Kinetic-Induced Moment Systems For Nonlinear Balance Laws

Dissertation
zur Erlangung des Doktorgrades
der Fakultät für Mathematik, Informatik
und Naturwissenschaften
der Universität Hamburg

vorgelegt
im Fachbereich Mathematik

von
Diana Cristina Gil Montoya
aus Medellín, Colombia

Hamburg
2017

Eidesstattliche Versicherung
Declaration on oath

Hiermit erklre ich an Eides statt, dass ich die vorliegende Dissertationsschrift selbst verfasst und keine anderen als die angegebenen Quellen und Hilfsmittel benutzt habe.

I hereby declare, on oath, that I have written the present dissertation by my own and have not used other than the acknowledged resources and aids.

Hamburg, den 29. März 2017
city and date

Unterschrift
signature

Als Dissertation angenommen vom Fachbereich

Mathematik der Universität Hamburg

Auf Grund der Gutachten von Prof. Dr. Jens Struckmeier

und Prof. Dr. Thomas Götz

Hamburg, den 22. November 2017

Prof. Dr. Michael Hinze

Leiter des Fachbereichs Mathematik

This thesis is dedicated to my Mother, Maria Gladis Montoya Valencia. Thanks to her efforts and to her understanding I was able to have a life in which I was free to pursue whatever I have set my mind to, no matter how weird and incomprehensible my ideas and points of view sounded to her. Because of her specially and my aunts that guided me at different points of my life (Nena, Gloria, Chila and Alba) I can be here.

To my supervisor Prof. Dr. Jens Struckmeier for his trust and support during all these years, which go back to my master studies.

And to my family in Hamburg, Aida, Johannes, Pedro, Antonio, Alessandro and my chosen life brothers Francesco, Juan David and Jose. All of them have made my life better and this process a lot more fun.

Contents

List of Tables

List of Figures

1. Introduction

Conservation laws are an important class of homogeneous hyperbolic partial differential equations (used to model wave motion and advective transport problems), where the total amount of the conserved quantity between two points changes only due to the flux past these points [22]. They form the mathematical foundation behind the study of fluid dynamics, which is broadly needed in the areas of geophysics, gas dynamics, acoustics, among others. Many of these physical problems give rise to nonlinearities, leading to discontinuous solutions like shock waves. This and the wide range of scales in which the different physical phenomena takes place bring often numerical difficulties, making more relevant the need of a deeper understanding of these equations origin.

Through out the study of rarefied gas flows, different macroscopic transport models have been developed as a more approachable alternative to the Boltzmann kinetic equation (from which they are also derived), specially for higher orders of the Knudsen numbers (Kn). In the limit of sufficiently small Kn, the Euler equations and the Navier-Stokes and Fourier equations can be derived, forming a link between the microscopic world of gas particles and the macroscopic one of fluid dynamics. One of the most promising is the *order of magnitude method* (OMM) which accomplishes stability at any order of Kn [36]. The OMM uses Chapman–Enskog–like asymptotic expansion techniques of the corresponding moments in terms of the Knudsen number, which plays the role of a relaxation parameter for the Boltzmann equation, the resulting moment systems are asymptotically closed without an additional closure relation.

Based on the previous stated connection between kinetic theory and conservation laws, we use the order of magnitude method in order to derive kinetic–induced moment systems for the spatially one–dimensional scalar and 2×2 system case of conservation laws from a given

Boltzmann-like kinetic equation, where Kn is represented now by the smallness parameter ε. The resulting partial differential equations are used first, as monitoring functions in order to detect particular flow structure like shock and rarefaction waves, resulting in novel grid-adaptive simulation tools and second, as a basis to derive novel parametrizations for subgrid closures.

This thesis is organized in five chapters. First, in chapter 2 we explain the basic concepts of conservation laws and kinetic theory. Second, in chapter 3 we describe the order of magnitude method and apply it to the scalar case and to a 2×2 system of balance laws (inhomogeneous conservation laws (2.7)), where we can prove that for $\varepsilon \to 0$, higher order moment systems tend to the original balance law plus a new function $W(x,t)$, which may act as a monitoring function to detect special solutions like shock and rarefaction waves. Third, in chapter 4 we perform numerical experiments in order to compare the original balance law with their corresponding moment system up to some order of accuracy. Initially, a static grid is used and the effects of different small values of ε are studied, then we include the new variable $W(x,t)$ as refinement criteria into adaptivity techniques and compare it with traditional mesh refinement approaches. Two main example are treated: the inviscid Burgers equation and the shallow water system. Finally, in chapter 5 we explore the spectral characteristics of the derived moment system for the inviscid Burgers case and the possibility to employ it as a "subgrid closure" model when using Fourier-Galerkin spectral approximations by comparing different amounts of resolved scales with different values of ε. In order to make the last chapter more readable, we include in Appendix A and B the complete set of figures of the numerical experiments used for it.

2. Preliminaries

During the following chapter, we will give an overview of basic concepts needed to have a better understanding of the succeeding chapters. The first section introduces the derivation of conservation laws together with two of its main approximation methods, the finite differences (FDM) and finite volumes methods (FVM). These concepts will be useful to understand the origin of the systems under study and the choice of numerical schemes for the corresponding numerical experiments. In the second section, we review the basic knowledge on kinetic theory, the modelling of gas flows and the connection with conservation laws, which are the key of the latter construction of kinetic-induced moment systems.

2.1 Conservation laws

Consider a one-dimensional density vector function $q(x,t)$ of m components, each one representing different conserved quantities. Given any smooth, bounded region $V \subset \mathbb{R}$, the total mass within V at a time t is given by

$$\int_V q(x,t)\mathrm{d}x \tag{2.1}$$

Since the aforementioned quantities should be conserved, their concentration is neither created or destroyed (principle of conservation) and thus the rate of change within V comes only from flux vector function $f(q)$, which controls the rate of loss or increase of $q(x,t)$ through the boundary ∂V. It makes then sense to write that for each time t, the following holds

$$\frac{\partial}{\partial t}\int_V q\mathrm{d}x = -\int_{\partial V} f(q)\cdot\nu\mathrm{d}S \tag{2.2}$$

where ν denotes the outward unit normal along V. By using the divergence theorem we can rewrite (2.2) as

$$\int_V q_t\mathrm{d}x = -\int_V f(q)_x\mathrm{d}x \tag{2.3}$$

and derive a general first order nonlinear PDE system of conservation laws

$$q_t + f(q)_x = 0 \quad \text{in } \mathbb{R} \times (0, t_{final}) \tag{2.4}$$

Definition 2.1.1. ***(Conservation laws)***

A system of conservation laws is a system of partial differential equations that can be written in the form

$$q_t + f(q)_x = 0, \tag{2.5}$$

where

$$q = (q_1, q_2, \cdots, q_m)^T, \quad f(q) = (f_1, f_2, \cdots, f_m)^T. \tag{2.6}$$

$q(x,t) \in \mathbb{R}^m$ *represents the vector of conserved variables and* $f \in \mathbb{R}^m$ *the flux vector, each* f_i *component is a function of the components* q_i *of* q *[40].*

We call an equation of the form (2.4) a system of *balance laws* when it is inhomogeneous, meaning that, there exits a source term $S(q) \neq 0 \in \mathbb{R}^m$ which contributes to changes in the physical variables under investigation. A *general one-dimensional nonlinear system of balanced laws* reads

$$q_t + f(q)_x = S(q) \quad \text{in } \mathbb{R} \times (0, t_{final}) \tag{2.7}$$

When $f(q) = aq$ with a constant value, the flux function is linear and we simply get the advection equation, in which case the solution translates uniformly. On the contrary, if $f(q)$ is nonlinear, the solution deforms as it evolves and *shock waves* appear, across which, the solution is discontinuous and (2.4) does not hold any more in the classical sense. Consider now a control volume in space $I = [x_L, x_R]$ then integrate (2.4) over it

$$\frac{\partial}{\partial t} \int_{x_L}^{x_R} q(x,t) \mathrm{d}x + \int_{x_L}^{x_R} \frac{\partial}{\partial x} f(q) \mathrm{d}x = 0 \tag{2.8}$$

subsequent integration of the second term by parts results in the *integral form* of (2.4),

$$\frac{\partial}{\partial t} \int_{x_L}^{x_R} q(x,t) \mathrm{d}x = f(q(x_L,t)) - f(q(x_R,t)) \tag{2.9}$$

this is an important definition since at a discontinuity in q, equation (2.9) will continue to hold if the *Rankine-Hugniot conditions* are satisfied. These conditions, relate the jump of the conserved quantities q and fluxes $f(q)$ across a shock wave with the propagation speed s of the discontinuity, they yield

$$s(q_R - q_L) = F(q_R) - F(q_L) \tag{2.10}$$

here q_L and q_R represent the states coming from the left and right side of the shock.

Additionally, the system (2.4) can be written in quasilinear form as

$$q_t + A(q) \cdot q_x = 0 \quad \text{in } \mathbb{R} \times (0, t_{final}) \tag{2.11}$$

where $A(q)$ is the Jacobian matrix of the flux vector.

Definition 2.1.2. ***(Jacobian Matrix)***

The Jacobian of the flux vector $f(q)$ in (2.4) is the matrix

$$A(q) = \frac{\partial f}{\partial q} = \begin{pmatrix} \partial f_1/\partial q_1 & \cdots & \partial f_1/\partial q_m \\ \partial f_2/\partial q_1 & \cdots & \partial f_2/\partial q_m \\ \vdots & \vdots & \vdots \\ \partial f_m/\partial q_1 & \cdots & \partial f_m/\partial q_m \end{pmatrix} \tag{2.12}$$

each entry $\partial f_i/\partial q_j$ corresponds to the partial derivative of the $i-$component of the flux vector $f(q)$ with respect to the $j-$component of the conserved quantities vector q [40].

Definition 2.1.3. ***(Eigenvalues)***

The eigenvalues λ_i of a matrix A are the roots of the characteristic polynomial

$$P(\lambda) = |A - \lambda I| = det(A - \lambda I) = 0 \tag{2.13}$$

where I is the identity matrix. They are also called the eigenvalues of the system [40].

In the physical sense, the eigenvalues will represent different speeds of propagation of information.

Definition 2.1.4. ***(Eigenvectors)***

A right eigenvector of a matrix A is a vector $r^i = [r_1^i, r_2^i, \cdots, r_m^i]^T$ satisfying $Ar^i = \lambda_i r^i$. In a similar way, a left eigenvector of a matrix A is a vector $l^i = [l_1^i, l_2^i, \cdots, l_m^i]^T$ such that $l^i A = \lambda_i l^i$ [40].

Definition 2.1.5. ***(Hyperbolic system)***

A system (2.4) is said to be hyperbolic if A has m real eigenvalues $\lambda_{i\,(i=1,\cdots,m)}$ and a corresponding set of m linearly independent right eigenvectors r^i. The system is strictly hyperbolic if all λ_i are distinct [40].

A system of m equations, will have m waves in the solution of the Riemann Problem and m characteristic fields defined by the characteristic speed $\lambda_i(q)$.

Definition 2.1.6. ***(Linearly degenerate field)*** *An $i-$characteristic field is said to be linearly degenerate if*

$$\bigtriangledown \lambda_i(q) \cdot r^i(q) = 0 \quad \forall q \in \mathbb{R}^m \tag{2.14}$$

where $\bigtriangledown \lambda$ represents the gradient with respect to the vector of conserved quantities q, i.e. $\bigtriangledown \lambda = \partial \lambda / \partial q$ [40].

If this is the case, nor shock nor rarefaction waves can occur in the $i-$characteristic field, instead a contact discontinuity appear, which is linear and propagates to the $i-$characteristic speed on each side without distorting.

Definition 2.1.7. ***(Genuinely nonlinear field)*** *An $i-$characteristic field is said to be genuinely nonlinear if*

$$\bigtriangledown \lambda_i(q) \cdot r^i(q) \neq 0 \quad \forall q \in \mathbb{R}^m \tag{2.15}$$

This property ensures that characteristics are always compressing or expanding as q varies, so either shocks or rarefaction waves can take place [40].

In order to give physical meaning to the Riemann Problem solution, a discontinuity separating left and right states, propagating at speed s, must satisfy the following *Entropy Condition*

$$\lambda_i(q_L) > s > \lambda_i(q_R) \tag{2.16}$$

so that the *i-th* characteristic is impinging on the discontinuity, while the other ones are crossing it. Furthermore,

$$\lambda_j(q_L) < s \text{ and } \lambda_j(q_R) < s \text{ for } j < i$$
$$\lambda_j(q_L) > s \text{ and } \lambda_j(q_R) > s \text{ for } j > i$$

where the eigenvalues are assumed to be ordered as $\lambda_1 < \lambda_2 < ... < \lambda_m$. For more details on the properties of conservation laws systems see [11],[20],[21],[22],[40].

Example 2.1.1. ***(Burgers Equation)***

Burgers Equation is one of the most fundamental nonlinear scalar conservation laws, defined by

$$\frac{\partial u}{\partial t} + \frac{\partial}{\partial x}\left(\frac{u^2}{2}\right) = 0 \tag{2.17}$$

where the velocity flux is given by $F(u) = \dfrac{u^2}{2}$, *thus* $F'(u) = u$. *In quasi-linear form the equation reads*

$$\frac{\partial u}{\partial t} + u\frac{\partial u}{\partial x} = 0 \tag{2.18}$$

and the characteristic speed is just $\lambda(u) = u$ *with its derivative* $\lambda'(u) = 1 > 0$, *meaning that the flux is convex and therefore larger values of* u *propagate faster than small ones.*

Example 2.1.2. ***(Isentropic gas dynamics)***

Consider the isentropic[1] *gas equations given by*

$$\frac{\partial \rho}{\partial t} + \frac{\partial}{\partial x}(\rho u) = 0 \tag{2.19}$$
$$\frac{\partial}{\partial t}(\rho u) + \frac{\partial}{\partial x}\big(\rho u^2 + P(\rho)\big) = 0 \tag{2.20}$$

[1] Adiabatic flow, i.e., without gain or loss of heat

where $\rho(t,x)$ denotes the gas density, $u(t,x)$ the velocity in $x-$direction and $P(\rho)$ the pressure. We choose a polytropic gas[2]*, meaning that the equation of state follows the relation*

$$P(\rho) = \kappa\rho^{\gamma}, \quad \kappa, \gamma \in \mathbb{R} \tag{2.21}$$

In quasi-linear form the previous system read

$$\begin{pmatrix} \rho \\ \rho u \end{pmatrix}_t + \begin{pmatrix} 0 & 1 \\ -u^2 + a^2 & 2u \end{pmatrix} \begin{pmatrix} \rho \\ \rho u \end{pmatrix}_x = \begin{pmatrix} 0 \\ 0 \end{pmatrix} \tag{2.22}$$

with $a = \gamma\kappa\rho^{\gamma-1}$. The eigenvalues are given by $\lambda_{1,2} = u \mp a$, which are real and distinct, then the system is strictly hyperbolic. The right and left eigenvectors are

$$r^1 = \begin{pmatrix} 1 \\ u - a \end{pmatrix}, \quad r^2 = \begin{pmatrix} 1 \\ u + a \end{pmatrix} \tag{2.23}$$

$$l^1 = (-(u+a), 1), \quad l^2 = (-(u-a), 1) \tag{2.24}$$

2.1.1 Numerical methods for conservation laws

Rarely, it is possible to find an analytical solution to systems like (2.4), specially if we want to get closer to real scenarios. Several successful numerical methods have been developed over the years, which approximate the solution of such problems along a given space and time interval. Here, we make an overview of two of the most important ones for Conservation Laws, which will then be used ahead to perform our numerical experiments.

Finite differences

Consider the scalar case of (2.4), the Finite Differences Method replaces the derivatives in the nonlinear first-order PDE with finite differences approximations, which are evaluated

[2]The internal energy is a function only of temperature, usually proportional to it.

in a finite number mesh instead of in a continuous domain. Let us define a spatial domain $[a, b]$ where (2.4) holds, the space discretization is then denoted by M equidistant points

$$x_i = a + i\Delta x, \qquad \forall \quad 0 \leq i \leq M - 1 \tag{2.25}$$

$\Delta x = (b - a)/(M - 1)$ is the cell width. In a similar way, the temporal discretization of the time domain $[0, t_{final}]$ is determined by the time levels

$$t_n = n\Delta t, \quad \forall \quad 0 \leq n \leq N \tag{2.26}$$

with $\Delta t = t_{final}/N$ the time step and $t_{final} = \Delta t \cdot N$. The finite mesh will be given by (2.25) and (2.26). A general explicit numerical method can be defined by the numerical operator

$$L_h(Q_i^n) \equiv Q_i^{n+1} - H(Q_{i-l}^n, \cdots, Q_i^n, Q_{i+1}^n, \cdots, Q_{i+r}^n) = 0 \tag{2.27}$$

which acts on discrete point values Q_i^n. The operator H is a real function of $(l + r + 1)$ variables, with l and r the scheme size. The *Local Truncation Error* to one time step is then defined as

$$\tau = \frac{L_h(q(x_i, t_n))}{\Delta t} \tag{2.28}$$

here the numerical operator is applied to the exact solution computed at the mesh point (x_i, t_n).

Definition 2.1.8. ***(Order of accuracy)***

A numerical method is of order of accuracy p in space and k in time if

$$\tau = O(\Delta x^p) + O(\Delta t^k) \tag{2.29}$$

Definition 2.1.9. ***(Consistency)***

A numerical method is said to be consistent with the partial differential equation if

$$\tau \to 0 \quad as \quad \Delta x \to 0 \quad (or \quad \Delta t \to 0) \tag{2.30}$$

The exact value of $q(x,t)$ in (2.4) evaluated at the grid point (x_i, t_n) is thus approximated by Q_i^n and its respective partial time and space derivatives (∂_t,∂_x) by one of the following finite differences approximations.

- *forward differences* (1^{st} order accurate)

$$\partial_t q(x_i,t_n) = \frac{Q_i^{n+1} - Q_i^n}{\Delta t} + O(\Delta t) \tag{2.31a}$$

$$\partial_x q(x_i,t_n) = \frac{Q_{i+1}^n - Q_i^n}{\Delta x} + O(\Delta x) \tag{2.31b}$$

- *backward differences* (1^{st} order accurate)

$$\partial_t q(x_i,t_n) = \frac{Q_i^n - Q_i^{n-1}}{\Delta t} + O(\Delta t) \tag{2.32a}$$

$$\partial_x q(x_i,t_n) = \frac{Q_i^n - Q_{i-1}^n}{\Delta x} + O(\Delta x) \tag{2.32b}$$

- *centred differences* (2^{nd} order accurate)

$$\partial_t q(x_i,t_n) = \frac{Q_i^{n+1} - Q_i^{n-1}}{2\Delta t} + O(\Delta t^2) \tag{2.33a}$$

$$\partial_x q(x_i,t_n) = \frac{Q_{i+1}^n - Q_{i-1}^n}{2\Delta x} + O(\Delta x^2) \tag{2.33b}$$

The above approximation will be of use later during the implementation of our numerical experiments.

Additionally, for conservation laws one could use a conservative scheme like (2.41) to solve the scalar case of (2.4), which reads

$$Q_i^{n+1} = Q_i^n - \frac{\Delta t}{\Delta x}\left[F_{i+\frac{1}{2}} - F_{i-\frac{1}{2}}\right] \tag{2.34}$$

given that changes in the conservative quantity come only from the fluxes to left and right hand side of the domain. Details follow in the next section.

Definition 2.1.10. ***(Courant-Friedrichs-Lewy condition)***

In the case of an explicit discrete scheme, the domain of dependence of the PDE is contained in the domain of dependence of the numerical scheme if

$$\lambda_{max}^{n}\frac{\Delta t}{\Delta x} \leq CFL_{max} \tag{2.35}$$

with $\lambda_{max}^{n} = \max_{i}|\lambda_{i}^{n}|$ *the largest characteristic speed at time* n *and* $CFL_{max} = 1$ *the linearised stability limit for convection dominated problems [24].*

Remark 2.1.1. *For diffusion dominated problems the mesh restriction includes*

$$\nu\frac{\Delta t}{\Delta x^{2}} \leq CFL_{max} \tag{2.36}$$

with ν *the diffusion coefficient and* $CFL_{max} = 1/2$

The previous *CFL condition* is a necessary condition for stability and convergence as the grid is refined ($\Delta t, \Delta x \to 0$). A more detailed description on the general construction of finite differences schemes and their properties can be found in [23], [28], [40].

Finite volumes

Consider now the nonlinear system (2.4), the Finite Volume Method is based in the integral form (2.9), which continues to hold along discontinuities. Instead of making approximations at grid points like the finite differences method, the domain is divided into grid cells, and the numerical solution gives an approximation of the average value of $q(x,t)$ on each one. Defining $C_i = (x_{i-\frac{1}{2}}, x_{i+\frac{1}{2}})$ the *i-th* grid cell, the average value of $q(x,t)$ over the *i-th* interval at time t_n, is given by

$$Q_{i}^{n} \approx \frac{1}{\Delta x}\int_{C_i} q(x,t_n)\mathrm{d}x \tag{2.37}$$

where $\Delta x = x_{i+\frac{1}{2}} - x_{i-\frac{1}{2}}$. In each time step, these values will change only by the fluxes through the edges of the grid cells and the total mass within the computational domain will be preserved. Recall the integral form (2.9)

$$\frac{\partial}{\partial t}\int_{C_i} q(x,t)\mathrm{d}x = f(q(x_{i-\frac{1}{2}},t)) - f(q(x_{i+\frac{1}{2}},t)) \tag{2.38}$$

We want to approximate Q_i^{n+1} which is the value of the cell average in the next time step. Integrating (2.9) over a time interval $[t_n, t_{n+1}]$ and dividing by Δx we get

$$\frac{1}{\Delta x}\int_{C_i} q(x,t_{n+1})\mathrm{d}x = \frac{1}{\Delta x}\int_{C_i} q(x,t_n)\mathrm{d}x - \frac{1}{\Delta x}\left[\int_{t_n}^{t_{n+1}} f(q(x_{i+\frac{1}{2}},t))\mathrm{d}t - \int_{t_n}^{t_{n+1}} f(q(x_{i-\frac{1}{2}},t))\mathrm{d}t\right] \tag{2.39}$$

If we define $F^n_{i\mp\frac{1}{2}}$ as the approximation of the flux average along $x = x_{i\mp\frac{1}{2}}$, i.e.

$$F^n_{i\mp\frac{1}{2}} \approx \frac{1}{\Delta t}\int_{t_n}^{t_{n+1}} f(q(x_{i\mp\frac{1}{2}},t))\mathrm{d}t \tag{2.40}$$

then (2.39) may be written as

$$Q_i^{n+1} = Q_i^n - \frac{\Delta t}{\Delta x}\left[F^n_{i+\frac{1}{2}} - F^n_{i-\frac{1}{2}}\right] \tag{2.41}$$

where $F^n_{i\mp\frac{1}{2}}$ is the approximation of the flux average along $x = x_{i\mp\frac{1}{2}}$ in the time interval $[t_n, t_{n+1}]$. The real flux is giving by $f(q)$ where $q(x,t)$ is the exact solution.

$$F^n_{i\mp\frac{1}{2}} \approx \frac{1}{\Delta t}\int_{t_n}^{t_{n+1}} f(q(x_{i\mp\frac{1}{2}},t))\mathrm{d}t \tag{2.42}$$

However, since we do not know the exact solution it is not possible to evaluate the time integrals of the flux exactly and thus it is necessary to construct a good approximation of the flux function based on the approximate cell averages Q^n. The idea behind it, is to use a *piecewise constant* function defined by the cell averages Q_i^n (2.37) as initial data to compute the *numerical flux* $F_{i\mp\frac{1}{2}}$ at cell interfaces $x_{i\mp\frac{1}{2}}$, so it will be a function of the states on the left and on the right of the interfaces.

$$F_{i+\frac{1}{2}} = F_{i+\frac{1}{2}}(Q_i^n, Q_{i+1}^n) \tag{2.43}$$

Several numerical fluxes can be found in the literature ([15],[22],[40]), from the simplest one called central flux given by

$$F^c_{i+\frac{1}{2}} = \frac{1}{2}\left(f(Q_i^n) + f(Q_{i+1}^n)\right) \tag{2.44}$$

passing through the Lax-Friedrichs, the Lax-Wendroff and the FORCE which increase in complexity, and reaching the most accurate and complex one called the *Godunov flux*

$$F^{GO}_{i+\frac{1}{2}} = f(Q^{GO}_{i+\frac{1}{2}}) \tag{2.45}$$

where the Godunov state $Q^{GO}_{i+\frac{1}{2}} = Q^{RP}(0,t)$ is the exact solution at the cell interface of the local Riemann Problem, which yields

$$Q_t + f_x = 0 \tag{2.46a}$$

$$Q(x,0) = \begin{cases} Q^n_i, & \text{if } x < 0 \\ Q^n_{i+1}, & \text{if } x \geq 0 \end{cases} \tag{2.46b}$$

Remark 2.1.2. *The exact computation of the local Riemann Problems in (2.46) can be complex and time-consuming, therefore the use of* ***approximated Riemann solvers*** *are rather common. One of the most popular and the one used in this work is the* ***Roe linearisation method****, which is first order accurate and follows the properties of hyperbolicity, consistency and conservation but is not entropy satisfying, the so called Harten-Hyman entropy fix is then used in case of sonic entropies to avoid this problem [22].*

In a similar way to the finite differences method, the CFL condition (Def. 2.1.10) will again impose a constraint onto the mesh velocity $(\Delta x/\Delta t)$ as a necessary condition for stability. In the case of first order hyperbolic systems with p eigenvalues $\lambda_{p,i}$ in cell i, it reads

$$S^n_{max}\frac{\Delta t}{\Delta x} \leq CFL_{max} \tag{2.47}$$

where $S^n_{max} = \max_i \left\{ \max_p \mid \lambda^n_{p,i} \mid \right\}$ is an estimate of the largest wave speed at time n along with $CFL_{max} = 1$.

Definition 2.1.11. ***(Consistency)***

The numerical flux is said consistent if all the arguments of $F_{i+\frac{1}{2}}$ are identical

$$F_{i+\frac{1}{2}}(Q,Q,\ldots,Q) = f(Q) \tag{2.48}$$

Theorem 2.1.1. ***(Lax-Wendroff 1960)***

If a conservative method is ***consistent*** *and* ***stable*** *then its numerical solution is* ***convergent*** *and it converges to a weak integral solution of the conservation law.*

The respective proof can be found in [21].

Fractional-step methods

When discretizing a Balance Law (2.7), instead of solving the entire system, an easier approach is the use of *fractional-step methods*. The idea is to split the complete system into two sub-problems, that can be solved separately. The first problem will consist in the homogeneous conservation law system which can be resolved by using a finite volume method in time step Δt, later this solution will be used as initial condition in the discretization of the second problem, which will change accordingly with the nature of the source term. Therefore, the solution of the previous system will be equivalent to solve

$$\frac{\partial q}{\partial t} + \frac{\partial}{\partial x} f(q) = 0 \tag{2.49a}$$

$$\frac{\partial q}{\partial t} = S(q) \tag{2.49b}$$

2.2 Basic concepts of kinetic theory

2.2.1 Boltzmann equation and BGK relaxation model

The Boltzmann equation describes the statistical distribution of the density of particles $f(t, x, \xi)$ which at time t and position x moves with velocity ξ. It is formed by the effects of the free advection of particles (left hand side) and the collisions between them, since involves exchange of energy and momentum (right hand side). It reads,

$$\frac{\partial}{\partial t} f + \xi \frac{\partial}{\partial x} f = \frac{1}{Kn} S(f) \tag{2.50}$$

with Kn the Knudsen number [3] and $S(f)$ the collision term. One of the different ways to express $S(f)$ in a simpler manner (and the one used here) is the Bhatnagar-Gross-Krook (BGK) model, which must satisfy balance of mass, momentum and energy depending on the problem,

$$S(f) = f_0 - f \tag{2.51}$$

[3] Ratio between the mean free path (average distance travelled by a particle between collisions) and the system typical length $Kn = \lambda / L$.

with f_0 the *local equilibrium function.* A deeper study on the Boltzmann equation and the BGK model can be found in [36].

Moments of $f(t, x, \xi)$

The moments derived from the Boltzmann equation are weighted averages of the distribution function much more approachable than f, given that f sometimes can be difficult to compute and is usually charge with a lot of information that might not be useful. They form a complete set of partial differential equations [36], and follow

$$w_\alpha = \int_{\mathbb{R}} \xi^\alpha f(t, x, \xi)\, \mathrm{d}\xi \qquad \text{for} \quad \alpha = 0, 1, 2, \ldots \tag{2.52}$$

Remark 2.2.1. *The weighted averages of $f_0(t, x, \xi)$ are called equilibrium moments.*

2.2.2 Macroscopic transport equations for rarefied gas flows

The modelling of gas flows implies the numerical solution of the Boltzmann equation (2.50), which can be a quite complex and time demanding task, even for small values of the Knudsen number. However, the type of gas flow can be characterized by Kn offering alternative models to the kinetic equation (2.50) but derived directly from it, which will result in faster and more efficient macroscopic transport equations.

The simplest case is the *hydrodynamic regime* ($Kn \lesssim 0.01$), it can be accurately described by the laws of Navier-Stokes and Fourier, yet the NSF equations stop to be valid for the description of gas microflows in the *transitional regime* ($0.01 \lesssim Kn \lesssim 10$) where the processes demand a more detailed method. Simplified extended macroscopic models for rarefied gases [4] that replace (2.50) have been developed for $Kn \lesssim 1$, which include: the *Chapman-Enskog expansion* in powers of Kn, its higher orders have been proven unstable for time-dependent problems [13]; the *Grad's moment method*, which provides stable equations for any set of

[4] Flow of gases below standard atmospheric pressure, also called low-pressure gas flow [26].

moments considered basic variables, though it is not related to the Knudsen number and thus unclear which moment set needs to be considered for a given process [9, 16]; and the *Order of magnitude method* that combines the first two. The last method considers the infinite coupled set of all possible moment equations, at any order of Kn yields sets of moment equations produced from the requirement that the number of variables is a small as possible. The Chapman-Enskog expansion is used only to identify the Knudsen order of moments [37]. This method will be the base of our research on kinetic-induced moment systems for conservation laws, a deeper explanation will follow in Chapter 3. For a detailed review of the literature on rarefied gas flows approximation methods see [36].

For $Kn \gtrsim 1$ including the *free-molecular flow regime* ($Kn \gtrsim 10$) the only option is to solve the Boltzmann equation numerically either by direct numerical simulation (DNS) or direct simulation Monte Carlo (DSMC) [5].

2.2.3 Kinetic representation of conservation laws

On the other hand, one can also establish a connection between the kinetic equation (2.50) and a conservation laws system (2.4) through a valid kinetic representation. First, we define the *kinetic formulation* of a conservation laws, which according to Lions [25] is an equivalent equation to the original hyperbolic system based on an appropriate Boltzmann-like transport equation such that:

- consider a full family of entropy inequalities,
- it involves an additional variable ξ called kinetic or microscopic velocity.
- its ξ-moments recover the original equations and their entropy conditions.

A weaker version of this formulation and the one covered here is the so-called *kinetic representation*, it uses only the single entropy coming from the total energy and is based on the representation formula given by its equilibrium ξ-moments (the motivation for this and

a detailed construction of a kinetic formulation can be seen in [33]). Next, we will outline the construction of the kinetic representation for the isentropic gas dynamic system as an example.

Example 2.2.1. ***(Kinetic representation of isentropic gas dynamics)***
An equivalent equation to the isentropic gas dynamic system (2.19) is based on the representation formula

$$\begin{pmatrix} \rho \\ \rho u \\ \rho u^2 + \kappa \rho^\gamma \end{pmatrix} = \int_{\mathbb{R}} \begin{pmatrix} 1 \\ \xi \\ \xi^2 \end{pmatrix} f_0(\rho, \xi - u)\, \mathrm{d}\xi \tag{2.53}$$

which is valid under $f_0(\rho, \xi)$ defined as,

$$f_0(t, x, \xi) := f_0(\rho, \xi) = \rho^{1-\theta}\, \chi(\tfrac{\xi}{\rho^\theta}) \quad \textit{with} \quad \theta = \tfrac{\gamma - 1}{2} \tag{2.54}$$

and where the function $\chi(\omega) \in \mathbb{R}$ fulfils the properties

$$\chi(\omega) = \chi(-\omega) \geq 0 \qquad \textit{(even non-negative function)} \tag{2.55a}$$

$$\int_{\mathbb{R}} \chi(\omega)\, \mathrm{d}\omega = 1 \quad \textit{and} \quad \int_{\mathbb{R}} \omega^2 \chi(\omega)\, \mathrm{d}\omega = \kappa \tag{2.55b}$$

The succeeding proof is just a simple computation of the right hand side of (2.53). Now, by integrating w.r.t. ξ against weights 1 and ξ, and using the values in (2.53), we can check that $G(t, x, \xi)$ defined as

$$\frac{\partial}{\partial t} f_0(\rho, \xi - u) + \xi \frac{\partial}{\partial x} f_0(\rho, \xi - u) := G(t, x, \xi) \tag{2.56}$$

satisfies the conservation relations

$$\int_{\mathbb{R}} G\, \mathrm{d}\xi = 0 \quad \textit{and} \quad \int_{\mathbb{R}} \xi G\, \mathrm{d}\xi = 0 \tag{2.57}$$

It is possible to consider (2.56) as the limit when $\varepsilon \to 0$ of a Boltzmann-like equation with a BGK relaxation term, written as

$$\frac{\partial}{\partial t} f(t,x,\xi) + \xi \frac{\partial}{\partial x} f(t,x,\xi) = \frac{1}{\varepsilon}[f_0(\rho, \xi - u) - f(t,x,\xi)] \tag{2.58a}$$

$$\rho(t,x) = \int_{\mathbb{R}} f(t,x,\xi)\, \mathrm{d}\xi \tag{2.58b}$$

$$\rho u(t,x) = \int_{\mathbb{R}} \xi f(t,x,\xi)\, \mathrm{d}\xi \tag{2.58c}$$

where $\varepsilon \ll 1$ is a smallness parameter representing Kn and

$$G = \lim_{\varepsilon \to 0} \frac{1}{\varepsilon}[f_0(\rho, \xi - u) - f(t,x,\xi)]. \tag{2.59}$$

As mentioned in Perthame [33], the rigorous proof of this consideration is still an open problem.

The kinetic representation (2.56) can also be used for numerical purposes, it allows the construction of stable solvers for the numerical approximation of the flux needed in the finite volume method (2.41). The so called *kinetic schemes* use the moments of the numerical fluxes coming from the kinetic approach of the hyperbolic system to discretize the flux in (2.41). In the case of the isentropic gas dynamics (2.53) the fluxes are under the flux splitting [5] form, where

$$F^n_{i+\frac{1}{2}} = F_+(\rho^n_i, u^n_i) + F_-(\rho^n_{i+1}, u^n_{i+1}), \tag{2.60a}$$

$$F_+(\rho, u) = \int_{\xi \geq 0} \xi \begin{pmatrix} 1 \\ \xi \end{pmatrix} f_0(\rho, \xi - u)\, \mathrm{d}\xi, \tag{2.60b}$$

$$F_-(\rho, u) = \int_{\xi \leq 0} \xi \begin{pmatrix} 1 \\ \xi \end{pmatrix} f_0(\rho, \xi - u)\, \mathrm{d}\xi. \tag{2.60c}$$

[5] A different approach to the Godunov method for identifying upwind directions in the FVM, it allows to write the scheme for one sign of the velocity [22],[40]

The details of the construction and properties of these type of schemes are not within the scope of this work. For further reading see [32], [33].

3. Kinetic-Induced Moment Systems

Based on the formulation of the *order of magnitude method* done by H. Struchtrup [35] which constructs a set of stable transport equations for rarefied gases at high orders of the Knudsen number, we want to derive a general kinetic-induced moment system for the one-dimensional nonlinear balance law in the scalar case and for a 2×2 system of equations. The moment system will depend on the smallness parameter $\varepsilon \ll 1$ (representing Kn from now on), which in the formal limit $\varepsilon \to 0$ yields the original balance laws.

3.1 Order of magnitude method (OMM)

As mentioned in section 2.2.2, the stability problems of the higher order expansions coming from the Chapman-Enskog method [10] and the lack of connection between the Knudsen number and the set of moment equations derived from the Grad's moment method [36] in rarefied gases modelling ($\varepsilon \lesssim 1$), were the motivation behind H. Struchtrup formulation of a new extended hydrodynamic model [35, 37] which combines the previous two methods in order to derive a set of equations capable to capture micro-scale effects at high orders of ε [36], i.e. when the typical length L is of the order of the gas mean free path λ. The computation of such equations with order of accuracy η_0 in ε follows:

1. **Determine the order of magnitude η of the moments.** Based on a Chapman-Enskog expansion with ε as smallness parameter, expand the moment w_α (2.52) according to

$$w_\alpha = \sum_{\beta=0} \varepsilon^\beta w_{\alpha,\beta} = w_{\alpha,0} + \varepsilon w_{\alpha,1} + \varepsilon^2 w_{\alpha,2} + \dots \tag{3.1}$$

   and determine the leading order η by inserting the expansion into the complete set of moment equations. The expansion of the Boltzmann equation (2.50) is transferred

from the phase space (as done by the Chapman-Enskog method [10]) to the moment space.

Definition 3.1.1. *A moment is said to be of leading order η, if $w_{\alpha,\beta} = 0 \ \forall \beta < \eta$.*

Remark 3.1.1. *It is important to underline that the order of magnitude method is not interested in the computation of the coefficients $w_{\alpha,\beta}$, but rather in their leading order.*

2. **Construct a moment set of equations with the minimum number of moments at order η.** New variables are introduced by linear combinations of the original moments, such that at a given order η the number of variables is minimal and form a unique set of moments, independent from their initial choice.

3. **Model reduction to a given order of accuracy η_0.** Delete all terms in the system that lead to contributions of the order $\eta > \eta_0$, according to the definition of order of accuracy adopted for the problem.

Therefore, the **order of magnitude method** constructs a unique stable moment system at any **order of accuracy η_0** based on the infinite moment system of the Boltzmann equation, the resulting transport equations contain the minimal number of moments at a given **order of magnitude η**. Both orders are measured in powers of the ε [36].

Next, we will use OMM based on a Boltzmann-like kinetic equation (with $\varepsilon \ll 1$) to construct a higher order moment system correlated with the one-dimensional scalar and the 2×2 system case of nonlinear balance laws (2.7) and study its properties.

3.2 Non-linear scalar balance laws

Based on the construction of a unique moment set for the one-dimensional transport equation using the order of magnitude method in [37], a similar moment system is constructed

in [38] such that at zeroth order accuracy in ε, it yields the general form of a one dimensional nonlinear balance law equation, where the nonlinear flux is given by $F(u) \in C^1(\mathbb{R})$ and the source term by $P(t,x,u) \in C^0(\mathbb{R}^2 \times \mathbb{R}_{>0})$.

$$\frac{\partial u}{\partial t} + \frac{\partial}{\partial x} F(u) = P(t,x,u) \tag{3.2}$$

3.2.1 Boltzmann-like kinetic equation and the infinite moment system

Considering an artificial kinetic equation of the form (2.50) plus BGK-relaxation (2.51), we denote by $\mu \in [-1,1]$ the velocity of the particles and $u_0 = u$ the zeroth moment of $f(x,t,\mu)$, defined as

$$u_0(x,t) = \int_{-1}^{1} \mu^0 \, f(t,x,\mu) \, \mathrm{d}\mu \tag{3.3}$$

The corresponding advection process is then given by $\xi = F'(u_0) + \mu$, with $F'(u_0)$ the local (macroscopic) convection speed coming from (3.2), so it will be possible to recover the correct nonlinear flux function $F(u_0)$. Consequently, the distribution function $f(x,t,\mu)$ obeys the kinetic equation

$$\frac{\partial f}{\partial t} + (F'(u_0) + \mu)\frac{\partial f}{\partial x} = \frac{1}{\varepsilon}(f_0 - f) \tag{3.4}$$

Proposition 3.2.1. *The final Boltzmann-like kinetic equation corresponding to (3.2) is given by*

$$\frac{\partial f}{\partial t} + (F'(u_0) + \mu)\frac{\partial f}{\partial x} = \frac{1}{\varepsilon}\left(\frac{u_0}{2} - f\right) + \frac{P(u_0)}{2} \tag{3.5}$$

Proof. Since we want to recover an scalar balance law, the zeroth moment of the collision term (right hand side of (3.4)) must balance the source term in (3.2), which means

$$\int_{-1}^{1} \mu^0 \, \frac{1}{\varepsilon}(f_0 - f) \, \mathrm{d}\mu = P(u_0) \tag{3.6a}$$

where $\mu^0 = 1$ and ε is a constant value, then

$$\int_{-1}^{1} (f_0 - f) \, \mathrm{d}\mu = \varepsilon P(u_0) \tag{3.6b}$$

$$\int_{-1}^{1} f_0 \,\mathrm{d}\mu - \int_{-1}^{1} f \,\mathrm{d}\mu = \varepsilon P(u_0). \tag{3.6c}$$

Moreover, the zeroth moment of $f(x,t,\mu)$ must only balance mass (in this case given by $u_0(x,t)$) as defined in (3.3), therefore we can write

$$\int_{-1}^{1} f_0 \,\mathrm{d}\mu = \int_{-1}^{1} f \,\mathrm{d}\mu + \varepsilon P(u_0) \tag{3.6d}$$

$$\int_{-1}^{1} f_0 \,\mathrm{d}\mu = u_0 + \varepsilon P(u_0) \quad \text{by (3.3)} \tag{3.6e}$$

and given that f_0 is independent of μ by definition, it is possible to compute the expression

$$f_0 = \frac{u_0}{2} + \frac{\varepsilon P(u_0)}{2}. \tag{3.6f}$$

Inserting (3.6f) into (3.4) we get (3.5). □

Remark 3.2.1. *In the case of scalar conservation laws the zeroth moment of the collision term (3.6a) must be equal zero.*

Proposition 3.2.2. ***(Infinite moment system)*** *Let u_α and w_α be the even and odd monomial moments of the distribution $f(x,t,\mu)$,*

$$\begin{aligned} u_\alpha &= \textstyle\int_{-1}^{1} \mu^{2\alpha} f \,\mathrm{d}\mu \qquad \textit{for} \quad \alpha = 0,1,2,\ldots \quad \textit{even}, \\ w_\alpha &= \textstyle\int_{-1}^{1} \mu^{(2\alpha-1)} f \,\mathrm{d}\mu \qquad \textit{for} \quad \alpha = 1,2,\ldots \quad \textit{odd}, \end{aligned} \tag{3.7}$$

respectively. Then, the infinite moment system reads,

$$\frac{\partial u_0}{\partial t} + F'(u_0)\frac{\partial u_0}{\partial x} + \frac{\partial w_1}{\partial x} = P(u_0) \tag{3.8a}$$

$$\frac{\partial w_\alpha}{\partial t} + F'(u_0)\frac{\partial w_\alpha}{\partial x} + \frac{\partial u_\alpha}{\partial x} = -\frac{1}{\varepsilon} w_\alpha \qquad \alpha = 1,2,\ldots \tag{3.8b}$$

$$\frac{\partial u_\alpha}{\partial t} + F'(u_0)\frac{\partial u_\alpha}{\partial x} + \frac{\partial w_{\alpha+1}}{\partial x} = \frac{1}{\varepsilon}\left[\frac{u_0}{(2\alpha+1)} - u_\alpha\right] + \frac{P(u_0)}{(2\alpha+1)} \qquad \alpha = 1,2,\ldots \tag{3.8c}$$

Proof. Multiplying the kinetic equation (3.5) by powers of μ and subsequent integration yield the system (3.8). □

Later use of the order of magnitude method allows the derivation of a scale-induced closure to a finite number of moment equations at a given order of accuracy in ε. In particular, the recovery of the general balance law equation (3.2) at zeroth order.

3.2.2 Order of magnitude method

According to the description made in section 3.1, the *order of magnitude method* will assign orders of magnitude to the moments, so that one may construct a new set of equations with the minimal amount of them at each order. Expanding all moments according to (3.1)

$$u_\alpha = \sum_{\beta=0} \varepsilon^\beta u_{\alpha,\beta} = u_{\alpha,0} + \varepsilon u_{\alpha,1} + \dots \tag{3.9a}$$

$$w_\alpha = \sum_{\beta=0} \varepsilon^\beta w_{\alpha,\beta} = w_{\alpha,0} + \varepsilon w_{\alpha,1} + \dots \tag{3.9b}$$

u_α is of leading order η if $u_{\alpha,\beta} = 0 \quad \forall \beta < \eta$. It holds in the same way for w_α.

Equilibrium (zeroth) and 1st order variables

Lemma 3.2.1. *The equilibrium values of the moments u_α and w_α are given by*

$$u_\alpha|_E = \frac{u_0}{2\alpha + 1} \tag{3.10a}$$

$$w_\alpha|_E = 0 \tag{3.10b}$$

Proof. The claim easily follows by considering (3.8) in the formal limit $\varepsilon \to 0$. We can see that all odd moments have no equilibrium value. □

Lemma 3.2.2. *The zeroth order term in the expansion (3.9) agrees with the equilibrium moments (3.10).*

$$u_{\alpha,0} = \frac{u_0}{2\alpha + 1} \tag{3.11a}$$

$$w_{\alpha,0} = 0, \qquad w_\alpha \quad \textit{is at least of the order} \quad O(\varepsilon^1) \tag{3.11b}$$

Proof. Inserting the Chapman-Enskog expansion (3.9) into the moment system (3.8) and balancing the leading order terms ε^{-1} we obtain (3.11). □

Thus w_α has no zeroth order contribution and all the even moments u_α can be written in terms of u_0, which now is considered as a base variable. Now we can define the first set of

non-equilibrium moments,

$$u_\alpha^{(1)} = u_\alpha - u_\alpha|_E = u_\alpha - \frac{u_0}{2\alpha+1}, \qquad \alpha = 1, 2, ... \tag{3.12a}$$

$$w_\alpha^{(1)} = w_\alpha - w_\alpha|_E = w_\alpha, \qquad \alpha = 1, 2, ... \tag{3.12b}$$

Theorem 3.2.1. *The first order of magnitude moment system reads*

$$\frac{\partial u_0}{\partial t} + F'(u_0)\frac{\partial u_0}{\partial x} + \frac{\partial w_1^{(1)}}{\partial x} = P(u_0) \tag{3.13a}$$

$$\frac{\partial w_\alpha^{(1)}}{\partial t} + F'(u_0)\frac{\partial w_\alpha^{(1)}}{\partial x} + \frac{\partial u_\alpha^{(1)}}{\partial x} = -\frac{1}{\varepsilon}\left[w_\alpha^{(1)} + \frac{\varepsilon}{2\alpha+1}\frac{\partial u_0}{\partial x}\right] \qquad \alpha = 1, 2, \ldots \tag{3.13b}$$

$$\frac{\partial u_\alpha^{(1)}}{\partial t} + F'(u_0)\frac{\partial u_\alpha^{(1)}}{\partial x} + \frac{\partial w_{\alpha+1}^{(1)}}{\partial x} = -\frac{1}{\varepsilon}\left[u_\alpha^{(1)} - \frac{\varepsilon}{2\alpha+1}\frac{\partial w_1^{(1)}}{\partial x}\right] \qquad \alpha = 1, 2, \ldots \tag{3.13c}$$

Proof. Inserting the new variables (3.12) into (3.8) and eliminating the time derivative of u_0, we can derive the new moment system (3.13). □

2nd order variables

Now the variables in the new moment system (3.13) are given by the equilibrium one u_0 and the non-equilibrium ones $u_\alpha^{(1)}$, $w_\alpha^{(1)}$. The latter are by construction at least of first order $O(\varepsilon)$, their subsequent expansion in a Chapman-Enskog series in ε reads,

$$u_\alpha^{(1)} = \sum_{\beta=1} \varepsilon^\beta u_{\alpha,\beta}^{(1)} = \varepsilon u_{\alpha,1}^{(1)} + \varepsilon^2 u_{\alpha,2}^{(1)} + \ldots \tag{3.14a}$$

$$w_\alpha^{(1)} = \sum_{\beta=1} \varepsilon^\beta w_{\alpha,\beta}^{(1)} = \varepsilon w_{\alpha,1}^{(1)} + \varepsilon^2 w_{\alpha,2}^{(1)} + \ldots \tag{3.14b}$$

Lemma 3.2.3. *The first order term in the expansion (3.14) reads,*

$$u_{\alpha,1}^{(1)} = 0, \qquad u_\alpha^{(1)} \quad \textit{is at least of the order} \quad O(\varepsilon^2) \tag{3.15a}$$

$$w_{\alpha,1}^{(1)} = -\frac{1}{2\alpha+1}\frac{\partial u_0}{\partial x} = \frac{3}{2\alpha+1} w_{1,1}^{(1)}, \quad \alpha = 2, 3, \ldots \tag{3.15b}$$

Proof. It follows by inserting again the expansion (3.15) into (3.13) and subsequent balance of the leading order terms ε^0. □

According to (3.15), there is no first order contribution in $u_\alpha^{(1)}$, while all the moments $w_\alpha^{(1)}$ can be expressed in terms of the gradient of the zeroth moment and are proven linearly dependent. Subsequently, to first order all the moments can be written in terms of u_0 and a part of its flux $w_1^{(1)}$, therefore they will be considered as the new base variables, while the rest of the moments are replaced by the second non-equilibrium variables, which are at least second order $O(\varepsilon^2)$.

$$u_\alpha^{(2)} = u_\alpha^{(1)} - u_\alpha^{(1)}|_E = u_\alpha^{(1)}, \qquad \alpha = 1, 2, \dots \tag{3.16a}$$

$$w_\alpha^{(2)} = w_\alpha^{(1)} - w_\alpha^{(1)}|_E = w_\alpha^{(1)} - \frac{3}{2\alpha+1} w_1^{(1)}, \qquad \alpha = 2, 3, \dots \tag{3.16b}$$

Theorem 3.2.2. *Let $u_0 = \widehat{u_0}$ and $w_1^{(1)} = \varepsilon \widehat{w_1}^{(1)}$ in the interest of indicating their order of magnitude in ε for convenience. The new moment system including second order of magnitude variables yields*

$$\frac{\partial \widehat{u_0}}{\partial t} + F'(\widehat{u_0}) \frac{\partial \widehat{u_0}}{\partial x} + \varepsilon \frac{\partial \widehat{w_1}^{(1)}}{\partial x} = P(\widehat{u_0}) \tag{3.17a}$$

$$\varepsilon \frac{\partial \widehat{w_1}^{(1)}}{\partial t} + \varepsilon F'(\widehat{u_0}) \frac{\partial \widehat{w_1}^{(1)}}{\partial x} + \frac{\partial u_1^{(2)}}{\partial x} = -\frac{1}{\varepsilon} \left[\varepsilon \widehat{w_1}^{(1)} + \frac{\varepsilon}{3} \frac{\partial \widehat{u_0}}{\partial x} \right] \tag{3.17b}$$

$$\frac{\partial u_\alpha^{(2)}}{\partial t} + F'(\widehat{u_0}) \frac{\partial u_\alpha^{(2)}}{\partial x} + \frac{\partial w_{\alpha+1}^{(2)}}{\partial x} = -\frac{1}{\varepsilon} \left[u_\alpha^{(2)} + \frac{4\alpha\varepsilon^2}{(2\alpha+3)(2\alpha+1)} \frac{\partial \widehat{w_1}^{(1)}}{\partial x} \right] \quad \alpha = 1, 2, \dots \tag{3.17c}$$

$$\frac{\partial w_\alpha^{(2)}}{\partial t} + F'(\widehat{u_0}) \frac{\partial w_\alpha^{(2)}}{\partial x} + \frac{\partial u_\alpha^{(2)}}{\partial x} = -\frac{1}{\varepsilon} \left[w_\alpha^{(2)} + \frac{3\varepsilon}{2\alpha+1} \frac{\partial u_1^{(2)}}{\partial x} \right] \qquad \alpha = 2, 3, \dots \tag{3.17d}$$

Proof. Following the same procedure as before, the new moment system (3.17) follows after insertion of (3.16) and replacement of the time derivative of $w_\alpha^{(1)}$. □

3rd order variables

In a similar way as before, we expand only the second order variables,

$$u_\alpha^{(2)} = \sum_{\beta=2} \varepsilon^\beta u_{\alpha,\beta}^{(2)} = \varepsilon^2 u_{\alpha,2}^{(2)} + \varepsilon^3 u_{\alpha,3}^{(2)} + \dots \tag{3.18a}$$

$$w_\alpha^{(2)} = \sum_{\beta=2} \varepsilon^\beta w_{\alpha,\beta}^{(2)} = \varepsilon^2 w_{\alpha,2}^{(2)} + \varepsilon^3 w_{\alpha,3}^{(2)} + \dots \tag{3.18b}$$

Lemma 3.2.4. *The second order terms in the expansion (3.18) read*

$$u_{\alpha,2}^{(2)} = -\frac{4\alpha}{(2\alpha+3)(2\alpha+1)} \frac{\partial \widehat{w_1}^{(1)}}{\partial x} = \frac{15\alpha}{(2\alpha+3)(2\alpha+1)} u_{1,2}^{(2)}, \quad \alpha = 2, 3, \dots \tag{3.19a}$$

$$w_{\alpha,2}^{(2)} = 0, \qquad w_\alpha^{(2)} \quad \textit{is at least of the order} \quad O(\varepsilon^3) \tag{3.19b}$$

Proof. One more time, the proof follows by inserting (3.18) into (3.17) and balancing the leading order terms ε^1. Hence, $w_\alpha^{(2)}$ has no second order contribution and $u_{\alpha,2}^{(2)}$ is linear dependent as expected. □

We continue in the same way as before and introduce the third non-equilibrium variables

$$u_\alpha^{(3)} = u_\alpha^{(2)} - u_\alpha^{(2)}|_E = u_\alpha^{(2)} - \frac{15\alpha}{(2\alpha+3)(2\alpha+1)} u_1^{(2)}, \qquad \alpha = 2, 3, \dots \tag{3.20a}$$

$$w_\alpha^{(3)} = w_\alpha^{(2)} - w_\alpha^{(2)}|_E = w_\alpha^{(2)}, \qquad \alpha = 2, 3, \dots \tag{3.20b}$$

Theorem 3.2.3. *Let the already expanded variable be defined as $u_1^{(2)} = \varepsilon^2 \widehat{u_1}^{(2)}$, the new moment system including third order of magnitude variables yields*

$$\frac{\partial \widehat{u_0}}{\partial t} + F'(\widehat{u_0}) \frac{\partial \widehat{u_0}}{\partial x} + \varepsilon \frac{\partial \widehat{w_1}^{(1)}}{\partial x} = P(\widehat{u_0}) \tag{3.21a}$$

$$\varepsilon \frac{\partial \widehat{w_1}^{(1)}}{\partial t} + \varepsilon F'(\widehat{u_0}) \frac{\partial \widehat{w_1}^{(1)}}{\partial x} + \varepsilon^2 \frac{\partial \widehat{u_1}^{(2)}}{\partial x} = -\frac{1}{\varepsilon} \left[\varepsilon \widehat{w_1}^{(1)} + \frac{\varepsilon}{3} \frac{\partial \widehat{u_0}}{\partial x} \right] \tag{3.21b}$$

$$\varepsilon^2 \frac{\partial \widehat{u_1}^{(2)}}{\partial t} + \varepsilon^2 F'(\widehat{u_0}) \frac{\partial \widehat{u_1}^{(2)}}{\partial x} + \frac{\partial w_2^{(3)}}{\partial x} = -\varepsilon \left[\widehat{u_1}^{(2)} + \frac{4}{15} \frac{\partial \widehat{w_1}^{(1)}}{\partial x} \right] \tag{3.21c}$$

$$\frac{\partial w_\alpha^{(3)}}{\partial t} + F'(\widehat{u_0}) \frac{\partial w_\alpha^{(3)}}{\partial x} + \frac{\partial u_\alpha^{(3)}}{\partial x} = -\frac{1}{\varepsilon} \left[w_\alpha^{(3)} + \frac{9(\alpha-1)\varepsilon^3}{(2\alpha+3)(2\alpha+1)} \frac{\partial \widehat{u_1}^{(2)}}{\partial x} \right] \qquad \alpha = 2, 3, \dots \tag{3.21d}$$

$$\frac{\partial u_\alpha^{(3)}}{\partial t} + F'(\widehat{u_0}) \frac{\partial u_\alpha^{(3)}}{\partial x} + \frac{\partial w_{\alpha+1}^{(3)}}{\partial x} = -\frac{1}{\varepsilon} \left[u_\alpha^{(3)} - \frac{15\alpha\varepsilon}{(2\alpha+3)(2\alpha+1)} \frac{\partial \widehat{w_2}^{(3)}}{\partial x} \right] \qquad \alpha = 2, 3 \dots \tag{3.21e}$$

The proof comes in the same systematic way as for (3.17).

Approximation for 3rd order variables

As we go further, the transport equations increase and their derivation become more complex, therefore we shall stop at the third order equations and consider only the leading terms given by the expansion of the highest order moments.

$$u_\alpha^{(3)} = \sum_{\beta=3} \varepsilon^\beta u_{\alpha,\beta}^{(3)} \tag{3.22a}$$

$$w_\alpha^{(3)} = \sum_{\beta=3} \varepsilon^\beta w_{\alpha,\beta}^{(3)} \tag{3.22b}$$

Lemma 3.2.5. *The third order terms in the expansion (3.22) read*

$$u_{\alpha,3}^{(3)} = 0, \qquad u_\alpha^{(3)} \quad \textit{is at least of the order} \quad O(\varepsilon^4) \tag{3.23a}$$

$$w_{\alpha,3}^{(3)} = -\frac{9(\alpha-1)}{(2\alpha+3)(2\alpha+1)} \frac{\partial \widehat{u_1}^{(2)}}{\partial x} = \frac{35(\alpha-1)}{(2\alpha+3)(2\alpha+1)} w_{2,3}^{(3)}, \quad \alpha = 3, 4, \dots \tag{3.23b}$$

Proof. After inserting (3.22) into (3.21) and balancing the leading orders ε^2 we get (3.23), where only the odd moments $w_\alpha^{(3)}$ have third order contribution and are linear dependent. □

Theorem 3.2.4. *Define again the first three variables: of zeroth order $u_0 = \widehat{u_0}$, of first order $w_1^{(1)} = \varepsilon^1 \widehat{w_1}^{(1)}$ and of second order $u_1^{(2)} = \varepsilon^2 \widehat{u_1}^{(2)}$. Furthermore, let the third non-equilibrium variables (3.20) consider only the first term in the expansion and be defined as*

$$u_\alpha^{(3)} = \varepsilon^3 \widehat{u_\alpha}^{(3)} = \varepsilon^3 u_{\alpha,3}^{(3)} \tag{3.24a}$$

$$w_\alpha^{(3)} = \varepsilon^3 \widehat{w_\alpha}^{(3)} = \varepsilon^3 w_{\alpha,3}^{(3)}. \tag{3.24b}$$

Then the closed moment system with variables up to third order of magnitude corresponding to the infinite system (3.21) reads

$$\frac{\partial \widehat{u_0}}{\partial t} + F'(\widehat{u_0}) \frac{\partial \widehat{u_0}}{\partial x} + \varepsilon \frac{\partial \widehat{w_1}^{(1)}}{\partial x} = P(\widehat{u_0}) \tag{3.25a}$$

$$\varepsilon \frac{\partial \widehat{w_1}^{(1)}}{\partial t} + \varepsilon F'(\widehat{u_0}) \frac{\partial \widehat{w_1}^{(1)}}{\partial x} + \varepsilon^2 \frac{\partial \widehat{u_1}^{(2)}}{\partial x} = -\left[\widehat{w_1}^{(1)} + \frac{1}{3} \frac{\partial \widehat{u_0}}{\partial x} \right] \tag{3.25b}$$

$$\varepsilon^2 \frac{\partial \widehat{u_1}^{(2)}}{\partial t} + \varepsilon^2 F'(\widehat{u_0}) \frac{\partial \widehat{u_1}^{(2)}}{\partial x} - \frac{9\varepsilon^3}{35} \frac{\partial^2 \widehat{u_1}^{(2)}}{\partial x^2} = -\varepsilon \left[\widehat{u_1}^{(2)} + \frac{4}{15} \frac{\partial \widehat{w_1}^{(1)}}{\partial x} \right] \tag{3.25c}$$

where the smallness parameter ε plays the role of an indicator of the leading order of each quantity.

Proof. It follows first by replacing (3.24) into (3.21) and then closing the system using the leading order terms of the third order variables (3.23). □

Remark 3.2.2. *The previous system contains the minimal number of elements from the infinite moment equations that are up to third order of magnitude.*

3.2.3 Model reduction by order of accuracy

Depending of the process under study, a reduced version of the moment system (3.25) based on the smallness parameter ε might be enough.

Definition 3.2.1. *A set of equations is said to be* ***accurate of order η_0****, when the part of the flux $w_1 = w_1^{(1)}$ is known within the order $O(\varepsilon^{\eta_0})$ [37].*

The previous definition will be used for proving the next four theorems.

Theorem 3.2.5. *The* ***zeroth order accuracy*** *model reduction of the moment system (3.25) is given by the 1D nonlinear balance law equation*

$$\frac{\partial u_0}{\partial t} + F'(u_0) \frac{\partial u_0}{\partial x} = P(u_0) \tag{3.26}$$

Proof. As we have shown before, $w_1^{(1)} = \varepsilon \widehat{w_1}^{(1)}$ in (3.25) is of leading order ε. Therefore, according to the Definition 3.2.1 it will vanishes to zeroth order in ε and (3.26) will follow. □

Theorem 3.2.6. *The* ***first order accuracy*** *system of (3.25) recovers the inhomogeneous balance laws equation with a linear diffusion term and diffusion coefficient of the order $O(\varepsilon)$.*

$$\frac{\partial u_0}{\partial t} + F'(u_0) \frac{\partial u_0}{\partial x} = \frac{\varepsilon}{3} \frac{\partial^2 u_0}{\partial x^2} + P(u_0) \tag{3.27}$$

Proof. Accordingly with the Definition 3.2.1, if we consider the first order in the smallness parameter ε, first we need (3.25a)

$$\frac{\partial \widehat{u_0}}{\partial t} + F'(\widehat{u_0})\frac{\partial \widehat{u_0}}{\partial x} + \varepsilon \frac{\partial \widehat{w_1}^{(1)}}{\partial x} = P(\widehat{u_0}) \tag{3.28}$$

together with the leading order contribution (of order ε^0) from (3.25b),

$$0 = -\frac{1}{\varepsilon}\left[\varepsilon \widehat{w_1}^{(1)} + \frac{\varepsilon}{3}\frac{\partial \widehat{u_0}}{\partial x}\right] \tag{3.29}$$

$$\widehat{w_1}^{(1)} = -\frac{1}{3}\frac{\partial \widehat{u_0}}{\partial x} \tag{3.30}$$

Combining both equations the system will yield (3.27). □

Theorem 3.2.7. *The* ***second order accuracy*** *system of (3.25) yields*

$$\frac{\partial u_0}{\partial t} + F'(u_0)\frac{\partial u_0}{\partial x} + \varepsilon \frac{\partial \widehat{w_1}^{(1)}}{\partial x} = P(u_0) \tag{3.31a}$$

$$\varepsilon \frac{\partial \widehat{w_1}^{(1)}}{\partial t} + \varepsilon F'(u_0)\frac{\partial \widehat{w_1}^{(1)}}{\partial x} + \frac{1}{3}\frac{\partial u_0}{\partial x} = -\widehat{w_1}^{(1)} \tag{3.31b}$$

Proof. Now we need to consider higher order contributions to $w_1^{(1)}$ in order to increase the order of accuracy. Hence, the terms of second leading order ε^1 in (3.25b) must be included. □

Remark 3.2.3. *Consider $F'(u_0)$ in (3.31) with only real eigenvalues and is diagonalizable, then we will have found an inhomogeneous hyperbolic system.*

Theorem 3.2.8. *The* ***third order accuracy*** *system of (3.25) recovers an inhomogeneous hyperbolic system with a diffusive correction of higher order.*

$$\frac{\partial u_0}{\partial t} + F'(u_0)\frac{\partial u_0}{\partial x} + \varepsilon \frac{\partial \widehat{w_1}^{(1)}}{\partial x} = P(u_0) \tag{3.32a}$$

$$\varepsilon \frac{\partial \widehat{w_1}^{(1)}}{\partial t} + \varepsilon F'(u_0)\frac{\partial \widehat{w_1}^{(1)}}{\partial x} + \frac{1}{3}\frac{\partial u_0}{\partial x} = -\widehat{w_1}^{(1)} + \varepsilon^2 \frac{4}{15}\frac{\partial^2 \widehat{w_1}^{(1)}}{\partial x^2} \tag{3.32b}$$

Proof. We will require the balance law (3.25a) plus the full equation (3.25b),

$$\frac{\partial u_0}{\partial t} + F'(u_0)\frac{\partial u_0}{\partial x} + \varepsilon \frac{\partial \widehat{w_1}^{(1)}}{\partial x} = P(u_0) \tag{3.33a}$$

$$\varepsilon\frac{\partial\widehat{w_1}^{(1)}}{\partial t}+\varepsilon F'(u_0)\frac{\partial\widehat{w_1}^{(1)}}{\partial x}+\varepsilon^2\frac{\partial\widehat{u_1}^{(2)}}{\partial x}=-\left[\widehat{w_1}^{(1)}+\frac{1}{3}\frac{\partial u_0}{\partial x}\right]. \tag{3.33b}$$

Since the second order variable $\widehat{u_1}^{(2)}$ appears, the leading order terms in (3.25c) must be also included,

$$0=-\left[\widehat{u_1}^{(2)}+\frac{4}{15}\frac{\partial\widehat{w_1}^{(1)}}{\partial x}\right] \tag{3.34}$$

$$\widehat{u_1}^{(2)}=-\frac{4}{15}\frac{\partial\widehat{w_1}^{(1)}}{\partial x} \tag{3.35}$$

Combining the equations the new system is given by (3.32). □

If we continue in the same way, it is possible to construct sets of equations of 4th and 5th order of accuracy.

3.2.4 Case 1: 1D Inviscid Burgers equation

We will base the numerical experiments of the previous developments in the inviscid Burgers equation, which is one of the most fundamental study cases for nonlinear scalar balance laws. Our equation reads,

$$\frac{\partial u}{\partial t}+\frac{\partial}{\partial x}\left(\frac{u^2}{2}\right)=0 \tag{3.36}$$

where the velocity flux is given by $F(u)=\dfrac{u^2}{2}$, thus $F'(u)=u$. And there is no source term, i.e. $P(x,t,u)=0$ and the equation is homogeneous. We can now immediately construct the reduced models up to 3rd order, by using the Theorems 2.2.5 until 2.2.8.

Zeroth order accuracy

Accordingly to (3.26) we can instantly observe that the zeroth order in ε will read the inviscid Burgers equation.

$$\frac{\partial u_0}{\partial t}+u_0\frac{\partial u_0}{\partial x}=0 \tag{3.37}$$

First order accuracy

Consistently, following (3.27) the first order in the smallness parameter, recovers the viscous Burgers equation, with diffusion coefficient of the order $O(\varepsilon)$.

$$\frac{\partial u_0}{\partial t} + u_0 \frac{\partial u_0}{\partial x} = \frac{\varepsilon}{3} \frac{\partial^2 u_0}{\partial x^2} \tag{3.38}$$

Second order accuracy

Again, in agreement with (3.31) the second order system yields an inhomogeneous strictly hyperbolic system, since $\lambda_{\mp} = u_0 \mp \frac{1}{\sqrt{3}}$ the eigenvalues of the homogeneous corresponding problem are real and distinct.

$$\frac{\partial u_0}{\partial t} + u_0 \frac{\partial u_0}{\partial x} + \varepsilon \frac{\partial \widehat{w_1}^{(1)}}{\partial x} = 0 \tag{3.39a}$$

$$\frac{\partial \widehat{w_1}^{(1)}}{\partial t} + u_0 \frac{\partial \widehat{w_1}^{(1)}}{\partial x} + \frac{1}{3\varepsilon} \frac{\partial u_0}{\partial x} = -\frac{1}{\varepsilon} \widehat{w_1}^{(1)} \tag{3.39b}$$

Third order accuracy

Finally, the third order system includes a linear diffusive correction of higher order in the previous second order system, with a diffusion coefficient of the order $O(\varepsilon)$.

$$\frac{\partial u_0}{\partial t} + u_0 \frac{\partial u_0}{\partial x} + \varepsilon \frac{\partial \widehat{w_1}^{(1)}}{\partial x} = 0 \tag{3.40a}$$

$$\frac{\partial \widehat{w_1}^{(1)}}{\partial t} + u_0 \frac{\partial \widehat{w_1}^{(1)}}{\partial x} + \frac{1}{3\varepsilon} \frac{\partial u_0}{\partial x} = -\frac{1}{\varepsilon} \widehat{w_1}^{(1)} + \frac{4\varepsilon}{15} \frac{\partial^2 \widehat{w_1}^{(1)}}{\partial x^2} \tag{3.40b}$$

3.3 Non-linear 2×2 system of balance laws

We will now consider the case of a general balance laws system with two unknowns, in which the left hand side is given by the corresponding conservative[1] system which is hyperbolic and the right hand side by the source terms which can alter in time the amount of each

[1] change in time of the unknowns plus the corresponding flux matrix

quantity. The system yields,

$$\frac{\partial}{\partial t}\begin{bmatrix} q(t,x) \\ z(t,x) \end{bmatrix} + \frac{\partial}{\partial x}\begin{bmatrix} z(t,x) \\ f(q,z) \end{bmatrix} = P(q,z) \tag{3.41}$$

where the fluxes are giving by $F(q) = z$ and $F(z)$ by a function of the form $f(q,z) = \frac{z^2}{q} + \kappa q^\gamma$ for which we have used as a model the isentropic gas dynamics equations, where the pressure is given by the equation of state $p(q) = \kappa q^\gamma$ for some constants $\kappa > 0$ and $1 < \gamma \leqslant 3$, (see [33]). The type of source term $P(q,z)$ considered corresponds to linear functions representing external forces which must follow one of the following structures, and where the function $\nu(x,t)$ is know and can also be a constant.

$$P(q,z) = \nu(x,t)\begin{bmatrix} 0 \\ q \end{bmatrix} \tag{3.42a}$$

$$P(q,z) = \nu(x,t)\begin{bmatrix} q \\ z \end{bmatrix} \tag{3.42b}$$

The balance laws system (3.41) is completed by the *entropy function* $E(q,z)$, corresponding to the total energy of the system,

$$E(q,z) = \underbrace{\frac{1}{2}\frac{z^2}{q}}_{\text{kinetic energy}} + \underbrace{\frac{\kappa}{\gamma - 1}q^\gamma}_{\text{potential energy}} \tag{3.43}$$

This is an obvious choice since an entropy function should be a conserved quantity, in this case the energy whenever the unknowns are smooth, but which has a source or a sink at discontinuities.

In our case, the energy will decrease in an admissible shock but will increase across an expansion shock. Consequently, it is also possible to define an *entropy flux* together with the *entropy inequality*, which satisfies for weak solutions

$$\frac{\partial E}{\partial t} + \frac{\partial}{\partial x}\left[\frac{z}{q}\left(E + \kappa q^\gamma\right)\right] \leq 0 \tag{3.44}$$

For smooth solutions the previous inequality becomes an equality. For more details in the properties and definition of entropy functions see [22].

3.3.1 Boltzmann-like kinetic equation and the infinite moment system

The corresponding artificial kinetic equation is of the form (2.50) including the acceleration giving through external forces $\Psi(x,t,\mu)$ (see [36]), with a BGK-relaxation term (2.51).

$$\frac{\partial f}{\partial t} + \mu\frac{\partial f}{\partial x} + \Psi(x,t,\mu)\frac{\partial f}{\partial \mu} = \frac{1}{\varepsilon}(f_0 - f) \tag{3.45}$$

where,

$$\Psi(\xi) = \nu(x,t) \quad \text{for (3.42a)} \qquad\qquad \Psi(\xi) = \nu(x,t)\mu \quad \text{for (3.42b).}$$

We will consider only the case (3.42a), the other case should follow in an analogous way.

Proposition 3.3.1. *The final Boltzmann-like kinetic equation corresponding to (3.41) with a source term given by (3.42a), yields*

$$\frac{\partial f}{\partial t} + \mu\frac{\partial f}{\partial x} + \nu(x,t)\frac{\partial f}{\partial \mu} = \frac{1}{\varepsilon}(f_0 - f) \tag{3.46}$$

The subsequent definition of the respective moments of the equilibrium distribution $f_0(x,t,\mu)$ follows the so-called *kinetic representation formula* (2.53), an equivalent system to (3.41) as explained in section 2.2.3.

$$\begin{pmatrix} q \\ z \\ \dfrac{z^2}{q} + \kappa q^\gamma \end{pmatrix} = \int_{\mathbb{R}} \begin{pmatrix} 1 \\ \mu \\ \mu^2 \end{pmatrix} f_0(x,t,\mu)\,\mathrm{d}\mu \tag{3.47}$$

Lemma 3.3.1. *The general moment of the equilibrium function $f_0(x,t,\mu)$ reads*

$$\frac{z^\alpha}{q^{\alpha-1}} + \frac{\alpha(\alpha-1)}{2}\kappa q^\gamma \left(\frac{z}{q}\right)^{\alpha-2} = \int_{\mathbb{R}} \mu^\alpha\, f_0(t,x,\mu)\,\mathrm{d}\mu, \qquad \textit{for} \quad \alpha = 0,1,2,\ldots \tag{3.48}$$

Proof. By using the conditions (2.55a) and (2.55a) described in section 2.2.3 for the function $f_0(x,t,\mu)$ in the representation formula (3.47), we can compute (3.48). □

Proposition 3.3.2. ***(Infinite moment system)*** *Let w_α be the monomial moments of the distribution $f(x,t,\mu)$*

$$w_\alpha = \int_{\mathbb{R}} \mu^\alpha f(t,x,\mu)\,\mathrm{d}\mu, \qquad \textit{for} \quad \alpha = 0,1,2,\ldots \tag{3.49}$$

and (3.48) the moments of $f_0(x,t,\mu)$. Then, the infinite moment system reads

$$\frac{\partial q}{\partial t} + \frac{\partial z}{\partial x} = 0 \tag{3.50a}$$

$$\frac{\partial z}{\partial t} + \frac{\partial w_2}{\partial x} - \nu(x,t)q = 0 \tag{3.50b}$$

$$\frac{\partial w_\alpha}{\partial t} + \frac{\partial w_{\alpha+1}}{\partial x} - \alpha\nu(x,t)w_{\alpha-1} = \frac{1}{\varepsilon}\left[\frac{z^\alpha}{q^{\alpha-1}} + \frac{\alpha(\alpha-1)}{2}\kappa q^\gamma \left(\frac{z}{q}\right)^{\alpha-2} - w_\alpha\right] \qquad \alpha = 2,3,\ldots \tag{3.50c}$$

Proof. The collision operator (right hand side of (3.46)) must balance mass and momentum, therefore at the zeroth and first moment, $f(t,x,\mu)$ must be in equilibrium, i.e

$$\int_{\mathbb{R}} (f_0 - f)\,\mathrm{d}\mu = 0 \tag{3.51a}$$

$$\int_{\mathbb{R}} \mu(f_0 - f)\,\mathrm{d}\mu = 0. \tag{3.51b}$$

Multiplying the kinetic equation (3.46) by the powers of μ and subsequent integration, yield the moment system (3.50). □

3.3.2 Order of magnitude method

Equilibrium (zeroth) and 1st order variables

Lemma 3.3.2. *The equilibrium values of the infinite moment system (3.50) agree with the moments of $f_0(t,x,\mu)$.*

$$w_\alpha|_E = \frac{z^\alpha}{q^{\alpha-1}} + \frac{\alpha(\alpha-1)}{2}\kappa q^\gamma \left(\frac{z}{q}\right)^{\alpha-2} \tag{3.52}$$

Proof. By considering (3.50) in the formal limit $\varepsilon \to 0$, equation (3.52) easily follows. □

Since we have define only one set of moments, we can see that for every α we have zeroth order contribution. Contrary to the scalar case, we will see that for the 2×2 system there are not vanishing moments. The first set of non-equilibrium moments are defined as,

$$w_\alpha^{(1)} = w_\alpha - w_\alpha|_E = w_\alpha - \frac{z^\alpha}{q^{\alpha-1}} + \frac{\alpha(\alpha-1)}{2}\kappa q^\gamma \left(\frac{z}{q}\right)^{\alpha-2}, \qquad \alpha = 2, 3, ... \tag{3.53}$$

Theorem 3.3.1. *The first order of magnitude moment system reads*

$$\frac{\partial q}{\partial t} + \frac{\partial z}{\partial x} = 0 \tag{3.54a}$$

$$\frac{\partial z}{\partial t} + \frac{\partial}{\partial x}\left(\frac{z^2}{q} + \kappa q^\gamma\right) + \frac{\partial w_2^{(1)}}{\partial x} = \nu q \tag{3.54b}$$

$$\frac{\partial w_2^{(1)}}{\partial t} - \frac{2z}{q}\frac{\partial w_2^{(1)}}{\partial x} + \frac{\partial w_3^{(1)}}{\partial x} - \kappa(\gamma-3)q^\gamma \frac{\partial}{\partial x}\left(\frac{z}{q}\right) = -\frac{1}{\varepsilon} w_2^{(1)} \tag{3.54c}$$

$$\begin{aligned} &\frac{\partial w_\alpha^{(1)}}{\partial t} - \frac{\alpha(\alpha-1)(\alpha-2)\kappa q^\gamma}{2}\frac{z^{\alpha-3}}{q^{\alpha-1}}\left(q\frac{\partial w_2^{(1)}}{\partial x} + \kappa\gamma q^\gamma \frac{\partial q}{\partial x}\right) \\ &-\alpha\frac{z^{\alpha-1}}{q^{\alpha-1}}\frac{\partial w_2^{(1)}}{\partial x} - \frac{\alpha(\alpha-1)\kappa(\gamma-3)q^\gamma}{2}\frac{z^{\alpha-2}}{q^{\alpha-2}}\frac{\partial}{\partial x}\left(\frac{z}{q}\right) + \frac{\partial w_{\alpha+1}^{(1)}}{\partial x} = \alpha\nu w_{\alpha-1}^{(1)} - \frac{1}{\varepsilon} w_\alpha^{(1)} \end{aligned} \tag{3.54d}$$

Proof. Replacing the new variables (3.53) in (3.50) we have for $\alpha = 3, 4, \ldots$

$$\frac{\partial q}{\partial t} + \frac{\partial z}{\partial x} = 0 \tag{3.55a}$$

$$\frac{\partial z}{\partial t} + \frac{\partial}{\partial x}\left(\frac{z^2}{q} + \kappa q^\gamma\right) + \frac{\partial w_2^{(1)}}{\partial x} = \nu q \tag{3.55b}$$

$$\frac{\partial w_2^{(1)}}{\partial t} + \frac{\partial}{\partial t}\left(\frac{z^2}{q} + \kappa q^\gamma\right) + \frac{\partial w_3^{(1)}}{\partial x} + \frac{\partial}{\partial x}\left(\frac{z^3}{q^2} + 3\kappa q^{\gamma-1} z\right) = 2\nu z - \frac{1}{\varepsilon} w_2^{(1)} \tag{3.55c}$$

$$\begin{aligned} &\frac{\partial w_\alpha^{(1)}}{\partial t} + \frac{\partial}{\partial t}\left(\frac{z^\alpha}{q^{\alpha-1}} + \frac{\alpha(\alpha-1)\kappa q^\gamma}{2}\frac{z^{\alpha-2}}{q^{\alpha-2}}\right) \\ &+\frac{\partial w_{\alpha+1}^{(1)}}{\partial x} + \frac{\partial}{\partial x}\left(\frac{z^{\alpha+1}}{q^\alpha} + \frac{\alpha(\alpha+1)\kappa q^\gamma}{2}\frac{z^{\alpha-1}}{q^{\alpha-1}}\right) \\ &-\alpha\nu w_{\alpha-1}^{(1)} - \alpha\nu\left(\frac{z^{\alpha-1}}{q^{\alpha-2}} + \frac{(\alpha-2)(\alpha-1)\kappa q^\gamma}{2}\frac{z^{\alpha-3}}{q^{\alpha-3}}\right) = -\frac{1}{\varepsilon} w_\alpha^{(1)} \end{aligned} \tag{3.55d}$$

And eliminating the second time derivative in (3.55c) and (3.55d), the infinite moment system (3.55) follows. □

Remark 3.3.1. *We can see that is necessary to write explicitly the moment equation for $w_2^{(1)}$ separately from the general moment equation for $w_\alpha^{(1)}$ since giving the source term the last one also depends on the previous moment $w_{\alpha-1}^{(1)}$, while for $\alpha = 2$ this contribution disappears with the replacement of the time derivative for space one. The system (3.54) now depends on the equilibrium variables $q(t,x) = w_0$, $z(t,x) = w_1$ and the non-equilibrium ones $w_\alpha^{(1)}$ for $\alpha = 2, 3, \ldots$*

2nd order variables

By construction the new variables are at least of first oder in ε, therefore their Chapman-Enskog expansion will read

,

$$w_\alpha^{(1)} = \sum_{\beta=1} \varepsilon^\beta w_{\alpha,\beta}^{(1)} = \varepsilon w_{\alpha,1}^{(1)} + \varepsilon^2 w_{\alpha,2}^{(1)} + \ldots \qquad \alpha = 2, 3, \ldots \tag{3.56}$$

Lemma 3.3.3. *The first order contribution $O(\varepsilon)$ of (3.56), yields*

$$w_{2,1}^{(1)} = (\gamma - 3)\kappa q^\gamma \frac{\partial}{\partial x}\left(\frac{z}{q}\right) \tag{3.57}$$

$$w_{\alpha,1}^{(1)} = \frac{\alpha(\alpha-1)}{2}\frac{z^{\alpha-2}}{q^{\alpha-2}}\left[w_{2,1}^{(1)} + (\alpha-2)\kappa^2\gamma\frac{q^{2\gamma-1}}{z}\frac{\partial q}{\partial x}\right], \quad \alpha = 3, 4, \ldots \tag{3.58}$$

Proof. Our claim follows by inserting (3.56) on (3.54) and balancing the leading order terms ε^0 . □

We can then write the infinite first non-equilibrium $\alpha-moments$ in terms of the equilibrium variables and $w_2^{(1)}$, making it possible to close the system if desired. Again, we define a new set of non-equilibrium variables as a linear combination of the previous ones,which are at least of second order $O(\varepsilon^2)$,

$$w_\alpha^{(2)} = w_\alpha^{(1)} - w_\alpha^{(1)}|_E = w_\alpha^{(1)} - \frac{\alpha(\alpha-1)}{2}\frac{z^{\alpha-2}}{q^{\alpha-2}}\left[w_2^{(1)} + \varepsilon(\alpha-2)\kappa^2\gamma\frac{q^{2\gamma-1}}{z}\frac{\partial q}{\partial x}\right], \quad \alpha = 3, 4... \tag{3.59}$$

Theorem 3.3.2. *Let $q = \widehat{q}$, $z = \widehat{z}$ and $w_2^{(1)} = \varepsilon\widehat{w_2}^{(1)}$ in the interest of making explicit the magnitude of the already expanded variables. The new moment system including second order of magnitude variables yields*

$$\frac{\partial \widehat{q}}{\partial t} + \frac{\partial \widehat{z}}{\partial x} = 0 \tag{3.60a}$$

$$\frac{\partial \widehat{z}}{\partial t} + \frac{\partial}{\partial x}\left(\frac{\widehat{z}^2}{\widehat{q}} + \kappa\widehat{q}^{\gamma}\right) + \varepsilon\frac{\partial \widehat{w_2}^{(1)}}{\partial x} = \nu\widehat{q} \tag{3.60b}$$

$$\begin{aligned}\varepsilon\frac{\partial \widehat{w_2}^{(1)}}{\partial t} + \varepsilon\frac{\widehat{z}}{\widehat{q}}\frac{\partial \widehat{w_2}^{(1)}}{\partial x} + 3\varepsilon\widehat{w_2}^{(1)}\frac{\partial}{\partial x}\left(\frac{\widehat{z}}{\widehat{q}}\right) - \kappa(\gamma-3)\widehat{q}^{\gamma}\frac{\partial}{\partial x}\left(\frac{\widehat{z}}{\widehat{q}}\right)\\ +3\varepsilon\kappa^2\gamma\frac{\partial}{\partial x}\left(\widehat{q}^{2\gamma-2}\frac{\partial \widehat{q}}{\partial x}\right) + \frac{\partial w_3^{(2)}}{\partial x} = -\widehat{w_2}^{(1)}\end{aligned} \tag{3.60c}$$

$$\begin{aligned}\frac{\partial w_3^{(2)}}{\partial t} - \frac{3\varepsilon^2\widehat{w_2}^{(1)}}{\widehat{q}}\frac{\partial \widehat{w_2}^{(1)}}{\partial x} - \frac{3\widehat{z}}{\widehat{q}}\frac{\partial w_3^{(2)}}{\partial x} - 3\varepsilon\kappa\widehat{q}^{\gamma-2}\left(\gamma\widehat{w_2}^{(1)}\frac{\partial \widehat{q}}{\partial x} + \widehat{q}\frac{\partial \widehat{w_2}^{(1)}}{\partial x}\right)\\ -3\varepsilon\kappa^2\gamma\widehat{q}^{2\gamma-1}\left[\frac{\partial^2}{\partial x^2}\left(\frac{\widehat{z}}{\widehat{q}}\right) + \frac{2(\gamma-2)}{\widehat{q}}\frac{\partial \widehat{q}}{\partial x}\frac{\partial}{\partial x}\left(\frac{\widehat{z}}{\widehat{q}}\right)\right] + \frac{\partial w_4^{(2)}}{\partial x} = -\frac{1}{\varepsilon}w_3^{(2)}\end{aligned} \tag{3.60d}$$

$$\begin{aligned}\frac{\partial w_\alpha^{(2)}}{\partial t} + \frac{\alpha(\alpha-1)}{2}\frac{\widehat{z}^{\alpha-3}}{\widehat{q}^{\alpha-3}}\left[-\frac{\widehat{z}}{\widehat{q}}\frac{\partial w_3^{(2)}}{\partial x} - (\alpha-2)\varepsilon^2\frac{\widehat{w_2}^{(1)}}{\widehat{q}}\frac{\partial \widehat{w_2}^{(1)}}{\partial x}\right]\\ -\frac{\alpha(\alpha-1)(\alpha-2)\varepsilon\kappa\widehat{q}^{\gamma}}{2}\frac{\widehat{z}^{\alpha-3}}{\widehat{q}^{\alpha-3}}\left[\frac{1}{\widehat{q}}\frac{\partial \widehat{w_2}^{(1)}}{\partial x} + \gamma\frac{\widehat{w_2}^{(1)}}{\widehat{q}^2}\frac{\partial \widehat{q}}{\partial x}\right]\\ +\frac{\alpha(\alpha-1)(\alpha-2)\varepsilon\kappa^2\gamma\widehat{q}^{2\gamma}}{2}\frac{\widehat{z}^{\alpha-3}}{\widehat{q}^{\alpha-1}}\left[\frac{\widehat{z}}{\widehat{q}}\frac{\partial^2 \widehat{q}}{\partial x^2} - \frac{\partial^2 \widehat{z}}{\partial x^2} - 2(\gamma-3)\frac{\partial \widehat{q}}{\partial x}\frac{\partial}{\partial x}\left(\frac{\widehat{z}}{\widehat{q}}\right)\right]\\ -\frac{\alpha(\alpha-1)(\alpha-2)(\alpha-3)\varepsilon\kappa^2\gamma\widehat{q}^{2\gamma}}{2\widehat{z}}\frac{\widehat{z}^{\alpha-3}}{\widehat{q}^{\alpha-1}}\left[\varepsilon\frac{\partial \widehat{w_2}^{(1)}}{\partial x} + \kappa\gamma\widehat{q}^{\gamma-1}\frac{\partial \widehat{q}}{\partial x}\right]\frac{\partial \widehat{q}}{\partial x}\\ +\frac{\partial w_{\alpha+1}^{(2)}}{\partial x} - \alpha\nu w_{\alpha-1}^{(2)} = -\frac{1}{\varepsilon}w_\alpha^{(2)}\end{aligned} \tag{3.60e}$$

Proof. By performing the change of variables on (3.54) with (3.59) and replacing the appearing second time derivatives, the infinite moment system (3.60) follows. □

3rd order variables

As done previously, we now expand the second order variables according to the Chapman-Enskog expansion

$$w_\alpha^{(2)} = \sum_{\beta=2} \varepsilon^\beta w_{\alpha,\beta}^{(2)} = \varepsilon^2 w_{\alpha,2}^{(2)} + \varepsilon^3 w_{\alpha,3}^{(2)} + \dots \qquad \alpha = 3, 4, \dots \tag{3.61}$$

Lemma 3.3.4. *The second order contribution in ε of (3.61) are giving by*

$$w_{3,2}^{(2)} = 3\kappa \widehat{q}^{\gamma-1} \left(\frac{\gamma \widehat{w_2}^{(1)}}{\widehat{q}} \frac{\partial \widehat{q}}{\partial x} + \frac{\partial \widehat{w_2}^{(1)}}{\partial x} + \kappa\gamma \widehat{q}^{\gamma} \left[\frac{\partial^2}{\partial x^2} \left(\frac{\widehat{z}}{\widehat{q}} \right) + \frac{2(\gamma-2)}{\widehat{q}} \frac{\partial \widehat{q}}{\partial x} \frac{\partial}{\partial x} \left(\frac{\widehat{z}}{\widehat{q}} \right) \right] \right) \tag{3.62}$$

$$w_{\alpha,2}^{(2)} = \frac{\alpha(\alpha-1)(\alpha-2)}{6} \frac{\widehat{z}^{\alpha-3}}{\widehat{q}^{\alpha-3}} \left[w_{3,2}^{(2)} + \frac{3(\alpha-3)\kappa^3\gamma^2 \widehat{q}^{3\gamma-3}}{\widehat{z}} \left(\frac{\partial \widehat{q}}{\partial x} \right)^2 \right], \quad \alpha = 4, 5 \dots \tag{3.63}$$

Proof. Once again, the proof follows by inserting (3.61) into (3.60) and balancing the leading order terms ε. □

As usual, we define now the third order non-equilibrium variables, in order to replace the previous ones for $\alpha = 4, 5, \dots$ in (3.60).

$$w_\alpha^{(3)} = w_\alpha^{(2)} - \frac{\alpha(\alpha-1)(\alpha-2)}{6} \frac{\widehat{z}^{\alpha-3}}{\widehat{q}^{\alpha-3}} \left[w_3^{(2)} + \frac{3\varepsilon^2(\alpha-3)\kappa^3\gamma^2 \widehat{q}^{3\gamma-3}}{\widehat{z}} \left(\frac{\partial \widehat{q}}{\partial x} \right)^2 \right] \tag{3.64}$$

Theorem 3.3.3. *Let the already expanded variable be defined as $q = \widehat{q}$, $z = \widehat{z}$, $w_2^{(1)} = \varepsilon \widehat{w_2}^{(1)}$ and $w_3^{(2)} = \varepsilon^2 \widehat{w_3}^{(2)}$, the new moment system including third order of magnitude variables yields*

$$\frac{\partial \widehat{q}}{\partial t} + \frac{\partial \widehat{z}}{\partial x} = 0 \tag{3.65a}$$

$$\frac{\partial \widehat{z}}{\partial t} + \frac{\partial}{\partial x} \left(\frac{\widehat{z}^2}{\widehat{q}} + \kappa \widehat{q}^{\gamma} \right) + \varepsilon \frac{\partial \widehat{w_2}^{(1)}}{\partial x} = \nu \widehat{q} \tag{3.65b}$$

$$\begin{aligned} \varepsilon \frac{\partial \widehat{w_2}^{(1)}}{\partial t} + \varepsilon \frac{\widehat{z}}{\widehat{q}} \frac{\partial \widehat{w_2}^{(1)}}{\partial x} + 3\varepsilon \widehat{w_2}^{(1)} \frac{\partial}{\partial x} \left(\frac{\widehat{z}}{\widehat{q}} \right) - \kappa(\gamma-3) \widehat{q}^{\gamma} \frac{\partial}{\partial x} \left(\frac{\widehat{z}}{\widehat{q}} \right) \\ + 3\varepsilon\kappa^2\gamma \frac{\partial}{\partial x} \left(\widehat{q}^{2\gamma-2} \frac{\partial \widehat{q}}{\partial x} \right) + \varepsilon^2 \frac{\partial \widehat{w_3}^{(2)}}{\partial x} = -\widehat{w_2}^{(1)} \end{aligned} \tag{3.65c}$$

$$\varepsilon^2\frac{\partial\widehat{w_3}^{(2)}}{\partial t}-\frac{3\widehat{z}}{\widehat{q}}\frac{\partial w_3^{(2)}}{\partial x}-3\varepsilon\kappa\widehat{q}^{\gamma-2}\left(\gamma\widehat{w_2}^{(1)}\frac{\partial\widehat{q}}{\partial x}+\widehat{q}\frac{\partial\widehat{w_2}^{(1)}}{\partial x}\right)$$
$$-\frac{3\varepsilon^2\widehat{w_2}^{(1)}}{\widehat{q}}\frac{\partial\widehat{w_2}^{(1)}}{\partial x}-3\varepsilon\kappa^2\gamma\widehat{q}^{2\gamma-1}\left[\frac{\partial^2}{\partial x^2}\left(\frac{\widehat{z}}{\widehat{q}}\right)+\frac{2(\gamma-2)}{\widehat{q}}\frac{\partial\widehat{q}}{\partial x}\frac{\partial}{\partial x}\left(\frac{\widehat{z}}{\widehat{q}}\right)\right] \tag{3.65d}$$
$$+4\varepsilon^2\frac{\partial}{\partial x}\left[\frac{\widehat{z}}{\widehat{q}}\widehat{w_3}^{(2)}+3\kappa^3\gamma^2\widehat{q}^{3\gamma-4}\left(\frac{\partial\widehat{q}}{\partial x}\right)^2\right]+\frac{\partial w_4^{(3)}}{\partial x}=-\varepsilon\widehat{w_3}^{(2)}$$
$$\frac{\partial\widehat{w_4}^{(3)}}{\partial t}-4\frac{\widehat{z}}{\widehat{q}}\frac{\partial\widehat{w_4}^{(3)}}{\partial x}-4\varepsilon^2\kappa\gamma\widehat{q}^{\gamma-2}\widehat{w_3}^{(2)}\frac{\partial\widehat{q}}{\partial x}-4\varepsilon^3\frac{\widehat{w_3}^{(2)}}{\widehat{q}}\frac{\partial\widehat{w_2}^{(1)}}{\partial x}$$
$$-12\varepsilon^2\kappa^3\gamma^2\widehat{q}^{3\gamma-4}\frac{\partial\widehat{q}}{\partial x}\left[3(\gamma-3)\frac{\partial\widehat{q}}{\partial x}\frac{\partial}{\partial x}\left(\frac{\widehat{z}}{\widehat{q}}\right)-\frac{2\widehat{z}}{\widehat{q}}\frac{\partial^2\widehat{q}}{\partial x^2}+2\frac{\partial^2\widehat{z}}{\partial x^2}\right] \tag{3.65e}$$
$$-12\varepsilon^2\kappa^2\gamma\widehat{q}^{2\gamma-3}\frac{\partial\widehat{q}}{\partial x}\frac{\partial\widehat{w_2}^{(1)}}{\partial x}+\frac{\partial\widehat{w_5}^{(3)}}{\partial x}=-\frac{1}{\varepsilon}w_4^{(3)}$$
$$\frac{\partial w_\alpha^{(3)}}{\partial t}-\frac{\alpha(\alpha-1)(\alpha-2)(\alpha-3)\varepsilon^2}{6}\frac{\widehat{z}^{\alpha-4}}{\widehat{q}^{\alpha-3}}\widehat{w_3}^{(2)}\left[\kappa\gamma\widehat{q}^{\gamma-1}\frac{\partial\widehat{q}}{\partial x}+\varepsilon\frac{\partial\widehat{w_2}^{(1)}}{\partial x}\right]$$
$$-\frac{\alpha(\alpha-1)(\alpha-2)}{6}\frac{\widehat{z}^{\alpha-3}}{\widehat{q}^{\alpha-3}}\frac{\partial\widehat{w_4}^{(3)}}{\partial x}$$
$$-\frac{\alpha(\alpha-1)(\alpha-2)(\alpha-3)\varepsilon^2\kappa^2\gamma\widehat{q}^{2\gamma-3}}{2}\frac{\widehat{z}^{\alpha-4}}{\widehat{q}^{\alpha-4}}\frac{\partial\widehat{q}}{\partial x}\frac{\partial\widehat{w_2}^{(1)}}{\partial x}$$
$$-\frac{3\alpha(\alpha-1)(\alpha-2)(\alpha-3)\varepsilon^2\kappa^3\gamma^2(\gamma-3)\widehat{q}^{3\gamma-4}}{2}\frac{\widehat{z}^{\alpha-4}}{\widehat{q}^{\alpha-4}}\left(\frac{\partial\widehat{q}}{\partial x}\right)^2\frac{\partial}{\partial x}\left(\frac{\widehat{z}}{\widehat{q}}\right) \tag{3.65f}$$
$$-\alpha(\alpha-1)(\alpha-2)(\alpha-3)\varepsilon^2\kappa^3\gamma^2\widehat{q}^{3\gamma-4}\frac{\widehat{z}^{\alpha-4}}{\widehat{q}^{\alpha-4}}\frac{\partial\widehat{q}}{\partial x}\left[-\frac{\widehat{z}}{\widehat{q}}\frac{\partial^2\widehat{q}}{\partial x^2}+\frac{\partial^2\widehat{z}}{\partial x^2}\right]$$
$$-\frac{\alpha(\alpha-1)(\alpha-2)(\alpha-3)(\alpha-4)\varepsilon^2\kappa^4\gamma^3\widehat{q}^{4\gamma-5}}{2\widehat{z}}\frac{\widehat{z}^{\alpha-4}}{\widehat{q}^{\alpha-4}}\left(\frac{\partial\widehat{q}}{\partial x}\right)^3$$
$$-\frac{\alpha(\alpha-1)(\alpha-2)(\alpha-3)(\alpha-4)\varepsilon^3\kappa^3\gamma^2\widehat{q}^{3\gamma-4}}{2\widehat{z}}\frac{\widehat{z}^{\alpha-4}}{\widehat{q}^{\alpha-4}}\left(\frac{\partial\widehat{q}}{\partial x}\right)^2\frac{\partial\widehat{w_2}^{(1)}}{\partial x}$$
$$+\frac{\partial w_{\alpha+1}^{(3)}}{\partial x}-\alpha\nu w_{\alpha-1}^{(3)}=-\frac{1}{\varepsilon}w_\alpha^{(3)}$$

Proof. The proof comes in the same systematic way as for (3.60). □

Approximation for 3rd order variables

We could continue repeating the previous steps infinitely, but as in the scalar case the results will become more difficult to handle, therefore we shall go as far as third order

variables considering only the leading order terms of their expansion.

$$w_\alpha^{(3)} = \sum_{\beta=3} \varepsilon^\beta w_{\alpha,\beta}^{(3)} = \varepsilon^3 w_{\alpha,3}^{(3)} + \varepsilon^4 w_{\alpha,4}^{(3)} + \dots \qquad \alpha = 4, 5, \dots \tag{3.66}$$

Lemma 3.3.5. *The third order contribution in (3.66) reads*

$$\begin{aligned} w_{4,3}^{(3)} &= 4\kappa\gamma\widehat{q}^{\gamma-2}\widehat{w_3}^{(2)}\frac{\partial\widehat{q}}{\partial x} + 12\kappa^2\gamma\widehat{q}^{2\gamma-3}\frac{\partial\widehat{q}}{\partial x}\frac{\partial\widehat{w_2}^{(1)}}{\partial x} \\ &\quad + 12\kappa^3\gamma^2\widehat{q}^{3\gamma-4}\frac{\partial\widehat{q}}{\partial x}\left[3(\gamma-3)\frac{\partial\widehat{q}}{\partial x}\frac{\partial}{\partial x}\left(\frac{\widehat{z}}{\widehat{q}}\right) - 2\frac{\widehat{z}}{\widehat{q}}\frac{\partial^2\widehat{q}}{\partial x^2} + 2\frac{\partial^2\widehat{z}}{\partial x^2}\right] \end{aligned} \tag{3.67}$$

$$w_{\alpha,3}^{(3)} = \frac{\alpha(\alpha-1)(\alpha-2)(\alpha-3)}{24}\frac{\widehat{z}^{\alpha-4}}{\widehat{q}^{\alpha-4}}\left[w_{4,3}^{(3)} + 12\kappa^4(\alpha-4)\gamma^3\frac{\widehat{q}^{4\gamma-5}}{\widehat{z}}\left(\frac{\partial\widehat{q}}{\partial x}\right)^3\right] \tag{3.68}$$

Proof. Balancing the terms of the order $O(\varepsilon^2)$ after inserting (3.66) into (3.65), we get (3.67). □

Theorem 3.3.4. *Define again the first three variables: of zeroth order $q = \widehat{q}$, $z = \widehat{z}$, of first order $w_2^{(1)} = \varepsilon\widehat{w_2}^{(1)}$ and of second order $w_3^{(2)} = \varepsilon^2\widehat{w_3}^{(2)}$. Furthermore, let the third non-equilibrium variable (3.64) consider only the first term in the expansion and be defined as*

$$w_\alpha^{(3)} = \varepsilon^3\widehat{w_\alpha}^{(3)} = \varepsilon^3 w_{\alpha,3}^{(3)} \tag{3.69}$$

Then the closed moment system with variables up to third order of magnitude corresponding to the infinite system (3.21) reads

$$\frac{\partial\widehat{q}}{\partial t} + \frac{\partial\widehat{z}}{\partial x} = 0 \tag{3.70a}$$

$$\frac{\partial\widehat{z}}{\partial t} + \frac{\partial}{\partial x}\left(\frac{\widehat{z}^2}{\widehat{q}} + \kappa\widehat{q}^\gamma\right) + \varepsilon\frac{\partial\widehat{w_2}^{(1)}}{\partial x} = \nu\widehat{q} \tag{3.70b}$$

$$\begin{aligned} \varepsilon\frac{\partial\widehat{w_2}^{(1)}}{\partial t} + \varepsilon\frac{\widehat{z}}{\widehat{q}}\frac{\partial\widehat{w_2}^{(1)}}{\partial x} + 3\varepsilon\widehat{w_2}^{(1)}\frac{\partial}{\partial x}\left(\frac{\widehat{z}}{\widehat{q}}\right) \\ -\kappa(\gamma-3)\widehat{q}^\gamma\frac{\partial}{\partial x}\left(\frac{\widehat{z}}{\widehat{q}}\right) + 3\varepsilon\kappa^2\gamma\frac{\partial}{\partial x}\left(\widehat{q}^{2\gamma-2}\frac{\partial\widehat{q}}{\partial x}\right) + \varepsilon^2\frac{\partial\widehat{w_3}^{(2)}}{\partial x} = -\widehat{w_2}^{(1)} \end{aligned} \tag{3.70c}$$

$$
\begin{aligned}
&\varepsilon^2\frac{\partial\widehat{w_3}^{(2)}}{\partial t}+\varepsilon^2\frac{\widehat{z}}{\widehat{q}}\frac{\partial\widehat{w_3}^{(2)}}{\partial x}+4\varepsilon^2\widehat{w_3}^{(2)}\frac{\partial}{\partial x}\left(\frac{\widehat{z}}{\widehat{q}}\right)\\
&-\frac{3\varepsilon^2\widehat{w_2}^{(1)}}{\widehat{q}}\frac{\partial\widehat{w_2}^{(1)}}{\partial x}+4\varepsilon^3\kappa\gamma\frac{\partial}{\partial x}\left(\widehat{q}^{\gamma-2}\widehat{w_3}^{(2)}\frac{\partial\widehat{q}}{\partial x}\right)\\
&+12\varepsilon^2\kappa^3\gamma^2\frac{\partial\widehat{q}}{\partial x}\left[\frac{\partial}{\partial x}\left(\widehat{q}^{3\gamma-4}\frac{\partial\widehat{q}}{\partial x}\right)+\widehat{q}^{3\gamma-4}\frac{\partial^2\widehat{q}}{\partial x^2}\right]\\
&+12\varepsilon^3\kappa^2\gamma\widehat{q}^{2\gamma-4}\left[(\gamma-3)\left(\frac{\partial\widehat{q}}{\partial x}\right)^2\frac{\partial\widehat{w_2}^{(1)}}{\partial x}+\widehat{q}\frac{\partial}{\partial x}\left(\frac{\partial\widehat{w_2}^{(1)}}{\partial x}\frac{\partial\widehat{q}}{\partial x}\right)\right]\\
&+108\varepsilon^3\kappa^3\gamma^2\widehat{q}^{3\gamma-5}\left(\frac{\partial\widehat{q}}{\partial x}\right)^2\left[(\gamma(\gamma-3)+6)\frac{\partial\widehat{q}}{\partial x}\frac{\partial}{\partial x}\left(\frac{\widehat{z}}{\widehat{q}}\right)+\gamma\widehat{q}\frac{\partial^2}{\partial x^2}\left(\frac{\widehat{z}}{\widehat{q}}\right)\right]\\
&+12\varepsilon^3\kappa^3\gamma^2\widehat{q}^{3\gamma-5}\left(\frac{\partial\widehat{q}}{\partial x}\right)^2\left[\frac{37\widehat{z}}{\widehat{q}}\frac{\partial^2\widehat{q}}{\partial x^2}-17\frac{\partial^2\widehat{z}}{\partial x^2}\right]\\
&+24\varepsilon^3\kappa^3\gamma^2\widehat{q}^{3\gamma-5}\left[(3\gamma-10)\frac{\partial\widehat{q}}{\partial x}\frac{\partial\widehat{z}}{\partial x}\frac{\partial^2\widehat{q}}{\partial x^2}\right]\\
&+24\varepsilon^3\kappa^3\gamma^2\widehat{q}^{3\gamma-5}\left[\widehat{q}\frac{\partial}{\partial x}\left(\frac{\partial\widehat{q}}{\partial x}\frac{\partial^2\widehat{z}}{\partial x^2}\right)-\widehat{z}\frac{\partial}{\partial x}\left(\frac{\partial\widehat{q}}{\partial x}\frac{\partial^2\widehat{q}}{\partial x^2}\right)\right]\\
&-3\varepsilon\kappa\widehat{q}^{\gamma}\left[\frac{\gamma\widehat{w_2}^{(1)}}{\widehat{q}^2}\frac{\partial\widehat{q}}{\partial x}+\frac{1}{\widehat{q}}\frac{\partial\widehat{w_2}^{(1)}}{\partial x}\right]\\
&-3\varepsilon\kappa^2\gamma\widehat{q}^{2\gamma-1}\left[\frac{\partial^2}{\partial x^2}\left(\frac{\widehat{z}}{\widehat{q}}\right)+2(\gamma-2)\frac{1}{\widehat{q}}\frac{\partial\widehat{q}}{\partial x}\frac{\partial}{\partial x}\left(\frac{\widehat{z}}{\widehat{q}}\right)\right]=-\varepsilon\widehat{w_3}^{(2)}
\end{aligned}
\tag{3.70d}
$$

where the smallness parameter ε plays the role of an indicator of the leading order of each quantity.

Proof. It follows first by replacing (3.69) into (3.65) and then closing the system using the leading order terms of the third order contribution variables (3.67). □

Remark 3.3.2. *The previous system contains the minimal number of elements from the infinite moment equations that are up to third order of magnitude.*

3.3.3 Model reduction by order of accuracy

Following the *order of accuracy* definition established for the scalar case (Def. 3.2.1), we now complete the order of magnitude method by reducing the moment system up to a third order of magnitude (3.70), based on the smallness parameter ε.

Theorem 3.3.5. *The **zeroth order accuracy** model reduction of the moment system (3.70) is given by the original one-dimensional 2×2 hyperbolic system*

$$\frac{\partial \widehat{q}}{\partial t} + \frac{\partial \widehat{z}}{\partial x} = 0 \tag{3.71a}$$

$$\frac{\partial \widehat{z}}{\partial t} + \frac{\partial}{\partial x}\left(\frac{\widehat{z}^2}{\widehat{q}} + \kappa \widehat{q}^{\gamma}\right) = \nu \widehat{q} \tag{3.71b}$$

Proof. According to the Definition 3.2.1, besides the equilibrium variables all the extra moments in (3.70) will vanish in ε, since their leading order is ε^1 or higher and (3.71) will follow. □

Remark 3.3.3. *The system of equations (3.71) has real and distinctive eigenvalues for $\kappa, \gamma \in \mathbb{R}_{>0}$.*

$$\lambda_{\mp} = \mp \sqrt{\kappa \gamma} q^{\frac{(\gamma-1)}{2}} \mp \frac{z}{q} \tag{3.72}$$

Theorem 3.3.6. *The **first order accuracy** model reduction of the moment system (3.70) yield an inhomogeneous hyperbolic system with a nonlinear diffusion term (unlike the linear one in the scalar case (3.27)) and an additional nonlinear mixed-derivative term, both of the order of $O(\varepsilon)$.*

$$\frac{\partial \widehat{q}}{\partial t} + \frac{\partial \widehat{z}}{\partial x} = 0 \tag{3.73a}$$

$$\frac{\partial \widehat{z}}{\partial t} + \frac{\partial}{\partial x}\left(\frac{\widehat{z}^2}{\widehat{q}} + \kappa \widehat{q}^{\gamma}\right) = -\varepsilon \kappa(\gamma - 3)\widehat{q}^{\gamma}\left[\frac{\gamma}{\widehat{q}}\frac{\partial \widehat{q}}{\partial x}\frac{\partial}{\partial x}\left(\frac{\widehat{z}}{\widehat{q}}\right) + \frac{\partial^2}{\partial x^2}\left(\frac{\widehat{z}}{\widehat{q}}\right)\right] + \nu \widehat{q} \tag{3.73b}$$

Proof. We are now searching for first order in ε, which means we will need the complete equation (3.70b) that includes the correction given by the third moment to the flux.

$$\frac{\partial \widehat{q}}{\partial t} + \frac{\partial \widehat{z}}{\partial x} = 0 \tag{3.74a}$$

$$\frac{\partial \widehat{z}}{\partial t} + \frac{\partial}{\partial x}\left(\frac{\widehat{z}^2}{\widehat{q}} + \kappa \widehat{q}^{\gamma}\right) + \varepsilon \frac{\partial \widehat{w_2}^{(1)}}{\partial x} = \nu \widehat{q} \tag{3.74b}$$

In order to close the system it is necessary to consider the leading order contribution ε^0 of the equation (3.70c)

$$0 = -\widehat{w_2}^{(1)} + \kappa(\gamma - 3)\widehat{q}^{\gamma}\frac{\partial}{\partial x}\left(\frac{\widehat{z}}{\widehat{q}}\right) \tag{3.75}$$

$$\widehat{w_2}^{(1)} = \kappa(\gamma-3)\widehat{q}^{\gamma}\frac{\partial}{\partial x}\left(\frac{\widehat{z}}{\widehat{q}}\right) \tag{3.76}$$

Replacing $\widehat{w_2}^{(1)}$ in (3.74), the system (3.73) will follow. □

Theorem 3.3.7. *The **second order accuracy** model reduction of the moment system (3.70) recovers an already closed system with a nonlinear correction of order $O(\varepsilon)$.*

$$\frac{\partial \widehat{q}}{\partial t} + \frac{\partial \widehat{z}}{\partial x} = 0 \tag{3.77a}$$

$$\frac{\partial \widehat{z}}{\partial t} + \frac{\partial}{\partial x}\left(\frac{\widehat{z}^2}{\widehat{q}} + \kappa\widehat{q}^{\gamma}\right) + \varepsilon\frac{\partial \widehat{w_2}^{(1)}}{\partial x} = \nu\widehat{q} \tag{3.77b}$$

$$\begin{aligned}\varepsilon\frac{\partial \widehat{w_2}^{(1)}}{\partial t} + \varepsilon\frac{\widehat{z}}{\widehat{q}}\frac{\partial \widehat{w_2}^{(1)}}{\partial x} + 3\varepsilon\widehat{w_2}^{(1)}\frac{\partial}{\partial x}\left(\frac{\widehat{z}}{\widehat{q}}\right) \\ -\kappa(\gamma-3)\widehat{q}^{\gamma}\frac{\partial}{\partial x}\left(\frac{\widehat{z}}{\widehat{q}}\right) = -3\varepsilon\kappa^2\gamma\frac{\partial}{\partial x}\left(\widehat{q}^{2\gamma-2}\frac{\partial \widehat{q}}{\partial x}\right) - \widehat{w_2}^{(1)}\end{aligned} \tag{3.77c}$$

Proof. To increase the order of accuracy to a second degree we just need to include the second order leading terms $O(\varepsilon)$ coming from (3.70c). □

It is possible to write the previous system (3.77) in conservation form by defining a new variable $f = \varepsilon\widehat{w_2}^{(1)} + \dfrac{\widehat{z}^2}{\widehat{q}} + \kappa\widehat{q}^{\gamma}$.

$$\frac{\partial \widehat{q}}{\partial t} + \frac{\partial \widehat{z}}{\partial x} = 0 \tag{3.78a}$$

$$\frac{\partial \widehat{z}}{\partial t} + \frac{\partial f}{\partial x} - \nu\widehat{q} = 0 \tag{3.78b}$$

$$\frac{\partial f}{\partial t} + \frac{\partial}{\partial x}\left[3\frac{\widehat{z}}{\widehat{q}}\left(f - \frac{2}{3}\frac{\widehat{z}^2}{\widehat{q}}\right)\right] - 2\nu\widehat{z} = -3\varepsilon\kappa^2\gamma\frac{\partial}{\partial x}\left(\widehat{q}^{2\gamma-2}\frac{\partial \widehat{q}}{\partial x}\right) - \frac{1}{\varepsilon}\left(f - \frac{\widehat{z}^2}{\widehat{q}} - \kappa\widehat{q}^{\gamma}\right) \tag{3.78c}$$

In quasilinear form, the conservative part of the previous system will read

$$\frac{\partial}{\partial t}\begin{pmatrix}\widehat{q}\\ \widehat{z}\\ f\end{pmatrix} + \begin{bmatrix}0 & 1 & 0\\ 0 & 0 & 1\\ 4\dfrac{\widehat{z}^3}{\widehat{q}^3} - 3f\dfrac{\widehat{z}}{\widehat{q}^2} & 3\dfrac{f}{\widehat{q}} - 6\dfrac{\widehat{z}^2}{\widehat{q}^2} & 3\dfrac{\widehat{z}}{\widehat{q}}\end{bmatrix}\frac{\partial}{\partial x}\begin{pmatrix}\widehat{q}\\ \widehat{z}\\ f\end{pmatrix} \tag{3.79}$$

with the respective eigenvalues of the Jacobian of the flux matrix,

$$\lambda_0 = \frac{\widehat{z}}{\widehat{q}} \qquad (3.80) \qquad\qquad \lambda_{\mp} = \frac{\widehat{z}}{\widehat{q}} \mp \sqrt{3\widehat{q}^4(f\widehat{q} - \widehat{z}^2)} \qquad (3.81)$$

by which (3.79) will be strictly hyperbolic as long as $(f\widehat{q} - \widehat{z}^2) > 0$.

Theorem 3.3.8. *The **third order accuracy** model reduction of the moment system (3.70) looks exactly like the second order accuracy one with an additional higher order correction term, which includes nonlinear diffusive and dispersive terms.*

$$\frac{\partial \widehat{q}}{\partial t} + \frac{\partial \widehat{z}}{\partial x} = 0 \qquad (3.82a)$$

$$\frac{\partial \widehat{z}}{\partial t} + \frac{\partial}{\partial x}\left(\frac{\widehat{z}^2}{\widehat{q}} + \kappa \widehat{q}^{\gamma}\right) + \varepsilon \frac{\partial \widehat{w_2}^{(1)}}{\partial x} = \nu \widehat{q} \qquad (3.82b)$$

$$\begin{aligned} \varepsilon \frac{\partial \widehat{w_2}^{(1)}}{\partial t} + \varepsilon \frac{\widehat{z}}{\widehat{q}} \frac{\partial \widehat{w_2}^{(1)}}{\partial x} + 3\varepsilon \widehat{w_2}^{(1)} \frac{\partial}{\partial x}\left(\frac{\widehat{z}}{\widehat{q}}\right) - \kappa(\gamma - 3)\widehat{q}^{\gamma} \frac{\partial}{\partial x}\left(\frac{\widehat{z}}{\widehat{q}}\right) = \\ -3\varepsilon\kappa^2\gamma \frac{\partial}{\partial x}\left(\widehat{q}^{2\gamma-2} \frac{\partial \widehat{q}}{\partial x}\right) - 3\varepsilon^2 \kappa \frac{\partial}{\partial x}\left[\frac{1}{\widehat{q}} \frac{\partial}{\partial x}\left(\widehat{q}^{\gamma} \widehat{w_2}^{(1)}\right)\right] \\ -3\varepsilon^2\kappa^2\gamma \frac{\partial}{\partial x}\left(\widehat{q}^{2\gamma-1}\left[\frac{\partial^2}{\partial x^2}\left(\frac{\widehat{z}}{\widehat{q}}\right) + 2(\gamma - 2)\frac{1}{\widehat{q}} \frac{\partial \widehat{q}}{\partial x} \frac{\partial}{\partial x}\left(\frac{\widehat{z}}{\widehat{q}}\right)\right]\right) - \widehat{w_2}^{(1)} \end{aligned} \qquad (3.82c)$$

Proof. We will now include the second order contribution in (3.70c) which adds to the previous second order accuracy system (3.77) the variable $\widehat{w_3}^{(2)}$.

$$\frac{\partial \widehat{q}}{\partial t} + \frac{\partial \widehat{z}}{\partial x} = 0 \qquad (3.83a)$$

$$\frac{\partial \widehat{z}}{\partial t} + \frac{\partial}{\partial x}\left(\frac{\widehat{z}^2}{\widehat{q}} + \kappa \widehat{q}^{\gamma}\right) + \varepsilon \frac{\partial \widehat{w_2}^{(1)}}{\partial x} = \nu \widehat{q} \qquad (3.83b)$$

$$\begin{aligned} \varepsilon \frac{\partial \widehat{w_2}^{(1)}}{\partial t} + \varepsilon \frac{\widehat{z}}{\widehat{q}} \frac{\partial \widehat{w_2}^{(1)}}{\partial x} + 3\varepsilon \widehat{w_2}^{(1)} \frac{\partial}{\partial x}\left(\frac{\widehat{z}}{\widehat{q}}\right) \\ -\kappa(\gamma - 3)\widehat{q}^{\gamma} \frac{\partial}{\partial x}\left(\frac{\widehat{z}}{\widehat{q}}\right) + 3\varepsilon\kappa^2\gamma \frac{\partial}{\partial x}\left(\widehat{q}^{2\gamma-2} \frac{\partial \widehat{q}}{\partial x}\right) + \varepsilon^2 \frac{\partial \widehat{w_3}^{(2)}}{\partial x} = -\widehat{w_2}^{(1)} \end{aligned} \qquad (3.83c)$$

Therefore, we must also take into account the leading order terms in (3.70d) in order to close the new system.

$$0 = -\widehat{w_3}^{(2)} + 3\kappa\widehat{q}^{\gamma}\left(\frac{\gamma \widehat{w_2}^{(1)}}{\widehat{q}^2} \frac{\partial \widehat{q}}{\partial x} + \frac{1}{\widehat{q}} \frac{\partial \widehat{w_2}^{(1)}}{\partial x} + \kappa\gamma\widehat{q}^{\gamma-1}\left[\frac{\partial^2}{\partial x^2}\left(\frac{\widehat{z}}{\widehat{q}}\right) + 2(\gamma - 2)\frac{1}{\widehat{q}} \frac{\partial \widehat{q}}{\partial x} \frac{\partial}{\partial x}\left(\frac{\widehat{z}}{\widehat{q}}\right)\right]\right)$$

$$\widehat{w_3}^{(2)} = 3\kappa\widehat{q}^{\gamma}\left(\frac{\gamma\widehat{w_2}^{(1)}}{\widehat{q}^2}\frac{\partial\widehat{q}}{\partial x} + \frac{1}{\widehat{q}}\frac{\partial\widehat{w_2}^{(1)}}{\partial x} + \kappa\gamma\widehat{q}^{\gamma-1}\left[\frac{\partial^2}{\partial x^2}\left(\frac{\widehat{z}}{\widehat{q}}\right) + 2(\gamma-2)\frac{1}{\widehat{q}}\frac{\partial\widehat{q}}{\partial x}\frac{\partial}{\partial x}\left(\frac{\widehat{z}}{\widehat{q}}\right)\right]\right)$$

$$\widehat{w_3}^{(2)} = 3\kappa\frac{1}{\widehat{q}}\left[\gamma\widehat{q}^{\gamma-1}\widehat{w_2}^{(1)}\frac{\partial\widehat{q}}{\partial x} + \widehat{q}^{\gamma}\frac{\partial\widehat{w_2}^{(1)}}{\partial x}\right] + 3\kappa^2\gamma\widehat{q}^{2\gamma-1}\left[\frac{\partial^2}{\partial x^2}\left(\frac{\widehat{z}}{\widehat{q}}\right) + 2(\gamma-2)\frac{1}{\widehat{q}}\frac{\partial\widehat{q}}{\partial x}\frac{\partial}{\partial x}\left(\frac{\widehat{z}}{\widehat{q}}\right)\right]$$

$$\widehat{w_3}^{(2)} = 3\kappa\frac{1}{\widehat{q}}\frac{\partial}{\partial x}\left(\widehat{q}^{\gamma}\widehat{w_2}^{(1)}\right) + 3\kappa^2\gamma\widehat{q}^{2\gamma-1}\left[\frac{\partial^2}{\partial x^2}\left(\frac{\widehat{z}}{\widehat{q}}\right) + 2(\gamma-2)\frac{1}{\widehat{q}}\frac{\partial\widehat{q}}{\partial x}\frac{\partial}{\partial x}\left(\frac{\widehat{z}}{\widehat{q}}\right)\right] \tag{3.84}$$

Inserting (3.84) into (3.83), the final system will yield (3.82). □

The homogeneous part will remain unaltered thus we can write it again in conservation form as in (3.79), keeping the same hyperbolic properties.

$$\frac{\partial\widehat{q}}{\partial t} + \frac{\partial\widehat{z}}{\partial x} = 0 \tag{3.85a}$$

$$\frac{\partial\widehat{z}}{\partial t} + \frac{\partial f}{\partial x} - \nu\widehat{q} = 0 \tag{3.85b}$$

$$\begin{aligned}\frac{\partial f}{\partial t} + \frac{\partial}{\partial x}\left[3\frac{\widehat{z}}{\widehat{q}}\left(f - \frac{2}{3}\frac{\widehat{z}^2}{\widehat{q}}\right)\right] - 2\nu\widehat{z} = \\ -3\varepsilon\kappa^2\gamma\frac{\partial}{\partial x}\left(\widehat{q}^{2\gamma-2}\frac{\partial\widehat{q}}{\partial x}\right) - 3\varepsilon\kappa\frac{\partial}{\partial x}\left[\frac{1}{\widehat{q}}\frac{\partial}{\partial x}\left(f\widehat{q}^{\gamma} - \widehat{z}^2\widehat{q}^{\gamma-1} - \kappa\widehat{q}^{2\gamma}\right)\right] \\ -3\varepsilon^2\kappa^2\gamma\frac{\partial}{\partial x}\left(\widehat{q}^{2\gamma-1}\left[\frac{\partial^2}{\partial x^2}\left(\frac{\widehat{z}}{\widehat{q}}\right) + 2(\gamma-2)\frac{1}{\widehat{q}}\frac{\partial\widehat{q}}{\partial x}\frac{\partial}{\partial x}\left(\frac{\widehat{z}}{\widehat{q}}\right)\right]\right) \\ -\frac{1}{\varepsilon}\left(f - \frac{\widehat{z}^2}{\widehat{q}} - \kappa\widehat{q}^{\gamma}\right)\end{aligned} \tag{3.85c}$$

3.3.4 Case 2: 1D Shallow water equations

For the numerical experiments of the 2×2 system, we will take as test case the one-dimensional homogeneous shallow water equations, with $\gamma = 2$, $\kappa = \frac{g}{2}$ and $\nu = 0$.

$$\frac{\partial h}{\partial t} + \frac{\partial(hu)}{\partial x} = 0 \tag{3.86a}$$

$$\frac{\partial(hu)}{\partial t} + \frac{\partial}{\partial x}\left(hu^2 + \frac{g}{2}h^2\right) = 0 \tag{3.86b}$$

Where $q(x,t) = h(x,t)$ represents the height of the water, $z(x,t) = h(x,t)u(x,t)$ the flow discharge with $u(x,t)$ the horizontal velocity and g stands for the gravitational acceleration. Replacing the new variables into (3.71), (3.73), (3.77), (3.83) we can construct the different closed systems for each order of accuracy.

Zeroth order accuracy

As expected from (3.71) at zeroth order in ε we recover the system of interest, in this case the 1D shallow water equations,

$$\frac{\partial \widehat{h}}{\partial t} + \frac{\partial (\widehat{h}\widehat{u})}{\partial x} = 0 \tag{3.87a}$$

$$\frac{\partial (\widehat{h}\widehat{u})}{\partial t} + \frac{\partial}{\partial x}\left(\widehat{h}\widehat{u}^2 + \frac{g}{2}\widehat{h}^2\right) = 0 \tag{3.87b}$$

First order accuracy

As we increase the accuracy in ε, accordingly with (3.73) nonlinear diffusive effects of the order of $O(\varepsilon)$ will appear affected by the gravitational force.

$$\frac{\partial \widehat{h}}{\partial t} + \frac{\partial (\widehat{h}\widehat{u})}{\partial x} = 0 \tag{3.88a}$$

$$\frac{\partial (\widehat{h}\widehat{u})}{\partial t} + \frac{\partial}{\partial x}\left(\widehat{h}\widehat{u}^2 + \frac{g}{2}\widehat{h}^2\right) = \varepsilon \frac{g}{2}\frac{\partial}{\partial x}\left(\widehat{h}^2 \frac{\partial \widehat{u}}{\partial x}\right) \tag{3.88b}$$

Second order accuracy

We can write directly the following systems in balance form by defining a new variable $f = \varepsilon \widehat{w_2}^{(1)} + \widehat{h}\widehat{u}^2 + \frac{g}{2}\widehat{h}^2$, as done for the general case.

$$\frac{\partial \widehat{h}}{\partial t} + \frac{\partial (\widehat{h}\widehat{u})}{\partial x} = 0 \tag{3.89a}$$

$$\frac{\partial (\widehat{h}\widehat{u})}{\partial t} + \frac{\partial f}{\partial x} = 0 \tag{3.89b}$$

$$\frac{\partial f}{\partial t} + \frac{\partial}{\partial x}\left[3\widehat{u}\left(f - \frac{2}{3}\widehat{h}\widehat{u}^2\right)\right] = -3\varepsilon \frac{g^2}{2}\frac{\partial}{\partial x}\left(\widehat{h}^2 \frac{\partial \widehat{h}}{\partial x}\right) - \frac{1}{\varepsilon}\left(f - \widehat{h}\widehat{u}^2 - \frac{g}{2}\widehat{h}^2\right) \tag{3.89c}$$

Together with the eigenvalues $\lambda_0 = \widehat{u}$ and $\lambda_\mp = \widehat{u} \mp \sqrt{3\widehat{h}(f - \widehat{h}\widehat{u}^2)}$, by which the system will be strictly hyperbolic if $\widehat{h} > 0$ and $(f - \widehat{h}\widehat{u}^2) > 0$.

Third order accuracy

Subsequently, in a similar way we construct the third order accuracy system in ε, which includes higher order nonlinear diffusivity and dispersive effects to the second order accuracy system.

$$\frac{\partial \widehat{h}}{\partial t} + \frac{\partial (\widehat{h}\widehat{u})}{\partial x} = 0 \tag{3.90a}$$

$$\frac{\partial (\widehat{h}\widehat{u})}{\partial t} + \frac{\partial f}{\partial x} = 0 \tag{3.90b}$$

$$\begin{aligned}\frac{\partial f}{\partial t} + \frac{\partial}{\partial x}\left[3\widehat{u}\left(f - \frac{2}{3}\widehat{h}\widehat{u}^2\right)\right] &= -3\varepsilon\frac{g}{2}^2\frac{\partial}{\partial x}\left(\widehat{h}^2\frac{\partial \widehat{h}}{\partial x}\right) - 3\varepsilon^2\frac{g}{2}^2\frac{\partial}{\partial x}\left(\widehat{h}^3\frac{\partial^2 \widehat{u}}{\partial x^2}\right) \\ &\quad - 3\varepsilon\frac{g}{2}\frac{\partial}{\partial x}\left[\frac{1}{\widehat{h}}\frac{\partial}{\partial x}\left(f\widehat{h}^2 - \widehat{h}^3\widehat{u}^2 - \frac{g}{2}\widehat{h}^4\right)\right] \\ &\quad - \frac{1}{\varepsilon}\left(f - \widehat{h}\widehat{u}^2 - \frac{g}{2}\widehat{h}^2\right)\end{aligned} \tag{3.90c}$$

3.4 Shock and rarefaction wave detector

3.4.1 Scalar case

For the scalar case, replacing $u_0 = u$ and $\widehat{w_1}^{(1)} = W$ for convenience, in the formal limit $\varepsilon \to 0$, the system (3.32) reads

$$\frac{\partial u}{\partial t} + F'(u)\frac{\partial u}{\partial x} = P(u) \tag{3.91a}$$

$$W = -\frac{1}{3}\frac{\partial u}{\partial x} \tag{3.91b}$$

Therefore, as ε goes to zero we have that if

$$\frac{\partial u}{\partial x} = 0 \to W = 0, \tag{3.92a}$$

$$\frac{\partial u}{\partial x} < 0 \to W > 0, \tag{3.92b}$$

$$\frac{\partial u}{\partial x} > 0 \to W < 0 \tag{3.92c}$$

Additionally, we could distinguish between shock and rarefaction waves, since

$$\begin{aligned} \frac{\partial u}{\partial x} &\to -\infty \quad W \to \infty \qquad \text{(shock wave)} \\ \frac{\partial u}{\partial x} &\to \infty \quad W \to -\infty \quad \text{(rarefaction wave)} \end{aligned}$$

The generic solutions for a nonlinear scalar balance law consist of one wave, that depending on the initial data will be either a shock or a rarefaction wave modified by the effects of the source term $P(u)$ with respect to the conservation law case.

Proposition 3.4.1. *In the formal limit $\varepsilon \to 0$, the system (3.32) yields the correct shock propagation which is independent of the source term.*

Proof. In order to prove that the third order moment system (3.32) yields the correct shock propagation and therefore it may act as an indicator to detect shock and rarefaction waves, consider a discontinuity located at $s(t)$ with $u(s(t^-), t) = -u(s(t^+), t)$ and $u(s(t^-), t) > 0$, such that its solution with evolve in a shock wave. The speed of the shock $\dot{s}(t)$ will be given by the Rankine-Hugoniot conditions [22]. Hence, from (3.91a) we can infer that for $0 < \varepsilon \ll 1$ the solution of $W(x,t)$ tends to a δ -function located at the point of the discontinuity $s(t)$. Scaling the variable x as

$$\eta = \frac{x - s(t)}{\varepsilon} \tag{3.93}$$

and introducing the scaled functions,

$$\widetilde{u}(\eta, t) = u(\varepsilon\eta + s(t), t) \tag{3.94a}$$

$$\widetilde{W}(\eta, t) = \varepsilon W(\varepsilon\eta + s(t), t) \tag{3.94b}$$

the system (3.32) will turn into

$$\varepsilon\frac{\partial \widetilde{u}}{\partial t} + (F'(\widetilde{u}) - \dot{s}(t))\frac{\partial \widetilde{u}}{\partial \eta} + \frac{\partial \widetilde{W}}{\partial \eta} = \varepsilon P(\widetilde{u}) \tag{3.95a}$$

$$\varepsilon\frac{\partial \widetilde{W}}{\partial t} + (F'(\widetilde{u}) - \dot{s}(t))\frac{\partial \widetilde{W}}{\partial \eta} + \frac{1}{3}\frac{\partial \widetilde{u}}{\partial \eta} = -\widetilde{W} + \frac{4}{15}\frac{\partial^2 \widetilde{W}}{\partial \eta^2} \tag{3.95b}$$

Again, taking the formal limit $\varepsilon \to 0$, the leading order of (3.95a) is given by

$$\frac{\partial \widetilde{W}}{\partial \eta} = (\dot{s}(t) - F'(\widetilde{u}))\frac{\partial \widetilde{u}}{\partial \eta} \tag{3.96}$$

Moreover by using equation (3.94b), equation (3.32a) can be written as

$$\frac{\partial u}{\partial t} + F'(u)\frac{\partial u}{\partial x} + \frac{1}{\varepsilon}\frac{\partial \widetilde{W}}{\partial \eta} = P(u) \tag{3.97}$$

since $\dfrac{\partial W}{\partial x} = \dfrac{1}{\varepsilon^2}\dfrac{\partial W}{\partial \eta}$. Now replacing (3.96) into (3.97), we will get

$$\frac{\partial u}{\partial t} + F'(u)\frac{\partial u}{\partial x} + \frac{1}{\varepsilon}(\dot{s}(t) - F'(\widetilde{u}))\frac{\partial \widetilde{u}}{\partial \eta} = P(u) \tag{3.98}$$

$$\frac{\partial u}{\partial t} + F'(u)\frac{\partial u}{\partial x} + \frac{1}{\varepsilon}(\dot{s}(t) - F'(u))\varepsilon\frac{\partial u}{\partial x} = P(u) \tag{3.99}$$

$$\frac{\partial u}{\partial t} + \dot{s}(t)\frac{\partial u}{\partial x} = P(u) \tag{3.100}$$

This demonstrates our claim. □

3.4.2 2×2 system

Similarly, for the 2×2 system replacing $\widehat{q} = q$, $\widehat{z} = z$ and $\widehat{w_2}^{(1)} = W$, in the formal limit $\varepsilon \to 0$ the system (3.82) will yield,

$$\frac{\partial q}{\partial t} + \frac{\partial z}{\partial x} = 0 \tag{3.101a}$$

$$\frac{\partial z}{\partial t} + \frac{\partial}{\partial x}\left(\frac{z^2}{q} + \kappa q^\gamma\right) = 0 \tag{3.101b}$$

$$W = \kappa(\gamma - 3)q^\gamma \frac{\partial}{\partial x}\left(\frac{z}{q}\right) \tag{3.101c}$$

Consequently, taking into account that $\kappa > 0$ and $q(x,t) > 0$ the limit behaviour of the variable $W(x,t)$ will be determined by the values of γ and $\dfrac{\partial}{\partial x}\left(\dfrac{z}{q}\right)$. For $1 < \gamma < 3$ the term $(\gamma - 3)$ will always be negative and therefore will have a similar case as in (3.92),

$$\frac{\partial}{\partial x}\left(\frac{z}{q}\right) = 0 \rightarrow W = 0, \qquad (3.102a) \qquad \frac{\partial}{\partial x}\left(\frac{z}{q}\right) < 0 \rightarrow W > 0, \qquad (3.102b)$$

$$\frac{\partial}{\partial x}\left(\frac{z}{q}\right) > 0 \rightarrow W < 0 \qquad (3.102c)$$

In the case where the balance laws system corresponds to the study of a fluid's movement (gas or liquid), such as the *isentropic gas Euler equations* and the *shallow water equations*, the flux of the mass variable $q(x,t)$ will be given by the product of the velocity of the fluid times the mass density $z(x,t) = u(x,t)q(x,t)$. Thus the ratio $\frac{z}{q}$ will be equal to $u(x,t)$ the velocity, and (3.102) will behave as (3.92) such that is possible again to distinguish between shock and rarefaction waves.

Proposition 3.4.2. *For the case $z(x,t) = q(x,t)u(x,t)$ the third order accuracy system (3.82) will yield (formally) the correct shock propagation in the limit $\varepsilon \to 0$.*

Proof. A similar analysis to the scalar case can be performed for the 2×2 system, in which we consider a two-shock solution for the third order accuracy system (3.82) in the limit of $\varepsilon \to 0$ by considering again as initial condition a discontinuity located at $s(t)$ with $q(x,0) = q_0$ a constant value and $u(s(t^-),t) = -u(s(t^+),t)$ with $u(s(t^-),t) > 0$. After scaling x as in (3.93), the scaled functions will read,

$$\widetilde{q}(\eta,t) = q(\varepsilon\eta + s(t),t) \qquad (3.103a)$$

$$\widetilde{z}(\eta,t) = z(\varepsilon\eta + s(t),t) \qquad (3.103b)$$

$$\widetilde{W}(\eta,t) = \varepsilon W(\varepsilon\eta + s(t),t) \qquad (3.103c)$$

into (3.82) we will have,

$$\varepsilon\frac{\partial\widetilde{q}}{\partial t} + \left[\frac{\widetilde{z}}{\widetilde{q}} - \dot{s}(t)\right]\frac{\partial\widetilde{q}}{\partial\eta} + \widetilde{q}\frac{\partial}{\partial\eta}\left(\frac{\widetilde{z}}{\widetilde{q}}\right) = 0 \qquad (3.104a)$$

$$\varepsilon\frac{\partial\widetilde{z}}{\partial t} + \left[\frac{2\widetilde{z}}{\widetilde{q}} - \dot{s}(t)\right]\frac{\partial\widetilde{z}}{\partial\eta} + \left[\kappa\gamma\widetilde{q}^{\gamma-1} - \frac{\widetilde{z}^2}{\widetilde{q}^2}\right]\frac{\partial\widetilde{q}}{\partial\eta} + \frac{\partial\widetilde{W}}{\partial\eta} = \varepsilon\nu\frac{\partial\widetilde{q}}{\partial\eta} \qquad (3.104b)$$

$$\varepsilon\frac{\partial\widetilde{W}}{\partial t}+\left[\frac{\widetilde{z}}{\widetilde{q}}-\dot{s}(t)\right]\frac{\partial\widetilde{W}}{\partial\eta}+\left[3\widetilde{W}-\kappa(\gamma-3)\widetilde{q}^{\gamma}\right]\frac{\partial}{\partial\eta}\left(\frac{\widetilde{z}}{\widetilde{q}}\right)=$$
$$-3\kappa^2\gamma\frac{\partial}{\partial\eta}\left(\widetilde{q}^{2\gamma-2}\frac{\partial\widetilde{q}}{\partial\eta}\right)-\frac{3}{\varepsilon}\kappa\frac{\partial}{\partial\eta}\left(\widetilde{q}^{\gamma-1}\frac{\partial^2\widetilde{W}}{\partial\eta^2}+\gamma\widetilde{q}^{\gamma-2}\frac{\partial\widetilde{q}}{\partial\eta}\frac{\partial\widetilde{W}}{\partial\eta}\right) \tag{3.104c}$$
$$-3\kappa\gamma\frac{\partial}{\partial\eta}\left[\widetilde{q}^{2\gamma-1}\left(\frac{\partial^2}{\partial\eta^2}\left(\frac{\widetilde{z}}{\widetilde{q}}\right)+2(\gamma-2)\frac{1}{\widetilde{q}}\frac{\partial\widetilde{q}}{\partial\eta}\frac{\partial}{\partial\eta}\left(\frac{\widetilde{z}}{\widetilde{q}}\right)\right)\right]-\widetilde{W}$$

and taking again the limit case of ε going to zero, the leading orders will yield,

$$\frac{\partial}{\partial\eta}\left(\frac{\widetilde{z}}{\widetilde{q}}\right)=\frac{1}{\widetilde{q}}\left[\dot{s}(t)-\frac{\widetilde{z}}{\widetilde{q}}\right]\frac{\partial\widetilde{q}}{\partial\eta} \tag{3.105a}$$
$$\frac{\partial\widetilde{W}}{\partial\eta}=\left[\dot{s}(t)-\frac{\widetilde{z}}{\widetilde{q}}\right]\widetilde{q}\frac{\partial}{\partial\eta}\left(\frac{\widetilde{z}}{\widetilde{q}}\right)-\kappa\gamma\widetilde{q}^{\gamma-1}\frac{\partial\widetilde{q}}{\partial\eta} \tag{3.105b}$$

We rewrite the second equation of (3.82) using only the scaled function for $W(x,t)$, which will replace $\dfrac{\partial W}{\partial x}=\dfrac{1}{\varepsilon^2}\dfrac{\partial\widetilde{W}}{\partial\eta}$ and the new limiting expression (3.105b),

$$\frac{\partial z}{\partial t}+\frac{\partial}{\partial x}\left(\frac{z^2}{q}+\kappa q^{\gamma}\right)+\frac{1}{\varepsilon}\left[\left(\dot{s}(t)-\frac{\widetilde{z}}{\widetilde{q}}\right)\widetilde{q}\frac{\partial}{\partial\eta}\left(\frac{\widetilde{z}}{\widetilde{q}}\right)-\kappa\gamma\widetilde{q}^{\gamma-1}\frac{\partial\widetilde{q}}{\partial\eta}\right]=\nu q \tag{3.106}$$
$$\frac{\partial}{\partial t}\left(\frac{z}{q}\right)+\frac{z}{q^2}\left(\frac{\partial q}{\partial t}+\frac{\partial z}{\partial x}\right)+\dot{s}(t)\frac{\partial}{\partial x}\left(\frac{z}{q}\right)=\nu q \tag{3.107}$$
$$\frac{\partial}{\partial t}\left(\frac{z}{q}\right)+\dot{s}(t)\frac{\partial}{\partial x}\left(\frac{z}{q}\right)=\nu q \tag{3.108}$$

Hence, our claim follows. □

Remark 3.4.1. *In the case of $\gamma=3$ the $W(x,t)$ will always tend to zero as $\varepsilon\to 0$ independently of the values of the gradient of the $z(x,t)$, for this reason this type of problem will not count with $W(x,t)$ as a shock, rarefaction wave detector.*

Remark 3.4.2. *The moment systems (3.32) and (3.82) yield only in the formal sense the correct shock propagation, since it has not been proven rigorously that in the limit $\varepsilon\to 0$ a solution of the moment systems exist.*

3.5 Summary

Starting from an artificial Boltzmann-like equation (previously defined in accordance with the nonlinear balance law of interest), it is possible to use *the order of magnitude method* to

recover the corresponding infinite kinetic-induced moment system containing higher orders terms coming from the balance law itself.

At each order of magnitude η, one can construct a closure relation for the respective infinite moment system, by expanding asymptotically the highest order moments and subsequently finding and balancing the leading order terms.

The previous closed system might contain a few terms that are not of our interest, thus it can be reduced to a desired order of accuracy η_0, in which the part of the flux $w_1^{(1)}$ is known within the order $O(\varepsilon^{\eta_0})$.

The *0-th order accuracy* system always attains the original nonlinear balance law and the *1st order accuracy* includes a diffusive term with a coefficient of the order $O(\varepsilon)$. Higher orders of accuracy introduce the coupling between the original balance law and higher order variables, produced via the smallness parameter ε.

For the scalar case, we focus on the *3rd order accuracy* system and for the 2×2 case, on the *2nd order accuracy* one. This is given since our interest lies (for the moment) on the effects coming from the $\varepsilon-$coupling with the next higher order moment and its corresponding diffusive correction. Both cases yield (formally) the correct shock propagation.

In the formal limit $\varepsilon \to 0$, the two previous systems tend to the original nonlinear balance law together with the variable $W(x,t) = \widehat{w}^{(1)}$, that for the Burgers and shallow water examples approximates to the inverse of the gradient, making it easy to identify where special solutions like rarefaction and shock waves take place.

4. Numerical Experiments

As mentioned before, we will focus on two model problems: the one dimensional Burgers equation for the scalar case and the shallow water equations for the 2×2 system case. For them and their corresponding closed moment systems discretization, we will use a finite differences scheme and a finite volumes one respectively, according to the numerical methods for conservation laws problems introduced in section 2.1.1. In the first section, the choice of grid will be static, i.e., it will not change in time, this will allow us to compare the model problems with their kinetic-induced moment systems and to prove that indeed as expected, the new variable $W(x,t)$ works like a shock/rarefaction detector. The second section uses an adaptive mesh, for which the refinement parameter is then given by $W(x,t)$ in order to discretize the original equations.

4.1 Static grid

4.1.1 Case 1: 1D Inviscid Burgers equation

According to the order of magnitude method, the third order accuracy moment system for the inviscid Burgers equation (3.40) with $u_0 = u$ and $\widehat{w_1}^{(1)} = W$, yields the following kinetic-induced moment system

$$\frac{\partial u}{\partial t} + u\frac{\partial u}{\partial x} + \varepsilon\frac{\partial W}{\partial x} = 0 \tag{4.1a}$$

$$\frac{\partial W}{\partial t} + u\frac{\partial W}{\partial x} + \frac{1}{3\varepsilon}\frac{\partial u}{\partial x} = -\frac{1}{\varepsilon}W + \frac{4\varepsilon}{15}\frac{\partial^2 W}{\partial x^2} \tag{4.1b}$$

where there is a linear coupling depending on ε, a diffusion coefficient ($D_b = 4\varepsilon/15$) of the order $O(\varepsilon)$ and a source term of the order $O(\varepsilon^{-1})$. The corresponding homogeneous problem with $Q = [u \quad W]^T$ reads,

$$Q_t + \begin{bmatrix} u & \varepsilon \\ \dfrac{1}{3\varepsilon} & u \end{bmatrix} Q_x = \begin{bmatrix} 0 \\ 0 \end{bmatrix} \tag{4.2}$$

which is strictly hyperbolic with two real and distinct eigenvalues $\lambda_{\mp} = u \mp \frac{1}{\sqrt{3}}$ that do not depend on ε.

The system (4.1) is discretized by using finite differences schemes with splitting of the source term (2.49), since the last one can be solved exactly. The first part of equation (4.1a) is just Burgers equation, which can be approximated using the conservative scheme (2.41) evaluated at the grid points with $Q_i^n = u_m^n$, $F_{i+\frac{1}{2}} = f_{ru}$ and $F_{i-\frac{1}{2}} = f_{lu}$. The second part follows a backward difference (2.32b) for the space derivative of $W(x,t)$,

$$u_m^{n+1} = u_m^n - \frac{\Delta t}{\Delta x}(f_{ru} - f_{lu}) - \frac{\Delta t}{\Delta x}\varepsilon(W_m^n - W_{m-1}^n). \tag{4.3}$$

The fluxes around u_m^n are defined by the *nonlinear upwind scheme* due to Roe, which is a consistent, first order accurate numerical solution for the discretization of the nonlinear flux term, it reads

$$F_{i+\frac{1}{2}}^n = \frac{1}{2}(f(Q_i^n) + f(Q_{i+1}^n)) - \left|\frac{f(Q_i^n) - f(Q_{i+1}^n)}{Q_i^n - Q_{i+1}^n}\right| \frac{(Q_{i+1}^n - Q_i^n)}{2} \tag{4.4}$$

we can then write,

$$f_{ru} = \frac{1}{4}(u_{m+1}^n u_{m+1}^n + u_m^n u_m^n) - \frac{1}{4}|u_{m+1}^n + u_m^n|(u_{m+1}^n - u_m^n) \tag{4.5a}$$

$$f_{lu} = \frac{1}{4}(u_{m-1}^n u_{m-1}^n + u_m^n u_m^n) - \frac{1}{4}|u_{m-1}^n + u_m^n|(u_m^n - u_{m-1}^n) \tag{4.5b}$$

Subsequent, the first part of the second equation (4.1b) is approximated again by (2.41) with $Q_i^n = W_m^n$, $F_{i+\frac{1}{2}} = f_{rw}$ and $F_{i-\frac{1}{2}} = f_{lw}$. For the second part, we use a backward difference (2.32b) for the space derivative of $u(x,t)$ and the diffusion term is done by a three-point stencil, the discretization yields

$$\widehat{W}_m^{n+1} = W_m^n - \frac{\Delta t}{\Delta x}(f_{rw} - f_{lw}) - \frac{\Delta t}{\Delta x}\frac{1}{3\varepsilon}(u_m^n - u_{m-1}^n) + \frac{\Delta t}{\Delta x}\frac{4\varepsilon}{15} \cdot \Lambda \tag{4.6}$$

$$W_i^{n+1} = \widehat{W}_m^{n+1} \cdot e^{-\Delta t/\varepsilon} \tag{4.7}$$

with the convection of W_m^n discretized by a first order accurate standard upwind scheme,

$$f_{rw} = \frac{1}{2}u_m^n(w_m^n + w_{m+1}^n) - \frac{1}{2}|u_m^n|(w_{m+1}^n - w_m^n) \tag{4.8a}$$

$$f_{lw} = \frac{1}{2}u_m^n(w_m^n + w_{m-1}^n) - \frac{1}{2}|u_m^n|(w_m^n - w_{m-1}^n) \tag{4.8b}$$

the diffusion term given by,

$$\Lambda = \frac{(W_{m+1}^n - 2W_m^n + W_{m-1}^n)}{\Delta x} \tag{4.9}$$

and where (4.7) comes from solving exactly the split source term $\dfrac{dW}{dt} = -\dfrac{1}{\varepsilon}W$.

In the case of first order hyperbolic PDEs, it is necessary to ensure stability, thus the initial time step Δt must fulfil the CFL-condition (2.47). For second order PDEs, in order to keep stability the restriction is more severe and the time step must satisfy (2.36). Therefore, as $\varepsilon \to 0$ the upper boundary for Δt will grow notably thanks to the diffusion coefficient $\nu = 4\varepsilon/15$, which depends on it. For both conditions we use $CFL = 0.9 * CFL_{max}$ and define the coarsest time step as

$$\Delta t = min\left(0.9 * \frac{\Delta x}{S_{max}^n}, 0.45 * \left[\frac{15(\Delta x^2)}{4\varepsilon}\right]\right) \tag{4.10}$$

where $S_{max}^n = \max_i \left\{ \max_p \mid \lambda_{p,i}^n \mid \right\}$, with $p = 2$ the number of eigenvalues.

For comparison reasons, the inviscid Burgers equation (2.17) is approximated by using as before the scheme (2.41) with the discrete fluxes given by (4.4), it will only need to satisfy the advection CFL-condition (2.35).

Results

- ***l2-error***

  The evolution in time of the 3rd order accuracy moment system using $\varepsilon = 0.001$ is contrasted with that of the approximated and exact solution of the inviscid Burgers equation in the domain $[-2, 8]$. The grid is giving by $M = 800$ corresponding to a $\Delta x = 0.0125$, which evolves until $t = 4$.

Initial conditions correspond to a shock developing Riemann problem with the discontinuity located at $x = 0$,

$$u(x,0) = \begin{cases} 2 & \text{if } x < 0 \\ 1 & \text{if } x \geq 0 \end{cases} \tag{4.11a}$$

$$W(x,0) = 0, \quad \text{only for (4.1b).} \tag{4.11b}$$

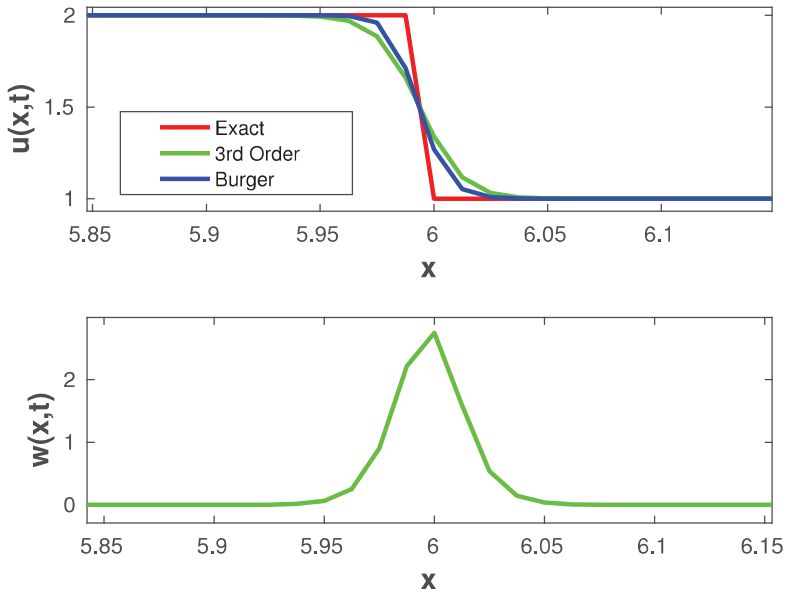

Figure 4.1: $\mathbf{u(x,t)}$, $\mathbf{W(x,t)}$ **at** $\mathbf{t = 4}$

At a first glance, Fig. 4.1 shows us the expected diffusion coming from the numerical methods and the accuracy of the variable $W(x,t)$ to act as a shock detector when ε is very small, both approximations perform quite similar, but yet the 3rd order system injects some extra diffusivity. The previously detected differences between solutions are quantified by the following discrete *l2-norm*, where Q_i^n is used to denote the approximated solution and q_i^n the exact one.

$$l_2^n = \sqrt{\frac{1}{M+1}\sum_{i=0}^{M} \mid Q_i^n - q_i^n \mid^2} \tag{4.12}$$

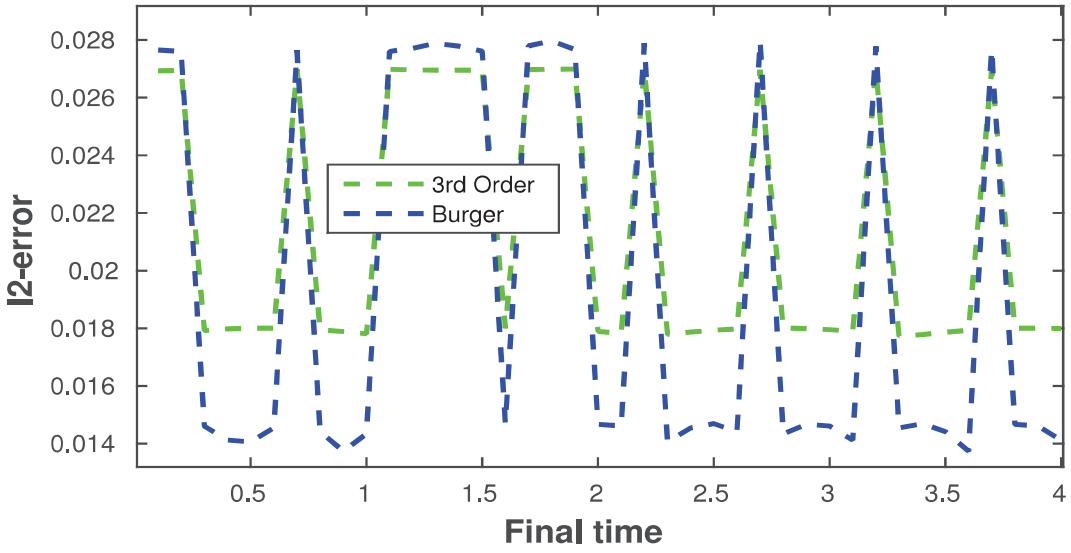

Figure 4.2: ***l2-error* time evolution**

As anticipated, Fig. 4.2 proves that for $\varepsilon = 0.001$ the differences between *l2-errors* as time advances is quite small. The 3rd order approximation error will always lie beneath the largest Burgers error value and above the smallest one, having a quite stable behaviour in time and with a rather close mean value, around 2.1×10^{-2} which of an order considered as a good performance.

As for the behaviour of the $l2-error$ corresponding to the 3rd order moment system with respect to the smallness parameter ε, we perform several computations by using five different values of it,

$$\boldsymbol{\varepsilon} = \quad \{0.0002,\ 0.0005,\ 0.001,\ 0.003,\ 0.010\} \tag{4.13}$$

and five different grid sizes Δx until $t = 4$,

Δx	
dx1	0.0077
dx2	0.01
dx3	0.0125
dx4	0.02
dx5	0.04

Table 4.1: Δx values for the 3rd order moment system discretization.

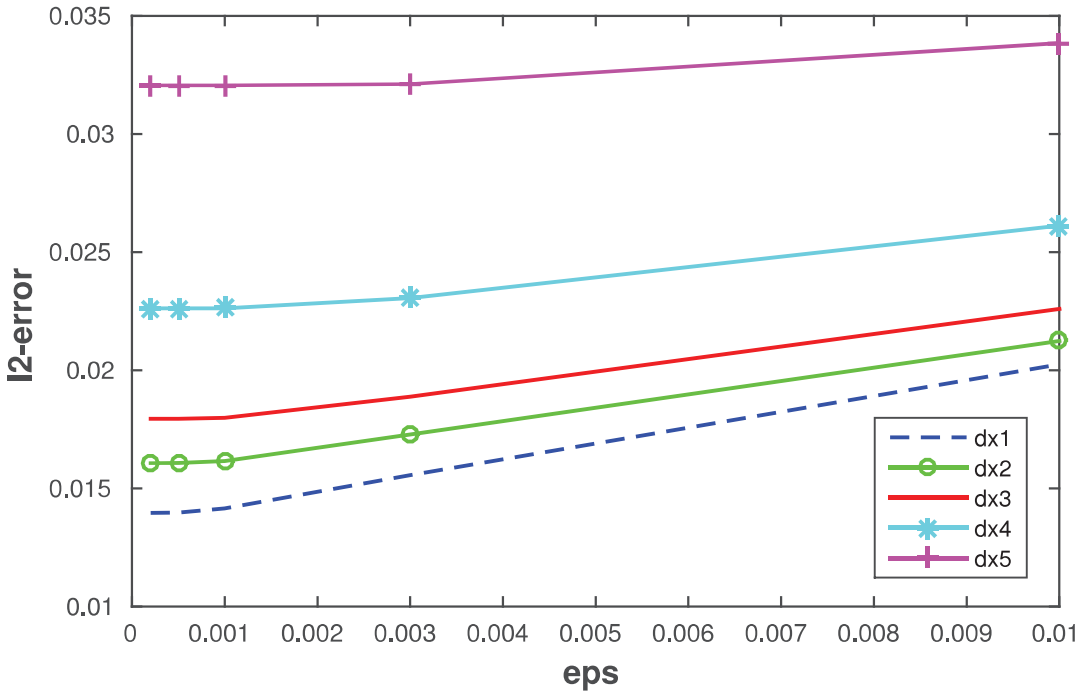

Figure 4.3: ***l2-error* performance of the 3rd order moment system w.r.t. ε and Δx**

As known, the kinetic system approximation grows apart from the inviscid Burgers equation as ε grows since its value increment the amount of diffusion on it, therefore for larger values of ε we will see that according with Fig. 4.3, the results on the *l2-error* time evolution (Fig. 4.2) will not be as similar as for $\varepsilon = 0.001$ and instead the one

corresponding to the 3rd order system will start increasing. There is nonetheless, a stable increment of the error for each space step and no evidence of the results blowing up for very small or large values of ε. Furthermore, again the errors evolution is of order 10^{-2}, which is satisfying.

- **Time step Δt**

  The magnitude of the time step for both numerical schemes depends as explained before from the stability conditions, which variate according with the size of the grid. The advective condition (2.47) coming from the inviscid Burgers approximation for the different grid sizes dx_i, yield the following Δt

Δx		Δt
dx1	0.0077	0.0035
dx2	0.01	0.0045
dx3	0.0125	0.0056
dx4	0.02	0.0090
dx5	0.04	0.0180

Table 4.2: Δt values for the inviscid Burgers equation according with the stability advective condition (2.47).

Parallel to it, the advective condition coming from the 3rd order system produces the following time steps in Table 4.3, that for the smallest four dx_i are of the order 10^{-3}. Moreover, the diffusive condition (2.36) affecting the 3rd order system depends also on ε, thus we need to track the evolution of Δt for changes in the step size as for changes in the smallness parameter (Fig. 4.4).

Δx		Δt
dx1	0.0077	0.0026
dx2	0.01	0.0035
dx3	0.0125	0.0044
dx4	0.02	0.0070
dx5	0.04	0.0140

Table 4.3: Δt values for the 3rd order moment system according with the stability advective condition (2.47).

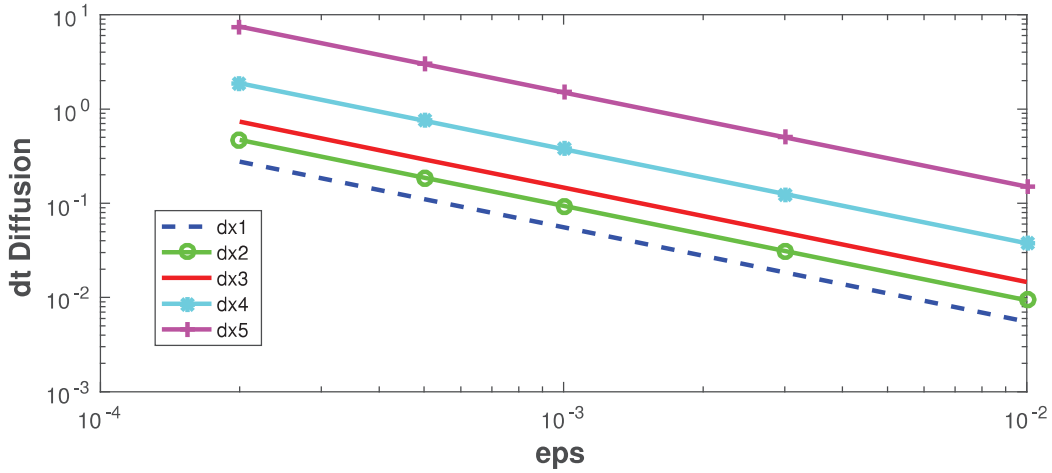

Figure 4.4: **Δt according with the diffusive condition (2.36) w.r.t different ε and Δx**

Presented in logarithmic scale, Fig. 4.4 shows that the increase of Δx will lead to a similar one of the time step, while the increase in ε will lead to a small decrease (depending on the value of Δx). However, for every Δx the time step coming from advection will be more restrictive than the diffusion one independently of the ε values, therefore the first one will be the one chosen by the numerical method.

At the same time, we do not compare the computational times, since we know that Burgers will always be faster than the 3rd order system considering that the first solves only one equation instead of two.

4.1.2 Case 2: 1D Inviscid shallow water equations

Unlike the Burgers equation case, for the shallow water equations it is enough to use the second order accuracy system (3.89) in order to have $W(x,t)$ acting as a shock/rarefaction detector at $\varepsilon \to 0$, since it already includes an extra equation for $\widehat{w_2}^{(1)}$ with a correction term which contains a diffusive part. Writing $\widehat{h} = h$, $\widehat{hu} = hu$ and $\widehat{w_2}^{(1)} = W$ we get

$$\frac{\partial h}{\partial t} + \frac{\partial (hu)}{\partial x} = 0 \tag{4.14a}$$

$$\frac{\partial (hu)}{\partial t} + \frac{\partial}{\partial x}\left(hu^2 + \frac{g}{2}h^2\right) + \varepsilon \frac{\partial W}{\partial x} = 0 \tag{4.14b}$$

$$\frac{\partial W}{\partial t} + u\frac{\partial W}{\partial x} + 3W\frac{\partial u}{\partial x} + \frac{g}{2\varepsilon}h^2\frac{\partial u}{\partial x} = -\frac{3}{2}g^2\left[h^2\frac{\partial^2 h}{\partial x^2} + 2h\left(\frac{\partial h}{\partial x}\right)^2\right] - \frac{1}{\varepsilon}W \tag{4.14c}$$

With $Q = [h \quad hu \quad f]^T$ and $f = \varepsilon W + hu^2 + \frac{g}{2}h^2$ the previous system in balance form reads

$$Q_t + \begin{bmatrix} 0 & 1 & 0 \\ 0 & 0 & 1 \\ 4u^3 - 3\frac{fu}{h} & 3\frac{f}{h} - 6u^2 & 3u \end{bmatrix} Q_x = \begin{bmatrix} 0 \\ 0 \\ -\frac{3}{2}\varepsilon g^2\left[h^2\frac{\partial^2 h}{\partial x^2} + 2h\left(\frac{\partial h}{\partial x}\right)^2\right] - \frac{1}{\varepsilon}\left(f - \widehat{h}\widehat{u}^2 - \frac{g}{2}\widehat{h}^2\right) \end{bmatrix} \tag{4.15}$$

where the diffusion part is nonlinear and of the order $O(\varepsilon)$ with a coefficient ($D_{sw} = 3\varepsilon g^2/2$), additionally the source term has an order of $O(\varepsilon^{-1})$. The conservative part of the system is equipped with three eigenvalues $\lambda_0 = u$ and $\lambda_\mp = u \mp \sqrt{3h(f - hu^2)}$, by which the system will be strictly hyperbolic if $h > 0$ and $(f - hu^2) > 0$.

The homogeneous part of (4.15) is discretized according to the finite volumes method (2.39) with a Godunov numerical flux (2.45), it reads

$$Q_i^{n+1} = Q_i^n - \frac{\Delta t}{\Delta x}\left[A^+ \Delta Q_{i-\frac{1}{2}} + A^- \Delta Q_{i+\frac{1}{2}}\right] \tag{4.16}$$

the fluctuations at cell interfaces are given by $A^{\mp}\Delta Q_{i-\frac{1}{2}}$, which stand for the net effect of all left-going and right-going waves from $x_{i-\frac{1}{2}}$ respectively and are define in the form,

$$A^- \Delta Q_{i-\frac{1}{2}} = F^n_{i-\frac{1}{2}} - f(Q_{i-1}) \tag{4.17}$$

$$A^+ \Delta Q_{i-\frac{1}{2}} = f(Q_i) - F^n_{i-\frac{1}{2}} \tag{4.18}$$

with $f(Q_i)$ the system flux evaluated at the specified point. The approximation of the fluctuations is done via the first order accurate Roe linearisation (2.1.2) and the Harten-Hyman entropy fix is used in case of sonic entropies. For details see [22]. The inhomogeneous part is discretized by applying a fractional-step method (2.49) and solving separately the problem,

$$Q_{\mathrm{t}} = \begin{pmatrix} 0 \\ 0 \\ -\frac{3}{2}\varepsilon g^2 \left[h^2 \frac{\partial^2 h}{\partial x^2} + 2h\left(\frac{\partial h}{\partial x}\right)^2\right] - \frac{1}{\varepsilon}\left(f - \widehat{h}\widehat{u}^2 - \frac{g}{2}\widehat{h}^2\right) \end{pmatrix}. \tag{4.19}$$

We use an explicit method with a first order accurate forward difference (2.31a) for the time derivative at t^n and a second order accurate central finite difference (2.33b) for the space derivatives at position x_i, where Q_i^* is the solution of the homogeneous system at each time step.

$$Q_i^{n+1} = Q_i^* + \Delta t(\gamma(Q_i^*)) \tag{4.20}$$

$$\frac{\partial Q}{\partial x} = \frac{Q_{i+1} - Q_{i-1}}{2\Delta x} \tag{4.21}$$

$$\frac{\partial^2 Q}{\partial x^2} = \frac{Q_{i+1} - 2Q_i + Q_{i-1}}{(\Delta x)^2} \tag{4.22}$$

We need to satisfy both stability conditions (2.47) and (2.36), therefore

$$\Delta t = min\left(0.9 * \frac{\Delta x_1}{S^n_{max}}, 0.45 * \left[\frac{2(\Delta x^2)}{3\varepsilon g^2}\right]\right) \tag{4.23}$$

where $S^n_{max} = \max_i \left\{ \max_p \mid \lambda^n_{p,i} \mid \right\}$, with $p = 3$ the number of eigenvalues. For the 1-D homogeneous shallow water system (3.86a) the same kind of discretization as for the homogeneous part of (4.15), which will just need the CFL-condition for advection (2.47).

Results

- ***l2-error***

  We compare the evolution in time of the 2nd order accuracy moment system ($\varepsilon = 0.001$) with the homogeneous shallow water equations in the domain $[-10, 10]$ using a static grid of $M = 1600$ and $\Delta x = 0.0125$ until $t = 1.8$. The initial conditions correspond to the dam break example, where a shock and rarefaction wave will form.

$$h(x,0) = \begin{cases} 2 & \text{if } x < 0 \\ 1 & \text{if } x \geq 0 \end{cases} \qquad (4.24a)$$

$$u(x,0) = 0, \qquad (4.24b)$$

$$W(x,0) = 0, \quad \text{only for (4.14c).} \qquad (4.24c)$$

  The solution given by the moment system is very close to the real shallow water approximation (Fig. 4.5), yet as could be expected it will add some extra diffusion to the numerical method coming from the extra equation which depends on the values of ε. As for the new variable $W(x,t)$, we can see that indeed for a very small ε it performs as a shock and rarefaction wave detector. In Figs. (4.6), (4.7) we can observe closely the diffusive effect for the rarefaction and the shock wave, in the first case given the smoothness of the wave the effect is milder while in the last case considering the sharpness of the solution we will see a higher impact.

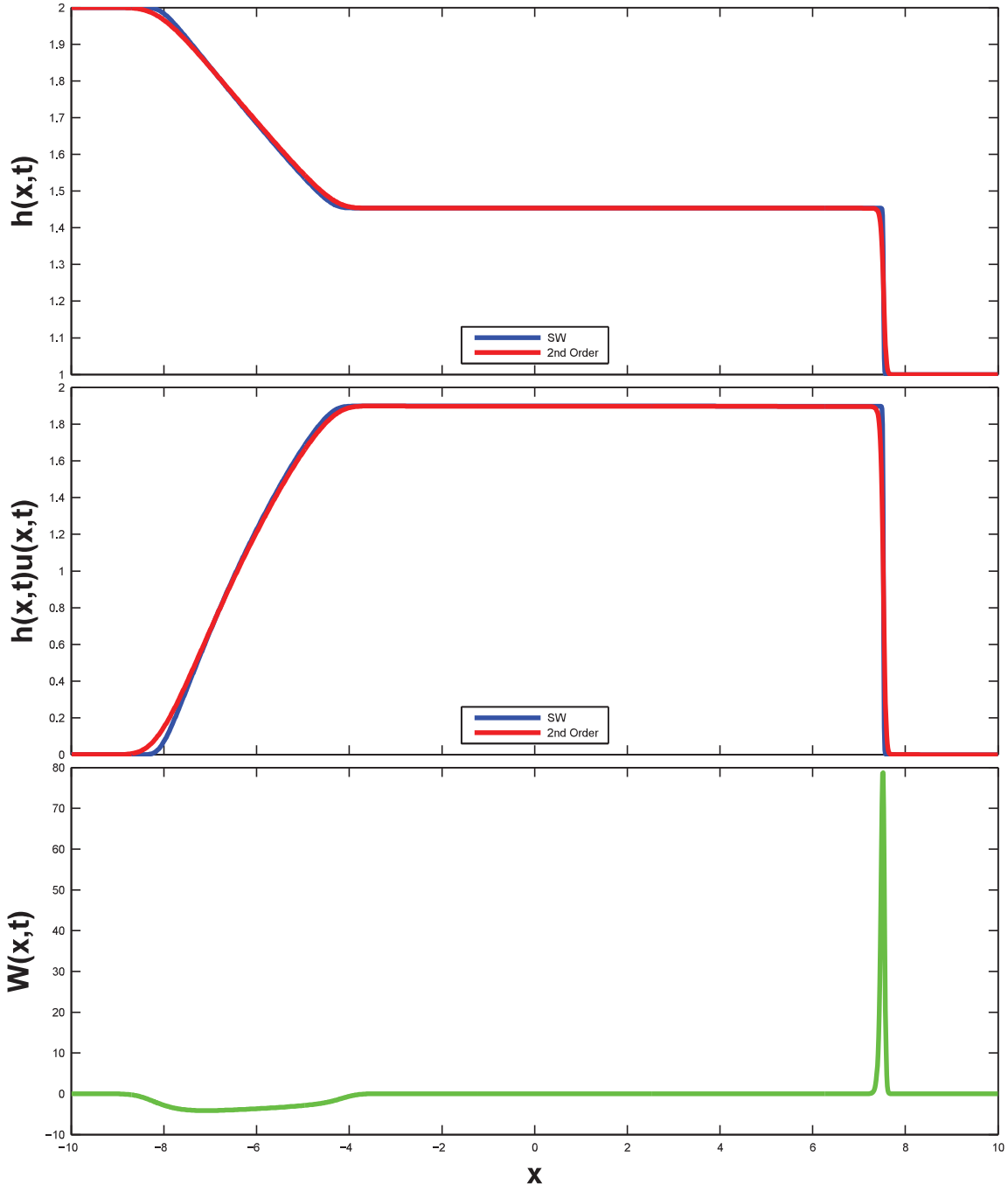

Figure 4.5: $\mathbf{h(x,t)}$, $\mathbf{h(x,t)u(x,t)}$, $\mathbf{W(x,t)}$ **at** $t = 1.8$

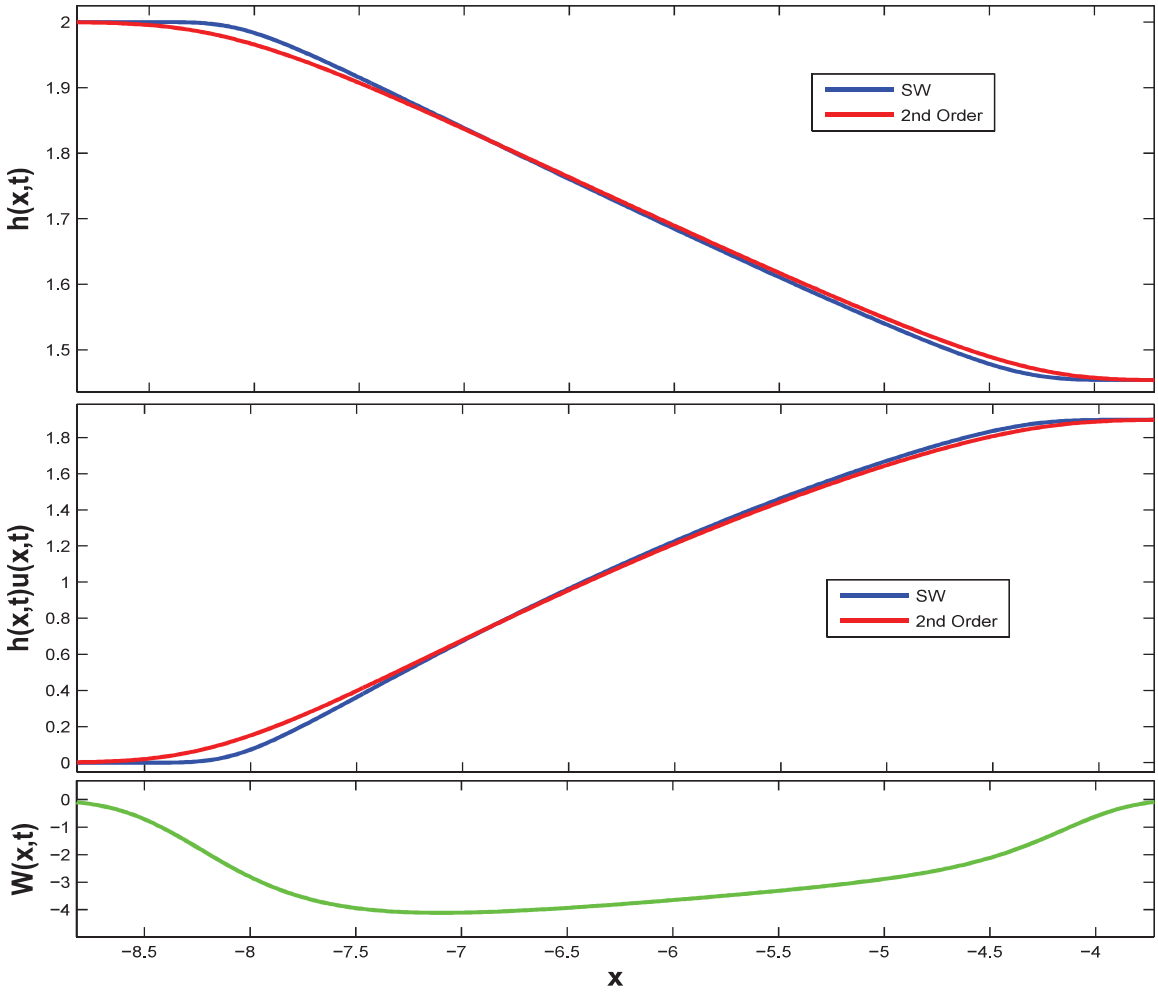

Figure 4.6: **Rarefaction wave at** $t = 1.8$

The measure of the solutions difference presented above is done via the *l2- discrete norm*, which for a two unknowns system yield

$$l_2^n = \sqrt{\frac{1}{M+1}\sum_{m=1}^{M}\left|\sqrt{\sum_{i=1}^{2} \mid Q_{m,i}^n - q_{m,i}^n \mid^2}\right|^2} \tag{4.25}$$

$Q_{m,i}^n$ and $q_{m,i}^n$ denotes the approximation of the moment system and the shallow water equations respectively, with *m: the quantity of unknowns.*

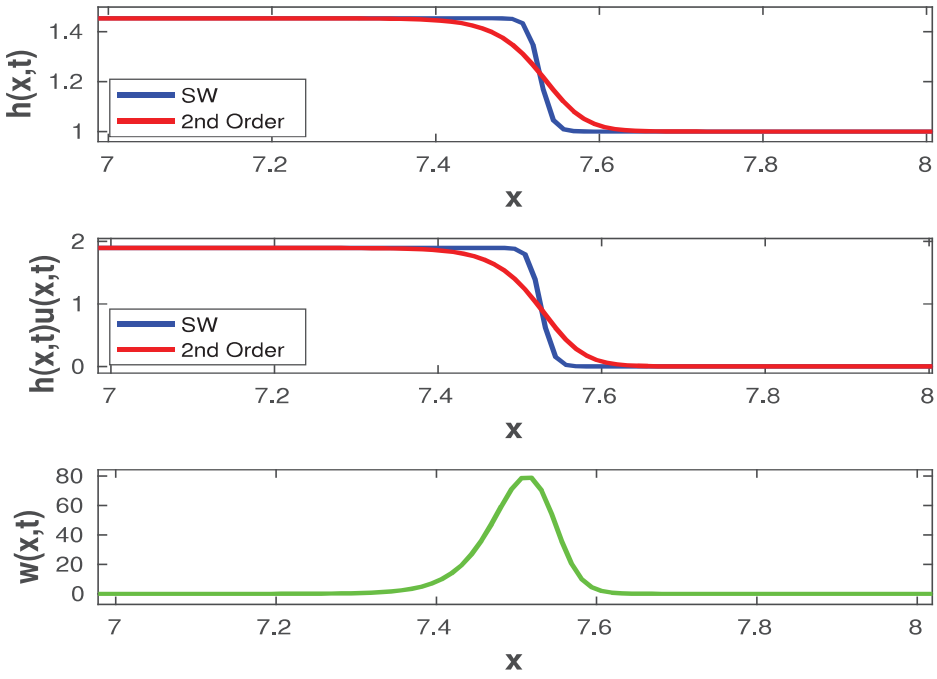

Figure 4.7: **Shock wave at** $t = 1.8$

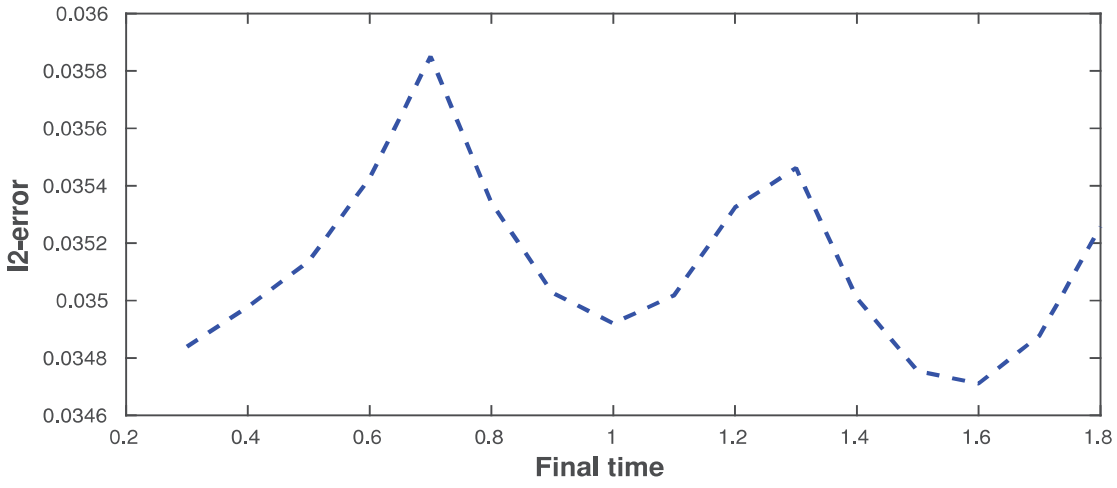

Figure 4.8: ***l2- error* time evolution**

The initial peak observed in Fig. 4.8 around $t = 0.7$ is considered of small relevance giving its magnitude, since as time evolves it tends to stabilize around the point 0.035 which can be considered a good result. Giving that the main contribution to the error comes from the extra diffusion added by the moment system, we measure the evolution of the *l2-error* for five different values of the smallness parameter ε,

$$\varepsilon = \quad \{0.0002,\ 0.0005,\ 0.0008,\ 0.001,\ 0.003\} \tag{4.26}$$

and five different grid sizes Δx until $t = 1.8$,

Δx	
dx1	0.0077
dx2	0.01
dx3	0.0125
dx4	0.02
dx5	0.04

Table 4.4: **Δx** values for the 3rd order moment system discretization.

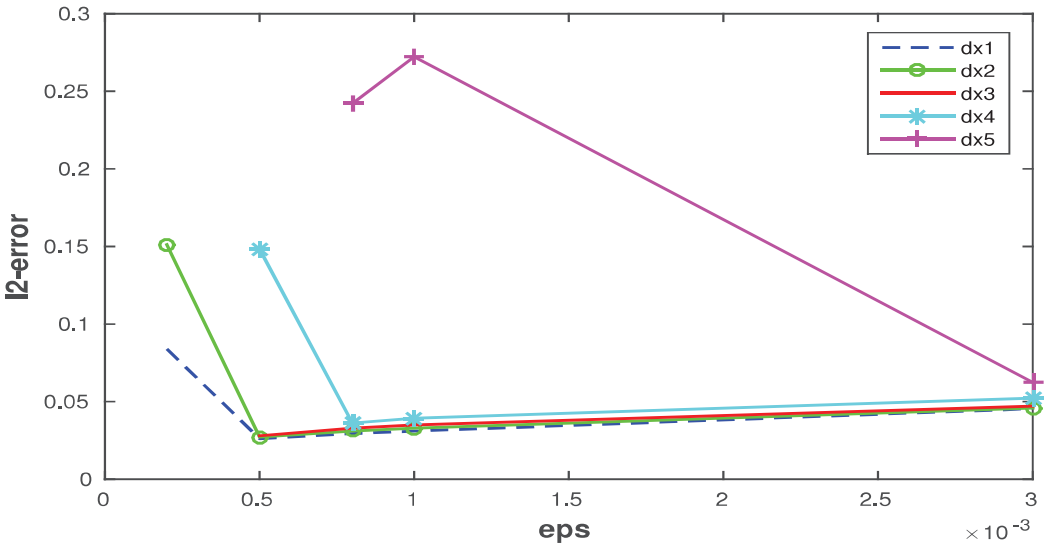

Figure 4.9: ***l2-error* performance w.r.t ε and Δx**

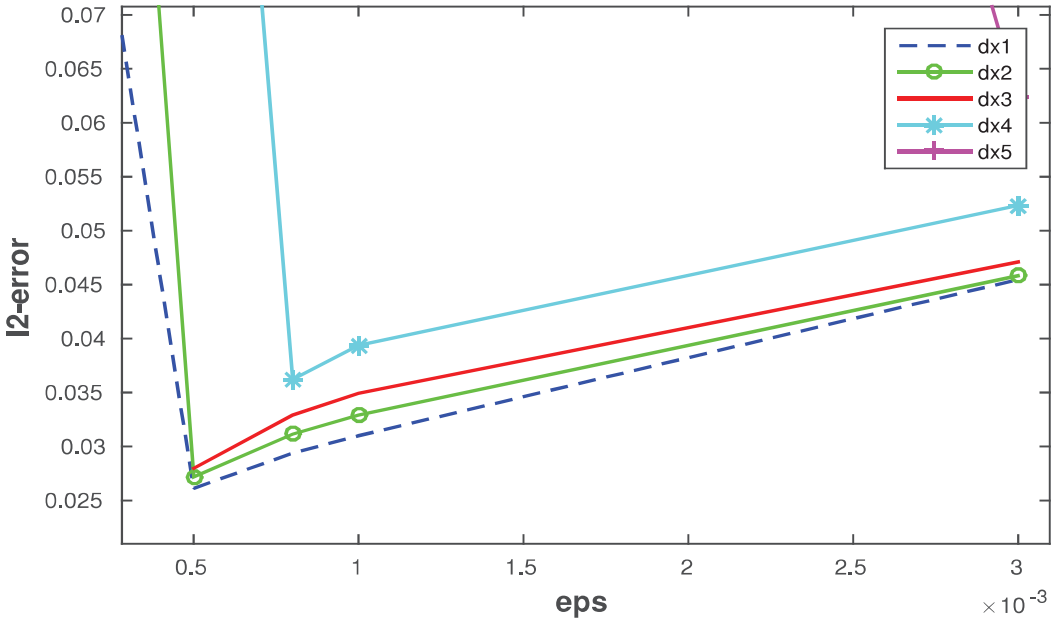

Figure 4.10: ***l2-error* performance w.r.t ε and Δx**

Fig. 4.9 shows that for each value of Δx there is a lower bound in ε which the numerical method can not handle any more making the error to jump. From that point onwards as ε moves away from zero the error will start to increase gradually as one would expect it. In the case of $dx5$, the space step has reach an upper bound for which only bigger values of the smallness parameter are admitted by the numerical method. Fig. 4.10 shows a closer look of the magnitude of the error according with the increase of ε.

- **Time step Δt**

  Coming from the stability condition for advection (2.47), in the case of the homogeneous shallow water system, the corresponding time steps for the different values of Δx used previously read

Δx		Δt
dx1	0.0077	0.0014
dx2	0.01	0.0018
dx3	0.0125	0.0022
dx4	0.02	0.0035
dx5	0.04	0.0071

Table 4.5: Δt values for the homogeneous shallow water equations according with the stability advective condition (2.47).

Since it must approximates only two equations instead of three, it will always perform faster than the moment system. In the case of the second order moment system, from advection we get

Δx		Δt
dx1	0.0077	0.0012
dx2	0.01	0.0015
dx3	0.0125	0.0019
dx4	0.02	0.0030
dx5	0.04	0.0032

Table 4.6: Δt values for the 2nd order moment system according with the stability advective condition (2.47).

And from diffusive condition (2.36), given that the stability condition depends also on the smallness parameter ε, we compute the corresponding time step (Fig. 4.11) using the same values (4.26) as before.

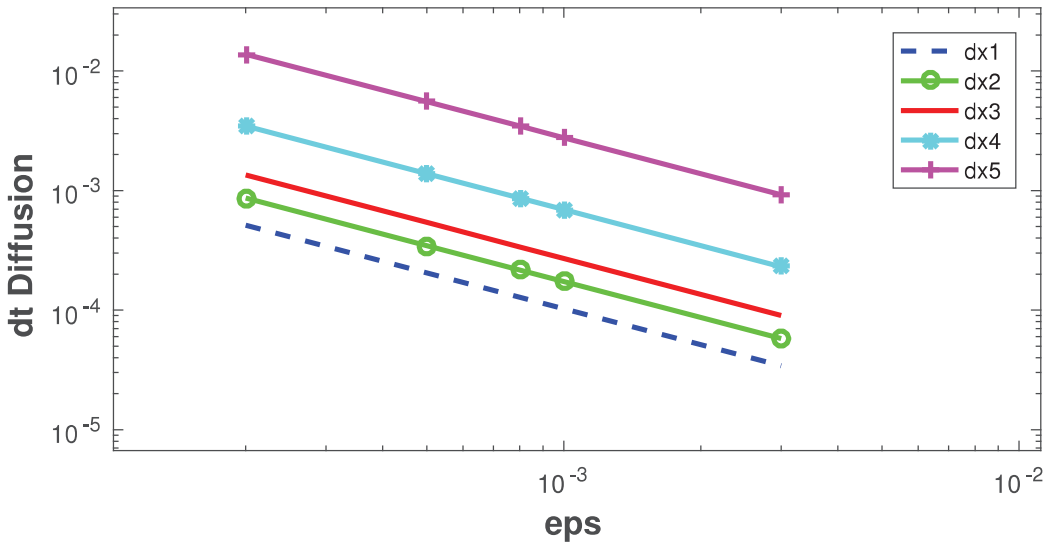

Figure 4.11: **Δt according with the diffusive condition (2.36) w.r.t different ε and Δx**

If we take a look to the range of Δx and ε in which the value of the *l2-error* stays stable, we will only consider $dx1$ until $dx4$ and $\varepsilon = \{0.8, 1, 3\} \times 10^{-3}$, in this range the diffusion time step is of the order of 10^{-4} and will always be smaller than the corresponding advection time step that is of the order of 10^{-3}, therefore the first will be the one chosen by the numerical method.

4.2 Adaptive mesh refinement

In this section, we will give a brief introduction to the concepts of adaptive discretization, specially its construction in a one-dimensional setting and how we can profit from the limit behaviour of the kinetic induced moment system in order to use the new variable $W(x,t)$ as the refinement criteria. We will keep on using during this chapter and along the rest of the thesis the two test cases introduced above (Burgers and shallow water equations) to perform the corresponding numerical experiments and subsequent comparison with the traditional refinement criteria applied to the original equations.

4.2.1 Definitions and the AMR 1D algorithm

The numerical solution of partial differential equations faces constantly computational limitations in order to achieve accurate and stable results. In the case of hyperbolic PDEs, it is usual to find physical problems where large regions embody a smooth slowly varying solution (where a coarse grid suffices) and small(local) regions where it varies rapidly (and a fine grid is needed). These localized special features can come from shocks development, steep gradients, discontinuities, spatial scales variations, boundary layers among others.

Until now many successful adaptive discretization techniques using Cartesian grids, over rectangular patches have been developed in [1, 2, 6, 3, 17, 18], we will focus in the last two to construct a one-dimensional AMR algorithm (where refined grid patches become intervals) in spite of testing the third order moment systems constructed previously.

The **AMR** technique adaptively places finer grids in regions needing a better numerical resolution over a coarse grid covering the domain [17], based on the behaviour of its own solution [3]. The refinement is by an integer ratio in space as well as in time and acts in a recursive manner.

Recursive AMR algorithm

Data: $Q(x^1, 0)$ initial condition

Result: $Q(x^1, t_{end})$ at the final time

$t = 0$

while $t < t_{end}$ **do**

  $Q(x^1, t) \xrightarrow{\Delta t^1} Q(x^1, t + \Delta t^1)$; /* Advances the current time solution one coarse time step Δt^1 */

  $l = 1$

  Check $refinement\_criteria(Q(x^l, t + \Delta t^l))$; /* Flags cells where refinement is needed */

  if *time to regrid* **then**

    $l = l + 1$

    $regrid(l)$; /* Computes new space and time steps $\Delta t^l, \Delta x^l$ and constructs the new grid */

    $t_l = t$

    while $t_l \leq t + \Delta t^1$ **do**

      $advance\_level(Q(x^l, t^l) \xrightarrow{\Delta t^l} Q(x^l, t_l + \Delta t^l))$

      $t_l = t_l + \Delta t^l$

    end

    if $l < l_{max}$ **then**

      Check $refinement\_criteria(Q(x^l, t + \Delta t^l))$

      if *time to regrid* **then**

        $l = l + 1$

        :

      end

    end

  end

  Update $Q(x^1, t + \Delta t^1)$; /* Computes new solution at $t + \Delta t^1$ */

  $t = t + \Delta t^1$

end

Algorithm 1: General recursive AMR algorithm

The previous algorithm describes in a general way how the AMR method advances the solution in time in a recursive manner, where the vector or matrix -according to the quantity of variables- $\boldsymbol{Q}(\boldsymbol{x}^l, \boldsymbol{t})$ contains the solution of each unknown at time t in the grid with level of refinement l. The whole process is divided in four stages [17]. The **Remesh Stage** is done in two steps: the **refine step** which evaluates the refinement criteria, flag the corresponding cells accordingly and cluster them into patches; and the **regrid step** that computes the physical location of the clusters and the corresponding solution values from the previous level. The most common monitoring functions [24] in which the decision of refinement is based are:

- **Richardson Extrapolation:** Error estimation, compares the solutions of one time step in $l-1$ with two steps l.

$$\left| \frac{Q(x_i^l, t_{n+1}) - Q(x_i^{l-1}, t_{n+1})}{\triangle t} \right| > tol \tag{4.27}$$

- **Spatial Gradient Estimate:** Max-Norm of the undivided difference of $Q(x_i^l, t_n)$ based in its two neighbours

$$|Q(x_{i+1}^l, t_n) - Q(x_{i-1}^l, t_n)| > tol \tag{4.28}$$

The flagging takes place in the cells where one of the previous functions -other functions like the curvature monitor proposed in [42] can also be used- exceeds some established tolerance (tol) given by the user, the proper setting of its value can cause some difficulties.

On the other hand, the refinement factor $\boldsymbol{r}$ -an integer- for nonlinear PDEs, must satisfy at each level the given conditions for stability and accuracy [17]. Consider Δx^l the corresponding spatial step at level l given by

$$\Delta x^l = \frac{\Delta x^{l-1}}{r} \quad , \qquad l = 2, 3, ..., l_{max} \tag{4.29}$$

In order to ensure stability, the initial time step in the AMR framework Δt_1 must satisfy the CFL-conditions (2.47) and (2.36), since the kinetic-induced moment system contains

also a diffusive term. For first order PDEs, to keep the ratio $\frac{\Delta t}{\Delta x}$ constant independently of the refinement level, the finer grid must be advanced r time steps for each coarser time step. Therefore,

$$\Delta t^l = \frac{\Delta t^{l-1}}{r} \quad , \qquad l = 2, 3, ..., l_{max}. \tag{4.30}$$

For second order PDE, the finer grid should have r^2 time steps for each coarser level to keep $\frac{\Delta t}{(\Delta x^2)}$ constant independently of the refinement level.

$$\Delta t^l = \frac{\Delta t^{l-1}}{r^2} \quad , \qquad l = 2, 3, ..., l_{max} \tag{4.31}$$

The **Advanced Stage** advances the solution for all clusters of the current level to a specified time. Here we illustrate two different numerical discretization in the AMR context, the finite differences and volumes method which we will use ahead. In the **finite differences** approach the solution of the unknown is node-centred, i.e. $Q(x_i^l, t_n)$ is a node value on the grid. The explicit FD scheme with $F(x^l_{i\pm\frac{1}{2}}, t_n)$ the flux function between (x_i, x_{i+1}) and (x_{i-1}, x_i) reads,

$$Q(x_i^l, t_{n+1}) = Q(x_i^l, t_n) - \frac{\Delta t^l}{\Delta x^l}\left(F(x^l_{i+\frac{1}{2}}, t_n) - F(x^l_{i-\frac{1}{2}}, t_n)\right) \tag{4.32}$$

We follow the AMR integration algorithm proposed in [17, 18] for a one-dimensional problem, constructed in a node-based adaptive framework. In the regridding step at a time n, the coarser nodes will share always the same position with a finer one (Fig. 4.12), the computation of the internal boundaries is done by interpolation between the internal boundary values of the coarser grid at forward time t^{l+1}_{n+1} and the ones on the finer grid at the current time t^l_n.

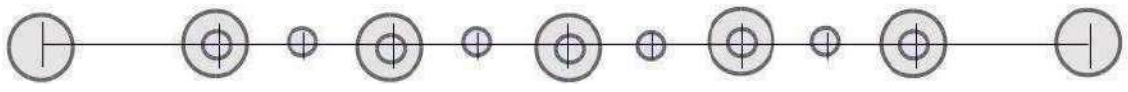

Figure 4.12: **Finite differences AMR grid**

Unlike the finite differences, the **finite volumes** method works in a cell-centred framework, i.e $Q(x_i^l, t_n)$ is the cell average and it is updated by the flux differences through the cell edges. The general scheme yields

$$Q(x_i^l, t_{n+1}) = Q(x_i^l, t_n) - \frac{\Delta t^l}{\Delta x^l}\left(F(x^l_{i+\frac{1}{2}}, t_n) - F(x^l_{i-\frac{1}{2}}, t_n)\right) \tag{4.33}$$

with

$$F(x^l_{i\pm\frac{1}{2}}, t_n) \approx \frac{1}{\Delta t^l}\int_{t_n}^{t_{n+1}} f(Q(x^l_{i\pm\frac{1}{2}}, t))dt \tag{4.34}$$

The AMR algorithm is proposed in [3] for the case of hyperbolic systems. The time integration will run until $t_n + \Delta t^1$ is reached, the internal boundaries are imposed using *ghost cells* which are computed by space-time interpolation from the coarser grid values (Fig. 4.13).

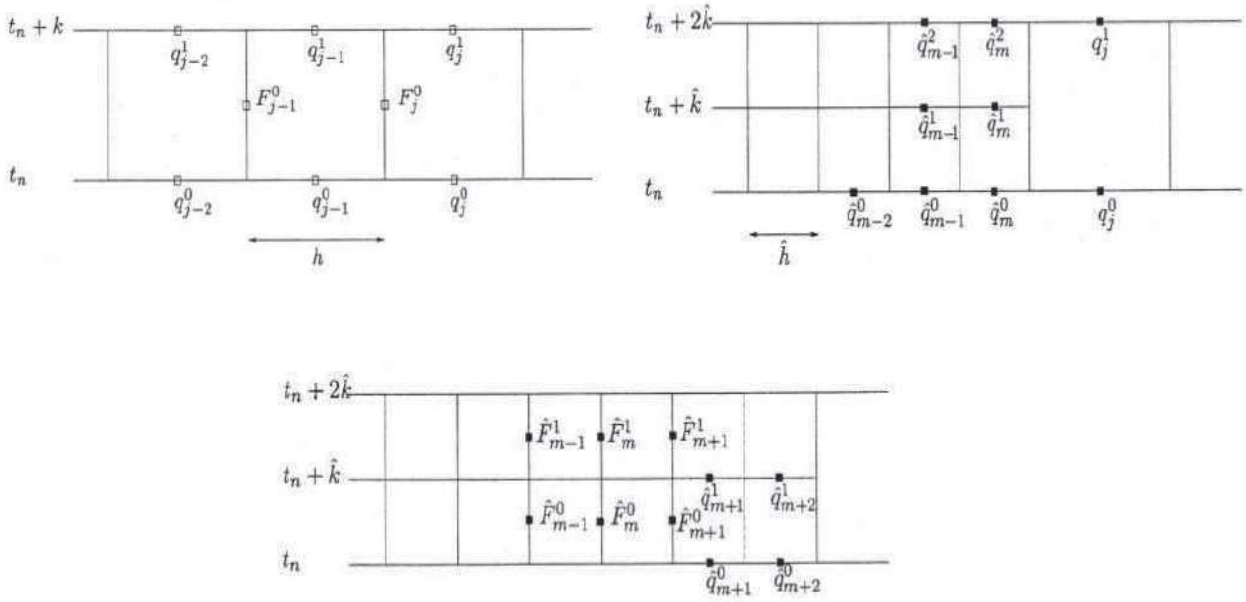

Figure 4.13: **Finite volumes AMR grid** [3]

Succeeding, the **Recursion Stage** makes a loop for every cluster until no further refinement is needed or until the maximum level l_{max} is reached. And finally, the **Projection Stage** updates the solution values on the coarsest grid according to the chosen numerical

discretization. For finite differences the fine grid solution is simply copied directly to the coarse nodes that overlap with the fine ones, in the case of finite volumes the coarser nodes values will be replaced by the average of the two adjacent finer ones.

4.2.2 $\mathbf{W(x,t)}$ as a refinement criteria

The new unknown $W(x,t)$ present in the third order moment systems (3.32) and the second order moment system (3.74) can be employed in the context of adaptive mesh refinement (AMR) as a refinement criteria, since as described in section (3.4) it behaves as a delta function in the case a shock or a rarefaction wave occurs. Different approaches in how to define the new refinement criteria were tested, at the end the one propose next showed the best results.

As the need of greater accuracy comes in cases of complicated flow structure, we can set the level of refinement accordingly with the steepness of the velocity gradient, given that in the limit of $\varepsilon \to 0$ the function $W(x,t)$ has the opposite behaviour of $\partial_x u$, consequently we expect in the case of shock waves a higher level of refinement. On that account, it is possible to define always in the limit of $\varepsilon \to 0$ an estimate of $\partial_x u$ depending on $W(x,t)$, coming from the moment system, which is produced by the original equation itself.

Consider

$$\partial_x U_i^n = f(W_i^n), \tag{4.35}$$

where $f(W_i^n)$ is a function which depends on the discrete values of $W(x,t)$ and represents an estimate of the respective gradient $\partial_x u$ at the point (i,n), it is recovered by considering the moment system in the formal limit $\varepsilon \to 0$. For our two examples, it is given by equations (3.91b) and (3.101c). Next we define,

$$|\partial_x U_i^n| : \text{absolute value of } \partial_x U_i^n \text{ at a given time } n \tag{4.36}$$

we can then establish a parameter $tolK$ which will denote accordingly with the type of

problem, yet more the kind of expected solution (if known) the steepness value for which more or less refinement is desired. At a fixed n all points in space where

$$|\partial_x U_i^n| \geq tolK \tag{4.37}$$

will be flagged for refinement. Our aim is to compare the previously defined monitor function with the traditional ones applied to the inviscid Burgers and the shallow water equations. For simplicity we choose the spatial gradient estimate (4.28).

4.2.3 Case 1: 1D Inviscid Burgers equation

In order to compute the **Advanced Stage** inside the adaptive mesh refinement algorithm we use the finite difference method described in (4.32). Moreover, the refinement function (4.36) for this case is defined accordingly with equation (3.91b)

$$|\partial_x U_i^n| = \mid -3 \cdot W_i^n \mid \tag{4.38}$$

Since we continue to use the same initial conditions (Riemann problem) as in the static grid case (5.21), we know that the solution will be a single shock wave moving in time as we have seen in Fig. 4.1. Therefore, we will refine always where $|\partial_x U_i^n| \neq 0$ according to (3.92) given that $W(x,t)$ will be zero everywhere except around the shock. The corresponding refinement tolerance for the third moment system would be then $tolK = 0$, since in a shock wave we will always want the maximum level of refinement.

Numerical data

We compare the results of the AMR integration algorithm for the inviscid Burgers equation (3.37) computed for three different tolerance values (tol) considering the spatial gradient estimate (4.28), and its corresponding third order kinetic system (4.1) considering the refinement criteria (4.38), with respect to the exact solution of the Burgers equation.

The first three solutions will be represented in the figures as *"Burgers Tol= tol"*, on the other hand, the computation of W_i^n coming from (4.1) will be also used as a refinement criteria for the inviscid Burgers represented by *"Burgers w/ $W(x,t)$"*, and for the kinetic system itself represented by *"Kims"*. Hence, we will be able to observe the corresponding changes in error and refined areas correspondingly with the following data,

* computational domain $[-2:8]$
* $\varepsilon = 0.001$
* $l_{max} = 4$
* refinement factor $r = 2$for
* $tol = [0.04, 0.6, 0.8]$, used (4.28)
* $tolK = 0$, used for (4.38)
* coarsest grid $M_1 + 1 = 251$
* finest grid $M_4 + 1 = 2001$, (if all the domain were refined)
* $\Delta x_1 = 0.04$
* $\Delta x_4 = 0.005$
* $t_{final} = 2.1$

Results

- **Refinement**

  Fig. (4.14) shows the refined areas with corresponding levels for each tolerance value, according with the respective refinement criteria for both AMR approximations. The first three results correspond to (4.28), the last one to (4.38) and the red plot represents the exact solution of the Riemann problem at $t = 2.1$.

  For (4.28) we have chosen such tolerance values that exhibit where the level of refinement starts decreasing. We can observe that the total *Kims* refined area is quite similar to the rest, but the part corresponding to $l = 4$ is bigger if we compare it

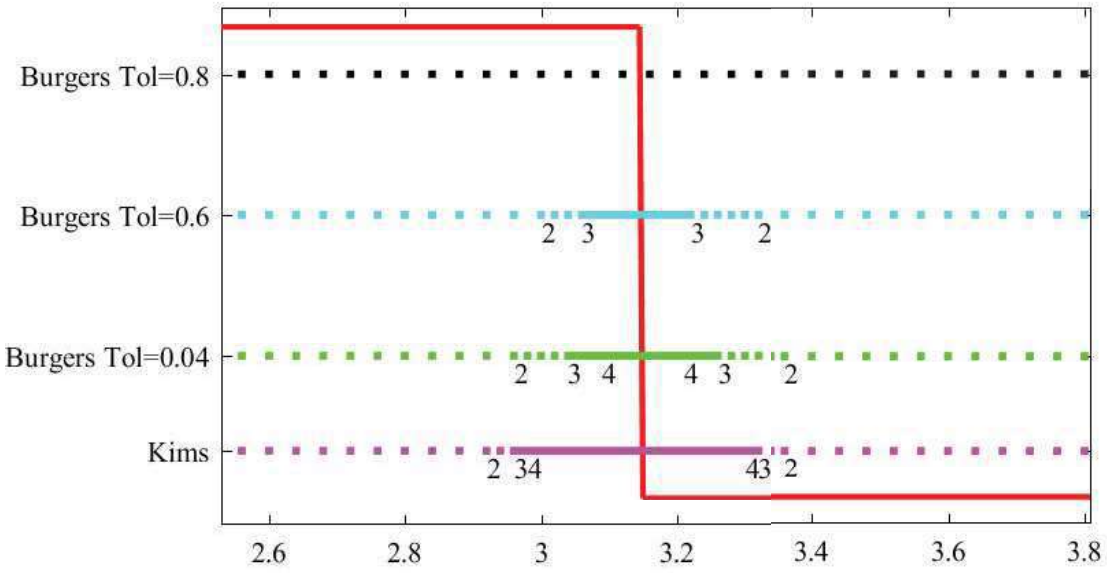

Figure 4.14: **Refinement levels at t = 2.1 for different tolerance values.**

with *Burgers Tol=0.04*, since in the first case the number of cells between levels is fixed to four from the start and it will not change given the established value for $tolK$. These are of course parameters that can be varied according to the problem and requirements of the user.

If we focus in the results coming from the spatial gradient estimate (4.28), we can see that in order to decrease the refinement we need to increase considerably *tol* but after it starts decreasing any small change will contract the refinement, showing in the case of a shock how sensitive it can be after a point to different tolerances. Ahead we would be able to see how this translates to the *l2-errors*.

- ***l2-error***

  We use the $l2 - norm$ (4.12) of the difference between approximated solutions Q_i^n (Burgers AMR and Kims AMR) and the inviscid Burgers equation exact solution q_i^n,

so to compute the error of our algorithms in the time interval $(0, 2.1]$.

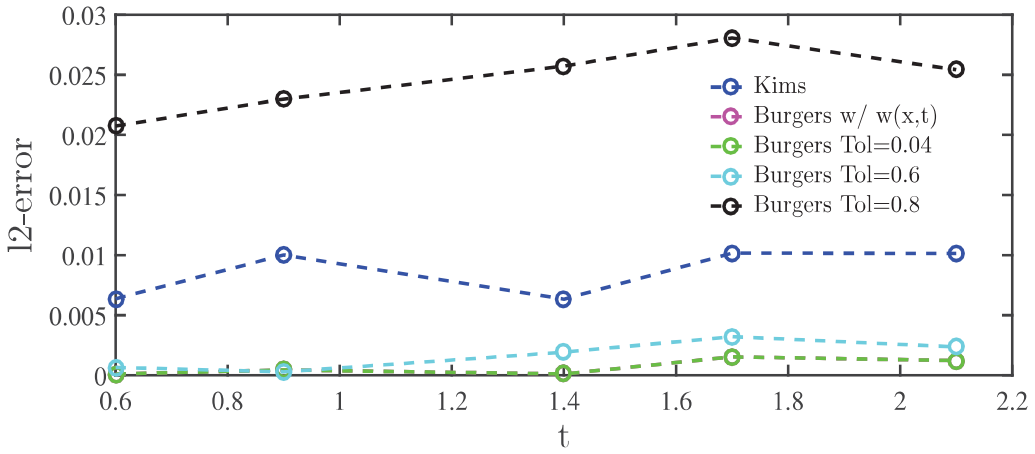

(a) l2-norm comparison between spatial gradient estimate for different tolerance values and KIMS refinement.

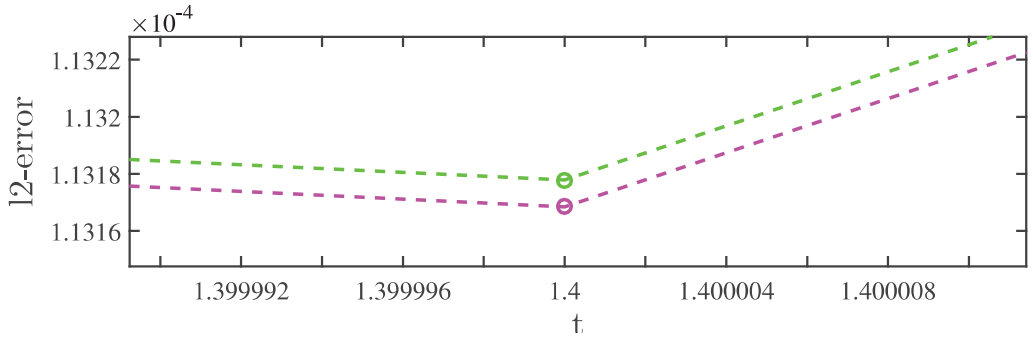

(b) Burgers l2-norm using spatial gradient estimate with $tol = 0.04$ and $w(x,t)$ from KIMS.

Figure 4.15: **l2-norm comparison.**

In Fig. 4.15a, it is possible to see that the evolution of the *l2-error* is coherent with the previous results of the refined area, as to lower levels of refinement we get higher errors. On the other hand, there is not a significant difference between the solutions with $tol = 0.04$ and $tol = 0.6$ being the latter just one level of refinement below, also as we could hope for, Fig. 4.15b shows that the adaptation made through $W(x,t)$

is almost the same as the best approximation done with spatial gradient estimate, which is of the order 10^{-2}. As a reference, we include the result of the kinetic system (KIMS), which has naturally the same refinement of *"Burgers w/ $W(x,t)$"* and as observed has a rather low error, also of the order 10^{-2}.

- **u(x,t)**

  Next we will show the comparison of the approximated solutions for $u(x,t)$ with respect to the exact one at the final time $t = 2.1$, by this point the discontinuity has travel past $x = 3.15$ (Fig. 4.16a).

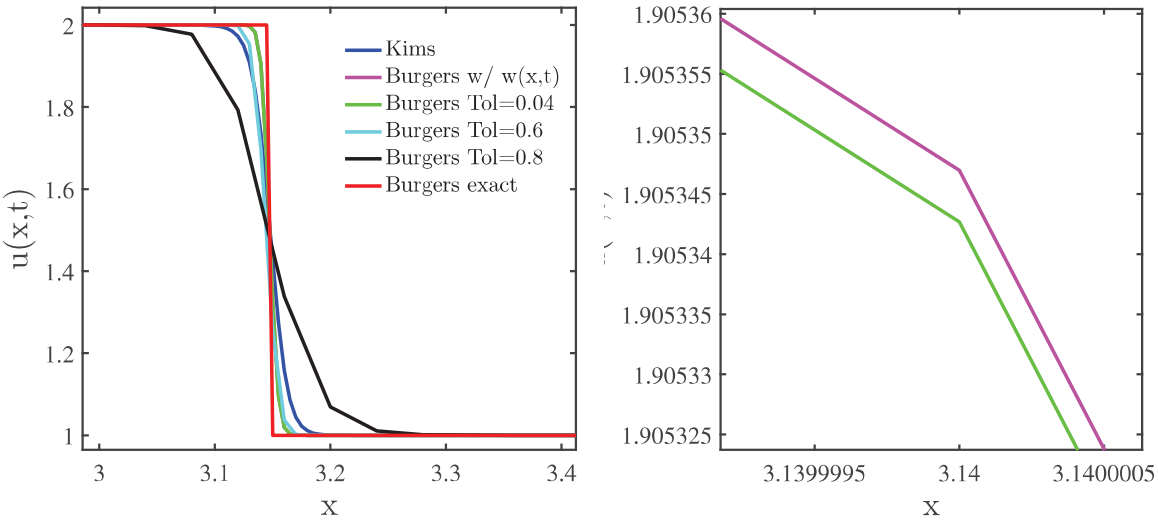

(a) $u(x,t)$ shock wave at $t = 2.1$ (b) Burgers with $tol = 0.04$ and $W(x,t)$

Figure 4.16: **Comparison of Burgers approximations with different tolerance values and the third order moment system (KIMS).**

Fig. 4.16a is indeed the reflection of what we have already observed, where the diffusive effect grows as the level of refinement decreases, increasing the error. Further in Fig. 4.16b, it becomes visible the closeness between the results *"Burgers Tol=0.04"*

and *"Burgers w/ $W(x,t)$"*.

- **Time step Δt_1**

  If we take a look to the maximal time steps in both AMR algorithms, we can notice that $\Delta t_{Burg} = 0.018$ is of the order 10^{-2} and $\Delta t_{kims,\varepsilon=0.001} = 0.014$ also of the order 10^{-2}, meaning that both have a quite similar computational effort. We do not compare the computational time of the numerical methods, since we know from advanced that the kinetic system is solving on top of the original equation (in this case the inviscid Burgers) an extra one, which will naturally take more time.

4.2.4 Case 2: 1D Inviscid shallow water equations

Following again the adaptivity routine described previously, we will now use the finite volume method (4.33) and (4.34) to compute the **Advance stage**. Additionally, the refinement function (4.36) is defined accordingly to (3.101c),

$$| \partial_x U_i^n | = \left| \frac{-2}{gh^2} \cdot W_i^n \right| \tag{4.39}$$

One more time, we use the same initial conditions as for the static grid case (4.24), which correspond to the breaking dam and as we know, in time it will develop into a rarefaction wave (for which the need of refinement is less) where $W(x,t)$ becomes a moderate negative curve and a shock wave (for which we will want to refine until the maximum level) where $W(x,t)$ behaves like a delta peak, as we have seen in Fig. 4.5. Hence, we can define the parameter *tolK* accordingly with the value of space gradient desired for different levels of refinement. In this case, we want the rarefaction wave to reach only $l = 2$ and thus the refinement criteria yield,

$$tolK = \begin{cases} 0 & \text{if } l < 2 \\ 1.5 & \text{if } 2 \leq l < 4 \end{cases} \tag{4.40}$$

Numerical data

The AMR for shallow water is computed by using three different tolerance values *tol* for the spatial gradient estimate (4.28) and $w(x,t)$ from the second order moment system together with *tolK* for (4.39). The results are compared with a reference solution coming from the approximation of the shallow water equations with a fine static grid.

In a similar way to the previous scalar example, the first three results for the shallow water equations are represented by *"SWE Tol= tol"*, the refinement of the shallow water equations done via W_i^n by *"SWE w/ W(x,t)"* and the refined second order kinetic system itself by *"Kims"*. The parameters used for the numerical computations read,

* computational domain $[-10:10]$
* $\varepsilon = 0.001$
* $l_{max} = 4$
* refinement factor $r = 2$
* $tol = [0.01, 0.1, 0.8]$
* coarsest grid $M_1 + 1 = 600$
* finest grid $M_4 + 1 = 4800$, (if all the domain were refined)
* $\Delta x_1 = 0.033$
* $\Delta x_4 = 0.0042$
* $t_{final} = 1.4$

Results

- **Refinement**

  Subsequently with the spatial gradient estimate (4.28), the levels of refinement corresponding to each *tol* value for the *shallow water system* are presented in figure 4.16 together with the *second order moment system (KIMS)* accordingly to section 3.2.2. In the first case, we have chosen tolerance values that display different refinements at

least for the rarefaction wave. Only the solution for $hu(x,t)$ is shown.

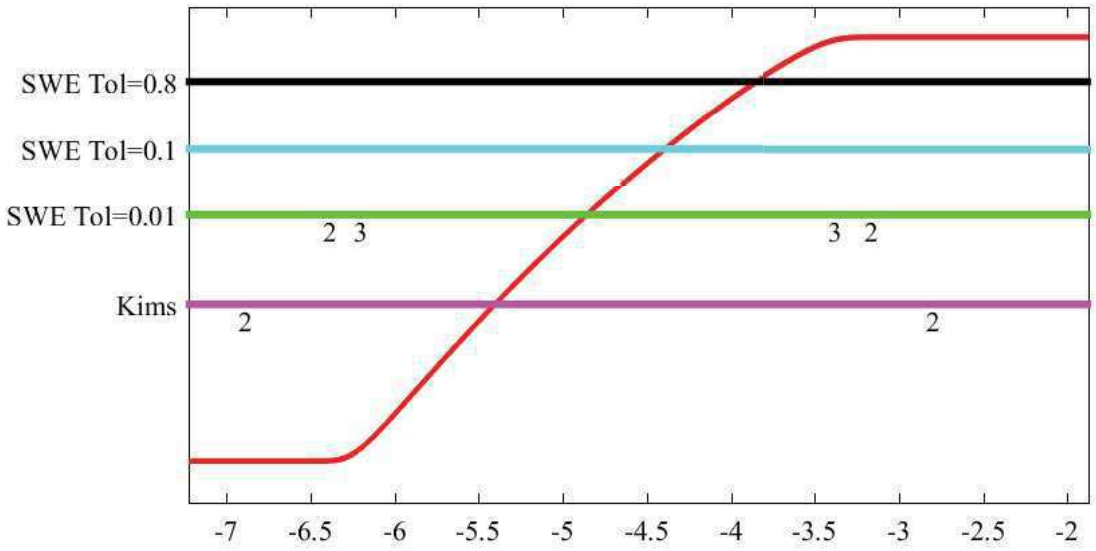

(a) Rarefaction wave for $h(x,t)u(x,t)$ at $t = 1.4$

In Fig. 4.17a we can see that along the rarefaction wave the lowest tolerance for (4.28) reaches until $l = 3$, but when we increase the value the refinement stops at $l = 1$. Again the refined area in *"Kims"* is just a little larger that the best approximation from the gradient estimate, and it goes up to $l = 2$ as established from the parameters (4.40). Furthermore, along the shock wave showed in Fig. 4.16b, for (4.28) the refinement decreases suddenly from the maximum level $l = 4$ to the initial grid just in the highest tolerance, and as in the Burgers case the refined region by *"Kims"* looks rather similar to the one corresponding to *"SWE Tol=0.01"* reaching out the maximum level as one should expect giving the drastic jump in the solution.

- **l2-error**

  According to the *l2-discrete norm* (4.25), with $Q^n_{m,i}$ the approximated AMR solution of the shallow water and the second order moment system, and $q^n_{m,i}$ the reference

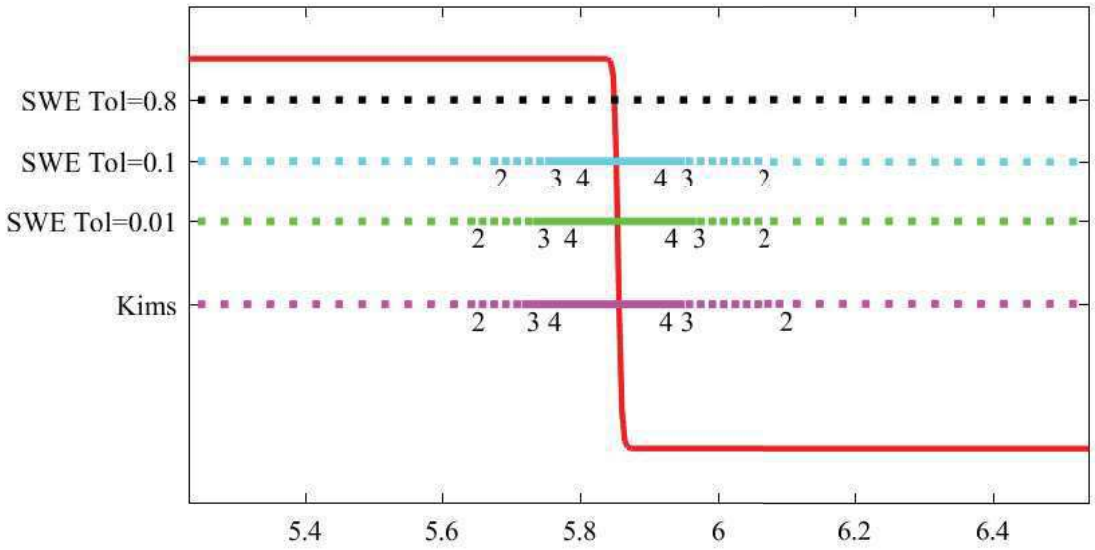

(b) Shock wave for $h(x,t)u(x,t)$ at $t = 1.4$

Figure 4.16: **Refinement of the SWE for $\mathbf{h(x,t)u(x,t)}$ at $\mathbf{t = 1.4}$.** Rarefaction wave (a), shock wave (b)

solution given by the approximation of the shallow water equations in a fine static mesh ($M + 1 = 4800$), Fig. 4.17 shows the comparison between approximations.

In line with the previous section, we can observe how the *l2-error* for *SWE Tol=0.8* increases substantially in comparison with the rest, since the grid stays at $l = 1$, as well as how the *"SWE w/ $W(x,t)$"* error stays between *"SWE Tol= 0.01"* and *"SWE Tol= 0.1"* given that the highest refinement level along the rarefaction are 2,3,1 respectively. It is of note that *"Kims"* error, which has the same refinement as *"SWE w/ $W(x,t)$"* is fairly low and stays comparatively close to *"SWE Tol= 0.1"* error, even overtaking it after some time.

- **$\mathbf{h(x,t)}$ and $\mathbf{h(x,t)u(x,t)}$**

  Conclusively Figs. 4.18a and 4.18b present the juxtaposition of the approximated

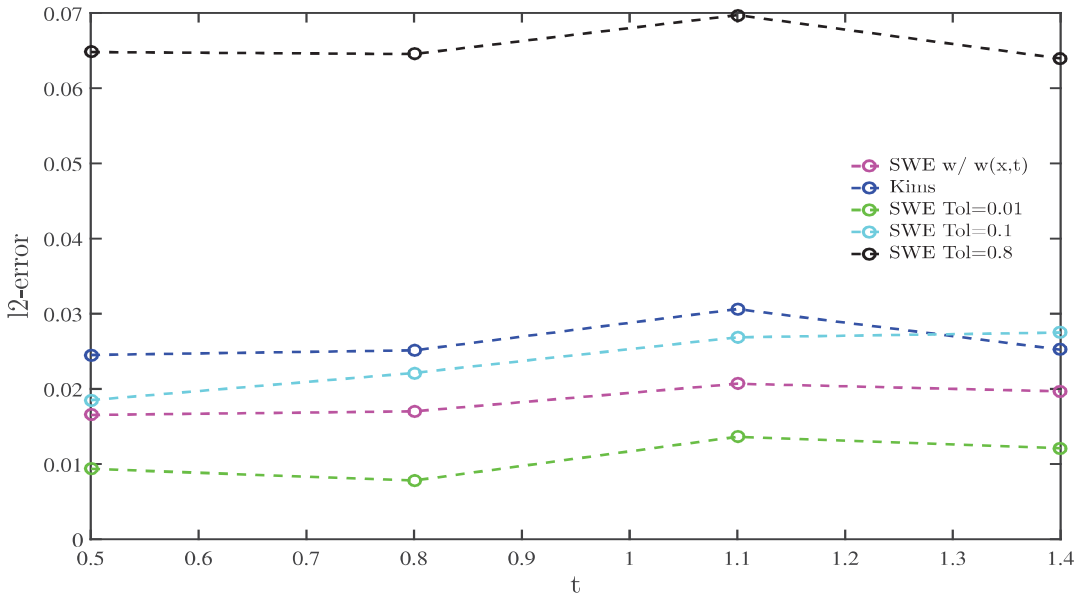

Figure 4.17: **Comparison of the l2-norm between the shallow water and the second order moment system (KIMS) with different tolerance values.**

solutions for both $h(x,t)$ and $h(x,t)u(x,t)$ including the reference solution defined previously for the computation of the error, which here is called *SWE Fix*. In order to visualize the divergence of the solutions in a clearer way, the rarefaction and shock waves are shown separately.

Figs. 4.19b and 4.19c display the beginning and end of the rarefaction wave, which coincide with the previous results. We can observe more diffusion coming from the second order moment approximations (*Kims*) and from highest tolerance value for the shallow water system (*SWE Tol=0.1* and *SWE Tol=0.8*), then becomes clear that the rarefaction approximation has the strongest influence on the error increment -which is aligned with the static mesh results at section 3.1.2-, given that for the shock wave (Fig. 4.20) almost all the cases are equally refined and we can note how close they are to each other (Fig. 4.20b).

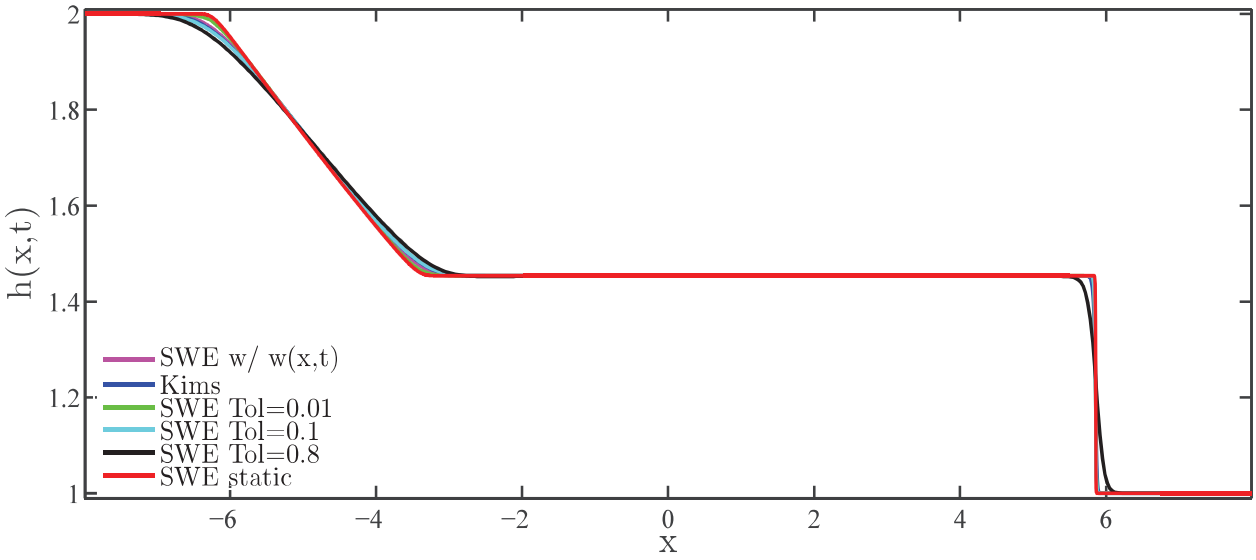

(a) $h(x,t)$ at $t = 1.4$

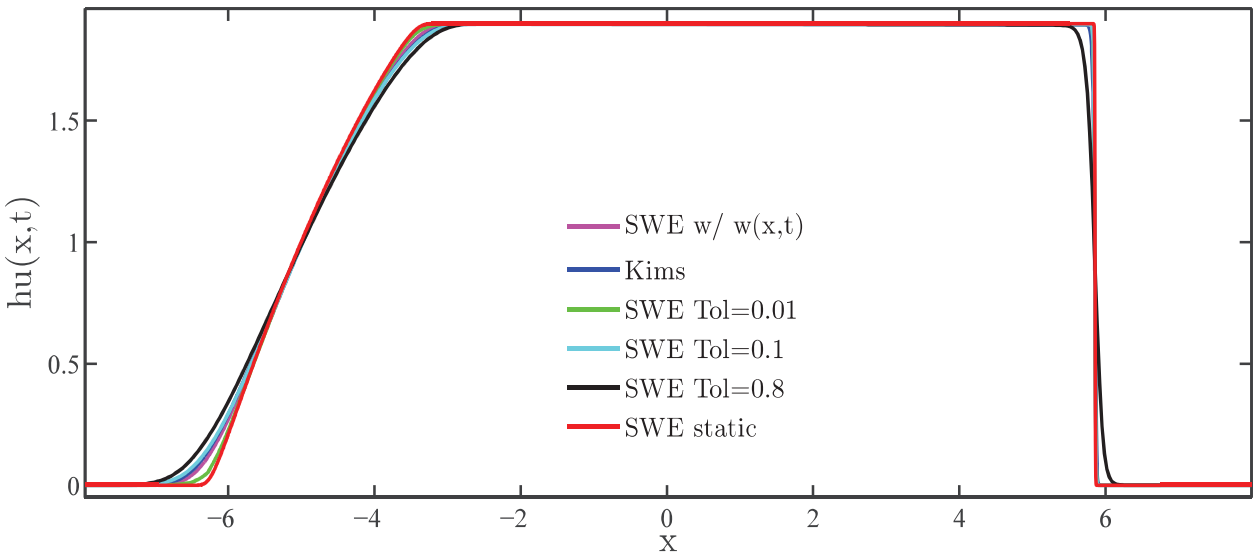

(b) $h(x,t)u(x,t)$ at $t = 1.4$

Figure 4.18: **Comparison between the shallow water and the second order moment system (KIMS) with different tolerance values.**

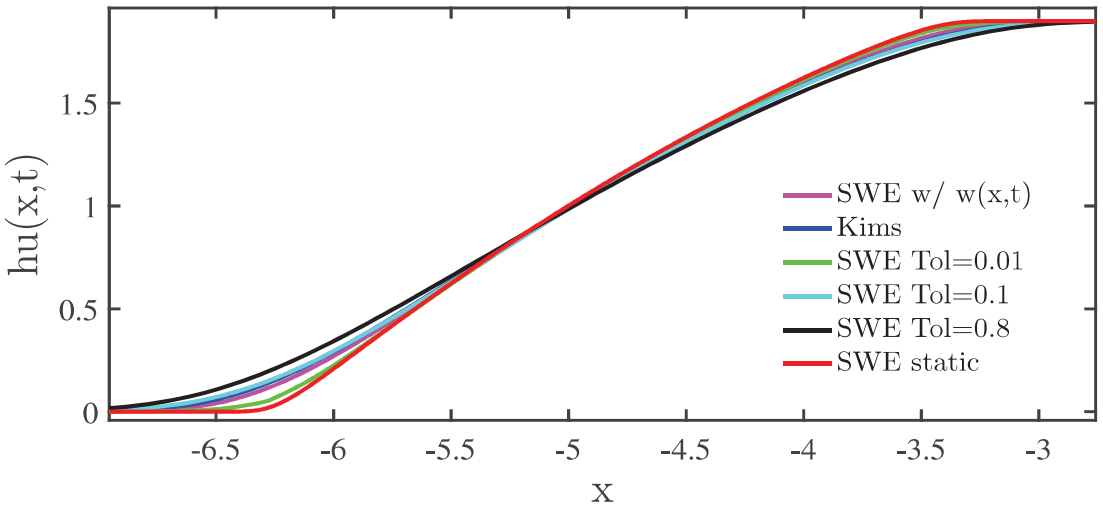

(a) $hu(x,t)$ rarefaction wave at $t = 1.4$

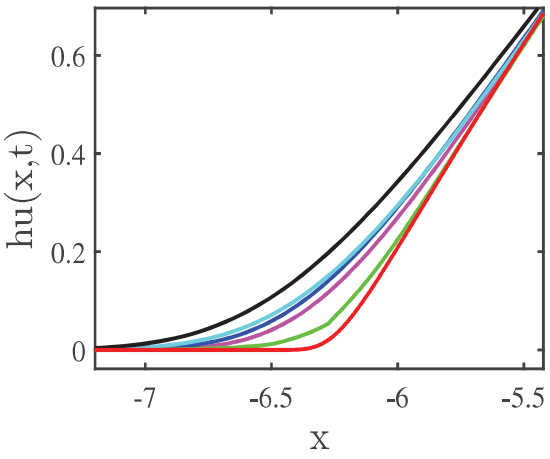

(b) Beginning of the wave

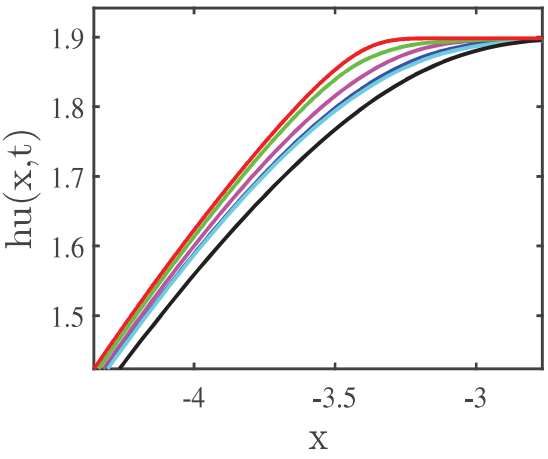

(c) End of the wave

Figure 4.19: **Comparison of SWE rarefaction wave approximations with different tolerance values and the second order moment system (KIMS).**

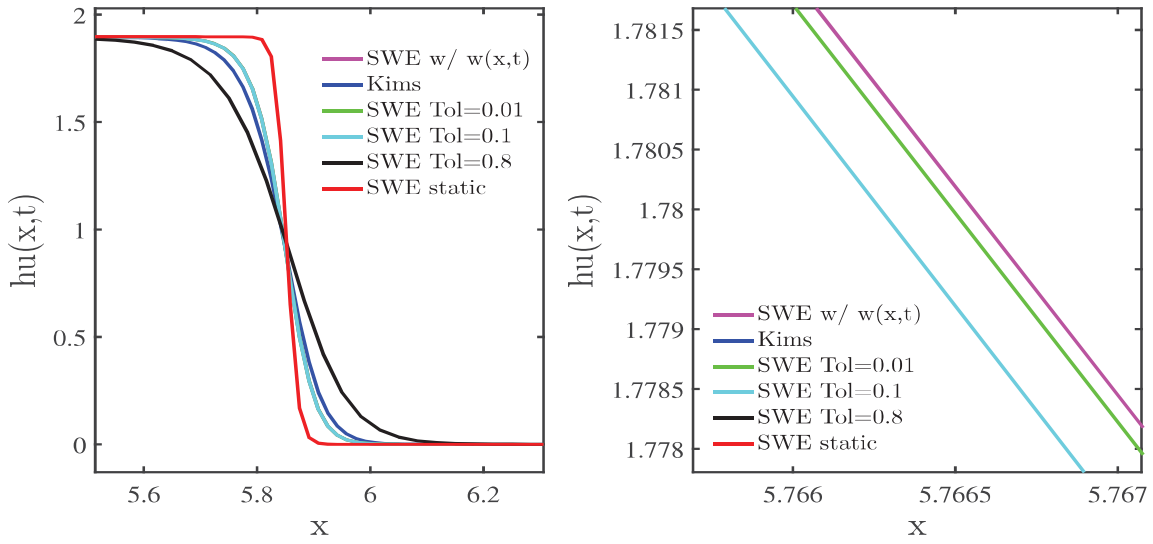

(a) $hu(x,t)$ shock wave at $t = 1.4$

(b) SWE with $tol = 0.01$ and $w(x,t)$

Figure 4.20: **Comparison of SWE shock wave approximations with different tolerance values and the third order moment system (KIMS).**

Fig. 4.20 shows again that the second order moment system introduces extra diffusivity to the shock. Nevertheless, there will be a lower level of refinement for the *SWE* in which the amount of diffusion reaches that of the *Kims* computed in a higher level of refinement as we could observe for the rarefaction wave.

4.3 Summary

The static grid numerical examples show that in both cases (Burgers and SWE), with a smallness parameter $\varepsilon = 0.001$, the new variable $W(x,t)$ in fact performs as a shock and rarefaction wave detector, behaving -as expected from Chapter 3- like the opposite of the gradient. Namely, around a shock wave it will behave as a positive $\delta-$peak, while around

a rarefaction wave it will have a moderate negative tendency, otherwise it will be equal to zero (Fig. 4.5). Therefore, it is possible to use W_i^n (the approximation of $W(x,t)$) as an alternative for the traditional refinement criteria in the context of adaptive mesh refinement.

As for the corresponding *l2-errors*, in the numerical approximation of the 3rd order moment system of Burgers equation, we could observed that by raising the value of ε, the error will increase steadily (Fig. 4.3). On the other hand, for the 2nd order moment system of the SWE, the steady increase of the error will depend on both parameters ε and Δx, since for very small values of ε or for not small enough values of Δx the error will blow up (Fig. 4.9). This could mean, that more complex systems will have stronger numerical restrictions on the parameters ε and Δx, thus in order to use the corresponding KIMS model we would have to check always in advance an appropriate setting for both parameters, so to avoid unstable approximations, which can be cumbersome.

Furthermore, when using W_i^n as a refinement criteria in AMR (4.35), it gives us the possibility to establish a proper gradient value for which less or more refinement shall be wanted. Hence, one can set a different maximum level of refinement depending of the expected solution. For example, if it is either a shock or a rarefaction wave. This feature will then allow the level refinement to be independent of some heuristic parameter specified according to the user's criteria, as it occurs with more traditional refinement parameters (4.27) and (4.28), instead we can use the gradient to determine more suitable refinement conditions.

The comparison between refinements of the original equations done via spatial gradient estimate (SGE) and via W_i^n shows that the area refined by the second method tends to be larger than the one by the first (Fig. 4.14,Fig. 4.16). Additionally, the latter is in both experiments almost the same to the best SGE result, which corresponds to the lowest tolerance value as one would expect (Fig. 4.2,Fig. 4.17). In other words, there is always a tolerance value (which needs to be found) for SGE that refines in the same way as W_i^n does

it, without the need of computing a kinetic-induced moment system which by default will need more computational time. Nevertheless, the use of W_i^n (if available), simplifies the task of defining the proper refinement parameters that give us the most accurate approximation, since it is not longer a random value but it is now connected to a mathematical characteristic of the problem itself, which in the long run will save us time.

5. Spectral Analysis

It is well know that discretizing the one-dimensional nonlinear diffusion equation by spectral methods, one often encounters convergence problems in the case of shock developing initial conditions [39]. This kind of solutions arise from very small viscosity ($\nu \to 0$), for which a considerably large amount of modes need to be considered in order to have a stable solution that includes the effect of small wavelength modes and resolves the resulting wave. Up to present time, different models like optimal prediction [4] and hyperviscosity [31] among others, have been developed trying to overcome this difficulty. Hereby, we try to established if the previous derived kinetic moment systems are equipped with spectral properties that allow some relaxation for the stability condition and provides an alternative model to the ones already found in the literature.

5.1 Fourier-Galerkin spectral approximation of the third order kinetic-induced moment system for Burgers equation

We are interested in studying the one-dimensional viscous Burgers equation (5.1) in the limit of vanishing viscosity ($\nu \to 0$), so we get closer to the inviscid problem (2.17).

$$\frac{\partial u}{\partial t} + u\frac{\partial u}{\partial x} = \nu\frac{\partial^2 u}{\partial x^2} \tag{5.1}$$

On the domain $x \in [0, 2\pi]$ with periodic Dirichlet boundary conditions $u(0,t) = u(2\pi,t) = 0$ the previous equation (5.1) will develop shock waves in time from smooth initial conditions, like sinusoidal waves. For $\nu = 0$ the shock will become a discontinuity [7].

The FG-spectral approximation, approximates the solution $u(x,t)$ of (5.1) by the Fourier

series[1],

$$u^N(x,t) = \sum_k \hat{u}_k(t) e^{ikx} \tag{5.2}$$

where the corresponding Fourier coefficients at each mode k are defined as

$$\hat{u}_k(t) := \frac{1}{2\pi} \left\langle u^N, e^{ikx} \right\rangle \tag{5.3}$$

with $\langle \cdot, \cdot \rangle$ the inner product[2], which uses e^{ikx} as test function. See [19] and [29].

Theorem 5.1.1. *Let $\overline{k}$ be the cut-off wavenumber, that truncates the Fourier series (5.2) of $u(x,t)$. The FG-spectral approximation of the viscous Burgers equation (5.1) satisfies the following nonlinear differential equation for modes within $\overline{k}$.*

$$\frac{\partial \hat{u}_k}{\partial t} + \frac{ik}{2} \sum_{n \in \mathbb{Z}_k(\overline{k})} \hat{u}_n \hat{u}_{k-n} = -\nu k^2 \hat{u}_k \qquad \forall \mid k \mid \leqslant \overline{k} \tag{5.4}$$

where the sum is over the set,

$$\mathbb{Z}_k(\overline{k}) = \{n/n \in \mathbb{Z}; |n|, |k-n| \leqslant \overline{k}\} \tag{5.5}$$

and yields,

$$\sum_{n \in \mathbb{Z}_k(\overline{k})} (\cdot) = \begin{cases} \sum\limits_{n=-\overline{k}+k}^{\overline{k}} (\cdot) & k \geqslant 0 \\ \\ \sum\limits_{n=-\overline{k}}^{\overline{k}+k} (\cdot) & k < 0 \end{cases} \tag{5.6}$$

[1]A Fourier series is an expansion of a periodic function in terms of an infinite sum of sines and cosines, which can also be extended to complex coefficients. It make use of the orthogonality relationships of the sine and cosine functions [12].

[2]The vector space of real functions whose domain is a closed interval $[a,b]$ is equipped with the inner product $\langle f, g \rangle = \int_a^b fg\, dx$. It satisfies the following four properties:

1. $\langle f, f \rangle \geq 0$, $\langle f, f \rangle = 0$ only if f is the constant zero function,
2. $\langle f, g \rangle = \langle g, f \rangle$. For complex-valued functions $\langle f, g \rangle = \overline{\langle g, f \rangle}$ the complex conjugate,
3. $\langle f, g + h \rangle = \langle f, g \rangle + \langle f, h \rangle$,
4. $\langle f, cg \rangle = c\langle f, g \rangle$ for any scalar c.

For details see [11].

Proof. In weak conservative form[3] with e^{ikx} as the test function, (5.1) yields

$$\overbrace{\langle \partial_t u, e^{ikx} \rangle}^{\text{a}} + \overbrace{\left\langle \partial_x^2 \left(\frac{1}{2} u^2 \right), e^{ikx} \right\rangle}^{\text{b}} = \overbrace{\langle \partial_x (\nu u), e^{ikx} \rangle}^{\text{c}}. \tag{5.7}$$

Using the Fourier series approximation of $u(x,t)$ by (5.2), together with integration by parts and periodicity we develop each term:

$$\begin{aligned} \mathbf{a} &= \langle \partial_t \sum_l \hat{u}_l(t) e^{ilx}, e^{ikx} \rangle = \langle \sum_l \partial_t \hat{u}_l(t) e^{ilx}, e^{ikx} \rangle \\ &= \sum_l \partial_t \hat{u}_l(t) \langle e^{ilx}, e^{ikx} \rangle = 2\pi \sum_l \partial_t \hat{u}_l(t) \delta_{lk} \\ &= \boxed{2\pi \partial_t \hat{u}_k(t)} \end{aligned} \tag{5.8a}$$

$$\begin{aligned} \mathbf{b} &= \left\langle \partial_x^2 \left(\frac{1}{2} u^2 \right), e^{ikx} \right\rangle = \langle -\frac{1}{2} u^2, \partial_x e^{ikx} \rangle \\ &= -\frac{1}{2} \langle \left(\sum_n \hat{u}_n(t) e^{inx} \right) \left(\sum_l \hat{u}_l(t) e^{ilx} \right), ike^{ikx} \rangle \\ &= -\frac{1}{2} \langle \sum_n \sum_l \hat{u}_n(t) \hat{u}_l(t) e^{i(n+l)x}, ike^{ikx} \rangle \\ &= \frac{ik}{2} \sum_{n+l=k} \hat{u}_n(t) \hat{u}_{k-n}(t) \langle e^{ikx}, ike^{ikx} \rangle \\ &= \boxed{ik\pi \sum_n \hat{u}_n(t) \hat{u}_{k-n}(t)} \end{aligned} \tag{5.8b}$$

$$\begin{aligned} \mathbf{c} &= \langle \partial_x^2 (\nu u), e^{ikx} \rangle = \nu \langle \partial_x^2 \sum_l \hat{u}_l(t) e^{ilx}, e^{ikx} \rangle \\ &= \nu \sum_l \hat{u}_l(t) \langle (il)^2 e^{ilx}, e^{ikx} \rangle = -\nu \sum_l l^2 \hat{u}_l(t) \langle e^{ilx}, e^{ikx} \rangle \\ &= -(2\pi)\nu \sum_l l^2 \hat{u}_l(t) \delta_{lk} = \boxed{-(2\pi)\nu k^2 \hat{u}_k(t)} \end{aligned} \tag{5.8c}$$

[3] An equation written in its weak form is no longer required to hold in the classical sense, instead requires a solution only with respect to certain test functions. These are then called weak solutions, which allow discontinuities [11].

Putting all terms together and dividing by 2π we obtain (5.1),

$$\boxed{\frac{\partial \hat{u}_k}{\partial t} + \frac{ik}{2} \sum_{n \in \mathbb{Z}_k(\overline{k})} \hat{u}_n \hat{u}_{k-n} = -\nu k^2 \hat{u}_k \qquad k \in \{-\overline{k}, ..., 0, ..., \overline{k}\},\ t \geq 0} \tag{5.9}$$

□

Remark 5.1.1. *As is well known, spectral methods work very good for viscous problems where the mesh parameter*

$$h = \pi/\overline{k} \tag{5.10}$$

is smaller than the shock width

$$l \ = \ \pi \ * \ \nu, \tag{5.11}$$

thus imposing the condition

$$h < l \tag{5.12}$$

One could state, that $\overline{k}$ should be approximately greater (or equal) than ν^{-1}, meaning that they are inversely proportional. The needed amount of resolved scales will then increase as we get closer to the inviscid case ($\nu = 0$), increasing naturally the numerical effort.

Consider again the third order moment system induced from the one-dimensional inviscid Burgers equation (4.1) with $0 < \varepsilon < 1$,

$$\frac{\partial u}{\partial t} + u\frac{\partial u}{\partial x} + \varepsilon \frac{\partial W}{\partial x} = 0 \tag{5.13a}$$

$$\frac{\partial W}{\partial t} + \frac{1}{3\varepsilon}\frac{\partial u}{\partial x} + u\frac{\partial W}{\partial x} = \frac{4\varepsilon}{15}\frac{\partial^2 W}{\partial x^2} - \frac{1}{\varepsilon}W. \tag{5.13b}$$

The additional term in (5.13a) which couples the first equation with the second one, introduces extra viscosity to the inviscid Burgers solution as we saw on the third chapter. One could expect, that the truncated FG-approximation of such a system acts as the truncated solution of Burgers equation with an included "subgrid model" if we compare it with LES (large eddy simulation) [34], in which the influence of small wavelength unresolved modes is included on the long wavelength resolved ones by means of an additional source term, yet in this case the extra modelling comes from the equation itself.

Theorem 5.1.2. *Let $\hat{u}_k$ and $\hat{w}_k$ be the Fourier coefficients of the solutions $u(x,t)$ and $W(x,t)$ respectively, and let $\overline{k}$ be again the cut-off wavenumber that truncates the Fourier series approximation (5.2) for both variables. The FG-spectral approximation of the third order moment system (5.13) satisfies the following nonlinear differential equations for modes within $\overline{k}$.*

$$\frac{\partial \hat{u}_k}{\partial t} + \frac{ik}{2} \sum_{n \in \mathbb{Z}_k(\overline{k})} \hat{u}_n \hat{u}_{k-n} + i\varepsilon k \hat{w}_k = 0 \tag{5.14a}$$

$$\frac{\partial \hat{w}_k}{\partial t} + i \sum_{n \in \mathbb{Z}_k(\overline{k})} n \hat{w}_n \hat{u}_{k-n} + \frac{ik}{3\varepsilon} \hat{u}_k = -\left(\frac{4\varepsilon}{15} k^2 + \frac{1}{\varepsilon}\right) \hat{w}_k \quad , \forall \mid k \mid \leqslant \overline{k} \tag{5.14b}$$

Proof. Using e^{ikx} as test function, the weak conservative form of (5.13b) and (5.13a) yield

$$\overbrace{\langle \partial_t u, e^{ikx} \rangle}^{\mathbf{a}} + \overbrace{\langle \partial_x (\frac{1}{2} u^2), e^{ikx} \rangle}^{\mathbf{b}} + \overbrace{\langle \partial_x (\varepsilon W), e^{ikx} \rangle}^{\mathbf{c}} = 0 \tag{5.15a}$$

$$\underbrace{\langle \partial_t W, e^{ikx} \rangle}_{\mathbf{d}} + \underbrace{\langle \partial_x (\frac{1}{3\varepsilon} u), e^{ikx} \rangle}_{\mathbf{e}} + \underbrace{\langle u \partial_x W, e^{ikx} \rangle}_{\mathbf{f}} = \underbrace{\langle \partial_x^2 (\frac{4\varepsilon}{15} W), e^{ikx} \rangle}_{\mathbf{g}} - \underbrace{\langle \frac{1}{\varepsilon} W, e^{ikx} \rangle}_{\mathbf{h}} \tag{5.15b}$$

One more time by replacing the Fourier series approximation of $u(x,t)$ and $W(x,t)$ according to (5.2), together with integration by parts and periodicity we develop each term. First for (5.15a), the terms **a** and **b** read the same as in the viscous Burgers case, (5.8a) and (5.8b) respectively. The last term **c** follows

$$\begin{aligned}
\mathbf{c} &= \langle \partial_x (\varepsilon W), e^{ikx} \rangle = \langle -\varepsilon W, \partial_x e^{ikx} \rangle = -\varepsilon \langle W, ike^{ikx} \rangle \\
&= ik\varepsilon \langle W, e^{ikx} \rangle = ik\varepsilon \langle \sum_l \hat{w}_l(t) e^{ilx}, e^{ikx} \rangle \\
&= ik\varepsilon \sum_l \hat{w}_l(t) \langle e^{ilx}, e^{ikx} \rangle = 2\pi ik\varepsilon \sum_l \hat{w}_l(t) \delta_{lk} \\
&= \boxed{2\pi ik\varepsilon \hat{w}_k(t)}
\end{aligned} \tag{5.16}$$

Putting (5.8a), (5.8b) and (5.16) together and dividing by 2π we reach (5.14a),

$$\boxed{\frac{\partial \hat{u}_k}{\partial t} + \frac{ik}{2} \sum_{n \in \mathbb{Z}_k(\overline{k})} \hat{u}_n \hat{u}_{k-n} + i\varepsilon k \hat{w}_k = 0 \qquad k \in \{-\overline{k}, ..., 0, ..., \overline{k}\},\ t \geq 0} \tag{5.17}$$

Next, we proceed as before for (5.15b):

$$\begin{aligned}\mathbf{d} &= \langle \partial_t \sum_l \hat{w}_l(t) e^{ilx}, e^{ikx} \rangle = \langle \sum_l \partial_t \hat{w}_l(t) e^{ilx}, e^{ikx} \rangle \\ &= \sum_l \partial_t \hat{w}_l(t) \langle e^{ilx}, e^{ikx} \rangle = 2\pi \sum_l \partial_t \hat{w}_l(t) \delta_{lk} \\ &= \boxed{2\pi \partial_t \hat{w}_k(t)}\end{aligned} \tag{5.18a}$$

$$\begin{aligned}\mathbf{e} &= \langle \partial_x (\frac{1}{3\varepsilon} \sum_l \hat{u}_l(t) e^{ilx}), e^{ikx} \rangle = \langle -\frac{1}{3\varepsilon} \sum_l \hat{u}_l(t) e^{ilx}, \partial_x e^{ikx} \rangle \\ &= \frac{ik}{3\varepsilon} \sum_l \hat{u}_l(t) \langle e^{ilx}, e^{ikx} \rangle = 2\pi \frac{ik}{3\varepsilon} \sum_l \hat{u}_l(t) \delta_{lk} \\ &= \boxed{2\pi \frac{ik}{3\varepsilon} \hat{u}_k(t)}\end{aligned} \tag{5.18b}$$

$$\mathbf{f} = \langle u \partial_x W, e^{ikx} \rangle = \boxed{2\pi \sum_n in \hat{w}_n(t) \hat{u}_{k-n}(t)} \tag{5.18c}$$

Note: $\sum_n in \hat{w}_n \hat{u}_{k-n} = (\widehat{uw_x})_k \longrightarrow$ Convolution sum

$$\begin{aligned}\mathbf{g} &= \frac{4\varepsilon}{15} \langle \partial_x^2 \sum_l \hat{w}_l(t) e^{ilx}, e^{ikx} \rangle = \frac{4\varepsilon}{15} \sum_l \hat{w}_l(t) \langle (il)^2 e^{ilx}, e^{ikx} \rangle \\ &= -\frac{4\varepsilon}{15} \sum_l l^2 \hat{w}_l(t) \langle e^{ilx}, e^{ikx} \rangle = -(2\pi) \frac{4\varepsilon}{15} \sum_l l^2 \hat{w}_l(t) \delta_{lk} \\ &= \boxed{-(2\pi) \frac{4\varepsilon}{15} k^2 \hat{w}_k(t)}\end{aligned} \tag{5.18d}$$

$$\begin{aligned}\mathbf{h} &= \frac{1}{\varepsilon} \langle \sum_l \hat{w}_l(t) e^{ilx}, e^{ikx} \rangle = \frac{1}{\varepsilon} \sum_l \hat{w}_l(t) \langle e^{ilx}, e^{ikx} \rangle \\ &= \frac{2\pi}{\varepsilon} \sum_l \hat{w}_l(t) \delta_{lk} = \boxed{\frac{2\pi}{\varepsilon} \hat{w}_k(t)}\end{aligned} \tag{5.18e}$$

Again, putting (5.18a), (5.18b), (5.18c), (5.18d) and (5.18e) together and dividing by 2π we recover (5.14b)

$$\boxed{\frac{\partial \hat{w}_k}{\partial t} + \sum_{n \in \mathbb{Z}_k(\overline{k})} in\hat{w}_n\hat{u}_{k-n} + \frac{ik}{3\varepsilon}\hat{u}_k = -\left(\frac{4\varepsilon}{15}k^2 + \frac{1}{\varepsilon}\right)\hat{w}_k \qquad k \in \{-\overline{k}, ..., 0, ..., \overline{k}\},\ t \geq 0} \tag{5.19}$$

□

For numerical purposes explained in the coming section, an artificial viscous term ν_* is included in (5.20a), the resulting ODE system will then read

$$\frac{\partial \hat{u}_k}{\partial t} + \frac{ik}{2} \sum_{n \in \mathbb{Z}_k(\overline{k})} \hat{u}_n\hat{u}_{k-n} + i\varepsilon k\hat{w}_k = \boxed{-\nu_* \mathbf{k^2}\hat{\mathbf{u}}_\mathbf{k}} \tag{5.20a}$$

$$\frac{\partial \hat{w}_k}{\partial t} + i \sum_{n \in \mathbb{Z}_k(\overline{k})} n\hat{w}_n\hat{u}_{k-n} + \frac{ik}{3\varepsilon}\hat{u}_k = -\left(\frac{4\varepsilon}{15}k^2 + \frac{1}{\varepsilon}\right)\hat{w}_k \quad ,\forall \mid k \mid \leqslant \overline{k}. \tag{5.20b}$$

ODEs systems (5.4) and (5.20) are solved numerically using the Matlab solver `ode45` based on an explicit Runge-Kutta 4 formula [27].

5.2 Numerical Experiments for a Fourier-Galerkin spectral approximation

Since we want to study a periodic problem, the initial condition for (5.1) will be given by the sinusoidal wave

$$u(x, 0) = -sin(x), \tag{5.21}$$

in wavenumber space the same condition reads,

$$\hat{u}_k(0) = \begin{cases} 0 & \text{for } \mid k \mid \neq 1 \\ ik/2 & \text{for } \mid k \mid = 1\ . \end{cases} \tag{5.22}$$

In time, the energy transfer to higher modes coming from the nonlinear hyperbolic equation (5.1) with $\nu \to 0$ will turn the smooth initial condition (5.21) into discontinuities, this

special feature will be our main interest through out this chapter. Additionally, we set $W(x,0) = 0$ as initial condition for KIMS (5.13).

In order to compare the spectral characteristics of the viscous Burgers equation (5.1) with those of the KIMS model (5.13) for $\nu \to 0$, we perform different numerical experiments in time with $\Delta t = 0.1$, following the procedure below:

1. We compute a benchmark solution (called here **DNS** in analogy to turbulent flows) by solving the viscous Burgers equation (5.1) in a fine grid able to resolve accurately the shock wave. The FG- approximation is done accordingly with (5.4) and its respective cut-off wavenumber $\overline{k}_{DNS}$ will be given by the viscosity value according to (5.12). This solution will work as a reference frame.

2. We solve the viscous Burgers equation (5.1) in a coarse grid such that $h \gg l$ (**Burgers**), using different viscosity values ν. For each ν the coarse solutions are computed using different cut-off wavenumber $\overline{k}$.

3. We solve the moment system (5.20) in a coarse grid such that $h \gg l$ for different values of ε. (**KIMS ε = ...**)

$$\varepsilon = \{0.0005,\ 0.001,\ 0.005,\ 0.01,\ 0.05,\ 0.1\} \tag{5.23}$$

The $l2 - error$ will helps us to quantify the differences between the previous experiments, it is defined in the resolved scales as:

$$l_2(t) = \sqrt{\frac{\sum_{k=0}^{N} |E(k) - E^N(k)|^2}{\sum_{k=0}^{N} E(k)^2}} \tag{5.24}$$

where $N = \overline{k}$ is the cut-off wavenumber of the coarse grid approximations 2. and 3. with $E^N(k)$ their respective solution. $E(k)$ refers to the benchmark solution (DNS). The results are presented in physical space $\{u^N(x,t)\}$ as in wavenumber space $\{E(k) =\mid \hat{u}_k \mid$, *Fourier*

coefficients magnitude} together with the $l2-error$ of the Fourier coefficients with respect to the DNS.

5.2.1 $\nu_* = 0$

First, we look into how the third order moment system (5.20) for Burgers equation performs numerically without including the artificial viscosity term in (5.20a), hence we consider $\nu_* = 0$. Then following the procedure previously described, we set a benchmark solution (**DNS**) with $\nu = 3.5 \times 10^{-4}$ together with $\overline{k}_{DNS}(N) = 3000$ according to the condition (5.12) and compare it with the coarse approximations of (5.20) for the different ε values in (5.23), and with the viscous Burgers approximation (5.4) using the three different viscosity values presented in (5.25).

$$\nu = \{0.00035,\ 0.001,\ 0.0035\}. \tag{5.25}$$

We now need to define the different coarse cut-off wavenumbers (N) in order to compute these coarse approximations for which ($h \gg l$) holds, they are

$$N = \{100,\ 75,\ 50,\ 25\}. \tag{5.26}$$

For each one of the previous cases, we analyse the numerical results obtained for $E(k)$ and $u^N(x,t)$ (for simplicity the latest will be referred as $u(x,t)$ from now on) at different time moments until $t = 3.5$ is reached, and present those whose outcome is most relevant.

Results

At early times ($\boldsymbol{t = 0.1}$), the solution presented in Fig. 5.1 for $N = 50$ stays smooth and the energy is conserved since the shock is not yet formed, consequently independent of the values used for the viscosity (Burgers) and epsilon (KIMS) the energy has a stable nonlinear decay as we move closer to the cut-off wavenumber, this will happen even for the smallest N value (see Fig. A.1 for the results on $N = 100, 75, 25$ at $t = 0.1$). For KIMS $\varepsilon = 0.1$ (the biggest value used for ε) there is small increase in the energy for modes approximately

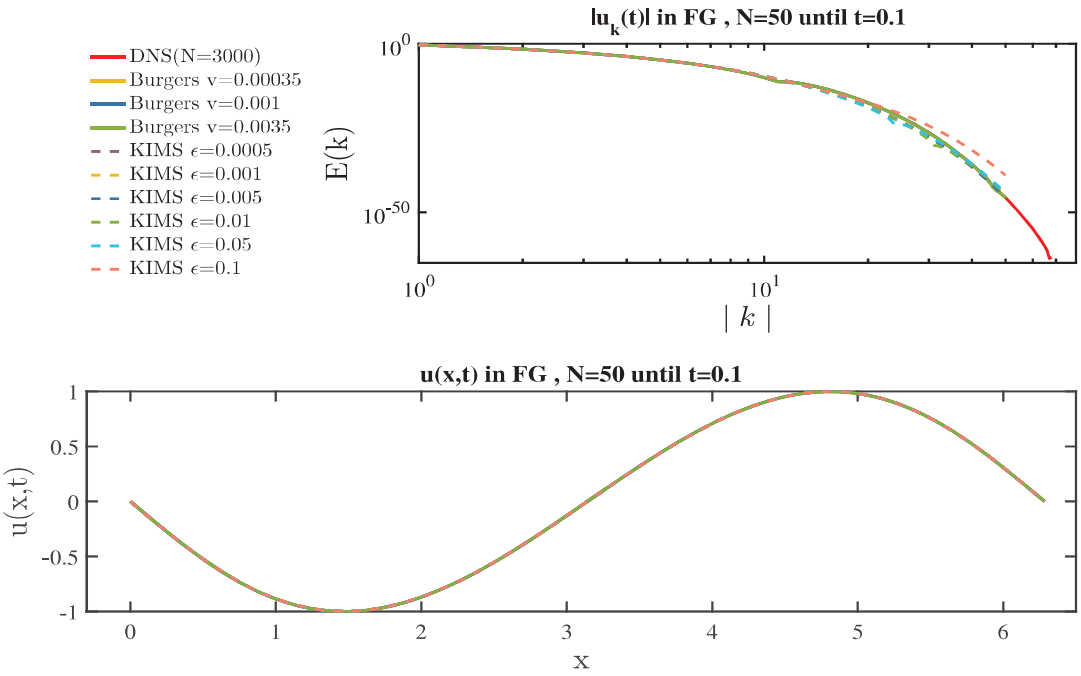

Figure 5.1: $E(k)$ **and** $u(x,t)$ **for the DNS and coarse grid solution** $N = 50$ **at** $t = 0.1$**.**

bigger than $k \approx 25$, which can be observed up to $N = 50$.

After $\boldsymbol{t = 1}$ the shocks around $x = 0$ and $x = 2\pi$ start to form, creating a sawtooth-like shape. The DNS corresponding energy decreases linearly (in a logarithmic scale) and we begin to see some differences with respect to the other solutions.

Two main events occur: First, for every viscous Burgers and KIMS with ε from 5×10^4 to 0.01 there is an accumulation of energy near the cut-off wavenumber, for the smallest values of ν and ε the energy increase starts sooner and the peaks reached by the oscillations are higher than for the rest. This pile of energy translates into small amplitude waves with a node around $x = \pi$ (Fig. 5.2a), which decreases amplitude as we reduce the number of resolved modes since the energy pile has also lower peaks (Fig. 5.2b). Second, the energy for KIMS $\varepsilon = \{0.05, 0.1\}$ decays sooner than that of the DNS approximation and has an almost linear behaviour without oscillations, thus it will not generate extra waves in the

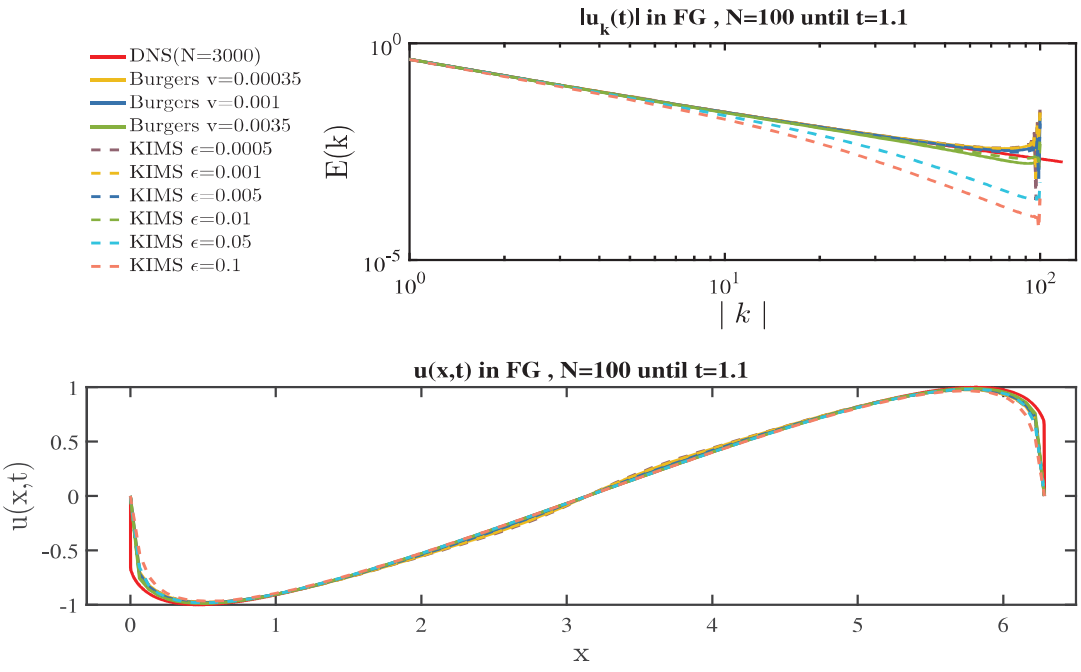

(a) $N = 100$

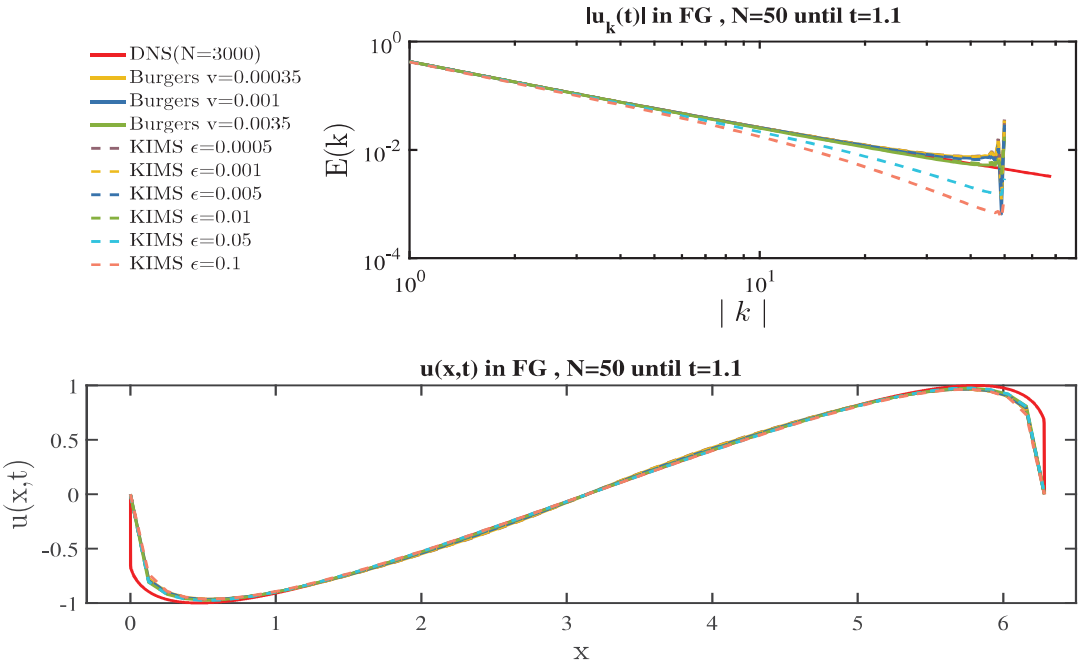

(b) $N = 50$

Figure 5.2: $E(k)$ **and** $u(x,t)$ **for the DNS and coarse grid solutions at** $t = 1.1$**.**

physical space solution.

Furthermore, the approximation of the forming shocks along all the different solutions looks rather similar, and we can observe how the steepness decreases from $N = 100$ to the smaller cut-off wavenumber $N = 50$. Additional results using $N = 75, 25$, can be see in Fig. A.2.

At $\boldsymbol{t = 3.5}$ when shock waves are already form, the energy transfer from smaller modes to bigger ones increases for some approximations, which will not converge in the physical space to the DNS.

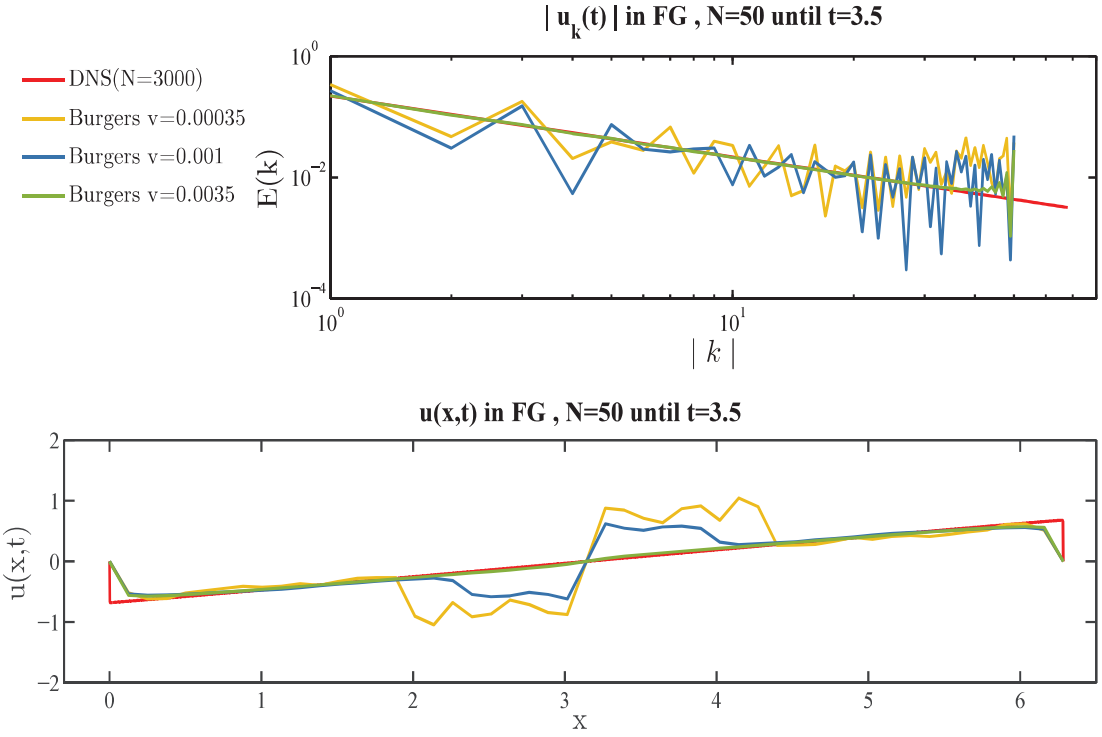

(a) $N = 50$ for Burgers with coarse grid

Namely, as we start reducing the number of resolved modes starting at $N = 100$ until $N = 25$, higher oscillations become more and more present for increasing viscosity in

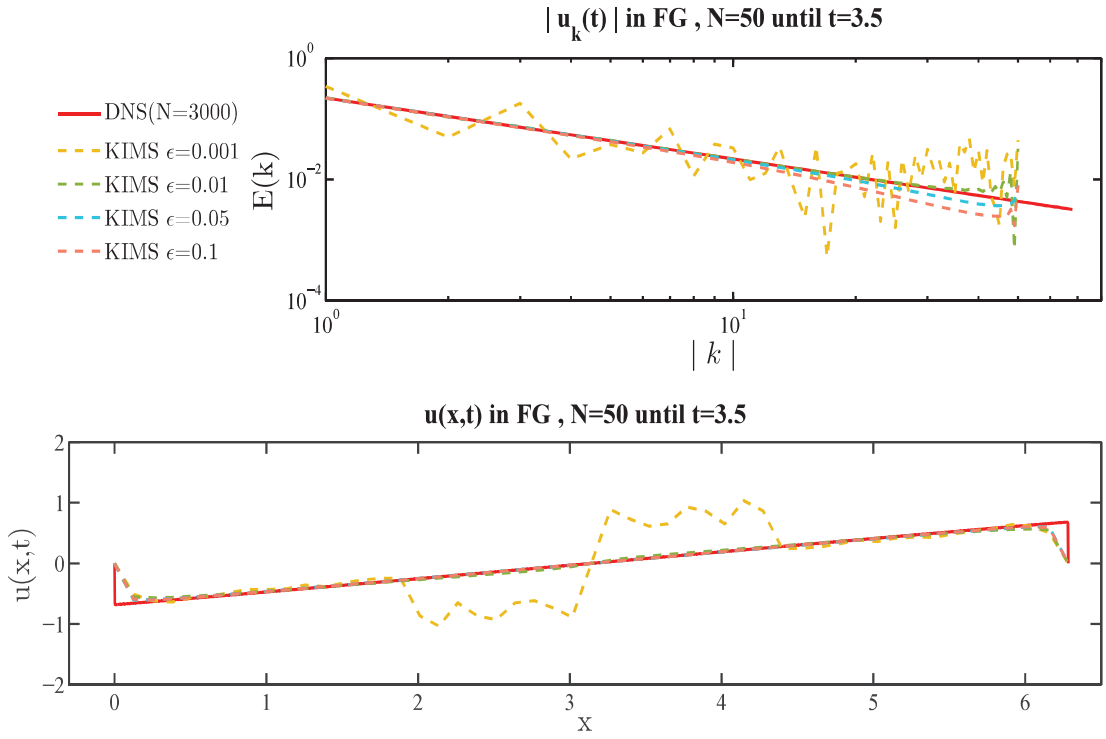

(b) $N = 50$ for KIMS with coarse grid

Figure 5.3: $E(k)$ **and** $u(x,t)$ **for the DNS and coarse grid solutions** $N = 50$ **at** $t = 3.5$**.**

the case of Burgers and for increasing ε in the case of KIMS. With $N = 50$, Burgers $\nu = \{0.35, 1\} \times 10^{-3}$ (Fig. 5.3a) together with KIMS $\varepsilon = \{0.5, 1, 5\} \times 10^{-3}$ (Fig. 5.3b) show to be unstable, we have reduced and divided the results in order to make them clearer, the complete solutions can be found in Fig. A.3c. It is then clear, that even for a small quantity of resolved modes, the remaining solutions KIMS $\varepsilon = \{0.05, 0.1\}$ (Fig. 5.3b) stay stable and converge to the DNS, yet keeping a slightly faster decaying energy as we observed at the previous time.

The complete set of results are shown in Fig. A.3, where we can observe that for $N = 100$ (Fig. A.3a) Burgers $\nu = 3.5 \times 10^{-4}$ and KIMS $\varepsilon = \{0.5, 1\} \times 10^{-3}$ present already bigger oscillations, later for $N = 75$ (Fig. A.3b) oscillations increase in Burgers $\nu = 1 \times 10^{-3}$,

for $N = 50$ (Fig. A.3c) in KIMS $\varepsilon = 5 \times 10^{-3}$ and for $N = 25$ (Fig. A.3d) in Burgers $\nu = 1 \times 10^{-3}$ and KIMS $\varepsilon = 0.01$.

Additionally, if we take a closer look to the approximation of the shock, the steepness of the shock wave will decrease accordingly to the amount of resolved modes included in the computations, as observed also at $t = 1.1$. On the other hand, the instabilities originated at $x = \pi$ will reach the shocks at lower values of the cut-off wavenumber where they have started. If we also observe closer the energy accumulation around the cut-off wavenumber, we can notice that less energy is transferred for smaller values of N. Fig. A.4 displays the results for all values of N at $t = 3.5$ zooming in the shock location.

- **l2-error**

Next, accordingly with (5.24) we compute the *l2-error* for different times and compare the results of the approximations already presented. We have by now made the distinction between two groups of solutions. The first one, consisting of Burgers with all the viscosity values and KIMS $\varepsilon = \{0.5, 1, 5, 10\} \times 10^{-3}$, and the second one KIMS $\varepsilon = \{0.05, 0.1\}$.

For the first group until the shock is formed at $t = 1$ the solutions are almost identical, after that the error will increase continuously starting for KIMS $\varepsilon = \{0.5, 1\} \times 10^{-3}$ and Burgers $\nu = 3.5 \times 10^{-4}$ with $N = 100$ (Fig. 5.4a), followed by Burgers $\nu = 1 \times 10^{-3}$ with $N = 75$ (Fig. 5.4b), then by KIMS $\varepsilon = 5 \times 10^{-3}$ with $N = 50$ (Fig. 5.4c) and finally by KIMS $\varepsilon = 0.01$ and Burgers $\nu = 3.5 \times 10^{-3}$ with $N = 25$ (Fig. 5.4d). It is of note, that the error increments occur first for the lowest values of viscosity and the smallness parameter and gradually as the resolved modes are decreased the next value follows. Moreover, we can identify pairs of parameters where the results behave quite similar, is the case of Burgers $\nu = 0.35 \times 10^{-3}$ with KIMS $\varepsilon = 1 \times 10^{-3}$, also Burgers $\nu = 1 \times 10^{-3}$ with KIMS $\varepsilon = 5 \times 10^{-3}$, and Burgers $\nu = 3.5 \times 10^{-3}$ with KIMS $\varepsilon = 10 \times 10^{-3}$.

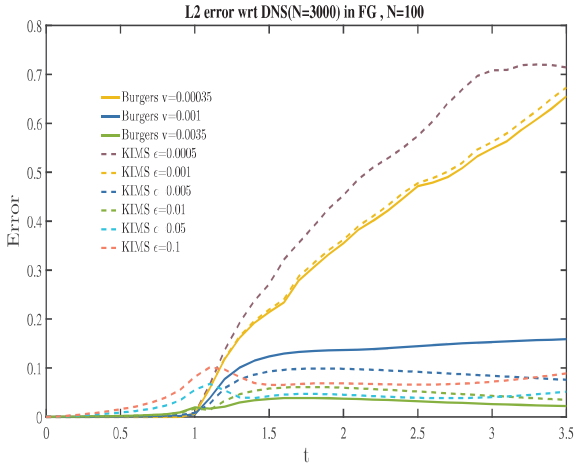

(a) $N = 100$

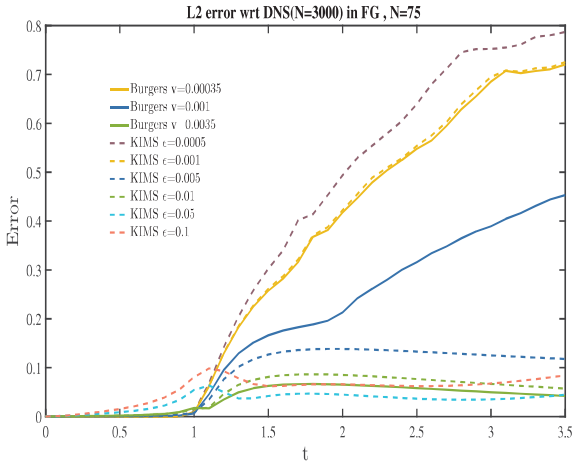

(b) $N = 75$

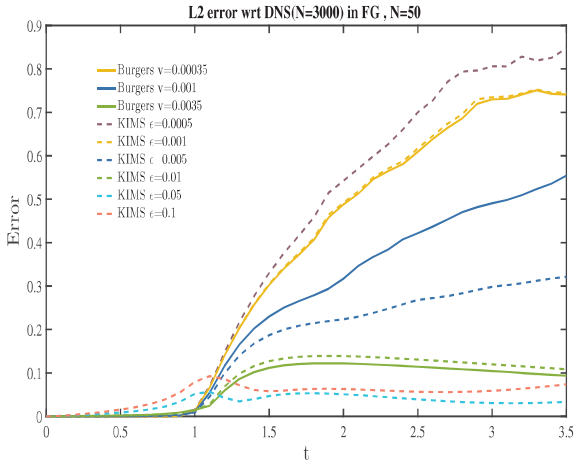

(c) $N = 50$

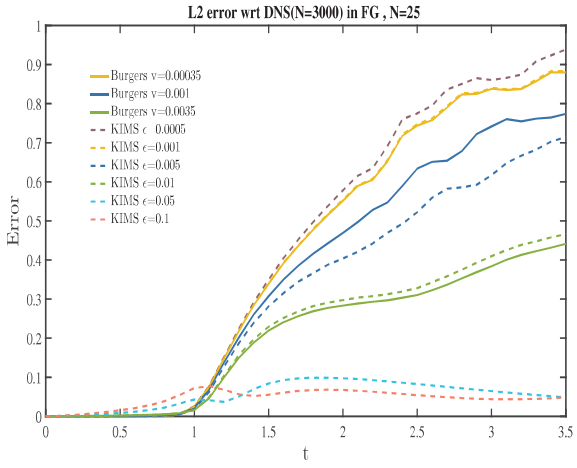

(d) $N = 25$

Figure 5.4: $l2$**-error as a function of time for** $u_0 = -sin(x)$**.**

The second group will have a higher jump around the time when the shock forms, followed by a decrease which leaves the error at a rather stable value along the changes of the cut-off wavenumber (Fig. 5.4). This means that for a ε around the order of $O(10^{-1})$ the

third order moment system (5.13) includes the significant effects of the unresolved modes into the resolved ones even for small N which provides a stable solution, nevertheless the steepness of the shock approximation will suffer the spared modes.

5.2.2 $\nu_* = \nu$

Next, we will include the artificial viscosity ν_* in (5.20a), which will take up on the same values as those used for the viscous Burgers equation (Table 5.1). Differently to the previous section with ($\nu_* = 0$), where only one DNS solution with its respective viscosity was defined to which all of the coarse grid cases of viscous Burgers and KIMS where compared to, here each one of the five viscous cases determines the amount of resolved modes (N_{DNS}) needed in order that the condition (5.12) holds, imposing the benchmark solution DNS corresponding to the case. This is done given that now the FG spectral approximation of KIMS (5.20) varies not only with respect to the parameter ε but with ν_* also.

#	$\boldsymbol{\nu}$	$\boldsymbol{l}$	$\boldsymbol{N_{DNS}}$	$\boldsymbol{h_{DNS}}$
1	$\mathbf{0.35 \times 10^{-3}}$	1.1×10^{-3}	**3000**	3.3×10^{-4}
2	$\mathbf{1 \times 10^{-3}}$	3.14×10^{-3}	**1010**	9.9×10^{-4}
3	$\mathbf{3.5 \times 10^{-3}}$	1.1×10^{-2}	**300**	3.3×10^{-3}
4	$\mathbf{10 \times 10^{-3}}$	3.14×10^{-2}	**110**	9.1×10^{-3}
5	$\mathbf{35 \times 10^{-3}}$	1.1×10^{-1}	**50**	2×10^{-2}

Table 5.1: Viscosity values with their respective shock width (5.11), cut-off wavenumber (5.12) and mesh parameter (5.10)

In the first place, we will compute the coarse grid approximations of the viscous Burgers (5.1) and of KIMS (5.20) for different ε values in (5.23), with a chosen viscosity ν given in Table 5.1, afterwards we compare them with the corresponding DNS solution. The choice of

the different cut-off wavenumbers (N) from Table 5.2 used to discretize the coarse grid examples is given accordingly with the related N_{DNS}, in order that they will agree with $h \gg l$.

$\boldsymbol{N}$	**500**	**250**	**200**	**150**	**100**
$\boldsymbol{h}$	2×10^{-3}	4×10^{-3}	5×10^{-3}	6.7×10^{-3}	1×10^{-2}

$\boldsymbol{N}$	**50**	**30**	**25**	**15**
$\boldsymbol{h}$	2×10^{-2}	3.3×10^{-2}	4×10^{-2}	6.7×10^{-2}

Table 5.2: Coarse cut-off wavenumbers N with their corresponding mesh parameter h given by (5.10)

The five different settings for the numerical experiments corresponding to each viscosity value in Table 5.1 read,

	$\boldsymbol{\nu}$	$\boldsymbol{N_1}$	$\boldsymbol{N_2}$	$\boldsymbol{N_3}$	$\boldsymbol{N_4}$
1	$\mathbf{0.35 \times 10^{-3}}$	500	250	100	50
2	$\mathbf{1 \times 10^{-3}}$	500	200	100	50
3	$\mathbf{3.5 \times 10^{-3}}$	150	50	25	–
4	$\mathbf{10 \times 10^{-3}}$	50	30	15	–
5	$\mathbf{35 \times 10^{-3}}$	25	15	–	–

Table 5.3: Coarse cut-off wavenumbers N chosen for each experiment

Results

We start by analysing **case 1** in Table 5.3. Fig. 5.5 shows as the kinetic energy decay in every solution for each value of N at initial times ($\boldsymbol{t = 0.5}$) for $N = 500$. We can observe an early agglomeration of the energy cascade for the DNS with the coarse Burgers solution

which start decaying sooner than the rest, together with the coarse KIMS solutions except for $\varepsilon = 0.1$ which is the highest ε value and the last one to decay. As we decrease N the energy cascade is then shortened without exhibiting mayor changes in its values. The results for each cut-off wavenumber in Table 5.3 with $\nu = 0.35 \times 10^{-3}$ can be seen in Fig. B.1.

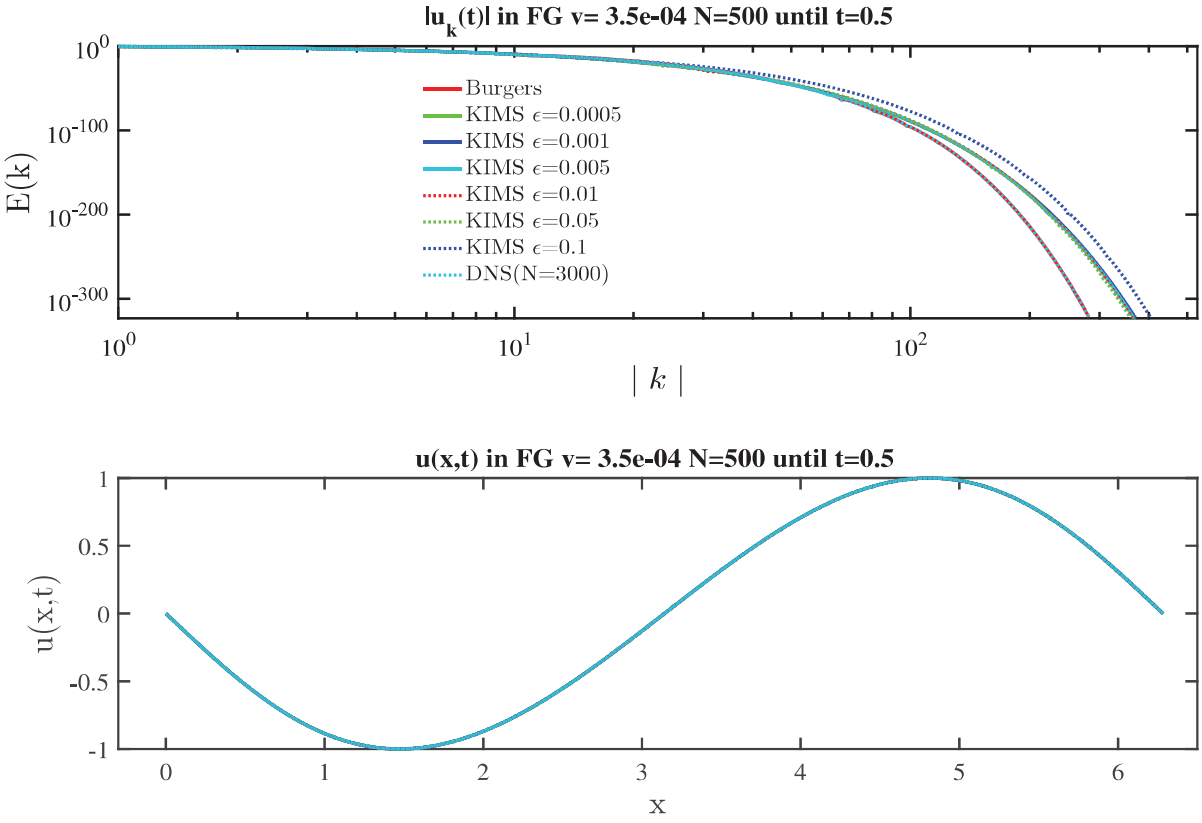

Figure 5.5: $E(k)$ **and** $u(x,t)$ **for the DNS and coarse grid solutions** $N = 250$ **at** $t = 0.5$**.**

The previous results are in-line with what we have already observed for $\nu_* = 0$, where the influence of viscosity and the smallness parameter are minimal for times prior to $t = 1$. In terms of $u(x,t)$ we still can not see significant differences in the solutions. As for the rest of cases described in Table 5.3, their outcome is quite similar for initial times to **case 1**, thus we do not extent this analysis to them.

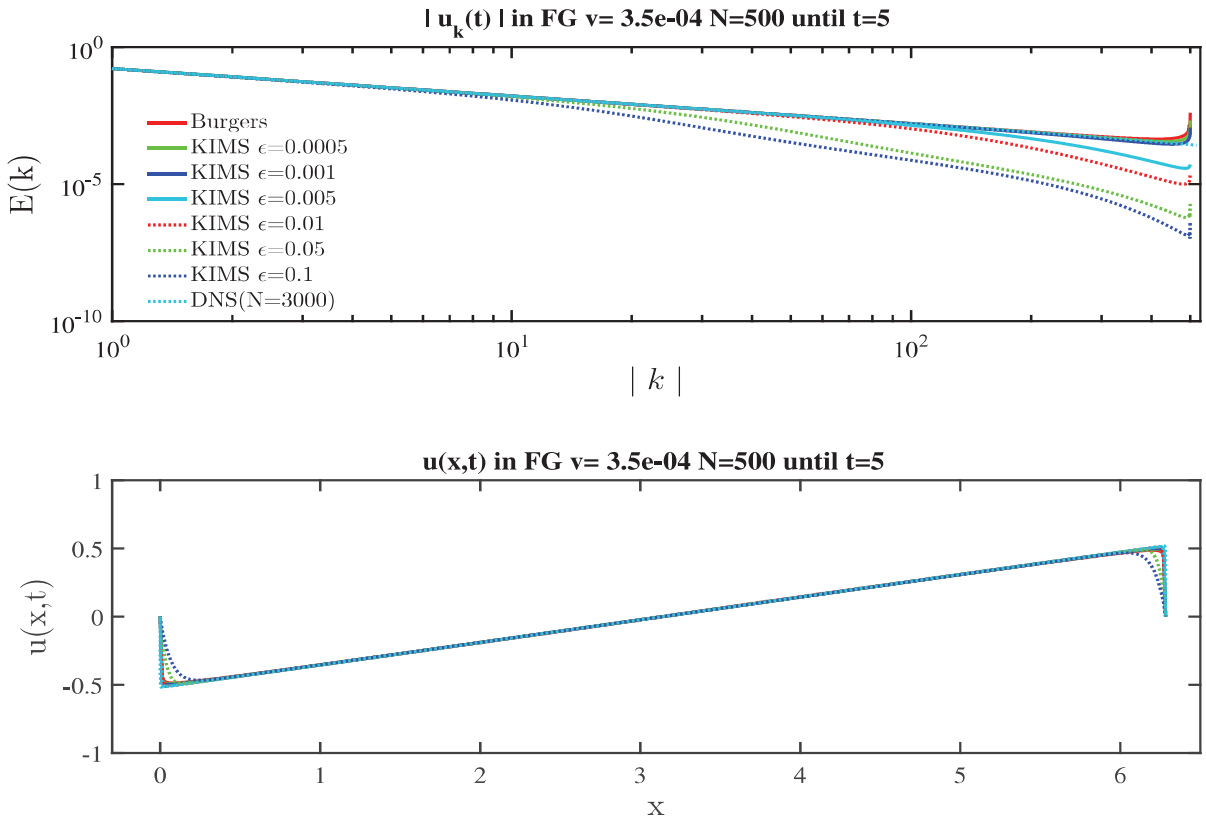

(a) $N = 500$

After $\boldsymbol{t = 1.5}$ the shock is forming and the energy starts to be transferred from the small scales to the modes near the cut-off wavenumber, by $\boldsymbol{t = 5}$ the shock is defined and decreasing, thus diminishing the kinetic energy decay. In **case 1** which uses the smallest viscosity value, as we decrease N from 500 to 50, we start observing oscillations which increase specially in the cut-off area, in the physical space these oscillations are translated into a jump in $u(x,t)$ around $x = \pi$, larger oscillations mean a larger and longer jump (Fig. 5.6). On the other hand, the smooth part of $u(x,t)$ showed by the DNS remains smooth for KIMS approximations with the biggest values of ε even for smallest amount of resolved scales $N = 50$ (Fig. B.2d).

For the biggest amount of resolved modes $N = 500$ (Fig. 5.6a) the coarse KIMS kinetic energy for $\varepsilon = \{1, 0.5\} \times 10^{-3}$ together with the coarse viscous Burgers will decay at the

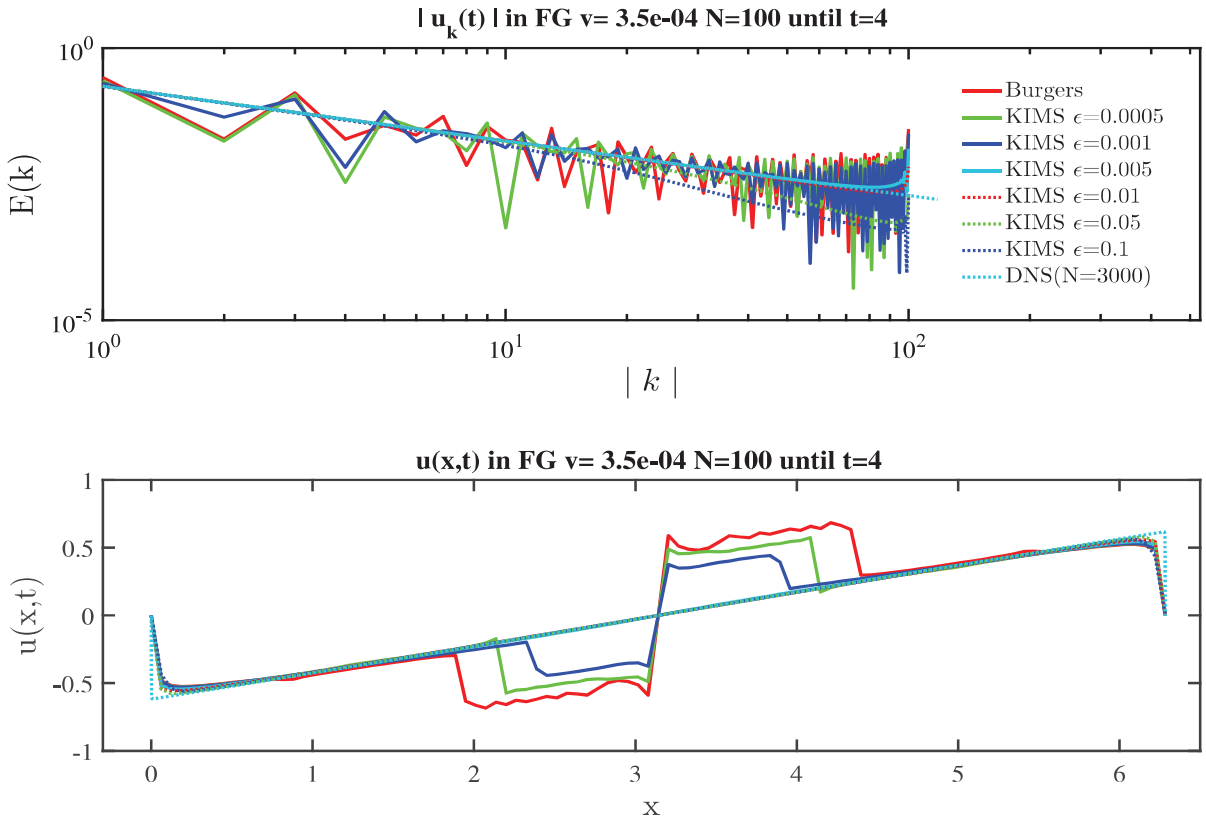

(b) $N = 100$

Figure 5.6: $E(k)$ **and** $u(x,t)$ **for the DNS and coarse grid solutions at** $t = 5$**.**

same rate as the DNS does, while the rest of solutions start decaying sooner beginning with the biggest $\varepsilon = 0.1$. By $N = 100$ in Fig. 5.6b the coarse viscous Burgers and KIMS with $\varepsilon = \{1, 0.5\} \times 10^{-3}$ have started to oscillate. The resting outcomes can be found in Fig. B.2, where we can see in detail that for $N = 250$ in Fig. B.2b only the coarse viscous Burgers oscillate, and by $N = 50$ in Fig. B.2d KIMS with $\varepsilon = 5 \times 10^{-3}$ joins the previous ones.

With regard to the shock approximation, in Fig. B.3 we show a closer look to the solutions behaviour around the shock area and the kinetic energy near the cut-off wavenumber. For $N = 500$ in Fig. B.3a only KIMS with $\varepsilon = \{0.1, 0.05\}$ have a significant difference with the DNS. As for $N = 250$ in Fig. B.3b the gap with respect to the DNS increases for the coarse

viscous Burgers and KIMS with the smallest values of ε which as seen in Chapter 3 will follow Burgers closely. Finally for $N = 50$ in Fig. B.3d the coarse viscous Burgers solution appears to bring the least accurate approximation of the shock wave.

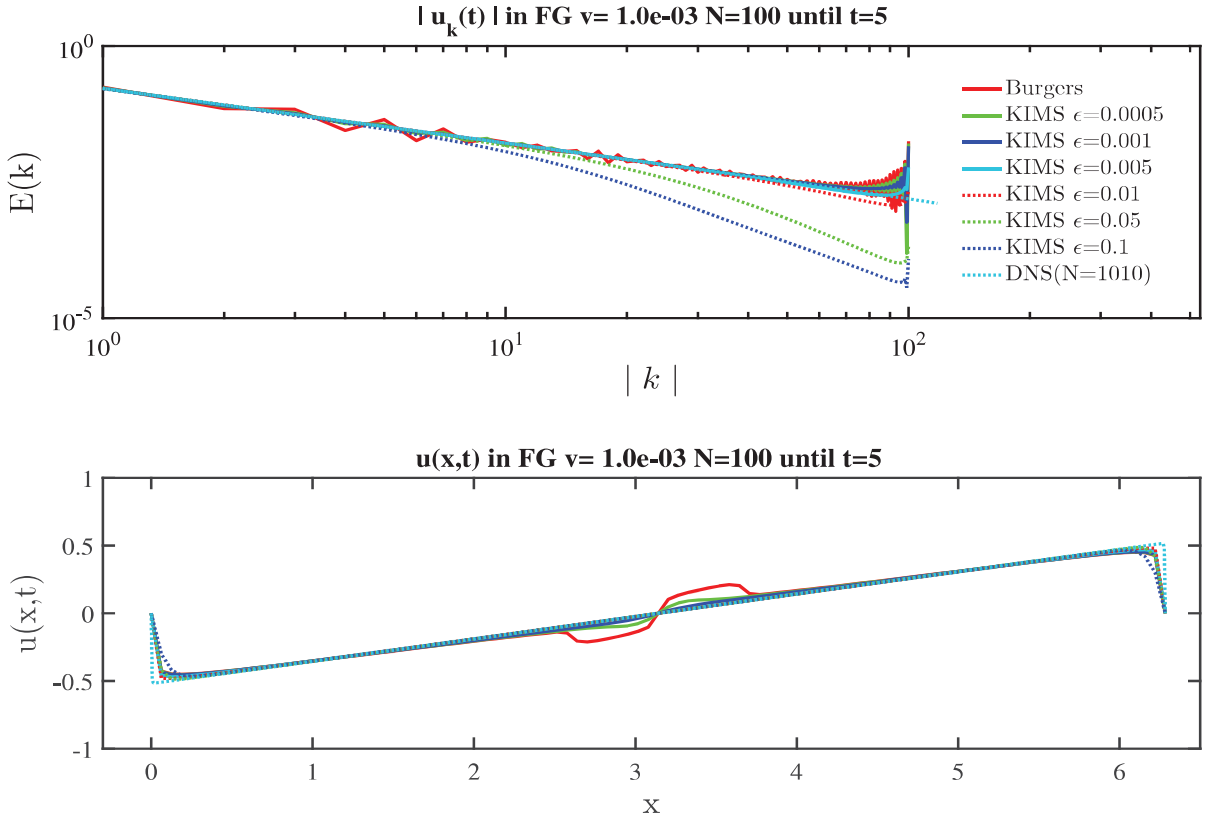

Figure 5.7: $E(k)$ **and** $u(x,t)$ **for the DNS and coarse grid solutions** $N = 100$ **at** $t = 5$**.**

We increase the viscosity value to $\nu = 1 \times 10^{-3}$ as we continue to **case 2**, therefore the number of resolved scales needed to achieve a stable approximation (N_{DNS}) is lower. The first coarse example with $N = 500$ contains half of the resolved scales with respect to the DNS, while previously it was a sixth. The behaviour of all the solutions span sticks to the same pattern seen before using a smaller viscosity, with the difference that in this case we start to observe oscillations only by $N = 100$ in Fig. 5.7 beginning with the coarse Burgers approximation, while for **case 1** this starts happening already for $N = 250$. By $N = 50$

KIMS with $\varepsilon = \{0.5, 1\} \times 10^{-3}$ have followed (Fig. B.4d). All of the numerical experiments for $N = 500, 200, 100, 50$ cab be seen in Fig. B.4.

Moreover, the shock resolution in this example is quite coherent with the one already observed in the previous case, not only in the way it evolves but also in the number of resolved scales. In Fig. B.5a ($N = 500$) we obtained some very good estimates, by $N = 50$ the distance with respect to the DNS has grown around the shock for all approximations in an almost equal magnitude. Details in Fig. B.5.

In **case 3** by increasing again the viscosity to $\nu = 3.5 \times 10^{-3}$ we get a cut-off wavenumber $N_{DNS} = 300$, less than half of the resolved scales used in the second example. We start the experiments by using half of the scales needed for stability $N = 150$ and go until one twelfth $N = 25$. The energy cascade looks quite stable for $N = (150, 50)$ presenting the same behaviour already seen in Fig. 5.6a for **case 1**, the corresponding results are showed in Figures B.6a and B.6b. Oscillations only appear for $N = 25$ in Fig. B.6c increasing in the usual approximations order and even touching KIMS $\varepsilon = 0.01$. As for the shock approximation, we do not get any surprises, there is a quite standard gap between DNS and the coarse solutions as the resolved scales are reduced, that is relatively similar to all, still KIMS with $\varepsilon = 0.1$ has a slightly better approximation of it by $N = 25$.

In **case 4** we have reached now a viscosity of order 10^{-2}. As we could observe in the previous experiments for bigger ν, oscillations appear along the energy cascade only for really coarse mesh with a smaller amplitude and frequency, which we can visualize in the Appendix Fig. B.8. Furthermore, for $N = 15$ (Fig. 5.8) is clear how oscillations reach faster KIMS approximations with bigger values of ε, going up until $\varepsilon = 0.01$. The behaviour of coarse approximations in terms of the shock resolution deteriorates faster than in the previous experiments, results are shown in Fig. B.9.

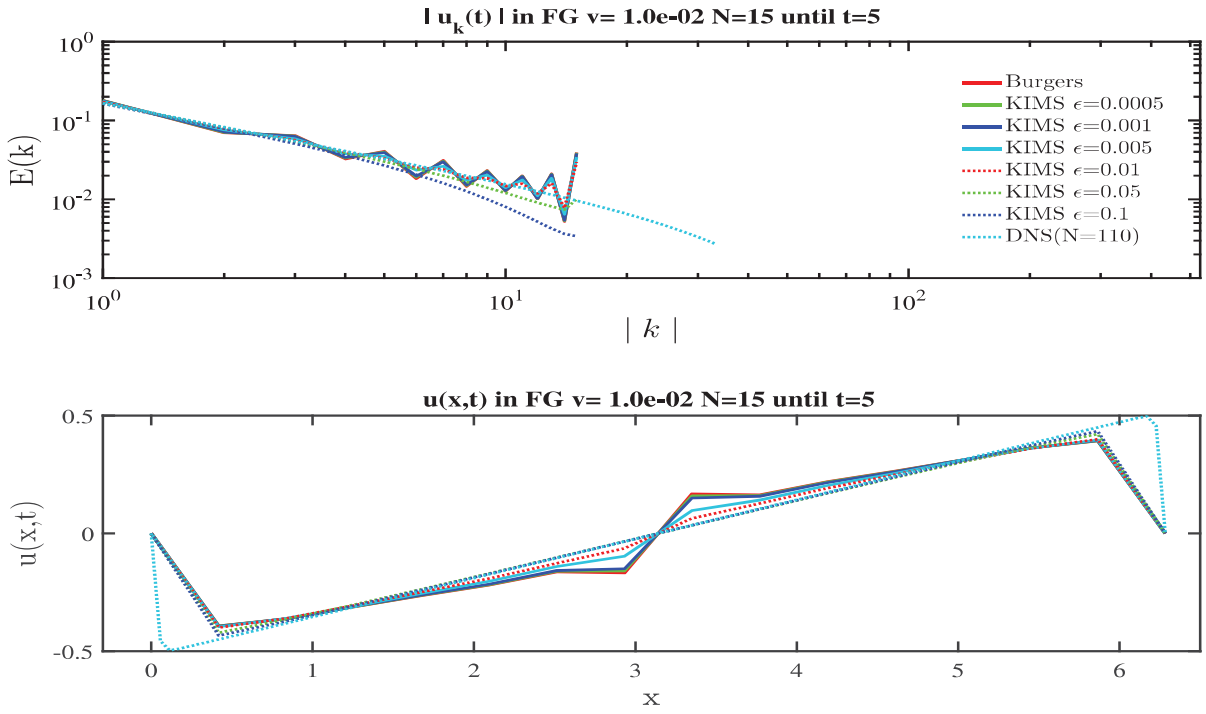

Figure 5.8: $E(k)$ and $u(x,t)$ for the DNS and coarse grid solutions $N = 15$ at $t = 5$.

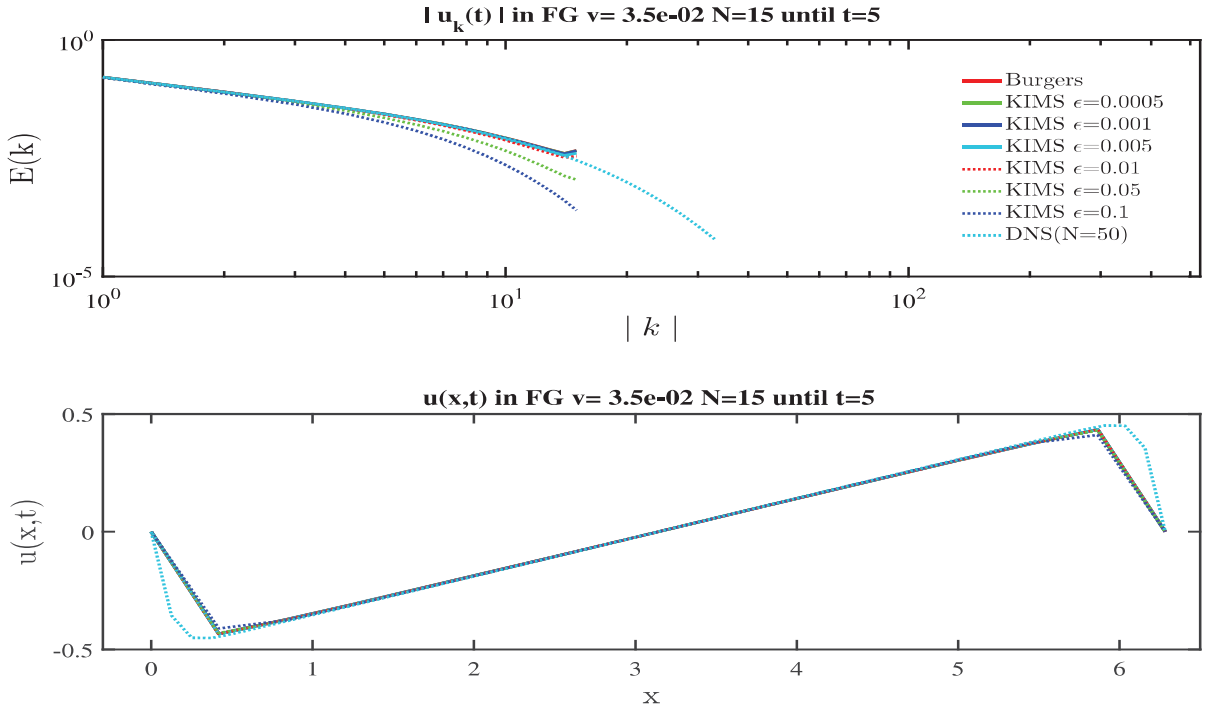

Figure 5.9: $E(k)$ and $u(x,t)$ for the DNS and coarse grid solutions $N = 15$ at $t = 5$.

With the last viscosity increase in **case 5**, we get the smallest cut-off wave number. In this case even for a small amount of resolved scales $N = 15$ (Fig. 5.9) there is no trace of oscillations along the energy cascade. In this case, the coarse viscous Burgers approximation keeps on being a good choice even for a really coarse mesh, this comes from the fact that $N = 15$ is just a third of the considered N_{DNS}. The complete ensemble of results are given in Fig. B.10.

- **l2-error**

Last of all, we monitor the accuracy evolution of each one of the five viscous numerical examples (Table 5.3) as we decrease the number of resolved scales N by computing the *l2-error* (5.24).

One more time, we begin with the smallest viscosity value in Table 5.3. In **case 1**, the coarse viscous Burgers and KIMS approximations with $\varepsilon = \{0.5, 1\} \times 10^{-3}$ expose a similar behaviour in time for every N. Until $t \approx 1$ we observe that there is almost no difference with the benchmark solution DNS, after that a big jump occurs around the same time where the shock is starting to form. For N in Fig. 5.10a we can see a pattern in the evolution, which at $t \approx 1.7$ reaches a maximum followed by a smooth decay until $t \approx 5$, where the shock is now disappearing. As we decrease N their $l2 - error$ increases notably, being the Burgers the first one to disrupt the pattern noticed before (Fig. 5.10b), but followed in the next cases by the two KIMS solutions (Figures 5.10c and 5.10d) and surpassing all the other approximations.

Furthermore, KIMS approximations with $\varepsilon = \{0.05, 0.1\}$ maintain a stable behaviour and magnitude throughout all the values of N, having an initial peak at $t \approx 1$ together with the shock formation and followed by a decrease around $t \approx 1.7$ with a subsequent increase which continues in time. We can see in Fig. 5.10a how these solutions have almost the opposite behaviour as the three ones discussed above. For $N = 500$ we get the highest

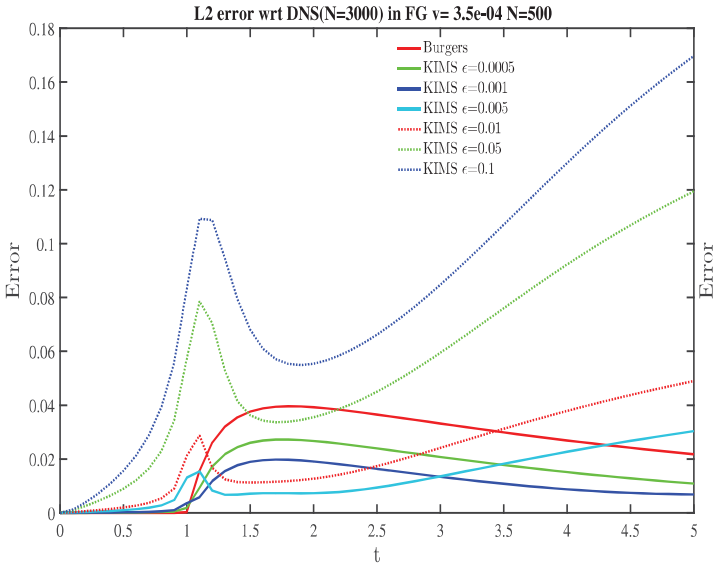

(a) $N = 500$

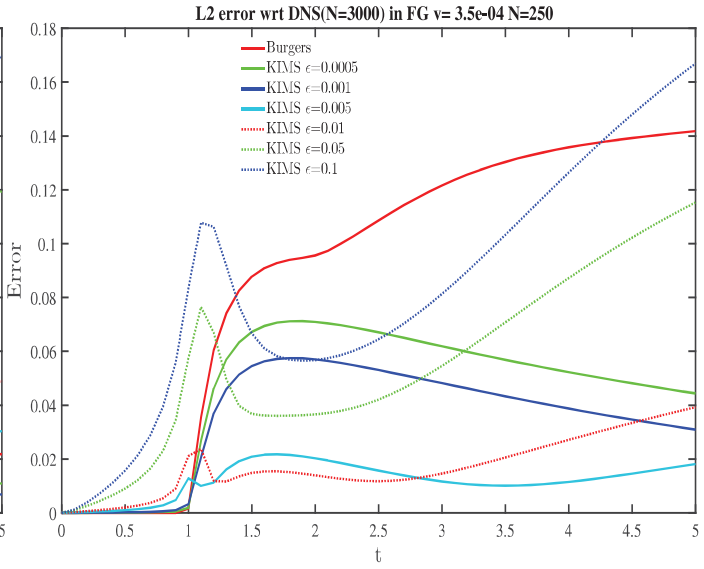

(b) $N = 250$

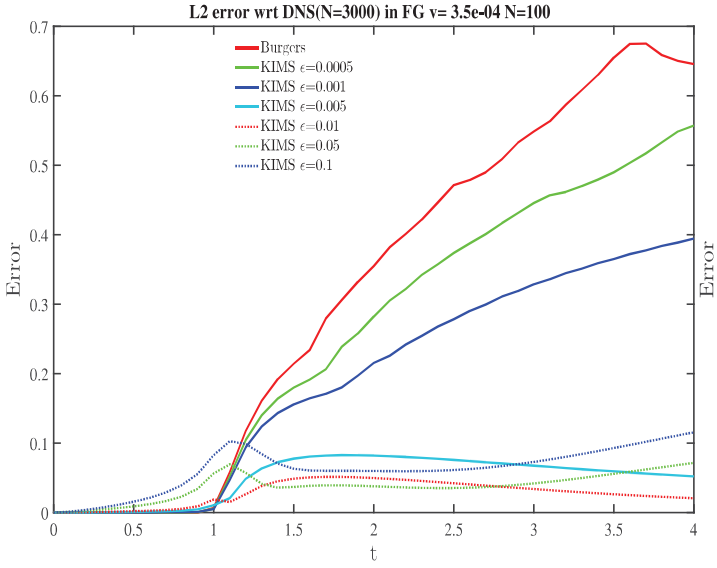

(c) $N = 100$

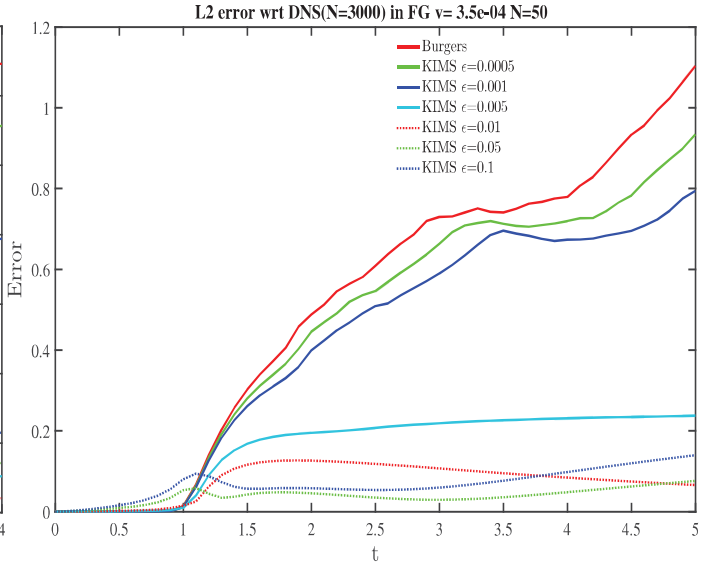

(d) $N = 50$

Figure 5.10: **Case 1: $l2$-error as a function of time for $u_0 = -sin(x)$.**

error at almost every time, but as other approximations error start increasing with the reduction of the resolved scales, we can observe how by $N = 50$ we get the lowest error almost everywhere.

Finally, KIMS approximations with $\varepsilon = \{0.5, 1\} \times 10^{-2}$ for $N = 500$ behave like those with the biggest ε values but with a smaller error, their behaviour transforms as N decreases taking a similar shape of the coarse viscous Burgers in Fig. 5.10a though increasing moderately the error value. In average, all through the span of cut-off wavenumbers they have the best performance, specially for the smaller one where in time the error tends to zero instead of increasing.

On the other hand, if we compare the results for $N = \{100, 50\}$ (Figs. 5.10c, 5.10d) with those obtained using $\nu_* = 0$ (Figs. 5.4b, 5.4c), we can observe that the artificial viscosity provides a marginally extra stability to the KIMS approximations.

Continuing with **case 2**, once more Fig. 5.11 show us that exists a pattern on the behaviour of every approximation for a diminishing N. However, in comparison with the previous case, the error coming from Burgers and KIMS with $\varepsilon = \{0.5, 1\} \times 10^{-3}$ is the lowest for $N = 500$ and starts to rise indefinitely only for a very coarse grid ($N = 50$). The rest of solutions as we decrease N perform in a similar way to the earlier example, which shows again that in average KIMS with $\epsilon = \{0.05, 0.1\}$ brings the best results.

Again, if we compare with the results obtained from $\nu_* = 0$ (Figs. 5.4b, 5.4c), we can notice that the artificial viscosity effect increases, as one would expect it, which means that KIMS approximations with smaller values of ε remain stable for lower cut-off wavenumbers. As we increase the viscosity values, we will see how these effects become stronger.

Already in **case 3**, Fig. 5.12 presents again -as one would hope- the same development for a decreasing N, yet in this case viscous Burgers and KIMS approximations from $\varepsilon = 0.5 \times 10^{-3}$ until $\varepsilon = 1 \times 10^{-2}$ have a resembling behaviour, performing really good for $N = 150$ and increasing in error at a comparable rate as N decreases, surpassing by $N = 25$ at least

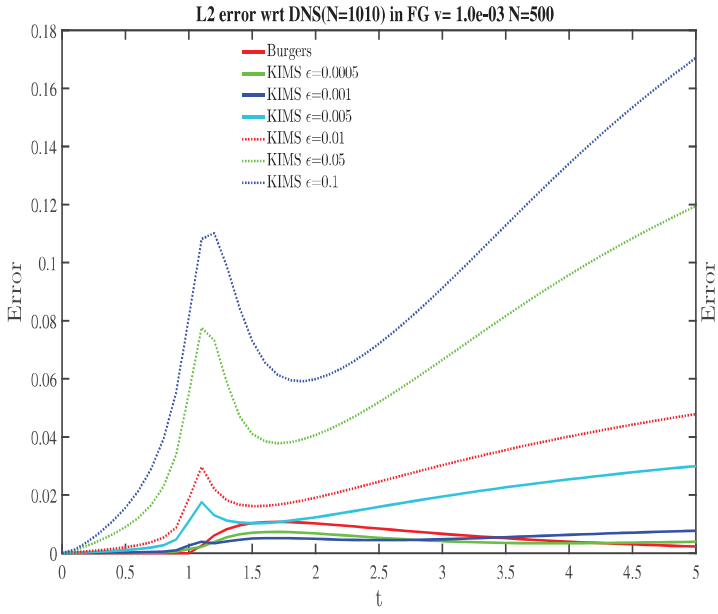

(a) $N = 500$

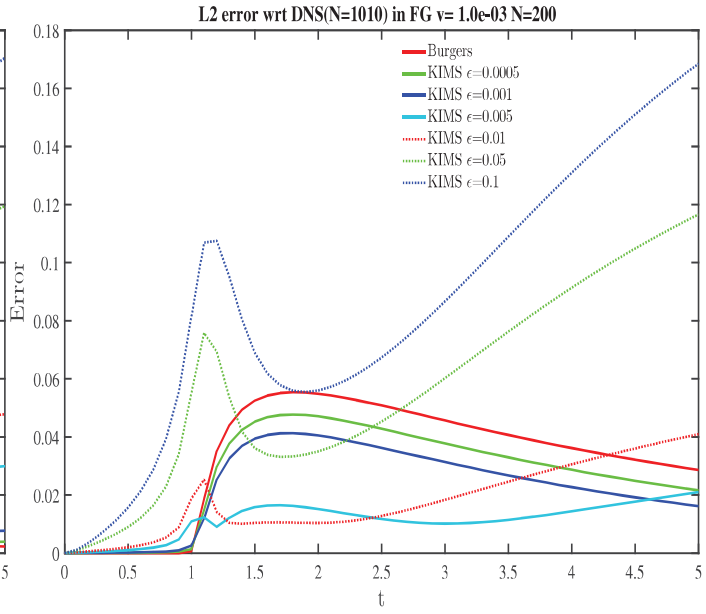

(b) $N = 200$

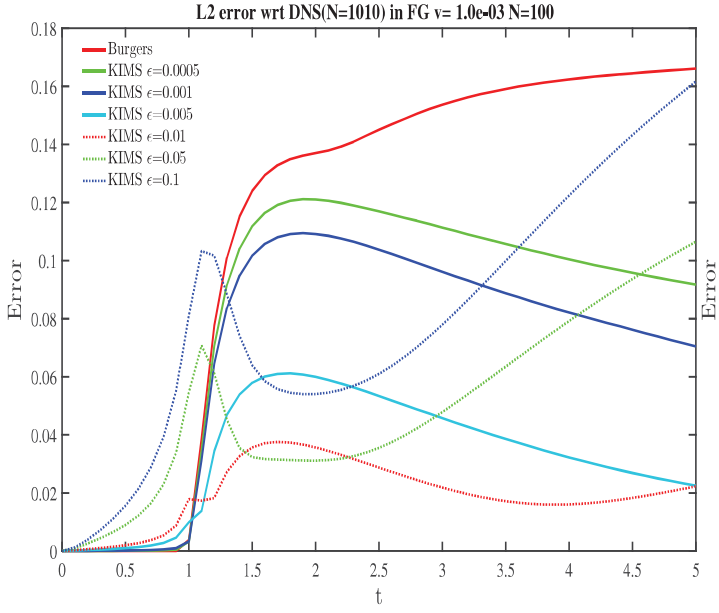

(c) $N = 100$

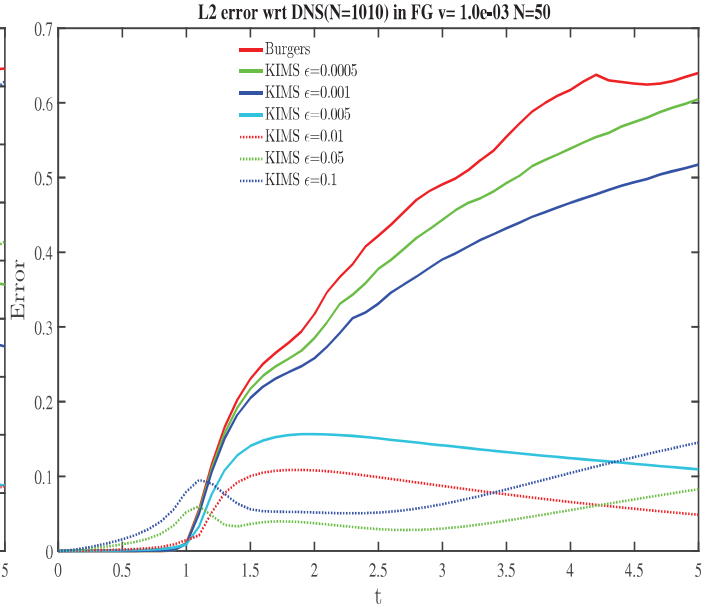

(d) $N = 50$

Figure 5.11: **Case 2:** $l2$**-error as a function of time for** $u_0 = -sin(x)$**.**

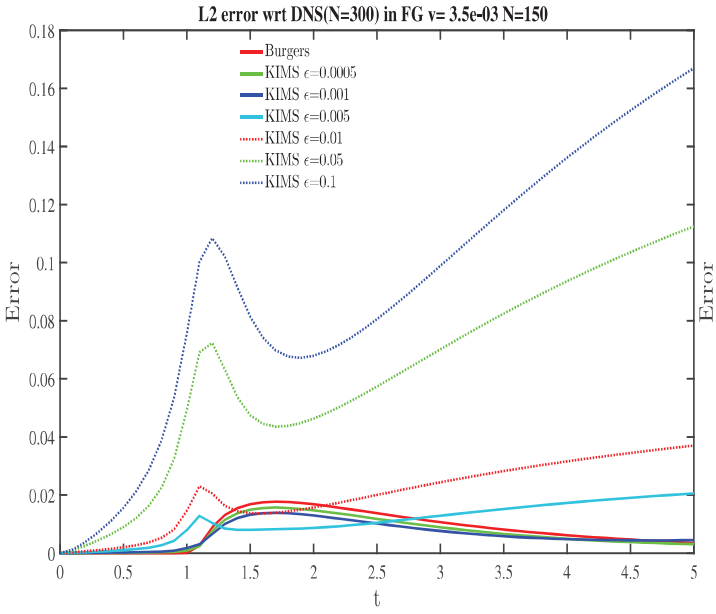

(a) $N = 150$

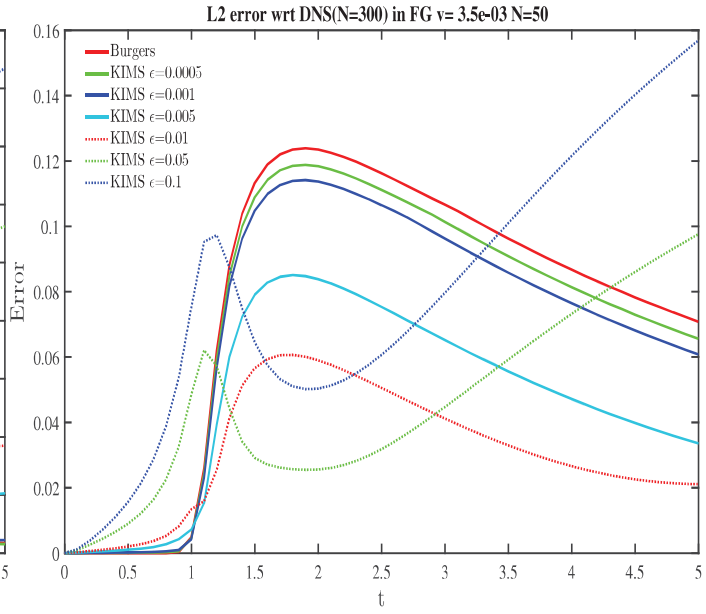

(b) $N = 50$

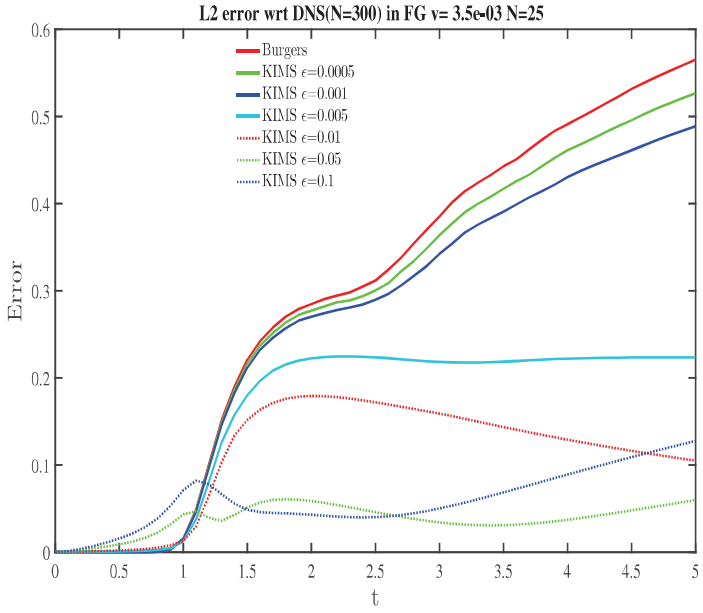

(c) $N = 25$

Figure 5.12: **Case 3:** $l2$**-error as a function of time for** $u_0 = -sin(x)$**.**

double the error coming from KIMS with $\varepsilon = \{0.1, 0.05\}$.

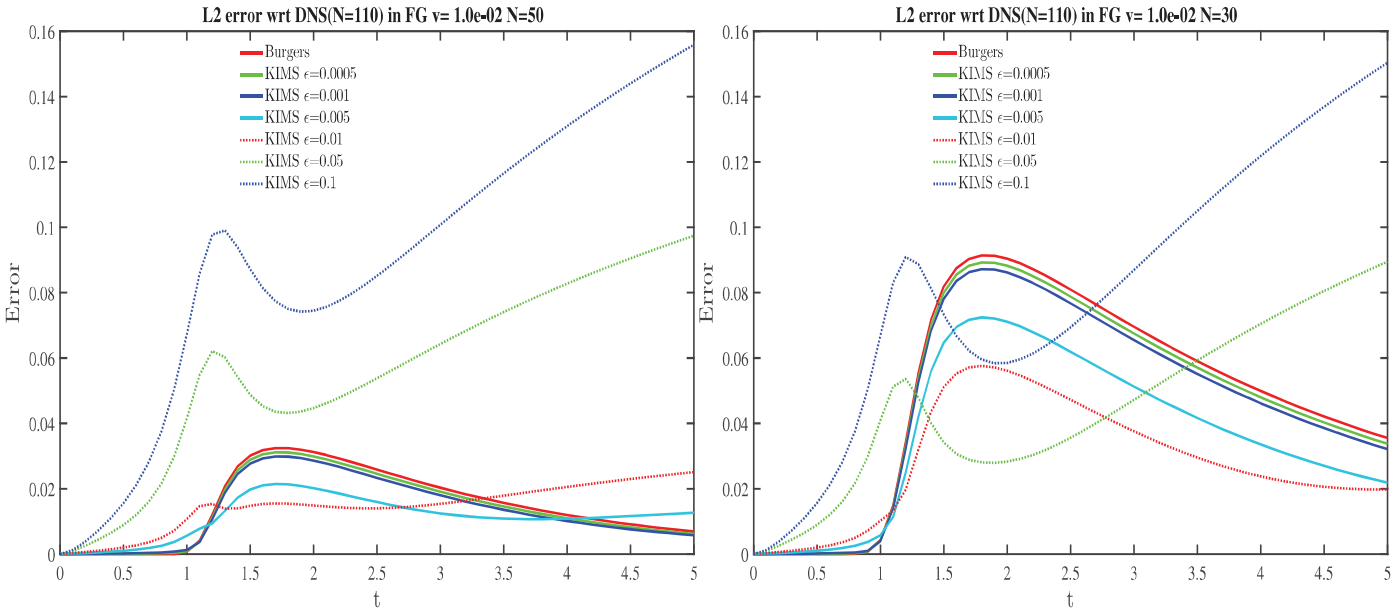

(a) $N = 50$ (b) $N = 30$

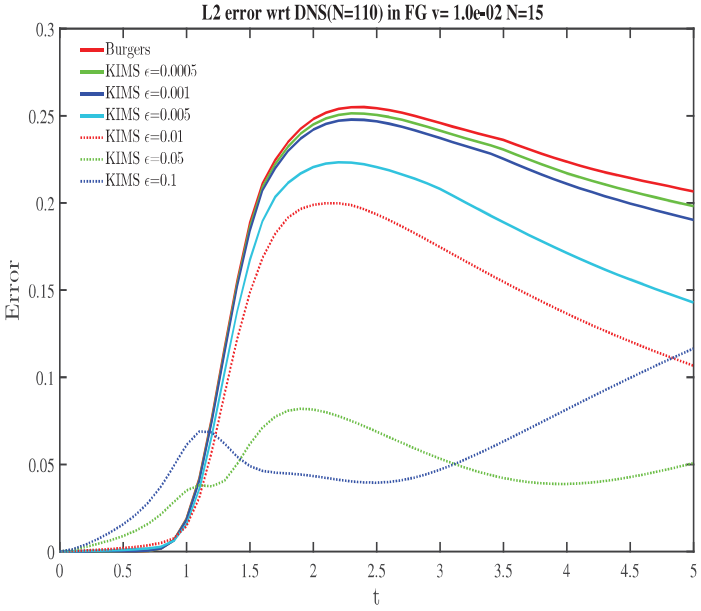

(c) $N = 15$

Figure 5.13: **Case 4: $l2$-error as a function of time for $u_0 = -sin(x)$.**

In coherence with the results already obtained for the Fourier modes magnitude and $u(x,t)$, for **case 4** the $l2-error$ even for $N=15$ does not blows up for any of the approximations. We observe in Fig. 5.14 the same pattern as in the third numerical example **case 3**, which for the lowest quantity of resolved scales the best outcome comes from KIMS with $\varepsilon = \{0.05, 0.1\}$.

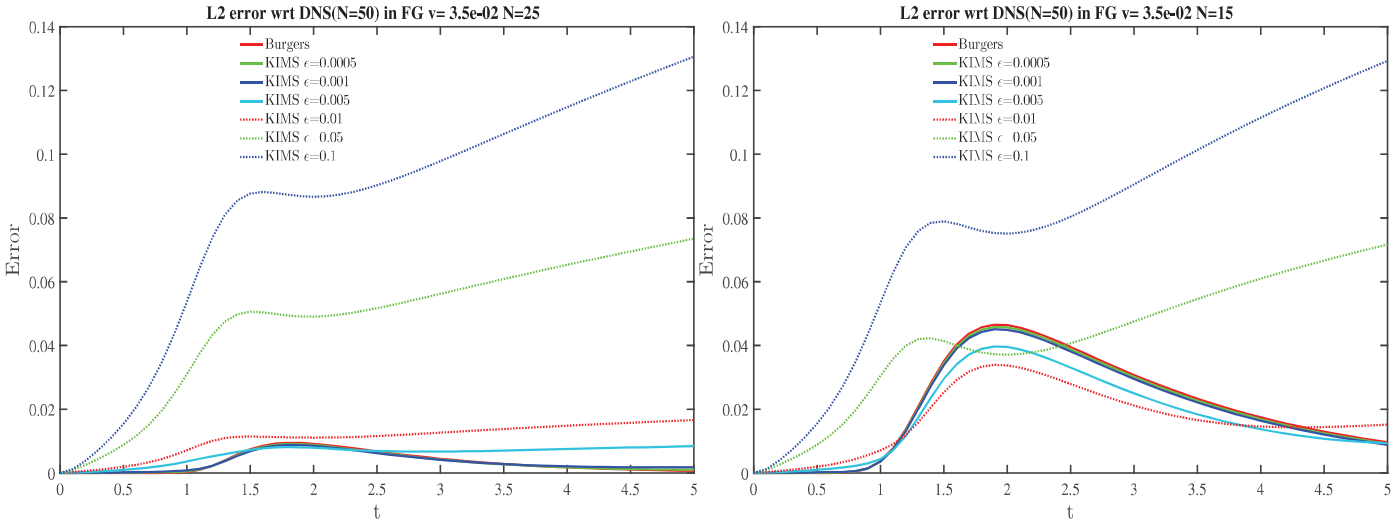

(a) $N = 25$ (b) $N = 15$

Figure 5.14: **Case 5: $l2$-error as a function of time for $u_0 = -sin(x)$.**

Finally, the **case 5** $l2-error$ in Fig. 5.14 shows a steady behaviour similar to what we have already seen. Nonetheless, KIMS with $\varepsilon = \{10, 5\} \times 10^{-3}$ continues on being in average the best choices.

5.3 Summary

In the presence of shock developing solutions, the discretization of the one-dimensional inviscid Burgers equation (2.17) by means of spectral methods will exhibit convergence problems, given that as the discontinuity forms the energy transfer to the higher modes

will significantly increase and large oscillations in the physical space will appear. One could tackle this problem by solving the viscous version of Burgers (5.1) in the limit of $\nu \to 0$. However, as the viscosity value gets closer to zero, the amount of resolved modes needed to achieve stability will be considerably larger (5.12), otherwise, oscillations will be developed again.

The kinetic-induced third order system for Burgers equation (5.13) is then expected to perform as a "subgrid closure" in terms of turbulent flows, in which the correct setting of the smallness parameter ε could account for the unresolved modes effect onto the resolved ones, specially when the stability condition (5.12) is not satisfied. The corresponding Fourier-Galerkin approximation (showed below) includes an artificial viscosity ν_* which is first set to zero, and then takes the viscosity values used to approximate the viscous Burgers equation

$$\frac{\partial \hat{u}_k}{\partial t} + \frac{ik}{2} \sum_{n \in \mathbb{Z}_k(\overline{k})} \hat{u}_n \hat{u}_{k-n} + i\varepsilon k \hat{w}_k = \boxed{-\nu_* \mathbf{k^2} \hat{\mathbf{u}}_\mathbf{k}}$$

$$\frac{\partial \hat{w}_k}{\partial t} + i \sum_{n \in \mathbb{Z}_k(\overline{k})} n \hat{w}_n \hat{u}_{k-n} + \frac{ik}{3\varepsilon} \hat{u}_k = -\left(\frac{4\varepsilon}{15} k^2 + \frac{1}{\varepsilon}\right) \hat{w}_k \quad , \forall \mid k \mid \leqslant \overline{k}$$

with $\overline{k}$ the cut-off wavenumber (called also N for numerical purposes). Several numerical experiments have been performed using different values of N for both cases of ν_*.

By setting $\nu_* = 0$, the numerical results before $t = 1$ when the shock has not formed yet, appear to be rather similar independently of the parameters (ν, ε, N) and two main behaviours show up: First, the Burgers approximations using every viscosity values, along with KIMS using the value of ε up to an order of $O(10^{-2})$, present an almost zero error being quasi identical to each other. Second, KIMS together with an ε of an order higher than $O(10^{-2})$ has an error increase around $t \approx 0.5$ which finds its peak at $t = 1$ where the shock lies. After $t = 1$ the shock forms and as the number of resolved modes (N) decreases the approximations stop converging, starting with those with the smallest values

of ν and ε, for KIMS with an ε of an order higher than $O(10^{-2})$ a decrease of the error and stabilization follows (Fig. 5.4), thus there is clear dependency between the stability requirement for KIMS and the values of ε. The above shows, that indeed the KIMS model is able to remove oscillations coming from the energy transfer during the development of the shock while using a significantly lower amount of resolved modes than the ones required by the condition (5.12), if the parameter ε is set accordingly. Still, the accuracy of the shock steepness is always compromised when decreasing the cut-off wavenumber.

Comparatively, setting $\nu_* = \nu$ the numerical approximations develop relatively similar to the previous case before the shock, specially for the smallest viscosity value. After $t = 1$, the increase in viscosity provides more damping and the needed amount of resolved scales (N) to remove oscillations in the physical space decreases in comparison to the results obtained with $\nu_* = 0$ (Fig. 5.10, Fig. 5.11, Fig. 5.12, Fig. 5.13, Fig. 5.14), in fact, it will be then possible for a particular N to set a value of ε larger than the one required in the case $\nu_* = 0$, so to improve the accuracy around the shock.

6. Conclusions

By means of the *Order of Magnitude Method*, it is possible to construct a kinetic-induced moment system (KIMS) with a desired order of accuracy η_0, which is asymptotically closed without an additional closure relation and couples the chosen balance law with its higher order variables via the smallness parameter ε by means of a Chapman–Enskog–like asymptotic expansion of the moments. At $zeroth - order$ accuracy it will always yield the original equations. Such kinetic-induced moment systems can be built for any conservation law system, for which an expression defining the equilibrium moments can be constructed. However, such an expression can be difficult to build and the derivation of the corresponding KIMS model will get more complex for larger systems and for higher accuracy orders.

Since our goal was to construct a system of equations that coupled the original balance law with its next higher order moment and corresponding diffusive correction, we focus on the 3rd order accuracy moment system for Burgers equation (3.40) and the 2nd order accuracy for the shallow water system of equations (3.89). The new variable $W(x,t)$ in the previous systems can then be used as a detector of special solutions that have an effect onto the velocity gradient, for example, shock and rarefaction waves, given that, in the formal limit $\varepsilon \to 0$ it will have an opposite behaviour to the gradient, while the moment system will still preserve the correct shock propagation. The preceding statement holds true for both of our study cases (Burgers and SWE).

In addition, the numerical experiments using a static grid show that the new variable $W(x,t)$ coming from the KIMS model, will behave accordingly with changes in the velocity gradient for a small enough ε as it was expected, acting as a delta function around shock waves, having a moderate negative tendency around rarefaction waves and equal to zero otherwise (Fig. 4.5), the speed of both waves will not be affected by the choice of ε. More-

over, the amount of extra diffusion inserted to the approximation of the original equations by higher order terms, decreases for smaller ε values, this effect is reflected in the decline of the *l2-error* as we lower ε. On the other hand, the KIMS model of the SWE is unstable for very small values of ε or for not small enough values of Δx (Fig. 4.9), meaning, that more complex systems will probably have stronger restrictions on the numerical parameters and an a priori validation of the chosen values is needed, which can be cumbersome.

Furthermore, $W(x,t)$ appears to be a good alternative choice of refinement criteria for adaptive mesh refinement techniques. Here, the desired gradient steepness would define the refinement area (4.35). Therefore, it allows easily to costume the desired maximum refinement level to different solutions (shocks, rarefactions) making it more flexible and independent of some heuristic parameter specified according to the user's criteria, as it occurs with more traditional refinement parameters (4.28) and (4.27), which will established more suitable conditions. Nevertheless, its numerical results come rather similar to those coming from spatial gradient estimate refinement criteria (4.28) with a very small tolerance value, yet, the computation of KIMS is more costly and may no be worth the extra features unless the moment system is already at hand. Still, since the refinement criteria will not longer depend of a random value but it is now connected to a mathematical characteristic of the problem itself, it will save us time in the long run and the computation of such systems might then be worth it for some cases.

On the other hand, a FG-spectral discretization of the 3rd order accuracy moment system for Burgers equation will indeed perform as a "subgrid closure" model, since it manages to include the effects of unresolved modes without having to satisfy the convergence condition (5.12), for which the mesh parameter must be smaller than the shock width. Particularly, the KIMS model is able to remove the oscillations coming from the increase in the energy transfer during the development of the shock wave generated by the Burgers equation, especially when the amount of resolved modes (N) is insufficient. This special feature will

allows to save in computational time without loosing stability. Nonetheless, it is necessary to chose the appropriate value of ε for the given amount of resolved modes (N), considering that for smaller N a larger ε is needed. The choices $\varepsilon = 0.05, 0.1$ showed no oscillations even for very small cut-off wavenumbers. However, it has a disadvantage, the shock steepness in the KIMS model approximation will suffer this reduction of resolved modes.

In the same way, if we consider an artificial viscosity term ν_* in KIMS spectral approximation for Burgers, the increase of this value will bring more damping and for less resolved modes the KIMS solution will converge even for very small values of ε, making the cut-off wavenumber for which the KIMS model approximation starts oscillating to decrease and giving the possibility to set a value of ε larger than the one required in the case $\nu_* = 0$ for a particular value of N, so to improve the steepness around the shock.

In conclusion, with this work we have shown that the *Order of Magnitude Method* coming from Kinetic Theory can be of use for the development of new techniques in the field of numerical analysis for Balance Laws. It has been presented how the ε-coupling of a new variable $W(x,t)$ derived from the original equations, allow us to optimize refinement regions in adaptive mesh refinement and also the amount of required resolved modes in FG-spectral approximations. However, we have repeatedly stated that the derivation of such kinetic-induced moment system can be complex and full of tedious computations. Here, we have just set the basis for further developments on the subject, a better understanding on how one could optimally set the smallness parameter ε in both cases is necessary.

References

[1] M. J. Berger and J. Oliger, *Adaptive mesh refinement for hyperbolic partial differential equations*, J. Comput. Phys., 53 (1984), pp. 484–512.

[2] M. J. Berger and P. Collela, *Local adaptive mesh refinement for shock hydrodynamics*, J. Comput. Phys., 82 (1989), pp. 64–84.

[3] M. J. Berger and R. J. Leveque, *Adaptive mesh refinement using wave-propagation algorithms for hyperbolic systems*, SIAM J., Vol. 35, 6 (1998), pp. 2298–2316.

[4] D. Bernstein *Optimal Prediction of Burgers's Equation*, Multiscale Model. Simul., 6 (2007), pp. 27–52.

[5] G. Bird, *Molecular Gas Dynamic and the Direct Simulation of Gas Flows*, Clarendon Press, Oxford, 1994.

[6] J. H. Bolstad, *An Adaptive Finite Difference Method for Hyperbolic Systems in One Space Dimension*, Ph.D. thesis, Stanford University, 1982.

[7] J. M. Burgers *The Nonlinear Diffusion Equation*, D. Reidel, Dordrecht, The Netherlands, 1974.

[8] C. Cercignani, *Theory and application of the Boltzmann equation*, Scottish Academic Press, Edinburgh, 1975.

[9] C. Cercignani, *Mathematical Methods in Kinetic Theory*, Springer, New York, 1990.

[10] S. Chapman and T.G. Cowling, *The Mathematical Theory of Non-Uniform Gases. An Account of the Kinetic Theory of Viscosity, Thermal Conduction and Diffusion in Gases*, 3rd. Edition, Cambridge University Press, London, 1970.

[11] L. Evans, *Partial Differential Equations*, 2nd. Edition, American Mathematical Society, Rhode Island, 2010.

[12] G. B. Folland, *Fourier Analysis and Its Applications*, Brooks/Cole, Pacific Grove (CA), 1992.

[13] L. S. García-Colín, R. M. Velasco and F. J. Uribe: *Beyond the Navier-Stokes equation: Burnett hydrodynamics*, Phys. Rep., 465 (2008), pp. 149–189.

[14] D. C. Gil and J. Struckmeier: *Kinetic-Induced Moment Systems for the Saint-Venant Equations*, TASK QUARTERLY, Vol. 17, 1-2 (2013), pp. 63–90.

[15] E. Godlewski and P. A. Raviart, *Numerical Approximation of Hyperbolic Systems of Conservation Laws*, Springer-Verlag, New York, 1996.

[16] H. Grad: *On the kinetic theory of rarefied gases*, Commun. Pure Appl. Math., 2 (1949), pp. 331–407.

[17] J. M. Hyman and S. Li, *Interactive and dynamic control of adaptive mesh refinement with nested Hierarchical grids*, Los Alamos National Laboratory Report, 1998.

[18] J. M. Hyman and S. Li, *Adaptive mesh refinement for finite difference WENO schemes*, Los Alamos National Laboratory Report, 2003.

[19] D. Kopriva, *Implementing Spectral Methods for Partial Differential Equations*, Springer-Verlag, Algorithms for Scientists and Engineers, Series: Scientific Computation, New York,2009.

[20] D. Kröner, *Numerical Schemes for Conservation Laws*, Wiley-Teubner, Chichester, 1997.

[21] P. D. Lax and B. Wendroff, *Systems of conservation laws*, Comm. Pure Appl. Math., 13(1960), pp. 217–237.

[22] R. J. Leveque, *Finite Volume Methods for Hyperbolic Problems*, Cambridge texts in Applied Mathematics, Cambridge, 2002.

[23] R. J. Leveque, *Finite Difference Methods for Ordinary and Partial Differential Equations*, SIAM, Philadelphia, 2007.

[24] R. J. LeVeque, M. J. Berger, et. al., *Clawpack Software 4.6, www.clawpack.org, July 2012.*

[25] P.L. Lions, B. Perthame and E. Tadmor, *Kinetic formulation of the isentropic gas dynamics and p-systems*, Commun. Math. Phys., 163 (1994), pp. 415–431.

[26] *Rarefied gas flow*, McGraw-Hill Concise Encyclopedia of Physics. (2002). Retrieved December 28 2016 from http://encyclopedia2.thefreedictionary.com/Rarefied+gas+flow

[27] Matlab, `http://de.mathworks.com/help/matlab/ref/ode45.html`

[28] K. W. Morton and D. F. Mayers, *Numerical Solution of Partial Differential Equations*, Cambridge University Press, Cambridge, 2005.

[29] A. Oberai, E. Colosqui and J. Wanderer, *Analytical estimates of the subgrid model for Burgers equation: Ramifications for spectral methods for conservation laws*, International Journal for Multiscale Computational Engineering, 6 (2008), pp. 299–307.

[30] A. Oberai and J. Wanderer, *A dynamic multiscale viscosity method for the spectral approximation of conservation laws*, Comput. Methods Appl. Mech. Engrg., 195 (2006), pp. 1778–1792.

[31] T. Passot and A. Pouquet *Hyperviscosity for compressible flows using spectral methods*, J. Comput. Phys., 75 (1988), pp. 300–313.

[32] B. Perthame and C. Simeoni, "A kinetic scheme for the Saint-Venant System with a source term," *CALCOLO*, 2001, No. 38, pp. 201–231.

[33] B. Perthame, *Kinetic Formulation of Conservation Laws*, OXFORD University Press, NY, 2002.

[34] P. Sagaut *Large eddy simulation for incompressible flows*, Springer-Verlag, New York, 2002.

[35] H. Struchtrup, *Stable transport equations for rarefied gases at high orders in the Knudsen number*, Phys. Fluids, 16 (2004), pp. 3921–3934.

[36] H. Struchtrup, *Macroscopic Transport Equations for Rarefied Gas Flows. Approximation Methods in Kinetic Theory*, Interaction of Mechanics and Mathematics, Springer-Verlag, Berlin, 2005.

[37] H. Struchtrup, *Unique moment set from the order of magnitude method*, Kinetic and Related Models, 5 (2012), pp. 417–440.

[38] J. Struckmeier, (*private communication*).

[39] E. Tadmor *Convergence of spectral methods for nonlinear conservation laws*, SIAM J. Numer. Anal., 195 (1989), pp. 30–44.

[40] E.F. Toro, *Riemann Solvers and Numerical Methods for Fluid Dynamics*, Springer-Verlag, Berlin, 1997.

[41] J. G. Verwer and J. G. Blom, *VLUGR2: A vectorized local uniform grid refinement code for PDEs in 2D*, CWI Report NM-R9307, 1993.

[42] J. G. Verwer and J. G. Blom, *VLUGR2: A vectorized local uniform grid refinement code for PDEs in 2D*, CWI Report NM-R9307, 1993.

A. $E(k)$ and $u(x,t)$ for $\nu_* = 0$

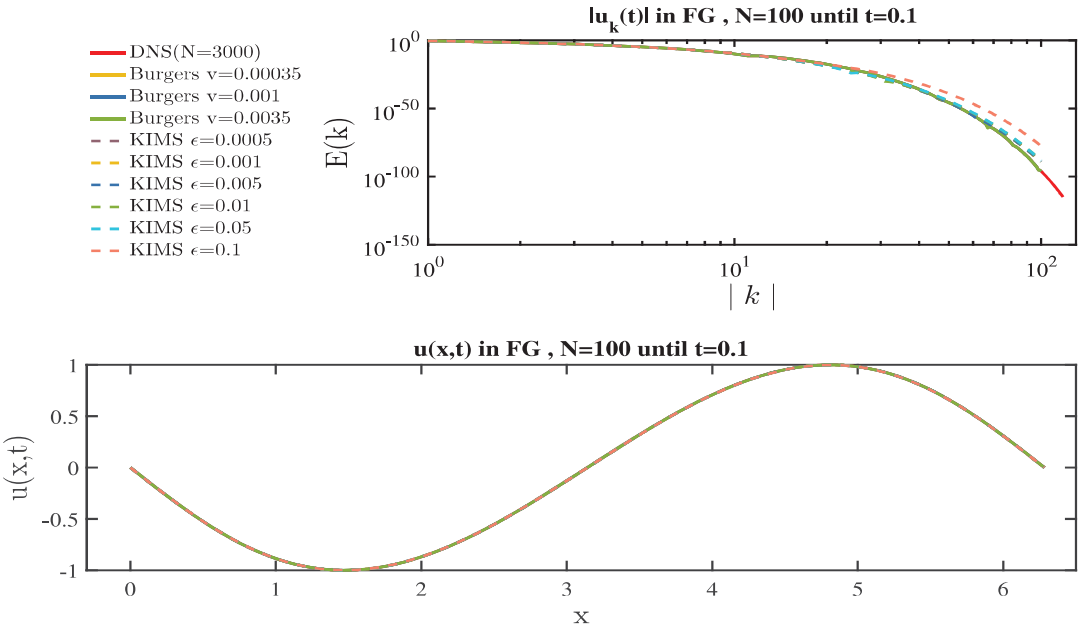

(a) $N = 100$

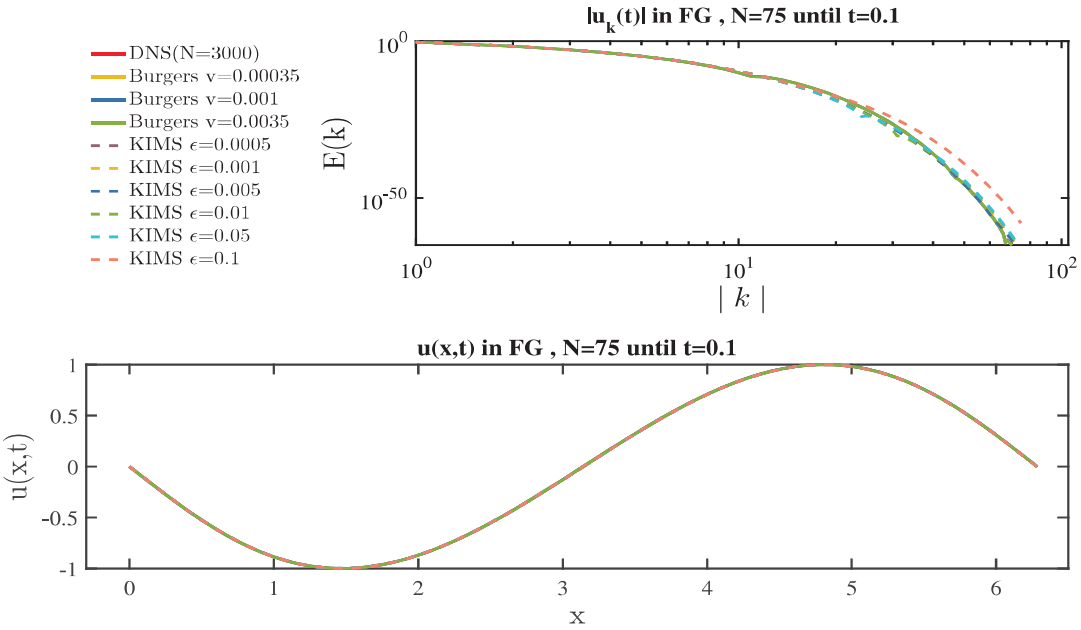

(b) $N = 75$

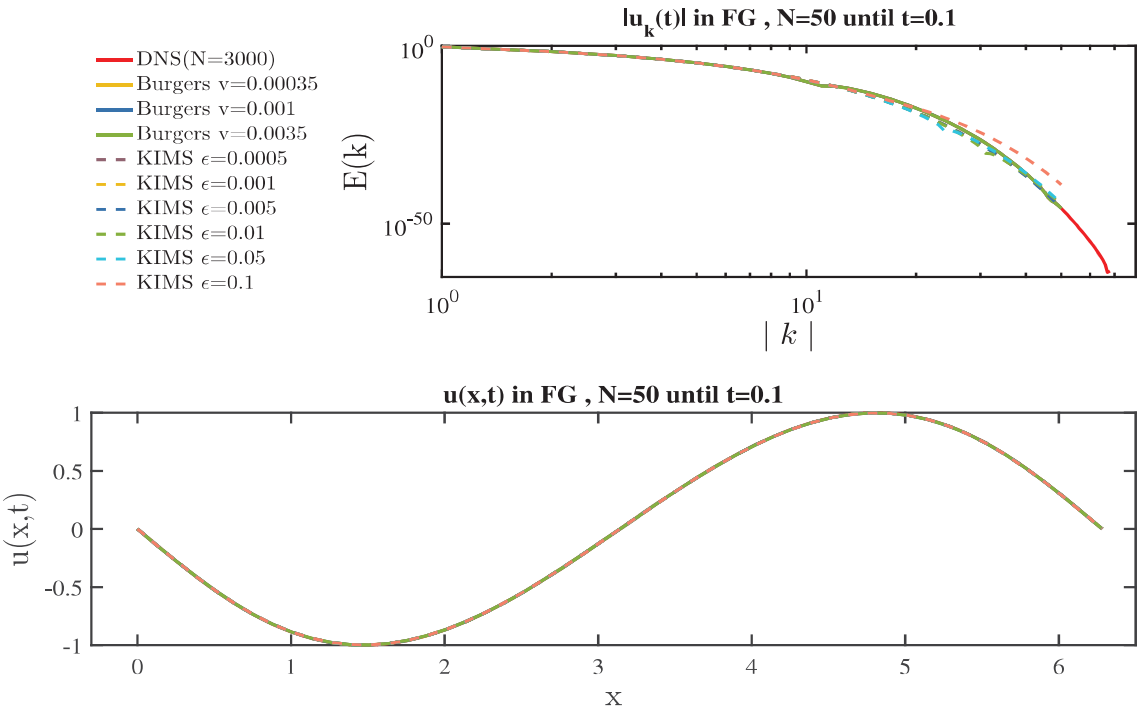

(c) $N = 50$

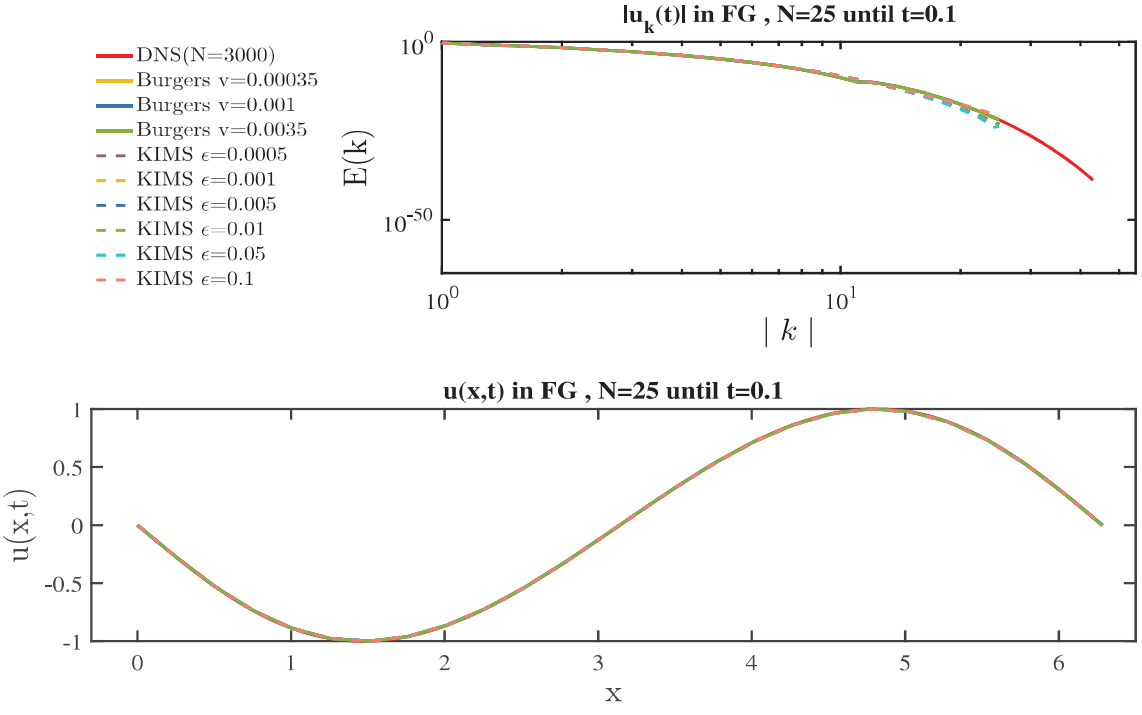

(d) $N = 25$

Figure A.1: $E(k)$ and $u(x,t)$ for the DNS and coarse grid solutions at $t = 0.1$.

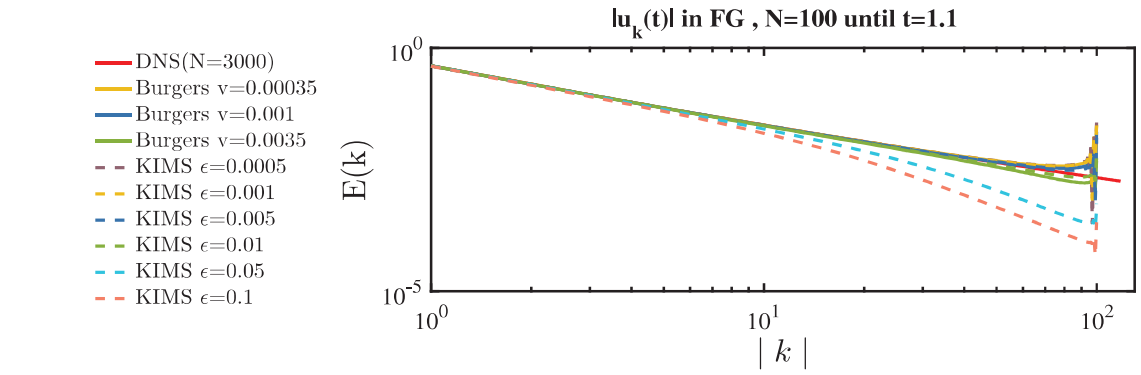
|u_k(t)| in FG , N=100 until t=1.1
DNS(N=3000)
Burgers v=0.00035
Burgers v=0.001
Burgers v=0.0035
KIMS ϵ=0.0005
KIMS ϵ=0.001
KIMS ϵ=0.005
KIMS ϵ=0.01
KIMS ϵ=0.05
KIMS ϵ=0.1
E(k)
| k |

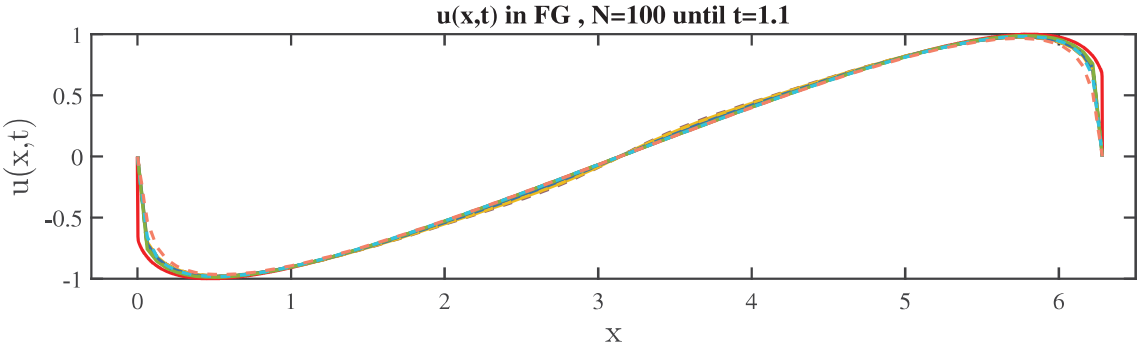
u(x,t) in FG , N=100 until t=1.1
u(x,t)
x

(a) $N = 100$

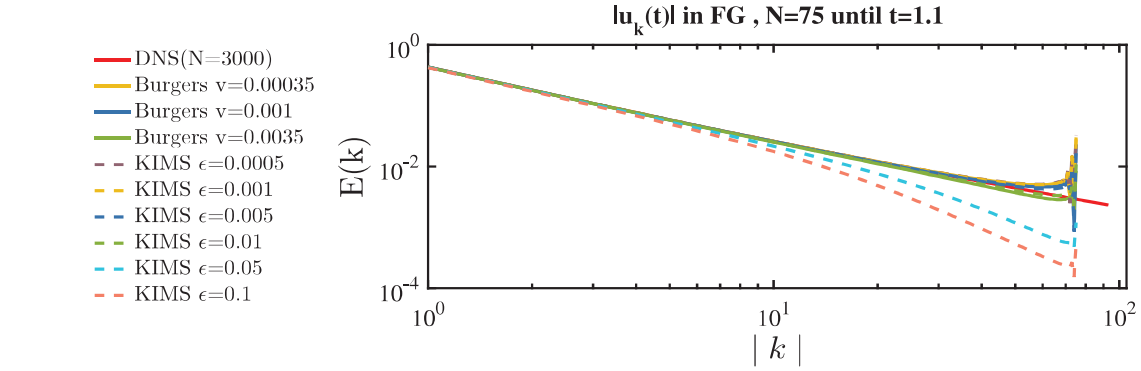
|u_k(t)| in FG , N=75 until t=1.1
DNS(N=3000)
Burgers v=0.00035
Burgers v=0.001
Burgers v=0.0035
KIMS ϵ=0.0005
KIMS ϵ=0.001
KIMS ϵ=0.005
KIMS ϵ=0.01
KIMS ϵ=0.05
KIMS ϵ=0.1
E(k)
| k |

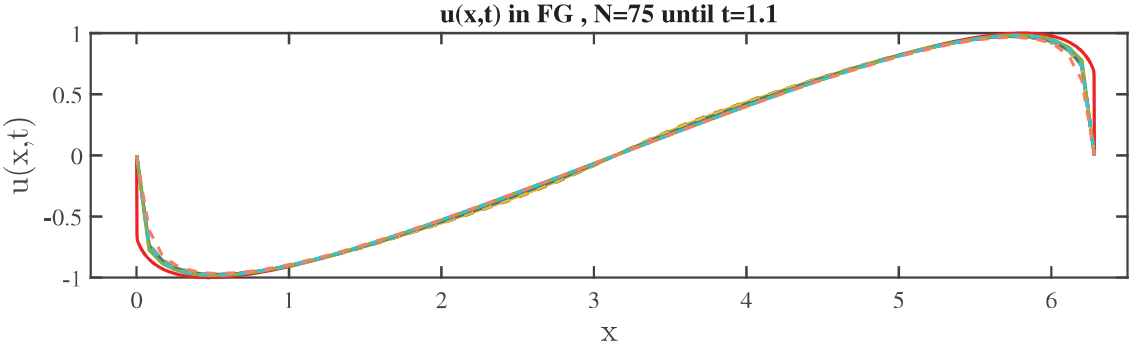
u(x,t) in FG , N=75 until t=1.1
u(x,t)
x

(b) $N = 75$

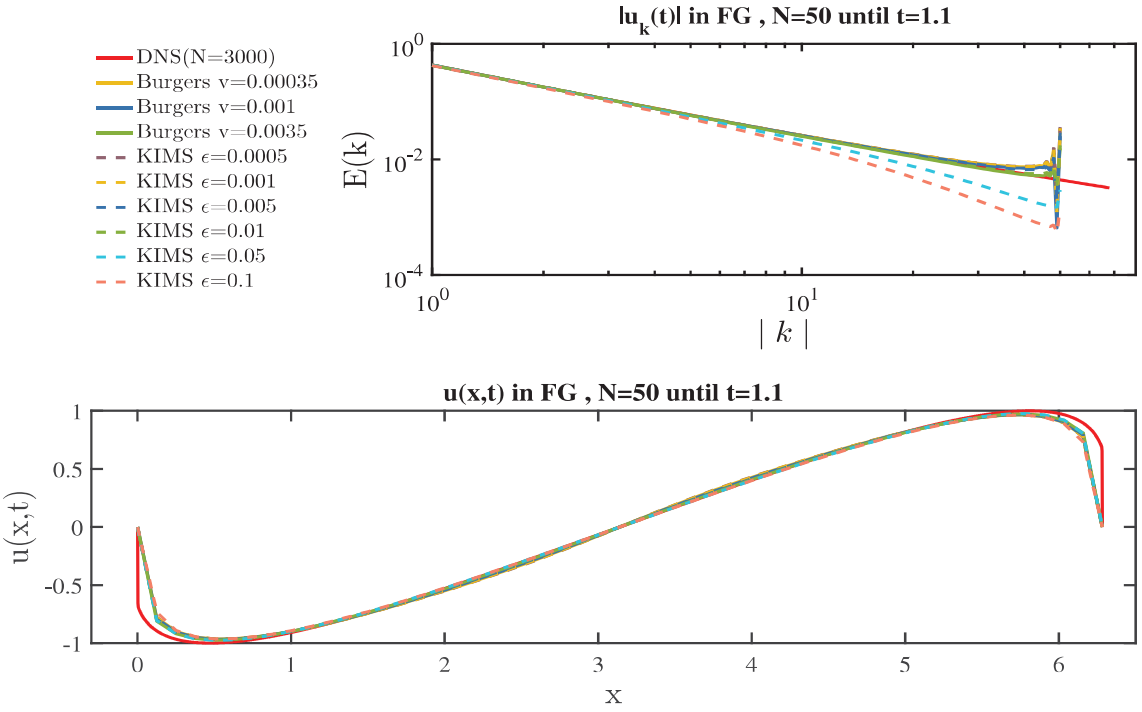

(c) $N = 50$

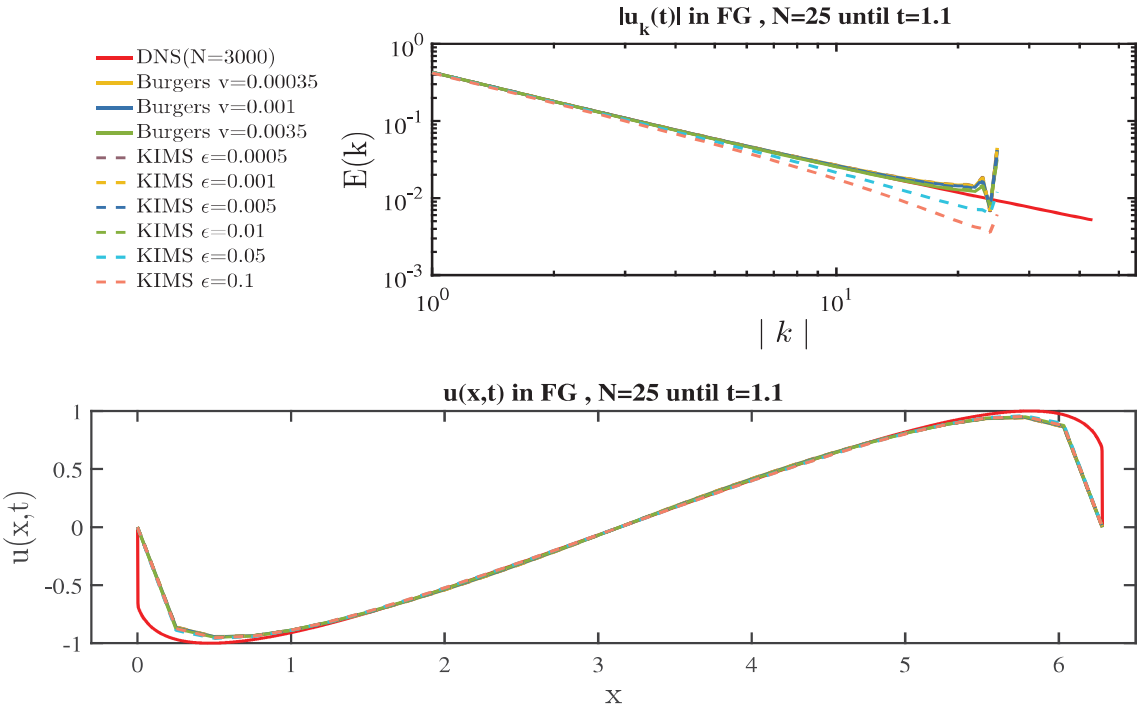

(d) $N = 25$

Figure A.2: $E(k)$ and $u(x,t)$ for the DNS and coarse grid solutions at $t = 1.1$.

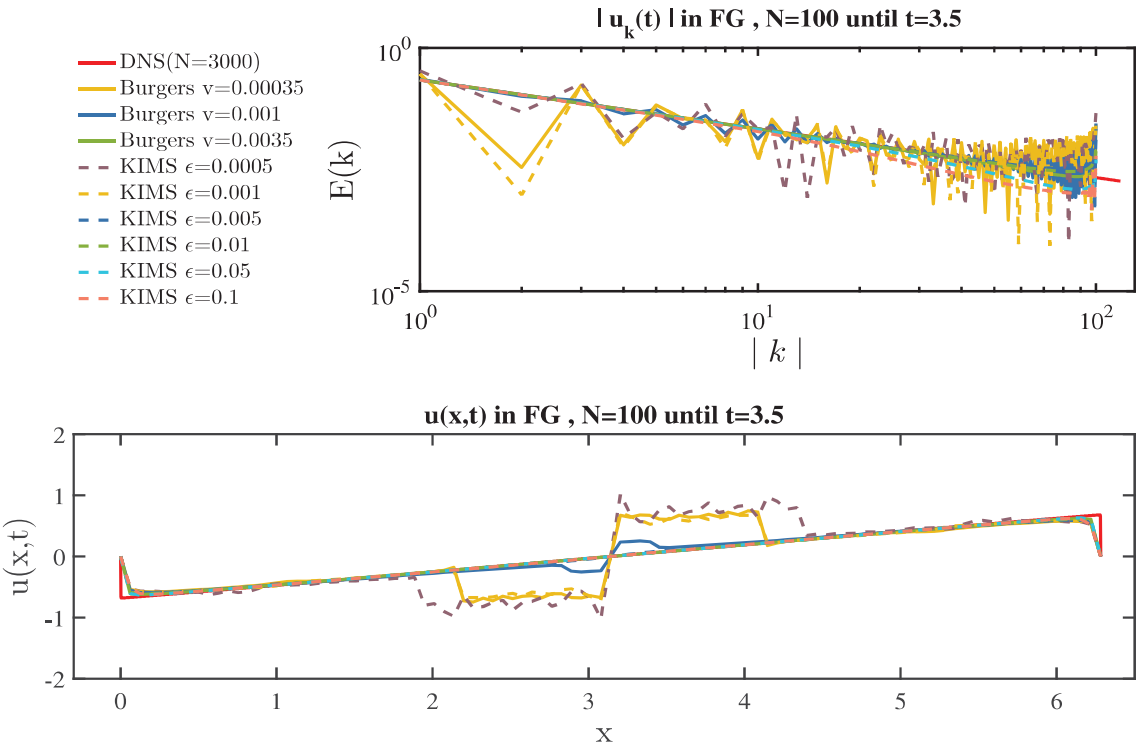
| u_k(t) | in FG , N=100 until t=3.5
DNS(N=3000)
Burgers v=0.00035
Burgers v=0.001
Burgers v=0.0035
KIMS ϵ=0.0005
KIMS ϵ=0.001
KIMS ϵ=0.005
KIMS ϵ=0.01
KIMS ϵ=0.05
KIMS ϵ=0.1
E(k)
| k |
u(x,t) in FG , N=100 until t=3.5
u(x,t)
x

(a) $N = 100$

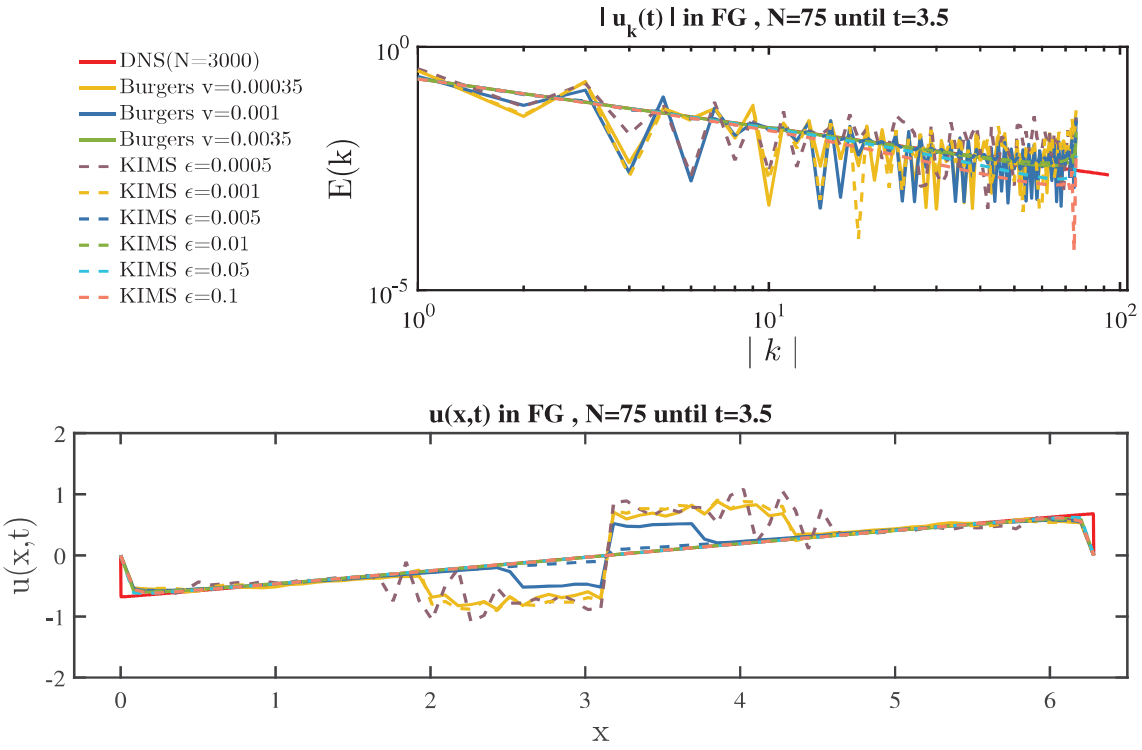
| u_k(t) | in FG , N=75 until t=3.5
DNS(N=3000)
Burgers v=0.00035
Burgers v=0.001
Burgers v=0.0035
KIMS ϵ=0.0005
KIMS ϵ=0.001
KIMS ϵ=0.005
KIMS ϵ=0.01
KIMS ϵ=0.05
KIMS ϵ=0.1
E(k)
| k |
u(x,t) in FG , N=75 until t=3.5
u(x,t)
x

(b) $N = 75$

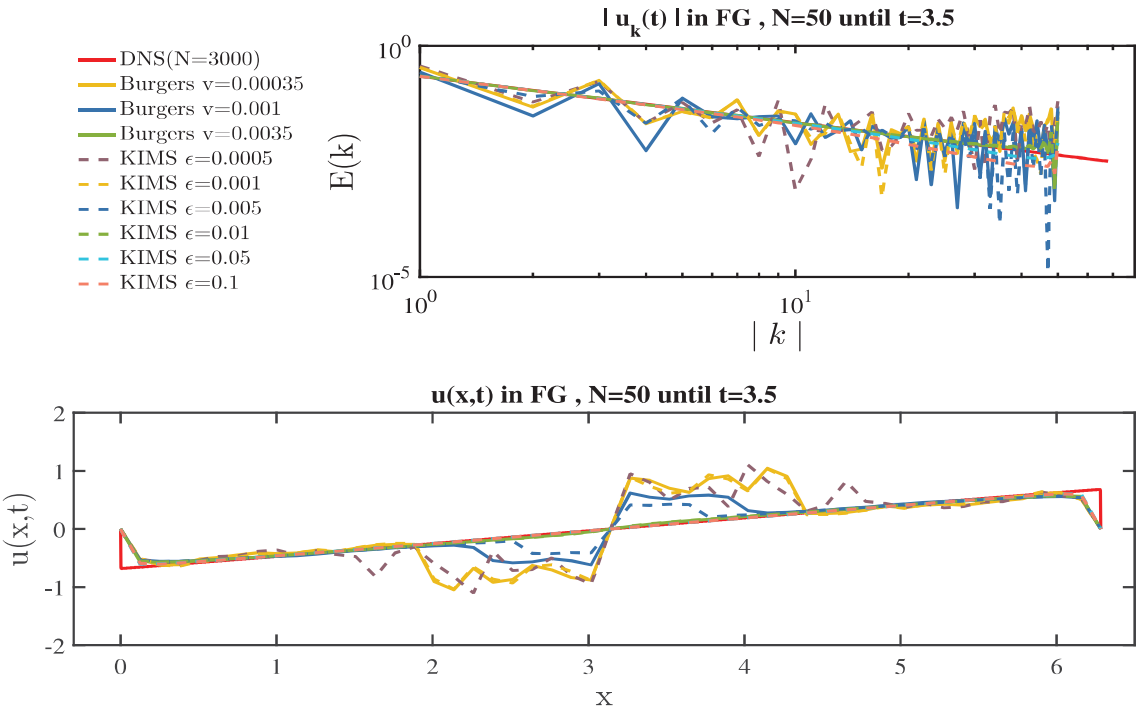

(c) $N = 50$

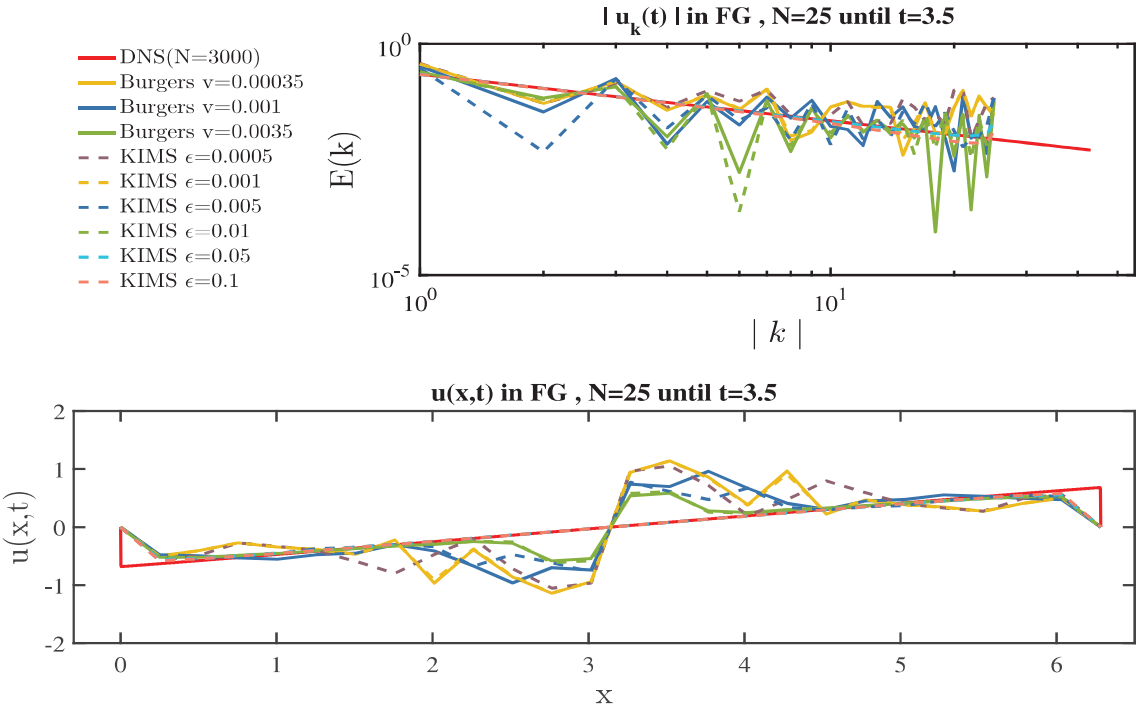

(d) $N = 25$

Figure A.3: $E(k)$ and $u(x,t)$ for the DNS and coarse grid solutions at $t = 3.5$.

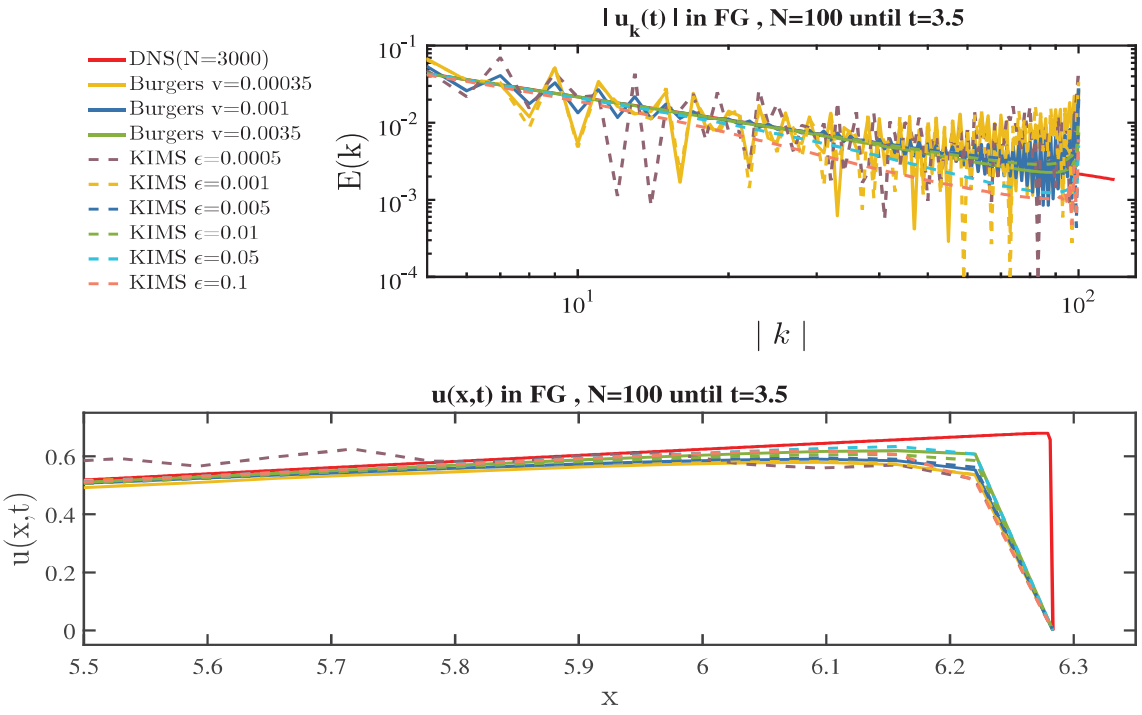
| u_k(t) | in FG , N=100 until t=3.5
DNS(N=3000)
Burgers v=0.00035
Burgers v=0.001
Burgers v=0.0035
KIMS ϵ=0.0005
KIMS ϵ=0.001
KIMS ϵ=0.005
KIMS ϵ=0.01
KIMS ϵ=0.05
KIMS ϵ=0.1
E(k)
| k |
u(x,t) in FG , N=100 until t=3.5
u(x,t)
x

(a) $N = 100$

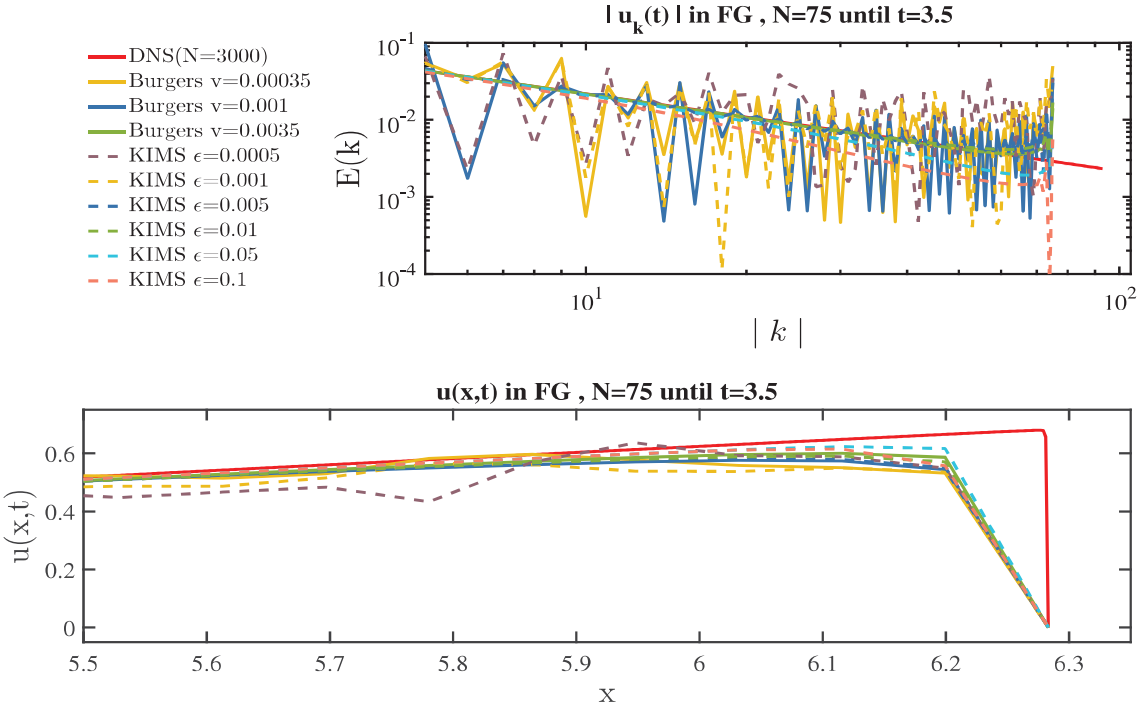
| u_k(t) | in FG , N=75 until t=3.5
DNS(N=3000)
Burgers v=0.00035
Burgers v=0.001
Burgers v=0.0035
KIMS ϵ=0.0005
KIMS ϵ=0.001
KIMS ϵ=0.005
KIMS ϵ=0.01
KIMS ϵ=0.05
KIMS ϵ=0.1
E(k)
| k |
u(x,t) in FG , N=75 until t=3.5
u(x,t)
x

(b) $N = 75$

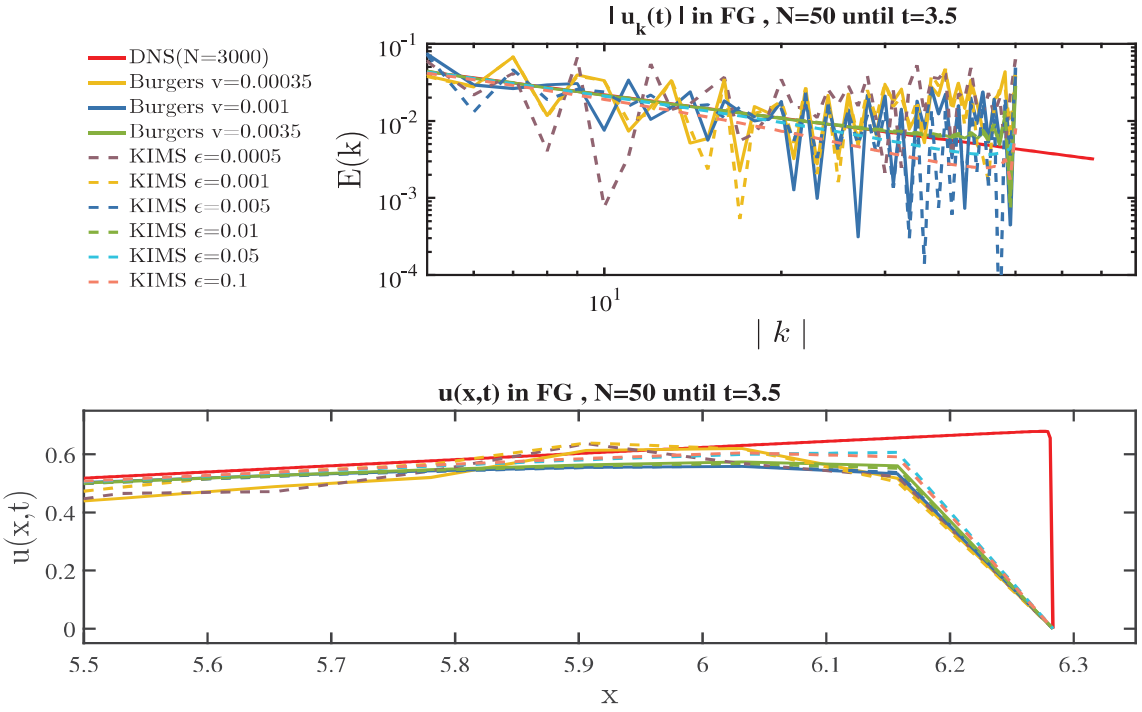

(c) $N = 50$

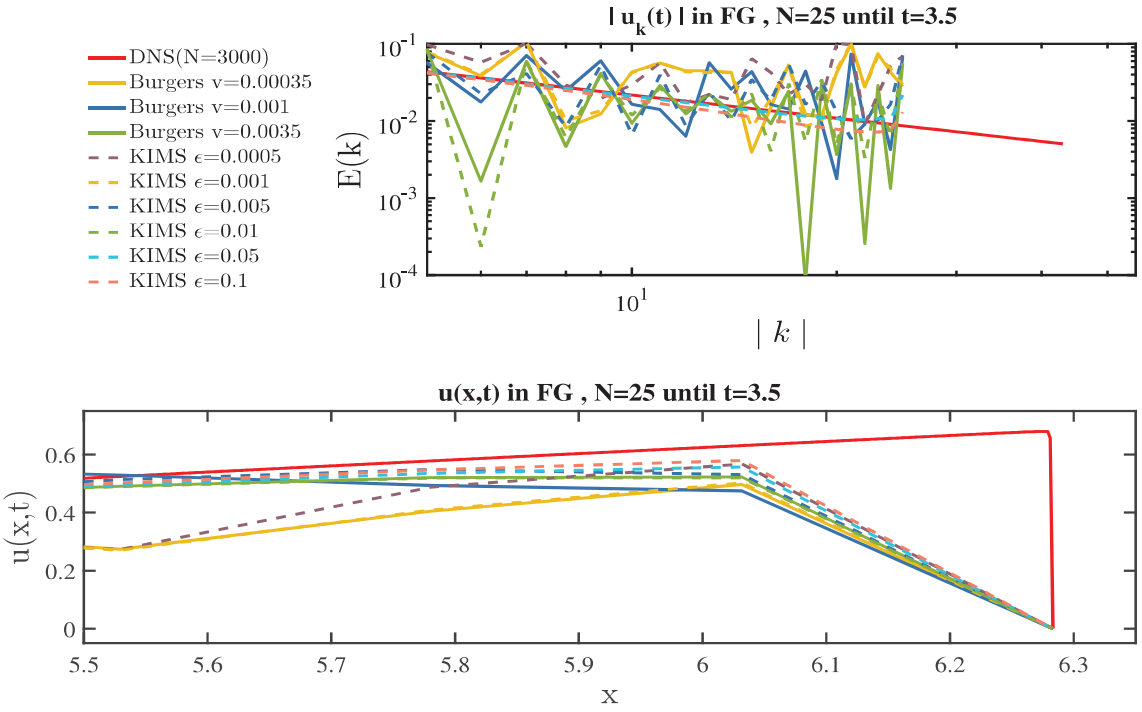

(d) $N = 25$

Figure A.4: $E(k)$ and $u(x,t)$ for the DNS and coarse grid solutions located at the shock area at $t = 3.5$.

B. $E(k)$ and $u(x,t)$ for $\nu_* = \nu$

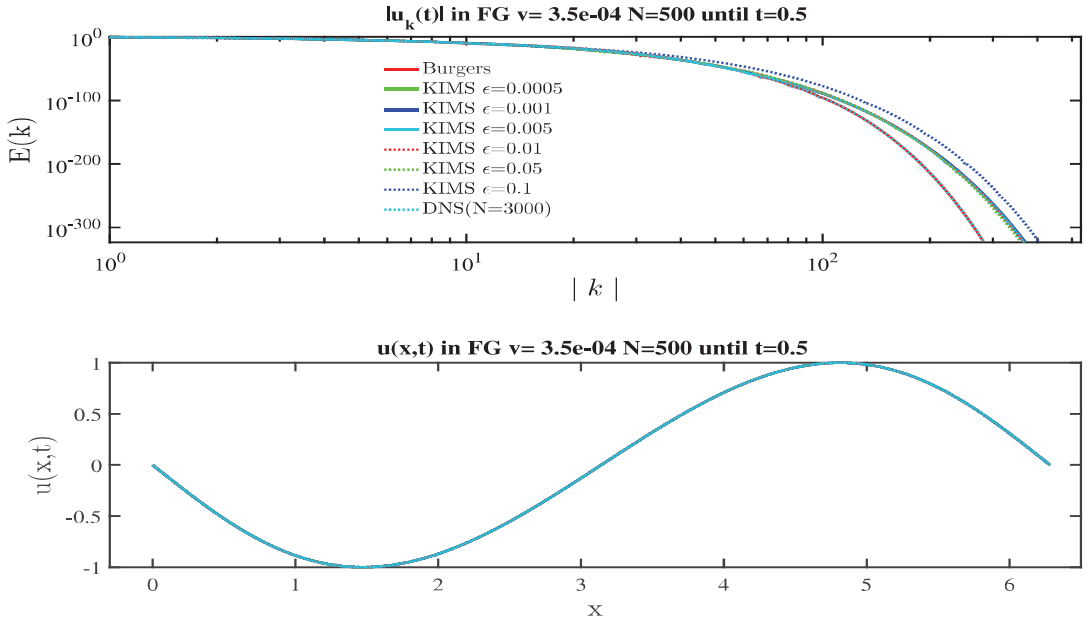

(a) $N = 500$

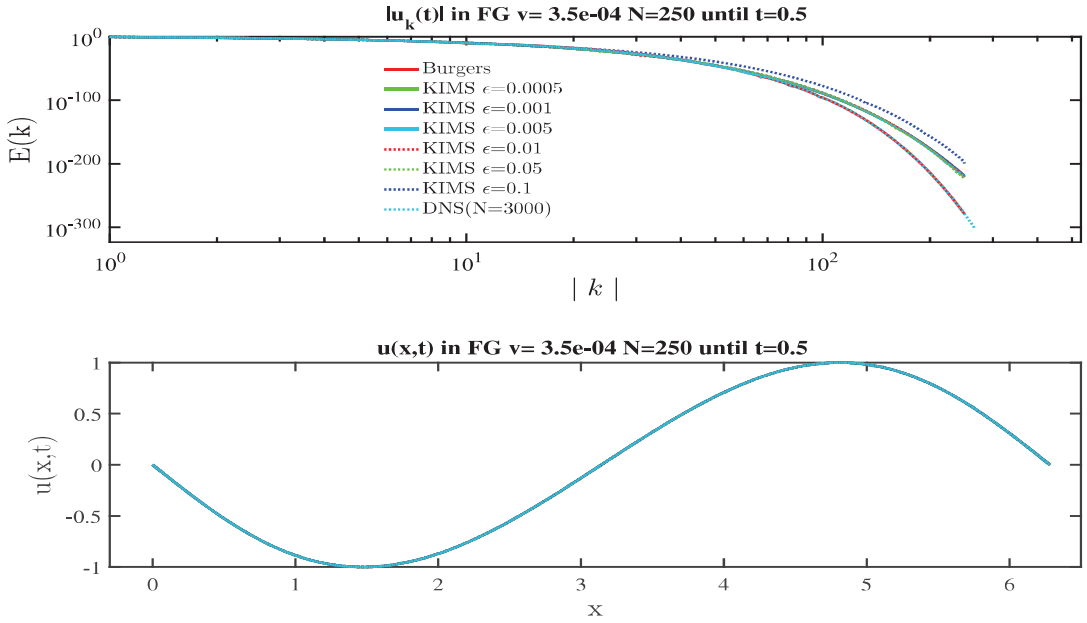

(b) $N = 250$

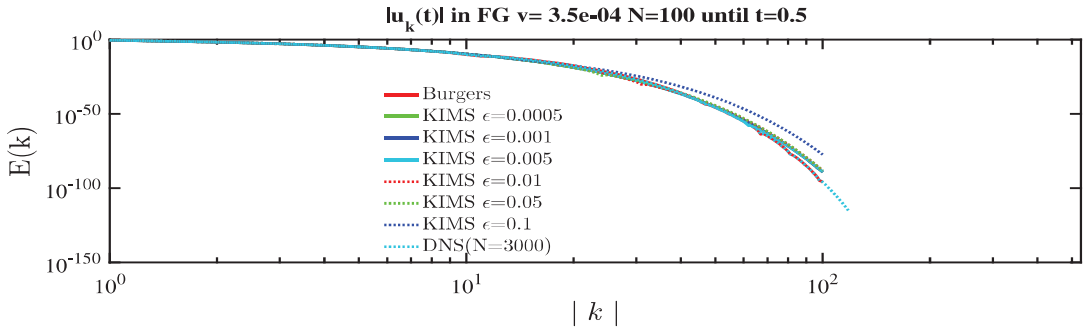

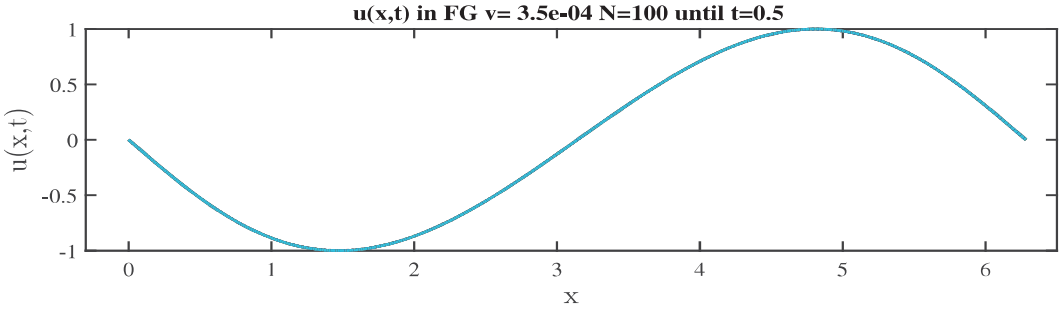

(c) $N = 100$

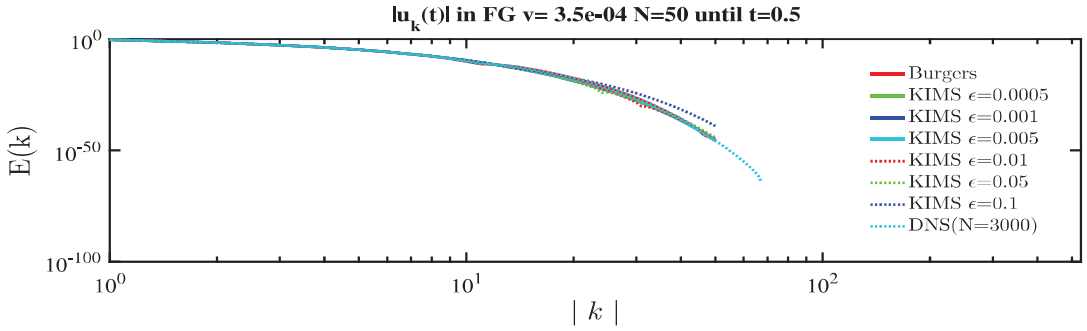

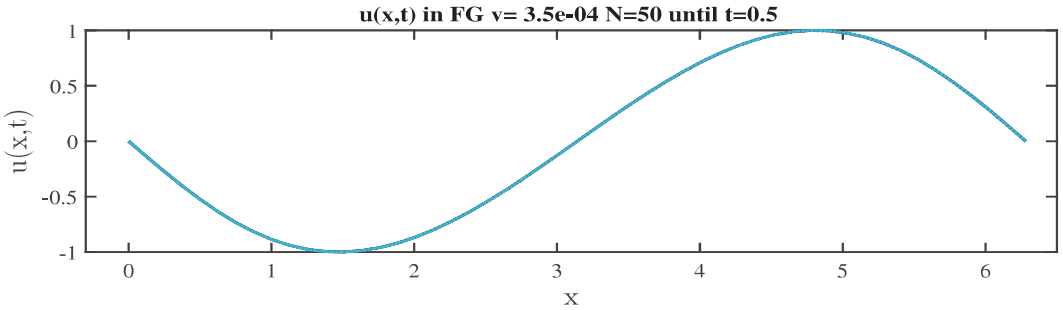

(d) $N = 50$

Figure B.1: $E(k)$ and $u(x,t)$ for the DNS and coarse grid solutions at $t = 0.5$.

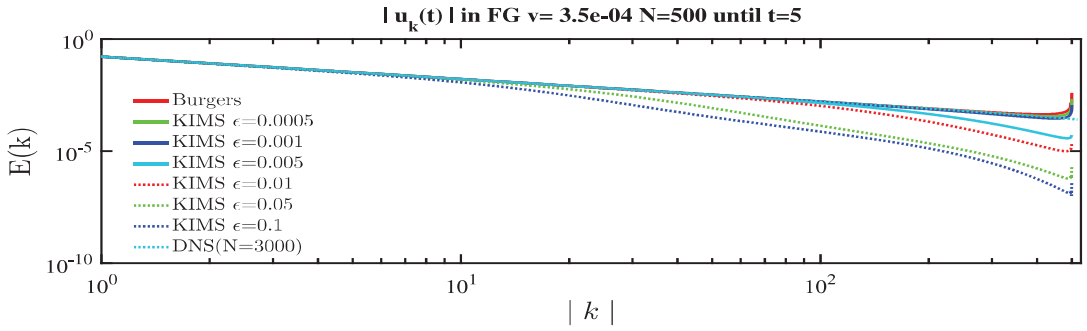
| u_k(t) | in FG v= 3.5e-04 N=500 until t=5
E(k)
| k |
Burgers
KIMS ϵ=0.0005
KIMS ϵ=0.001
KIMS ϵ=0.005
KIMS ϵ=0.01
KIMS ϵ=0.05
KIMS ϵ=0.1
DNS(N=3000)

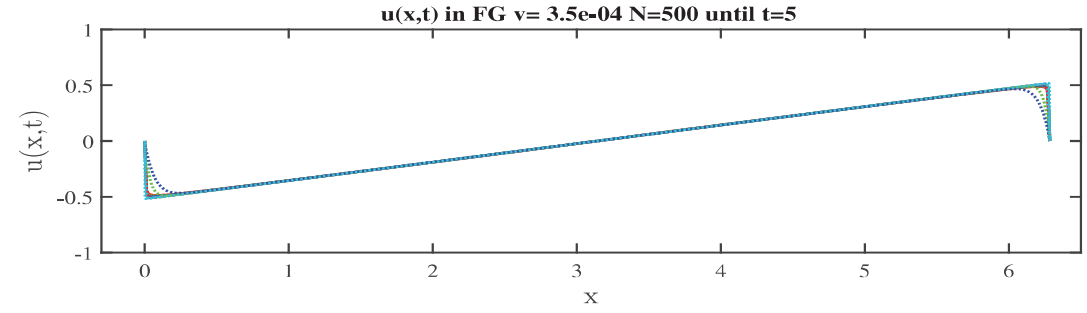
u(x,t) in FG v= 3.5e-04 N=500 until t=5
u(x,t)
x

(a) $N = 500$

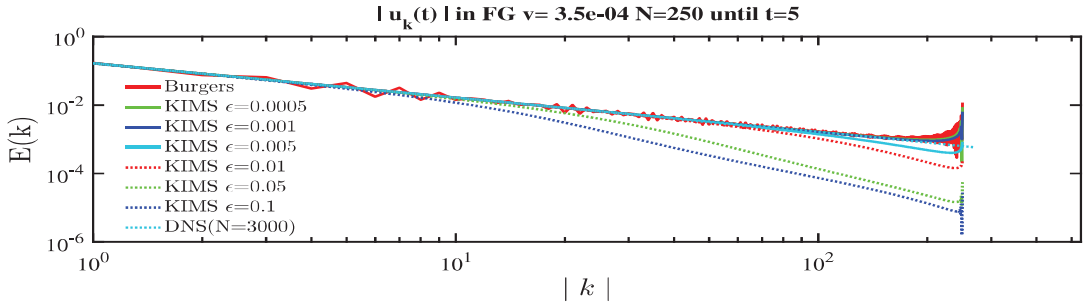
| u_k(t) | in FG v= 3.5e-04 N=250 until t=5
E(k)
| k |
Burgers
KIMS ϵ=0.0005
KIMS ϵ=0.001
KIMS ϵ=0.005
KIMS ϵ=0.01
KIMS ϵ=0.05
KIMS ϵ=0.1
DNS(N=3000)

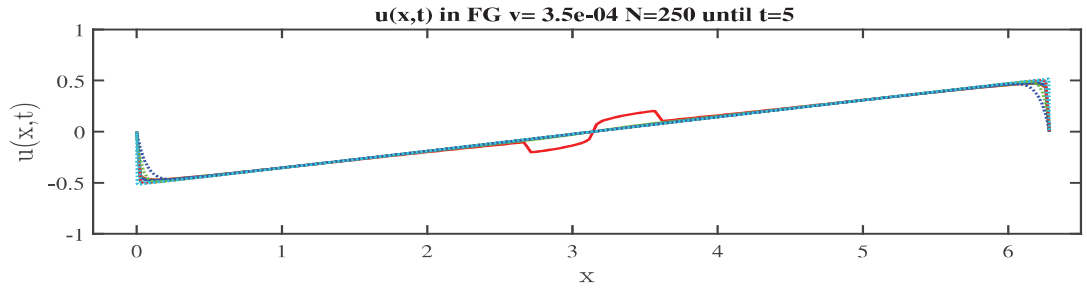
u(x,t) in FG v= 3.5e-04 N=250 until t=5
u(x,t)
x

(b) $N = 250$

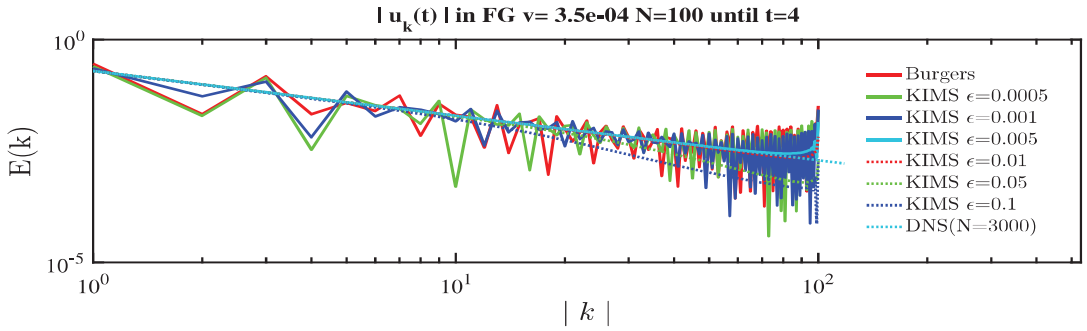

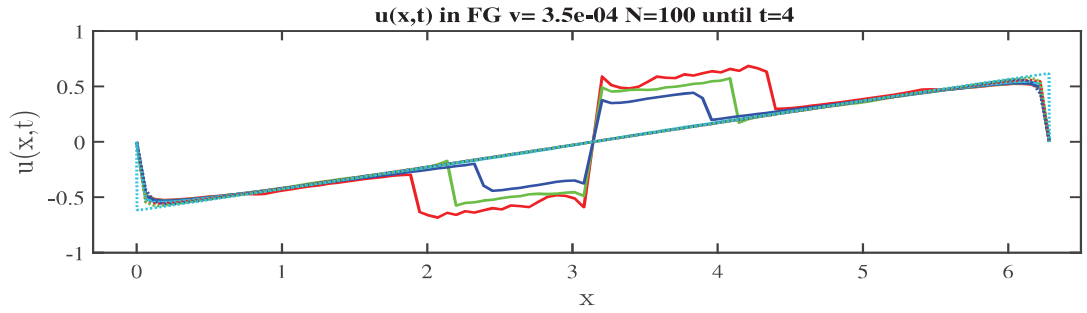

(c) $N = 100$

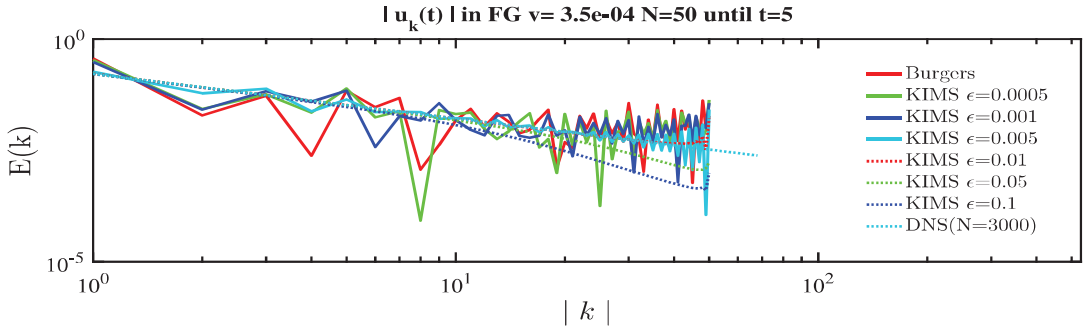

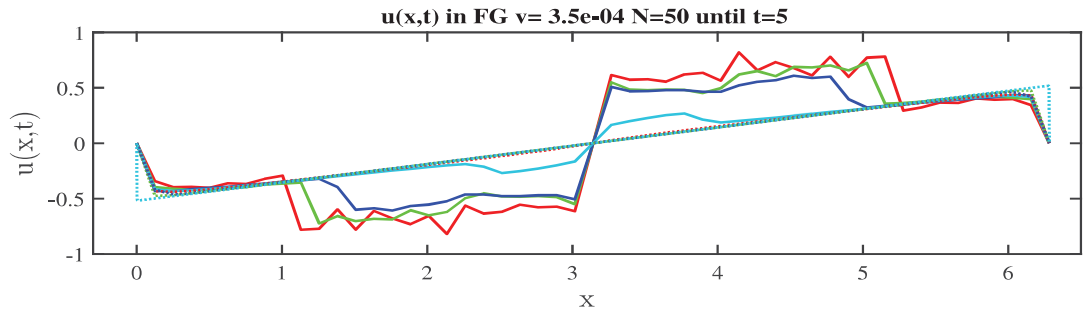

(d) $N = 50$

Figure B.2: $E(k)$ and $u(x,t)$ for the DNS and coarse grid solutions at $t = 5$.

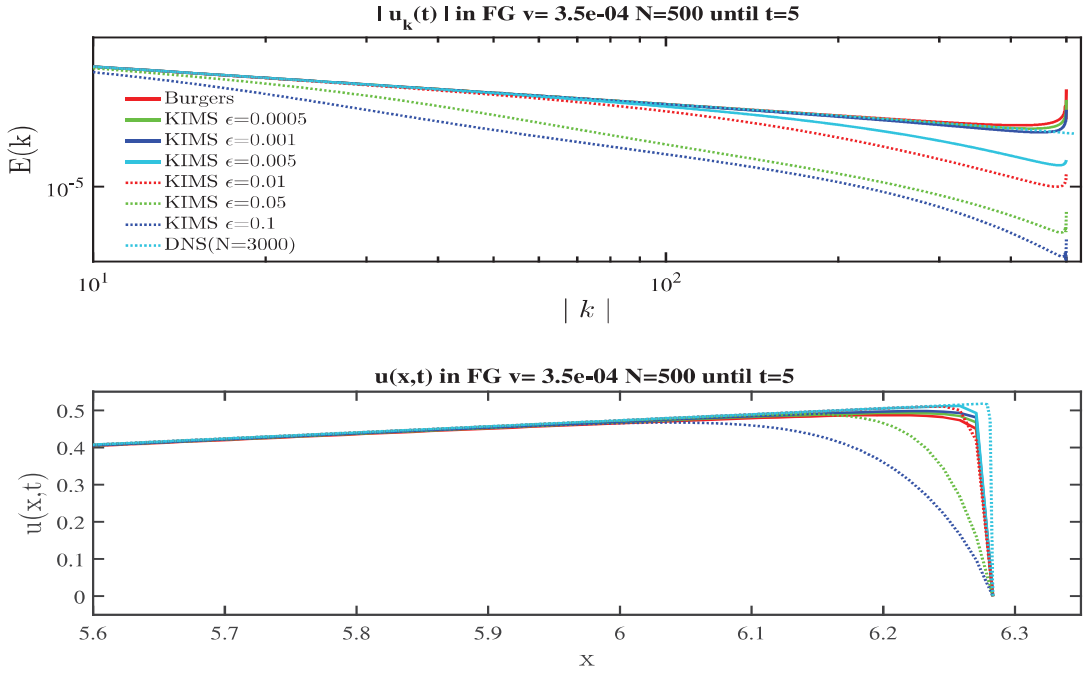
| u_k(t) | in FG v= 3.5e-04 N=500 until t=5
E(k)
10^-5
Burgers
KIMS ϵ=0.0005
KIMS ϵ=0.001
KIMS ϵ=0.005
KIMS ϵ=0.01
KIMS ϵ=0.05
KIMS ϵ=0.1
DNS(N=3000)
10^1
10^2
| k |
u(x,t) in FG v= 3.5e-04 N=500 until t=5
u(x,t)
0
0.1
0.2
0.3
0.4
0.5
5.6
5.7
5.8
5.9
6
6.1
6.2
6.3
x

(a) $N = 500$

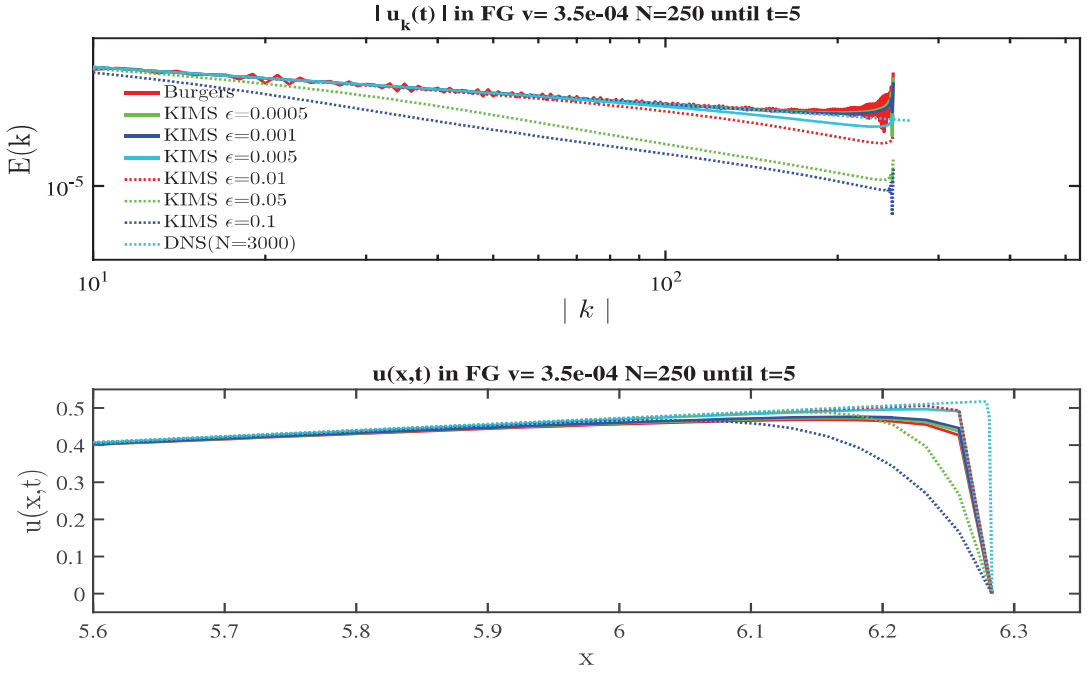
| u_k(t) | in FG v= 3.5e-04 N=250 until t=5
E(k)
10^-5
Burgers
KIMS ϵ=0.0005
KIMS ϵ=0.001
KIMS ϵ=0.005
KIMS ϵ=0.01
KIMS ϵ=0.05
KIMS ϵ=0.1
DNS(N=3000)
10^1
10^2
| k |
u(x,t) in FG v= 3.5e-04 N=250 until t=5
u(x,t)
0
0.1
0.2
0.3
0.4
0.5
5.6
5.7
5.8
5.9
6
6.1
6.2
6.3
x

(b) $N = 250$

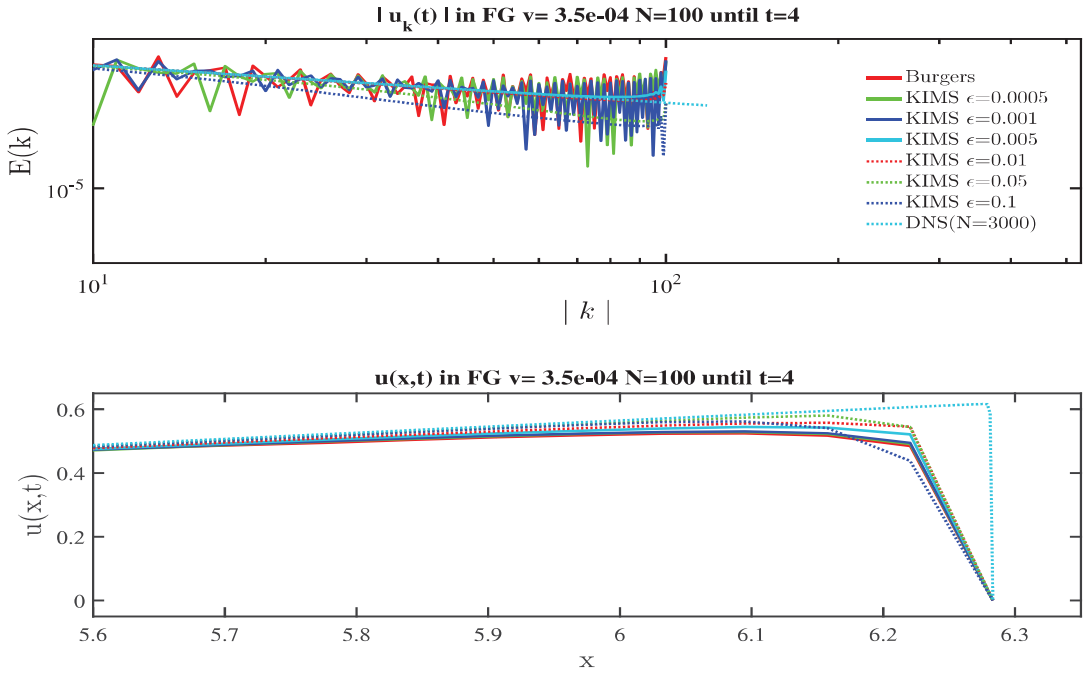

(c) $N = 100$

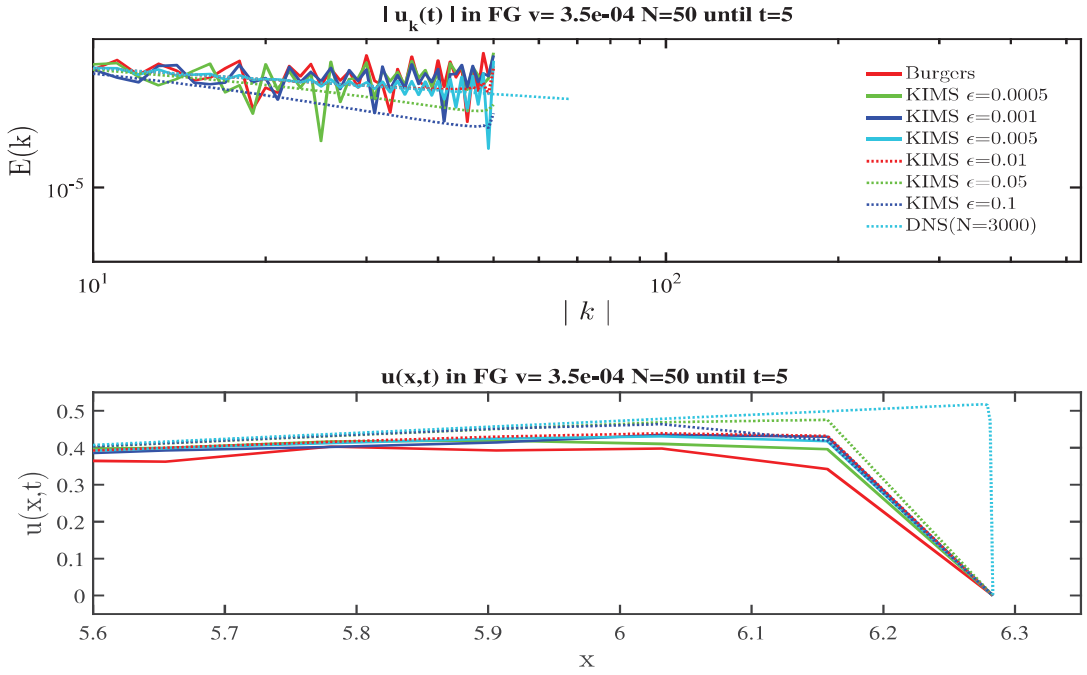

(d) $N = 50$

Figure B.3: $E(k)$ and $u(x,t)$ for the DNS and the coarse grid solutions at $t = 5$.

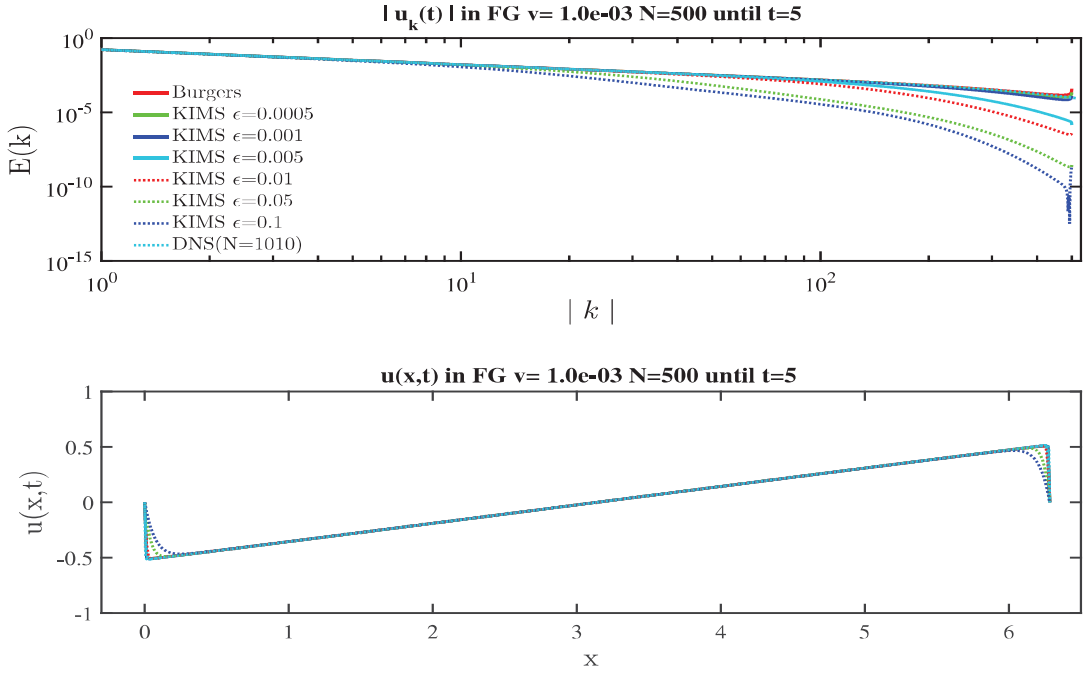
| u_k(t) | in FG v= 1.0e-03 N=500 until t=5
E(k)
| k |
Burgers
KIMS ϵ=0.0005
KIMS ϵ=0.001
KIMS ϵ=0.005
KIMS ϵ=0.01
KIMS ϵ=0.05
KIMS ϵ=0.1
DNS(N=1010)
u(x,t) in FG v= 1.0e-03 N=500 until t=5
u(x,t)
x

(a) $N = 500$

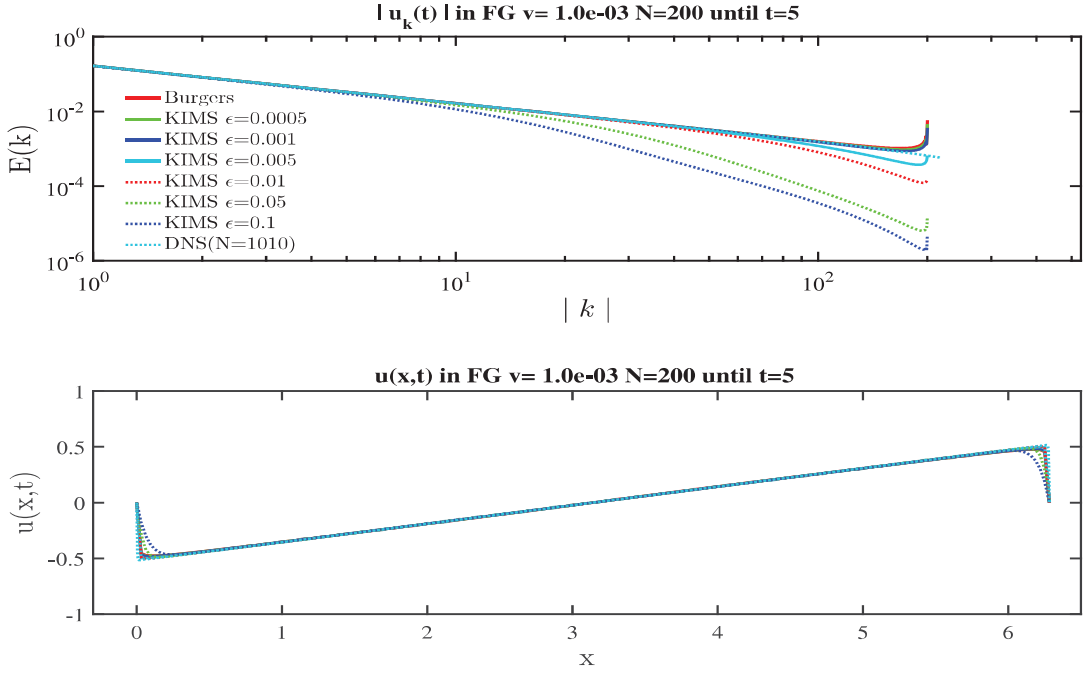
| u_k(t) | in FG v= 1.0e-03 N=200 until t=5
E(k)
| k |
Burgers
KIMS ϵ=0.0005
KIMS ϵ=0.001
KIMS ϵ=0.005
KIMS ϵ=0.01
KIMS ϵ=0.05
KIMS ϵ=0.1
DNS(N=1010)
u(x,t) in FG v= 1.0e-03 N=200 until t=5
u(x,t)
x

(b) $N = 200$

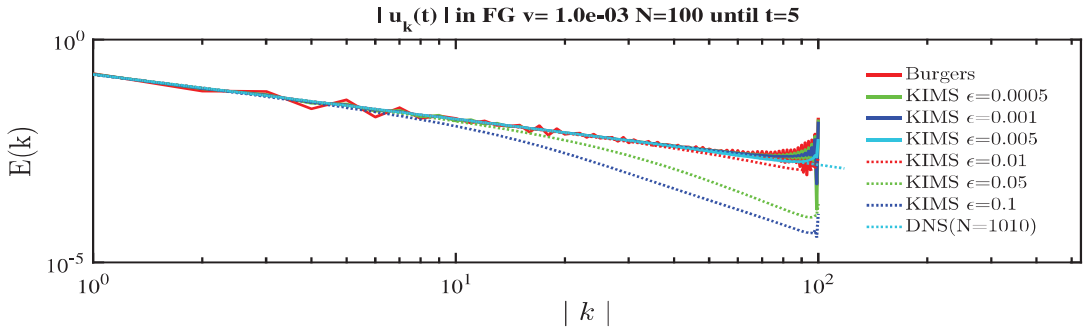

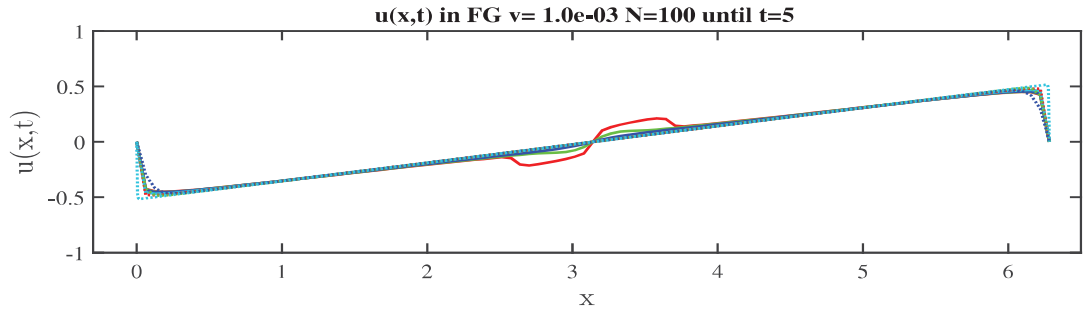

(c) $N = 100$

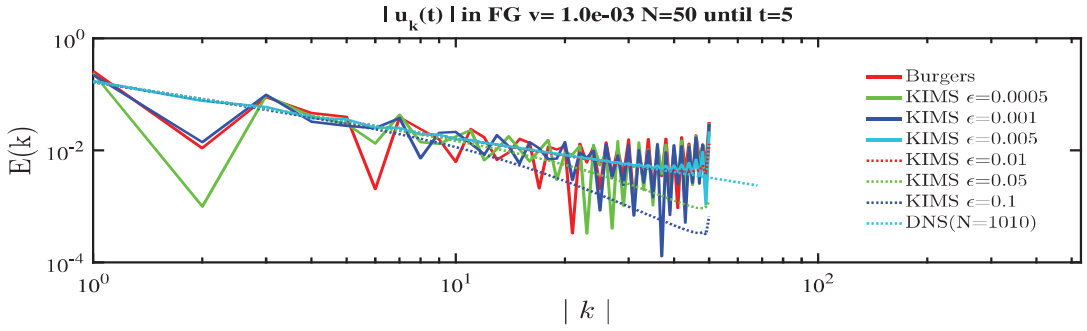

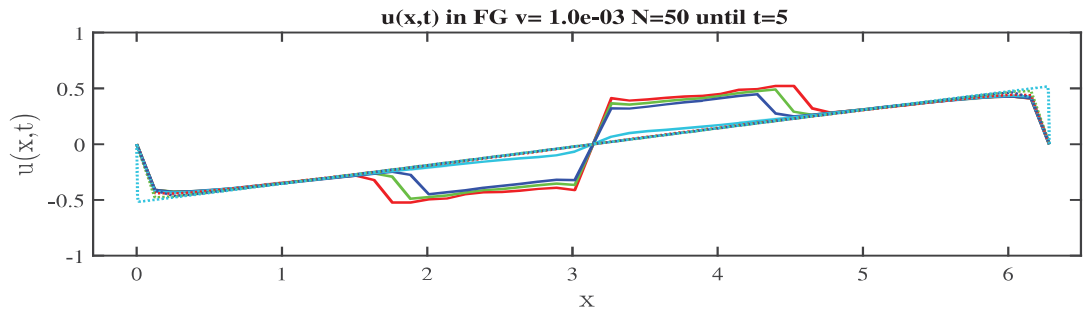

(d) $N = 50$

Figure B.4: $E(k)$ and $u(x,t)$ for the DNS and the coarse grid solutions at $t = 5$.

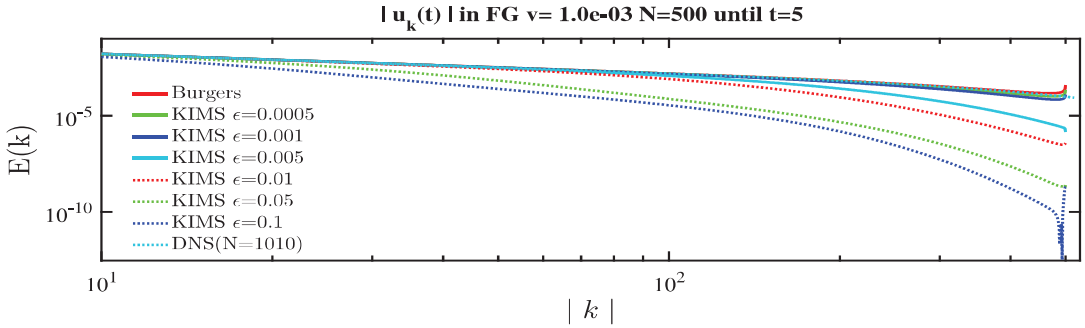
| u_k(t) | in FG v= 1.0e-03 N=500 until t=5
E(k)
10^-5
10^-10
10^1
10^2
| k |
Burgers
KIMS ϵ=0.0005
KIMS ϵ=0.001
KIMS ϵ=0.005
KIMS ϵ=0.01
KIMS ϵ=0.05
KIMS ϵ=0.1
DNS(N=1010)

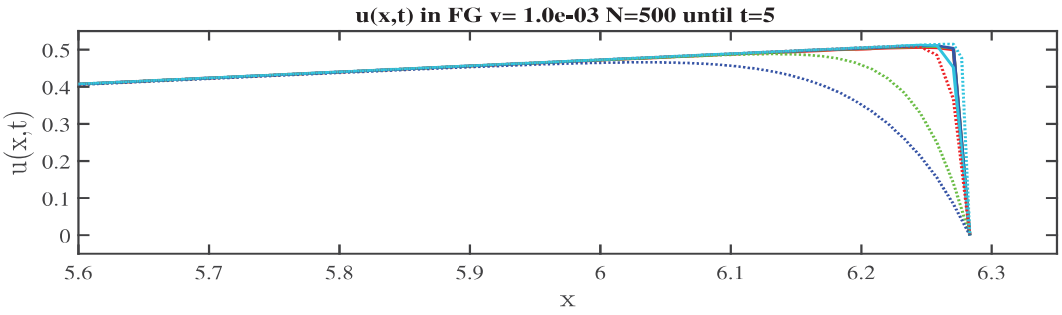
u(x,t) in FG v= 1.0e-03 N=500 until t=5
u(x,t)
0
0.1
0.2
0.3
0.4
0.5
5.6
5.7
5.8
5.9
6
6.1
6.2
6.3
x

(a) $N = 500$

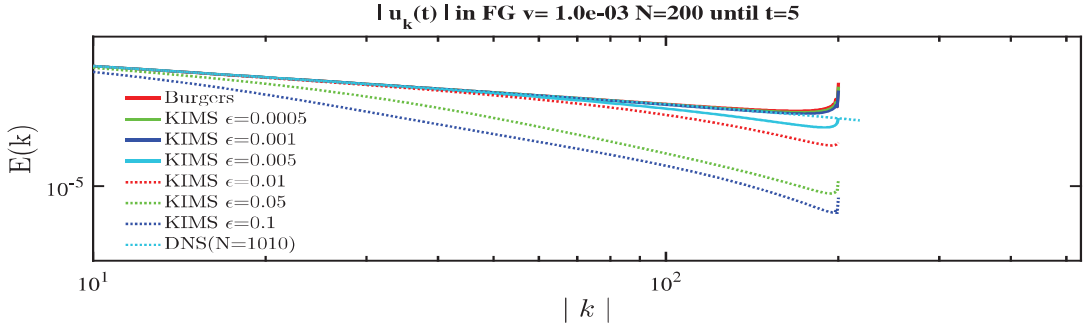
| u_k(t) | in FG v= 1.0e-03 N=200 until t=5
E(k)
10^-5
10^1
10^2
| k |
Burgers
KIMS ϵ=0.0005
KIMS ϵ=0.001
KIMS ϵ=0.005
KIMS ϵ=0.01
KIMS ϵ=0.05
KIMS ϵ=0.1
DNS(N=1010)

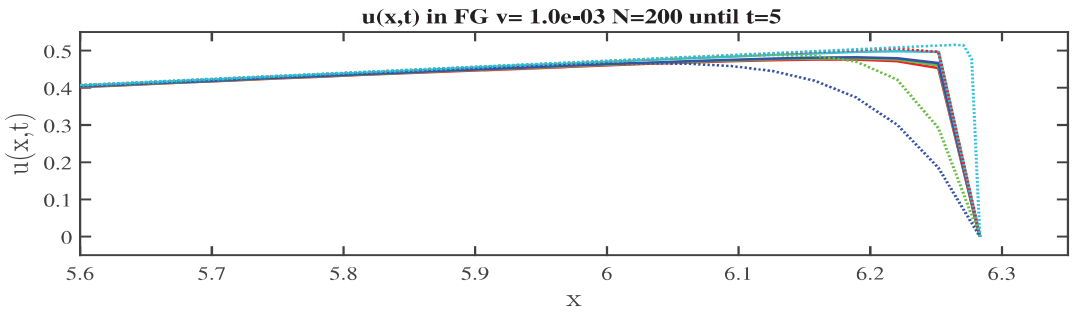
u(x,t) in FG v= 1.0e-03 N=200 until t=5
u(x,t)
0
0.1
0.2
0.3
0.4
0.5
5.6
5.7
5.8
5.9
6
6.1
6.2
6.3
x

(b) $N = 200$

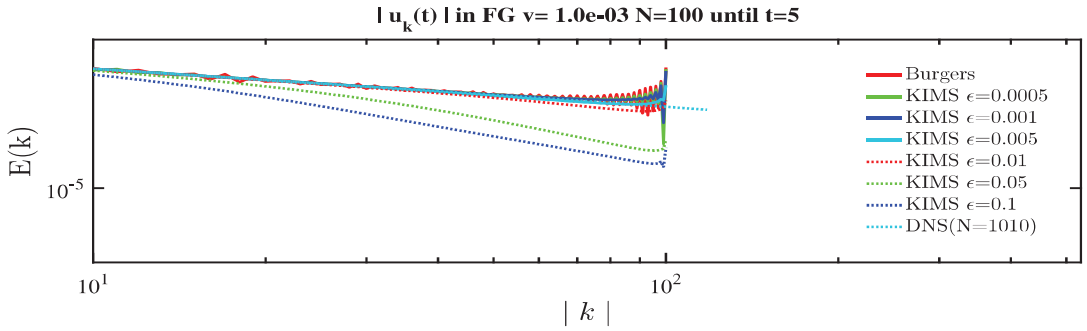

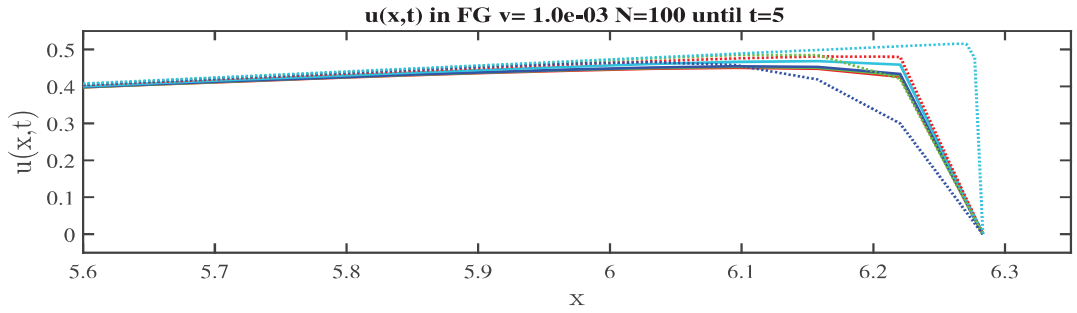

(c) $N = 100$

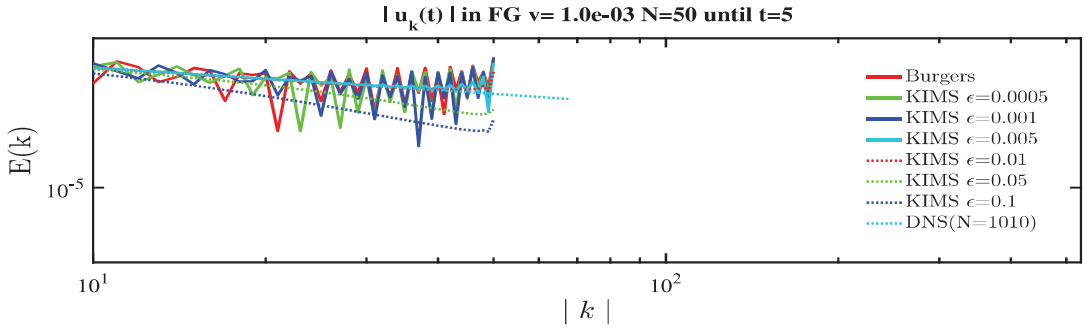

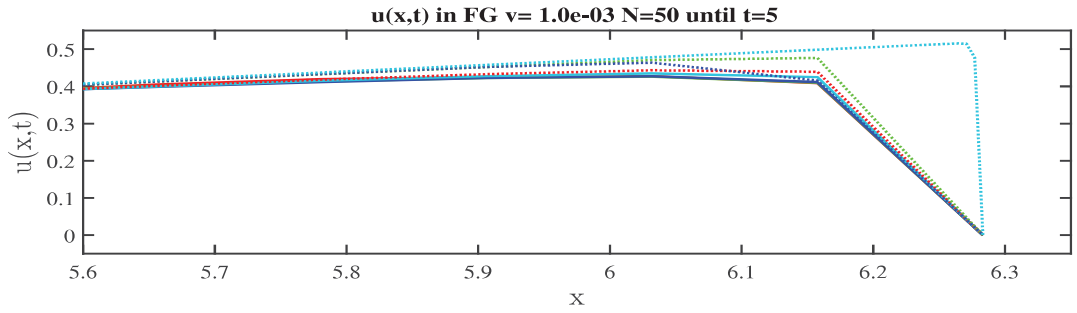

(d) $N = 50$

Figure B.5: $E(k)$ and $u(x,t)$ for the DNS and the coarse grid solutions at $t = 5$.

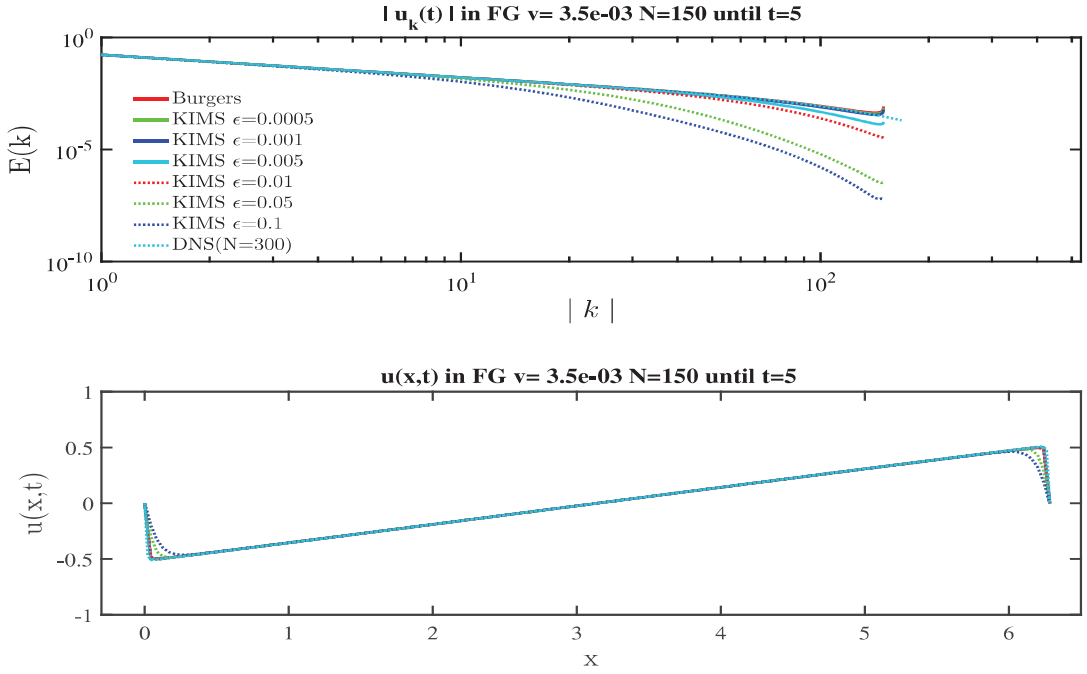
| u_k(t) | in FG v= 3.5e-03 N=150 until t=5
E(k)
| k |
Burgers
KIMS ϵ=0.0005
KIMS ϵ=0.001
KIMS ϵ=0.005
KIMS ϵ=0.01
KIMS ϵ=0.05
KIMS ϵ=0.1
DNS(N=300)
u(x,t) in FG v= 3.5e-03 N=150 until t=5
u(x,t)
x

(a) $N = 150$

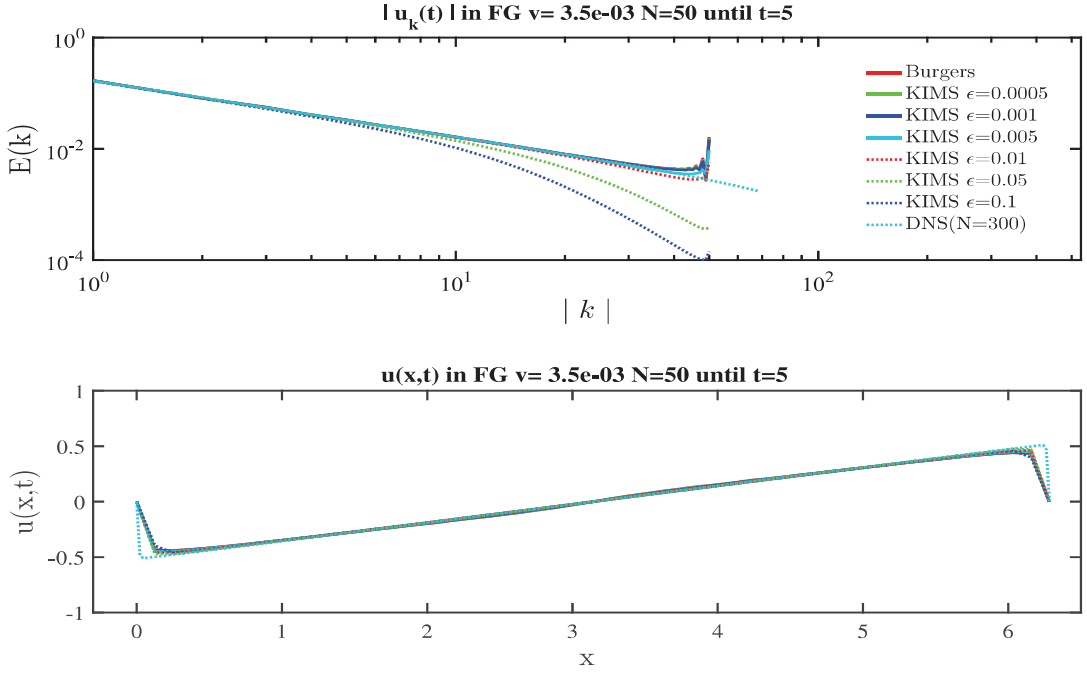
| u_k(t) | in FG v= 3.5e-03 N=50 until t=5
E(k)
| k |
Burgers
KIMS ϵ=0.0005
KIMS ϵ=0.001
KIMS ϵ=0.005
KIMS ϵ=0.01
KIMS ϵ=0.05
KIMS ϵ=0.1
DNS(N=300)
u(x,t) in FG v= 3.5e-03 N=50 until t=5
u(x,t)
x

(b) $N = 50$

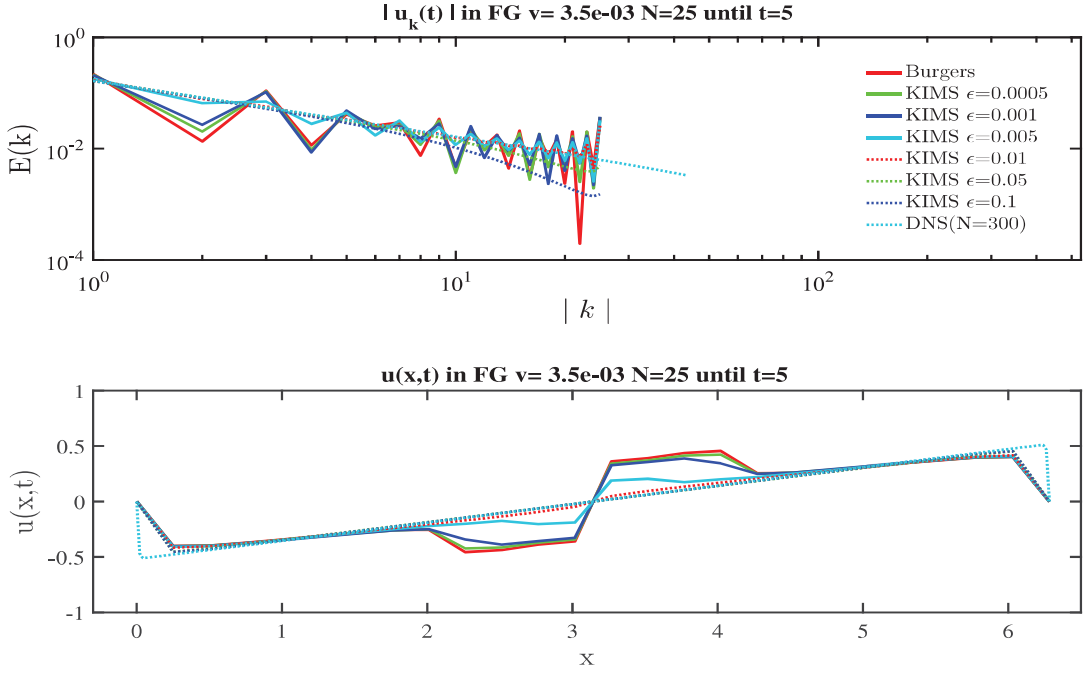

(c) $N = 25$

Figure B.6: $E(k)$ and $u(x,t)$ for the DNS and coarse grid solutions at $t = 5$.

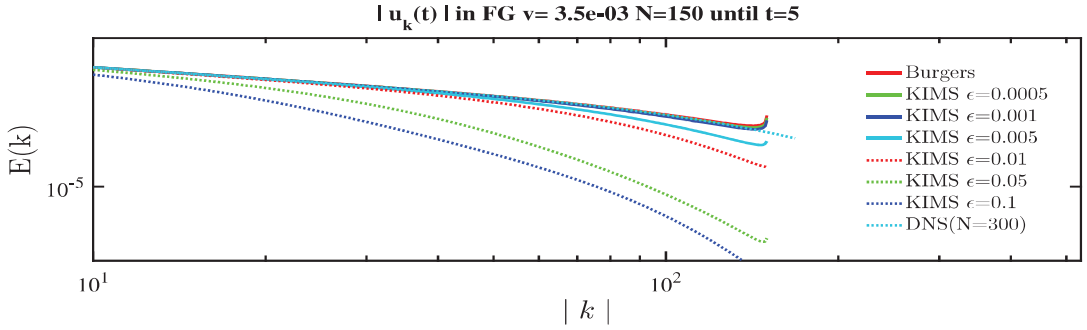
| u_k(t) | in FG v= 3.5e-03 N=150 until t=5
E(k)
10^-5
10^1
10^2
| k |
Burgers
KIMS ϵ=0.0005
KIMS ϵ=0.001
KIMS ϵ=0.005
KIMS ϵ=0.01
KIMS ϵ=0.05
KIMS ϵ=0.1
DNS(N=300)

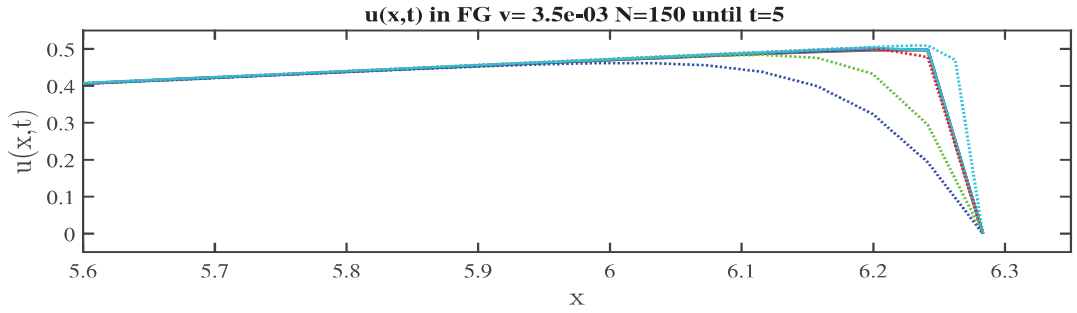
u(x,t) in FG v= 3.5e-03 N=150 until t=5
u(x,t)
0
0.1
0.2
0.3
0.4
0.5
5.6
5.7
5.8
5.9
6
6.1
6.2
6.3
x

(a) $N = 150$

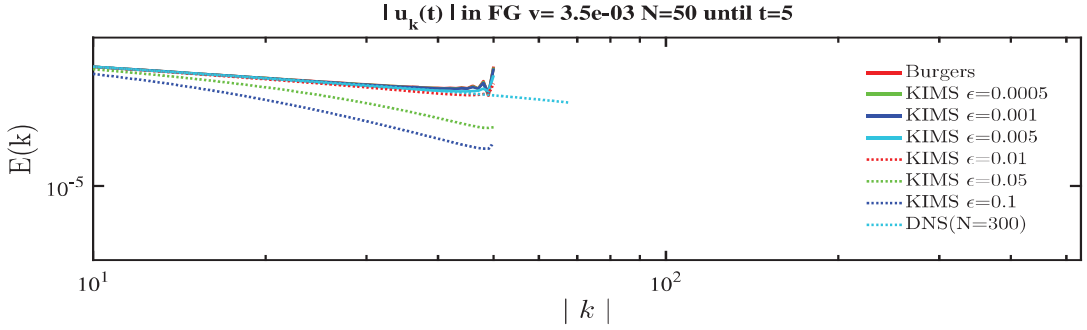
| u_k(t) | in FG v= 3.5e-03 N=50 until t=5
E(k)
10^-5
10^1
10^2
| k |
Burgers
KIMS ϵ=0.0005
KIMS ϵ=0.001
KIMS ϵ=0.005
KIMS ϵ=0.01
KIMS ϵ=0.05
KIMS ϵ=0.1
DNS(N=300)

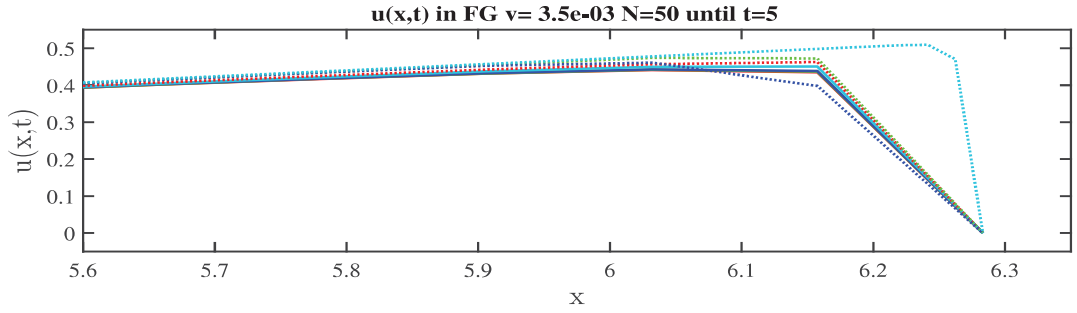
u(x,t) in FG v= 3.5e-03 N=50 until t=5
u(x,t)
0
0.1
0.2
0.3
0.4
0.5
5.6
5.7
5.8
5.9
6
6.1
6.2
6.3
x

(b) $N = 50$

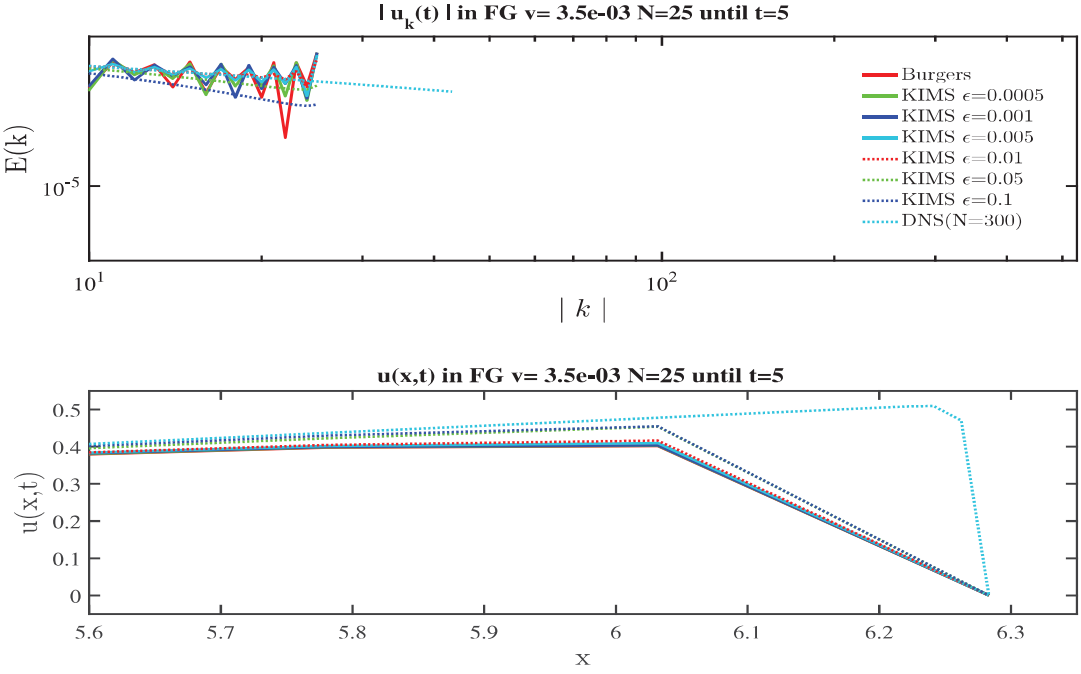

(c) $N = 25$

Figure B.7: $E(k)$ and $u(x,t)$ for the DNS and coarse grid solutions at $t = 5$.

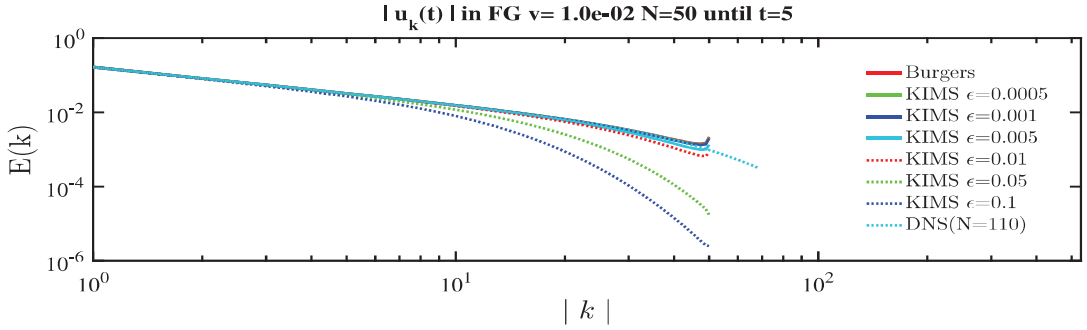
| u_k(t) | in FG v= 1.0e-02 N=50 until t=5
E(k)
| k |
Burgers
KIMS ϵ=0.0005
KIMS ϵ=0.001
KIMS ϵ=0.005
KIMS ϵ=0.01
KIMS ϵ=0.05
KIMS ϵ=0.1
DNS(N=110)

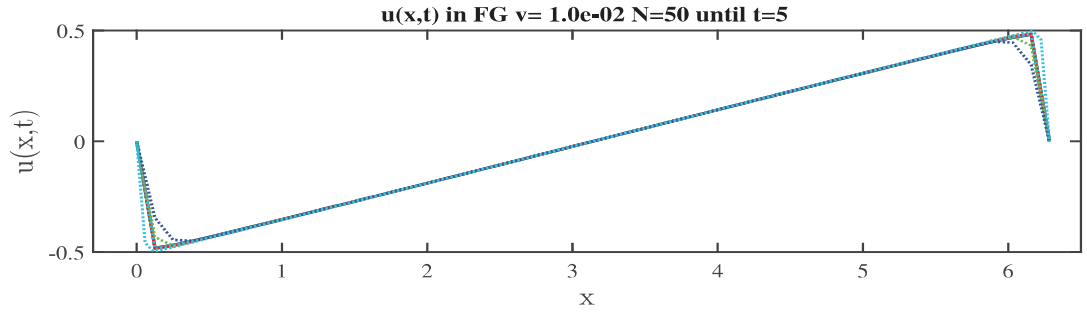
u(x,t) in FG v= 1.0e-02 N=50 until t=5
u(x,t)
x

(a) $N = 50$

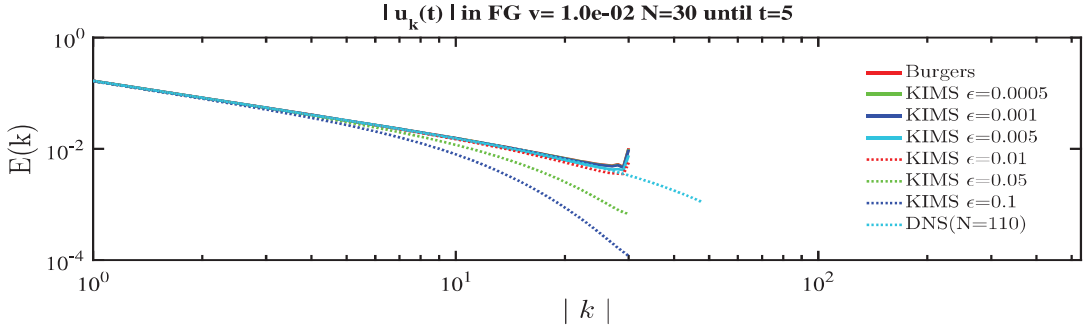
| u_k(t) | in FG v= 1.0e-02 N=30 until t=5
E(k)
| k |
Burgers
KIMS ϵ=0.0005
KIMS ϵ=0.001
KIMS ϵ=0.005
KIMS ϵ=0.01
KIMS ϵ=0.05
KIMS ϵ=0.1
DNS(N=110)

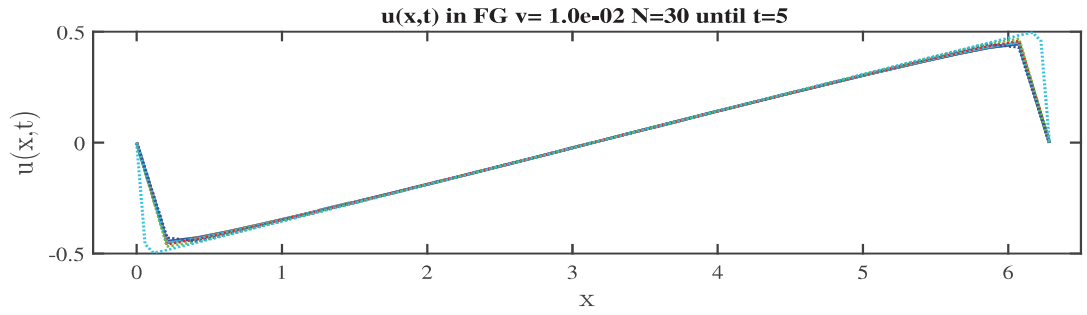
u(x,t) in FG v= 1.0e-02 N=30 until t=5
u(x,t)
x

(b) $N = 30$

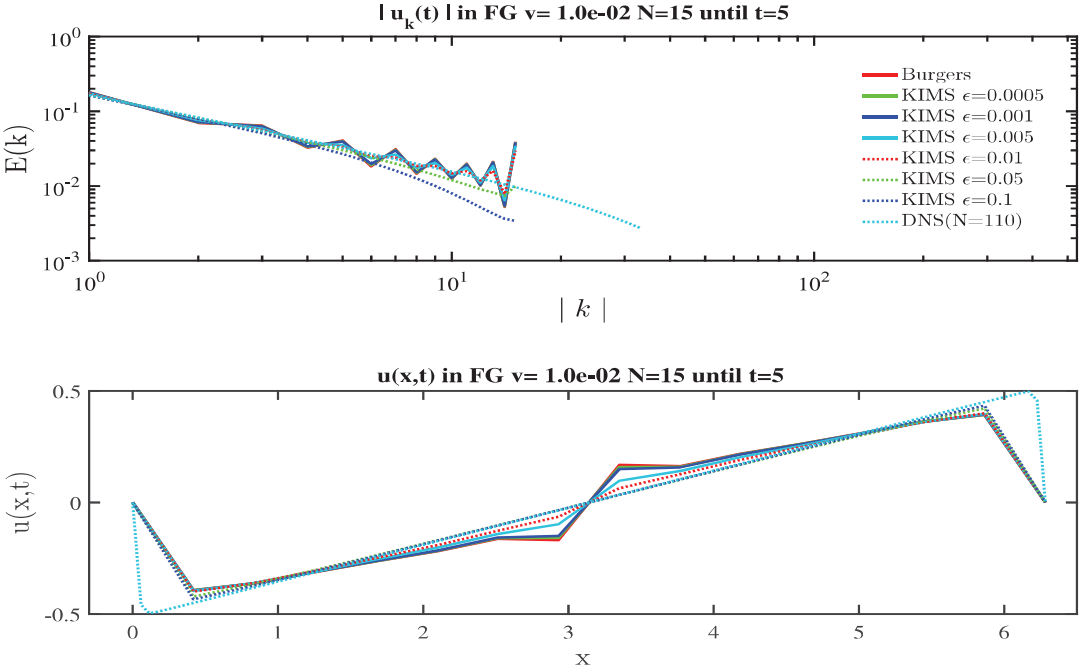

(c) $N = 15$

Figure B.8: $E(k)$ and $u(x,t)$ for the DNS and coarse grid solutions at $t = 5$.

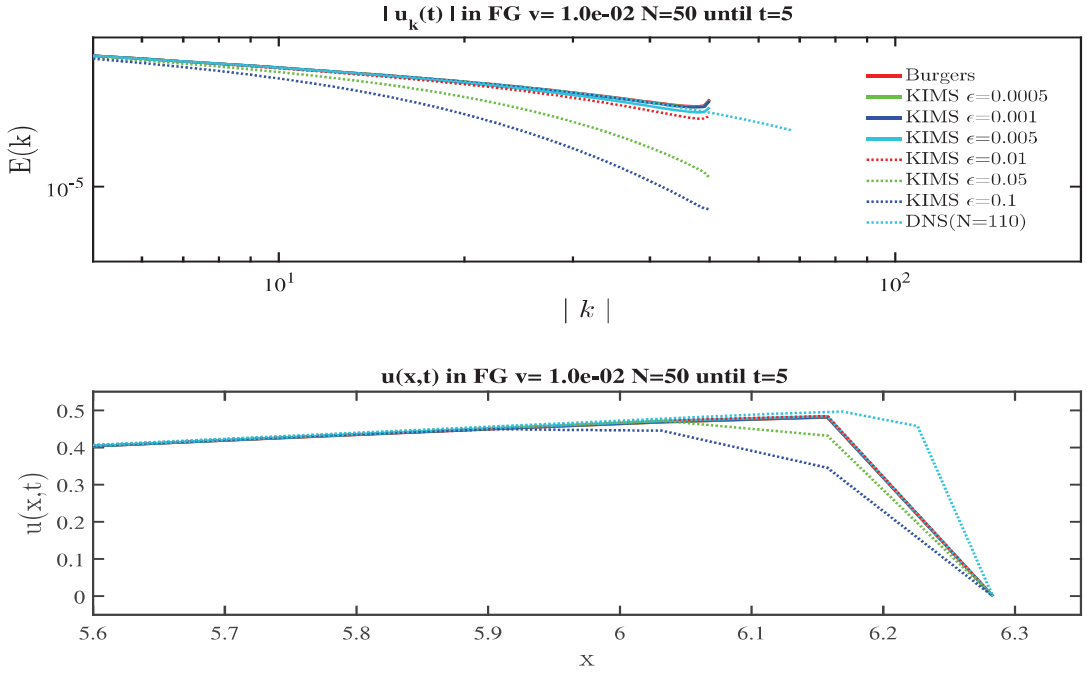
| u_k(t) | in FG v= 1.0e-02 N=50 until t=5
E(k)
10^-5
10^1
10^2
| k |
Burgers
KIMS ϵ=0.0005
KIMS ϵ=0.001
KIMS ϵ=0.005
KIMS ϵ=0.01
KIMS ϵ=0.05
KIMS ϵ=0.1
DNS(N=110)
u(x,t) in FG v= 1.0e-02 N=50 until t=5
u(x,t)
0
0.1
0.2
0.3
0.4
0.5
5.6
5.7
5.8
5.9
6
6.1
6.2
6.3
x

(a) $N = 50$

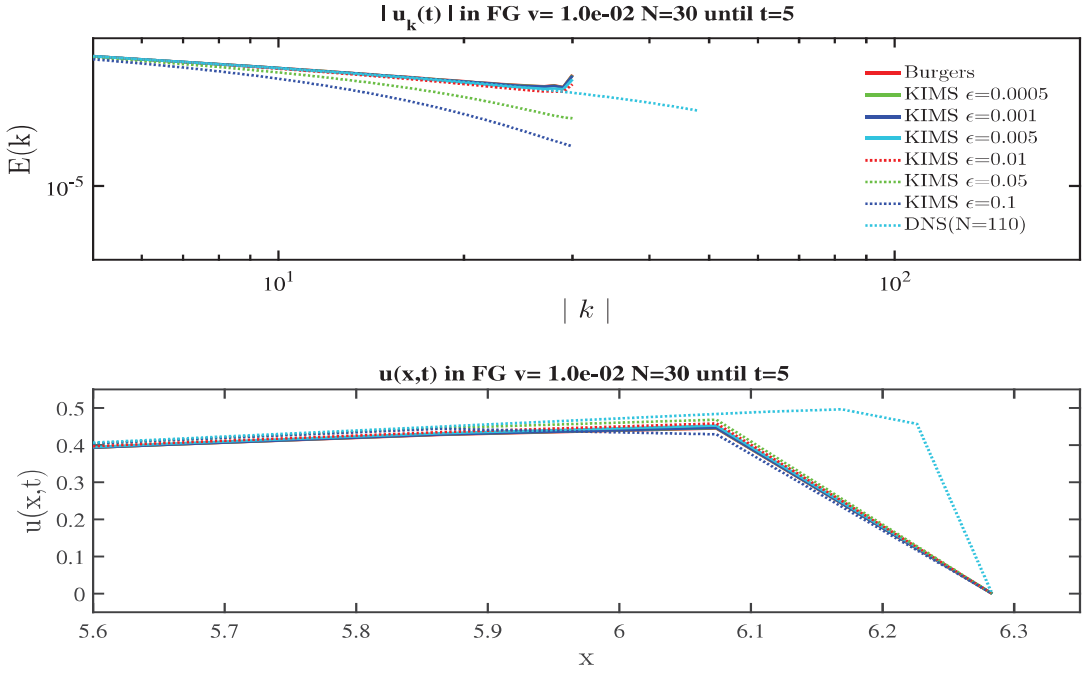
| u_k(t) | in FG v= 1.0e-02 N=30 until t=5
E(k)
10^-5
10^1
10^2
| k |
Burgers
KIMS ϵ=0.0005
KIMS ϵ=0.001
KIMS ϵ=0.005
KIMS ϵ=0.01
KIMS ϵ=0.05
KIMS ϵ=0.1
DNS(N=110)
u(x,t) in FG v= 1.0e-02 N=30 until t=5
u(x,t)
0
0.1
0.2
0.3
0.4
0.5
5.6
5.7
5.8
5.9
6
6.1
6.2
6.3
x

(b) $N = 30$

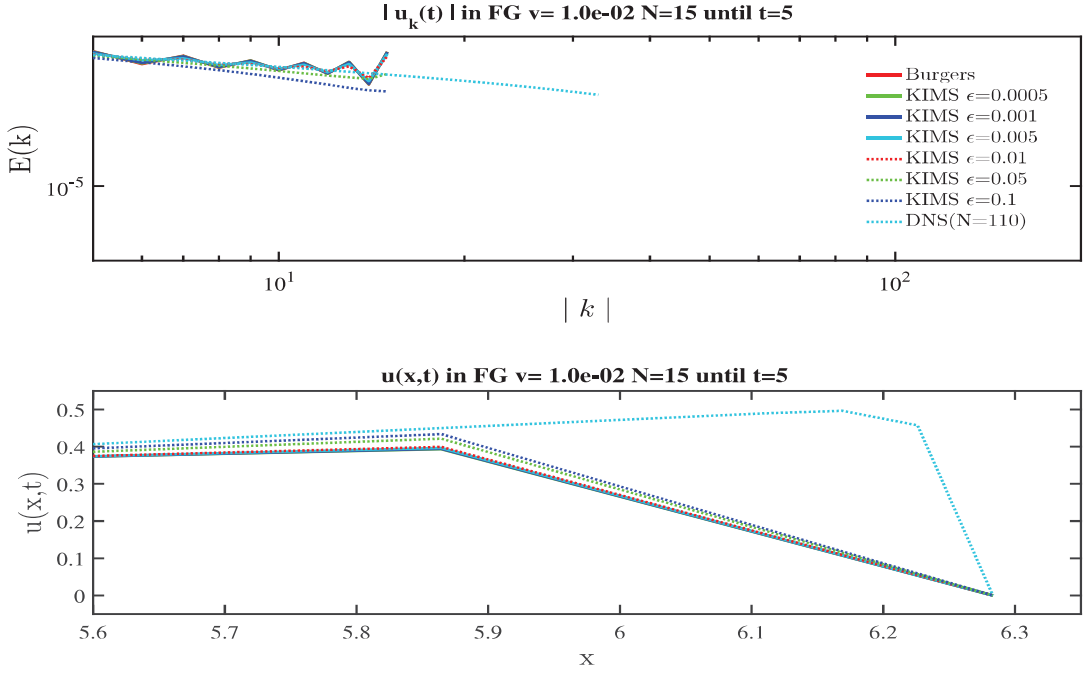

(c) $N = 15$

Figure B.9: $E(k)$ and $u(x,t)$ for the DNS and coarse grid solutions at $t = 5$.

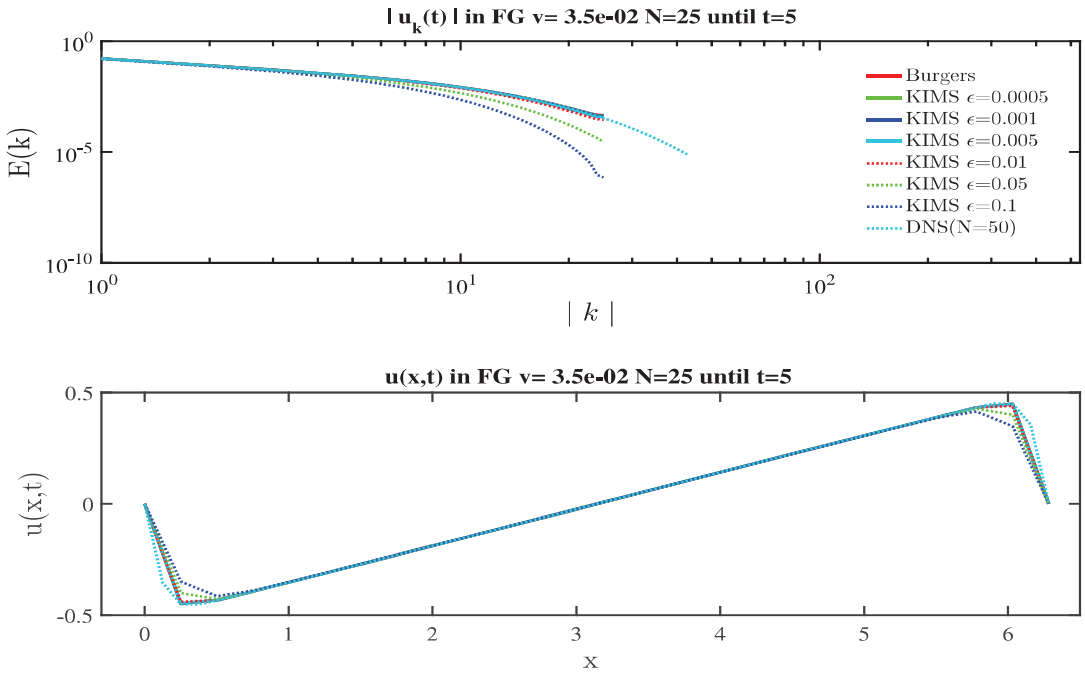

(a) $N = 25$

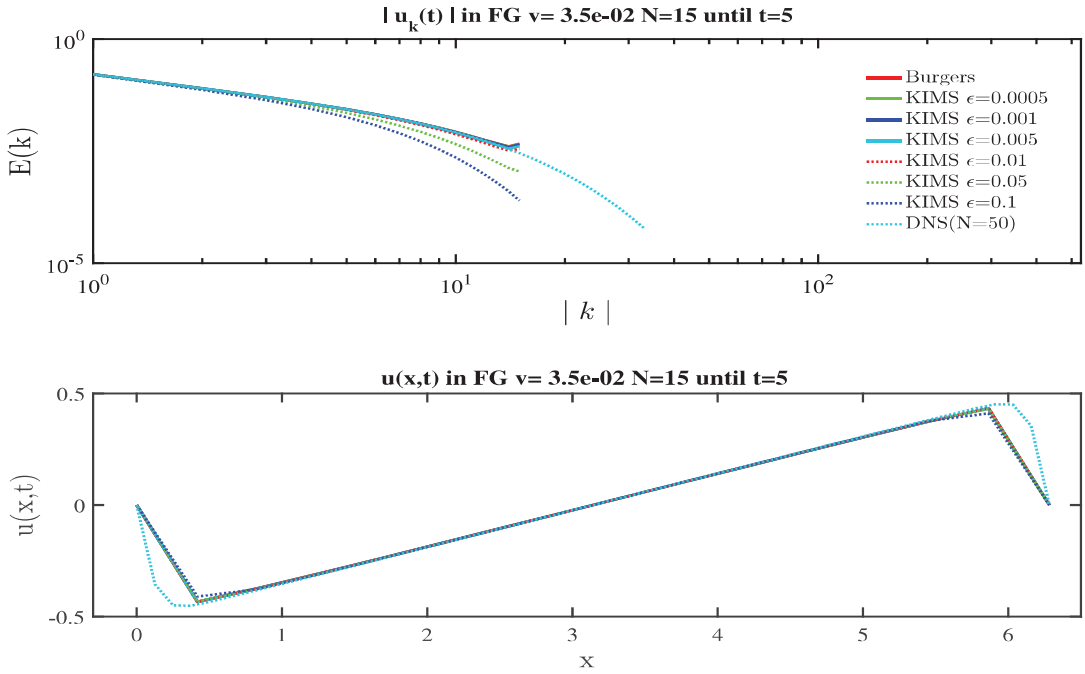

(b) $N = 15$

Figure B.10: $E(k)$ and $u(x,t)$ for the DNS and coarse grid solutions at $t = 5$.

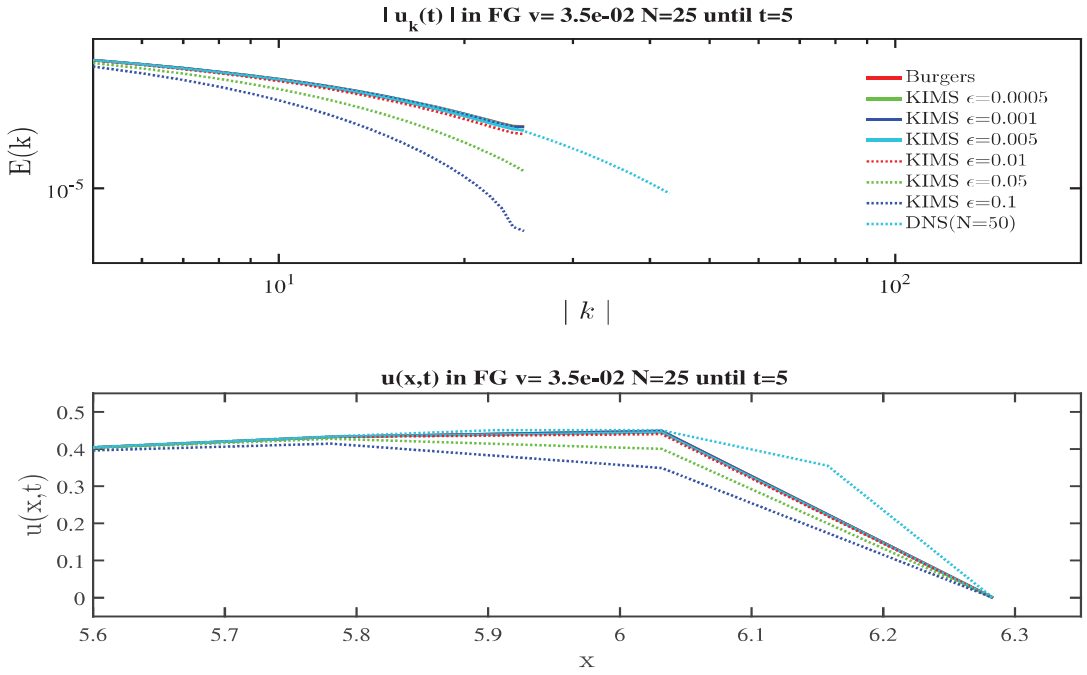

(a) $N = 25$

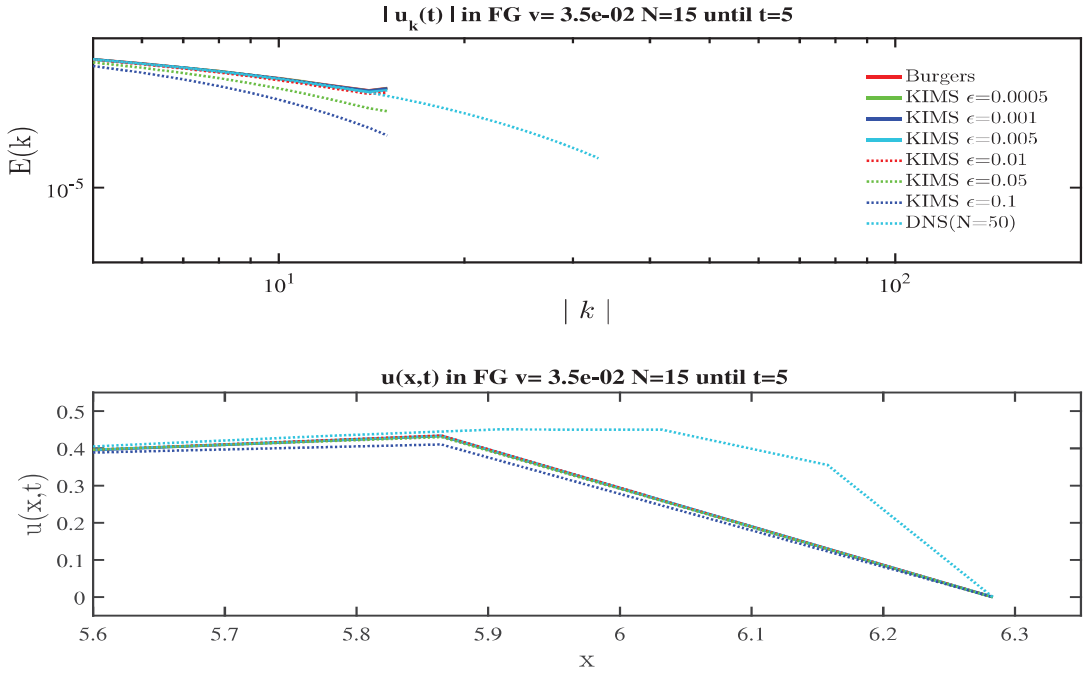

(b) $N = 15$

Figure B.11: $E(k)$ and $u(x,t)$ for the DNS and coarse grid solutions at $t = 5$.

Summary

Based on the relation between kinetic-like transport equations and non-linear balance laws, we use the order of magnitude method in order to derive kinetic-induced moment systems for the spatially one-dimensional scalar case and the 2×2 system, which will be then ε-coupled with their higher order terms. Next, we prove that in the formal limit $\varepsilon \to 0$, the higher order moment systems tend to the original balance law plus a new variable that we call $W(x,t)$, which may act as a monitoring function to detect special solutions like shock and rarefaction waves. Two main example are treated: the inviscid Burgers equation and the shallow water system, which are then used to perform numerical experiments where $W(x,t)$ is used as refinement criteria for adaptive techniques. In addition, we study the spectral characteristics of the derived moment system for the inviscid Burgers equation and its use as a "subgrid closure" model when using Fourier-Galerkin spectral approximations by comparing different amounts of resolved scales with different values of the smallness parameter ε.

Zusammenfassung

Basierend auf dem Verhältnis zwischen kinetisch geformten Transportgleichungen und nichtlinearem Gleichgewichtsgesetz, nutzen wir die Größenordnungsmethode, um kinetisch induzierte Momentsysteme für den räumlich eindimensionalen Skalarfall und das 2×2 System, welches dann ε-gekoppelte mit den Termen höherer Ordnung, abzuleiten. Als nächstes beweisen wir, dass im formalen Limes $\varepsilon \to 0$, das höhere Ordnungssystemmoment zum ursprünglichen Gleichgewichtsgesetz und einer neuen Variablen, die wir $W(x,t)$ nennen und die als Monitoringfunktion zum Aufdecken von speziellen Lösungen wie Schock- und Verdünnungswellen dienen kann, tendiert. Zwei Hauptbeispiele werden behandelt: die inviskose Burgersgleichung und das Flachwassersystem, welche dann genutzt werden, um numerische Experimente, bei denen $W(x,t)$ als Exaktifizierungskriterium für die Adaptivtechnik dient, durchzuführen. Zudem erforschen wir die Spektralcharakteristiken des erhaltenen Momentsystems für die inviskose Burgersgleichung und deren Nutzen als ein "Subnetz Abschluss" Model, indem wir die Fourier-Galerkin Spektralapproximationen durch den Vergleich von unterschiedlichen Mengen aufgelöster Skalen mit unterschiedlichen Werten des Kleinheitsparameters ε, benutzen.